TECHNICAL REPORT 76-1

E76-10337
CR-144477

FINAL REPORT

SKYLAB EREP 463 RESULTS

FAULT TECTONICS AND EARTHQUAKE HAZARDS IN PARTS OF SOUTHERN CALIFORNIA

January 1976

by

P. M. Merifield and D. L. Lamar
California Earth Science Corporation
1318 Second Street, Suite 27
Santa Monica, California 90401
Telephone: (213) 395-4528

and

Carl Gazley, Jr., J. V. Lamar, and R. H. Stratton
The Rand Corporation
Santa Monica, California 90405

for

David Amsbury, Technical Monitor
NASA Lyndon B. Johnson Space Center
Houston, Texas 77058

Sponsored by NASA Lyndon B. Johnson Space Center
Contract NAS 2-7693

TECHNICAL REPORT 76-1

FINAL REPORT

SKYLAB EREP 463 RESULTS

FAULT TECTONICS AND EARTHQUAKE HAZARDS IN PARTS OF SOUTHERN CALIFORNIA

January 1976

by

P. M. Merifield and D. L. Lamar
California Earth Science Corporation
1318 Second Street, Suite 27
Santa Monica, California 90401
Telephone: (213) 395-4528

and

Carl Gazley, Jr., J. V. Lamar, and R. H. Stratton
The Rand Corporation
Santa Monica, California 90406

for

David Amsbury, Technical Monitor
NASA Lyndon B. Johnson Space Center
Houston, Texas 77058

Sponsored by NASA Lyndon B. Johnson Space Center
Contract NAS 2-7698

PREFACE

This report describes the application of Skylab EREP imagery to the analysis of fault tectonics and earthquake hazards in parts of southern California. The work was accomplished over a two and one-half year period from 23 May 1973 to 31 January 1976 under Contract NAS 2-7698 sponsored by the National Aeronautics and Space Administration, Lyndon B. Johnson Space-craft Center. Dr. David Amsbury and Mr. Martin Miller served as technical monitors. A portion of the work was accomplished in cooperation with personnel of The Rand Corporation under a subcontract from California Earth Science Corporation (CalESCO). Digital data processing was done at the Image Processing Laboratory of the Jet Propulsion Laboratory under a subcontract from CalESCO. A portion of the work described herein was presented at the NASA Earth Resources Survey Symposium, Houston, Texas, June 1975, and published in the Proceedings, Vol. I-B, p. 779-798, NASA TM X-58168, JSC-09930.

CONTENTS

PART I

SUMMARY AND INTRODUCTION

by

P. M. Merifield and D. L. Lamar

CONTENTS

ILLUSTRATIONS

TABLES

SUMMARY OF SIGNIFICANT RESULTS

Summaries of significant results from parts II to VI of the report are presented below. The area covered by each part is shown on Fig. 1.

Part II: Faults and Linears on Skylab and Landsat Images of Peninsular Ranges, Southwestern California

Four previously unknown faults were discovered in basement terrane of the Peninsular Ranges; these have been named the San Ysidro Creek fault, Thing Valley fault, Canyon City fault, and Warren Canyon fault. In addition, fault gouge and breccia were recognized along the San Diego River fault zone. Prior to this investigation, the origin of the San Diego River linear was uncertain; a fault had been suggested on some published maps, but no field evidence had been presented. These faults are considered inactive because they are restricted to pre-Tertiary rocks and are cut by the active northwest trending faults; they appear to form an older strain system, consisting of northeast and east-west conjugate shears. Study of features on Skylab imagery and review of geologic and seismic data suggest that the risk of a damaging earthquake is greater along the northwestern portion of the Elsinore fault than along the southeastern portion.

Part III: The Garlock Fault: An Example of the Ability of EREP Imagery to Resolve Indicators of Active Faults

Physiographic indicators of active faulting along the Garlock fault identifiable in Skylab imagery include scarps, linear ridges, shutter ridges, faceted ridges, linear valleys, undrained depressions and offset drainage. A large proportion of indicators of recent faulting falls into the range of meters to tens of meters and is therefore resolved by the 190B camera. The 190A camera resolved a large percentage of these features but is less suitable for this purpose.

Part IV: Faults on Skylab Imagery of the Salton Trough Area, Southern California

Based on regional alignment of probable fault-controlled features visible on Skylab images, the following previously unrecognized fault segments are

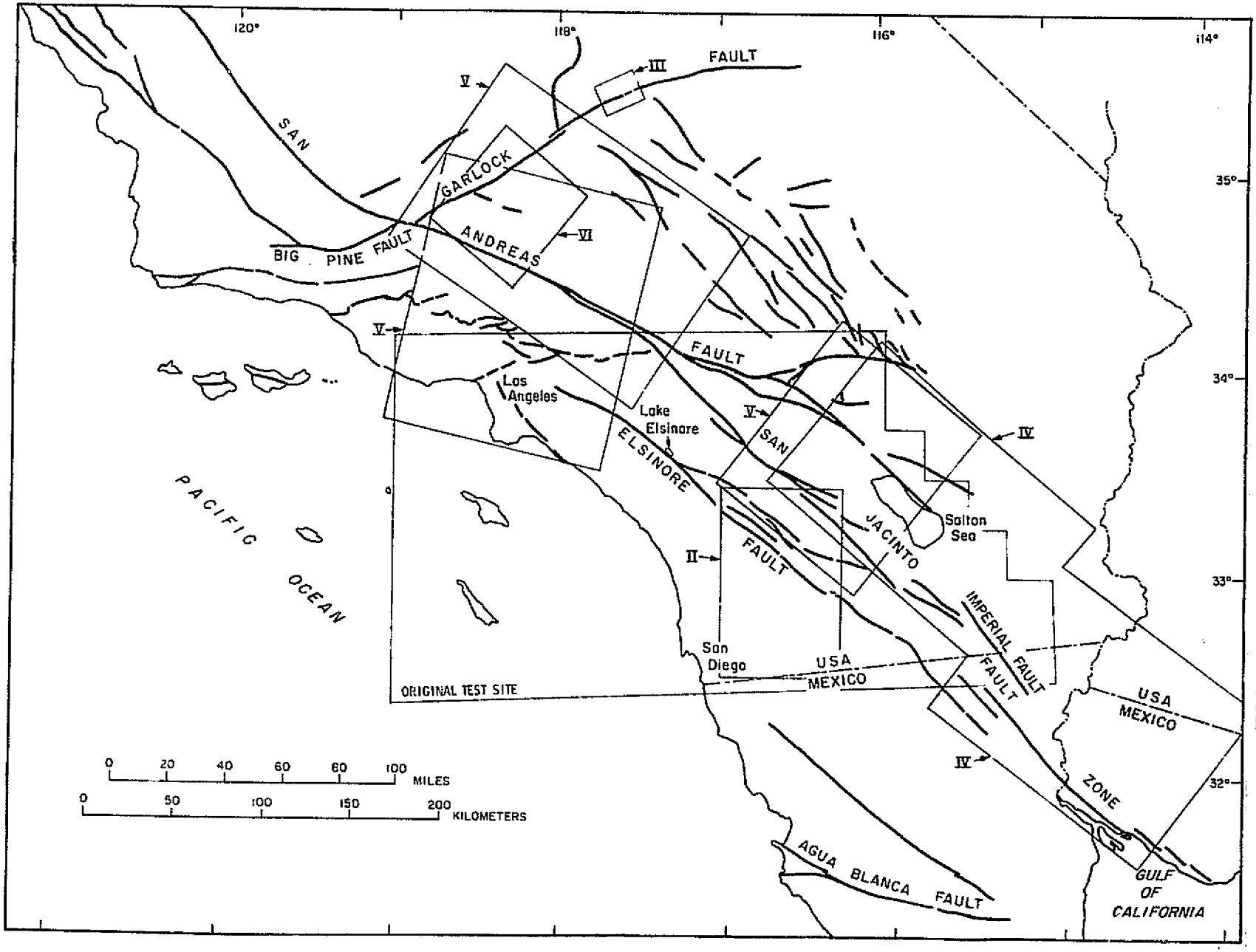

Fig. 1 - Map showing outline of original test site and areas actually studied. Roman numerals refer to individual parts of report; see text for descriptions of individual parts.

postulated: (1) An extension of a previously known fault in the San Andreas fault set located southeast of the Salton Sea. (2) An extension of the active San Jacinto fault zone along a tonal change in cultivated fields across Mexicali Valley; the tonal change may represent different soil conditions along opposite sides of a fault. Geophysical studies would be required to verify the existence of these fault segments. Long segments of previously mapped major high-angle faults are readily identifiable on Skylab images. Along active faults, distinctive topographic features such as scarps, offset drainage, shutter ridges, linear valleys, and linear ridges are visible. The following surface manifestations of ground water blockage in alluvium are also visible along branches of the San Andreas fault: spring alignments, oases, and linear differences in vegetation or land use along or on opposite sides of faults.

Part V: Enhancement Characteristics of Pseudocolor Transformations of Skylab and Landsat Images and Test Charts

For the Skylab and Landsat images studied, pseudocolor transformations offer no advantages over the original images in the recognition of faults in Skylab and Landsat images. Pseudocolor images provide some enhancement of certain features characterized by minor tonal differences on relatively flat surfaces. These include road intersections, street patterns, density of urban development and subtle tonal differences between surficial deposits on the Mojave Desert. Test charts of common symbols were prepared, and comparisons were made of the ability to identify symbols in black and white and pseudocolor images. The tests revealed no significant improvement in the ability to recognize symbols on the pseudocolor transformations. These results should be considered preliminary because of the limited number of images studied and subjects tested.

Part VI: Analysis of S-192 Imagery of the Western Mojave Desert, California

Alluvial deposits of different ages, a marble unit and iron oxide gossans of the Mojave Mining District are more readily differentiated on images prepared from ratios of individual bands of the S-192 multispectral

scanner data. The San Andreas fault was also made more distinct in the 8/2 and 9/2 band ratios by enhancement of vegetation differences on opposite sides of the fault. Our preliminary analysis indicates a significant earth resources potential for the discrimination of soil and rock types, including mineral alteration zones. This application should be actively pursued.

INTRODUCTION

Purpose and Objectives

Knowledge of the location and earthquake potential of faults is essential input for land-use planning and the siting of critical engineered structures, such as nuclear power plants, dams, hospitals and schools. Inactive faults, as well as active faults, are unsuitable sites for dams and reservoirs and constitute a hazard to tunneling operations. Fault gouge and breccia are poor foundation materials, and fault zones commonly provide the passageway for large volumes of subsurface water. In an accelerating effort to introduce geologic information into the land-use planning process, federal and state geologic agencies, in cooperation with universities and engineering-geologic consulting firms, are preparing fault maps of California (e.g., Jennings, 1973; Ziony et al., 1974). Faults are being classified by their geologic history of movement as a basis for their potential for future movement.

The general objectiv of this study is to contribute to a better understanding of the fault tectonics and earthquake hazards of southern California utilizing Skylab EREP data. Work was concentrated on the following more specific objectives.

(1) Determine the origin of photo linears revealed by Skylab imagery by means of geologic mapping supplemented by the study of existing geologic maps and aerial photography.

(2) Study the cross-cutting relationships between the principal northwest trending fault zones and fault sets with other trends to gain a better understanding of the tectonic history and earthquake potential on faults in southern California.

(3) Develop criteria for distinguishing active faults from inactive faults through recognition of geomorphic and ground water indicators of recent movement in Skylab imagery.

(4) Apply recently developed image-enhancement techniques, such as pseudocolor transformations and spectral band ratioing, to EREP data to improve photogeologic interpretation.

(5) Evaluate the relative merits of different EREP data, Landsat imagery and aerial photography at different scales in the study of faults and other geologic features.

(6) Develop an approach to improved usage of satellite imagery and define sensor requirements desirable for fault investigations in future space missions.

Areas Investigated and Data Utilized

The area of the primary test site as originally proposed and the areas actually studied, and described in each part of this report, are outlined on Fig. 1. The original test site included the Peninsular Ranges of southwestern California (described in Part II of this report) and the Salton Trough (Part IV) to the east. The basement terrane of the Peninsular Ranges was the main area of interest because prominent photo linears of unknown origin had been noted on Gemini and Apollo photographs by Dr. Paul D. Lowman of NASA Goddard Space Flight Center. The Salton Trough was included in order to study the appearance of faults in the San Andreas fault system, which are classic examples of major active faults.

The following additional investigations which pertained to the project objectives developed out of study of the Skylab images: (1) Continuation of faults in the Salton Trough south of the U.S.-Mexican border (Part IV). (2) The Garlock Fault zone on the Mojave Desert (Part III). (3) Faults and other features seen on ratio images from S-192 multiband spectral data of the western Mojave Desert (Part VI) and on pseudocolor images of the Mojave Desert and surrounding regions (Part V).

The Skylab images utilized in this investigation are outlined on Fig. 2. Owing to cloud cover, EREP data were not obtained for the coastal portion of the test site, and cloud-free images of the prime area of interest in the Peninsular Ranges were acquired only during SL-3, EREP Pass 43. Excellent imagery of the Salton Trough and areas to the northwest and southeast was obtained on SL-4. Photography from SL-2 was somewhat degraded, but nevertheless was especially useful because it covered areas not otherwise

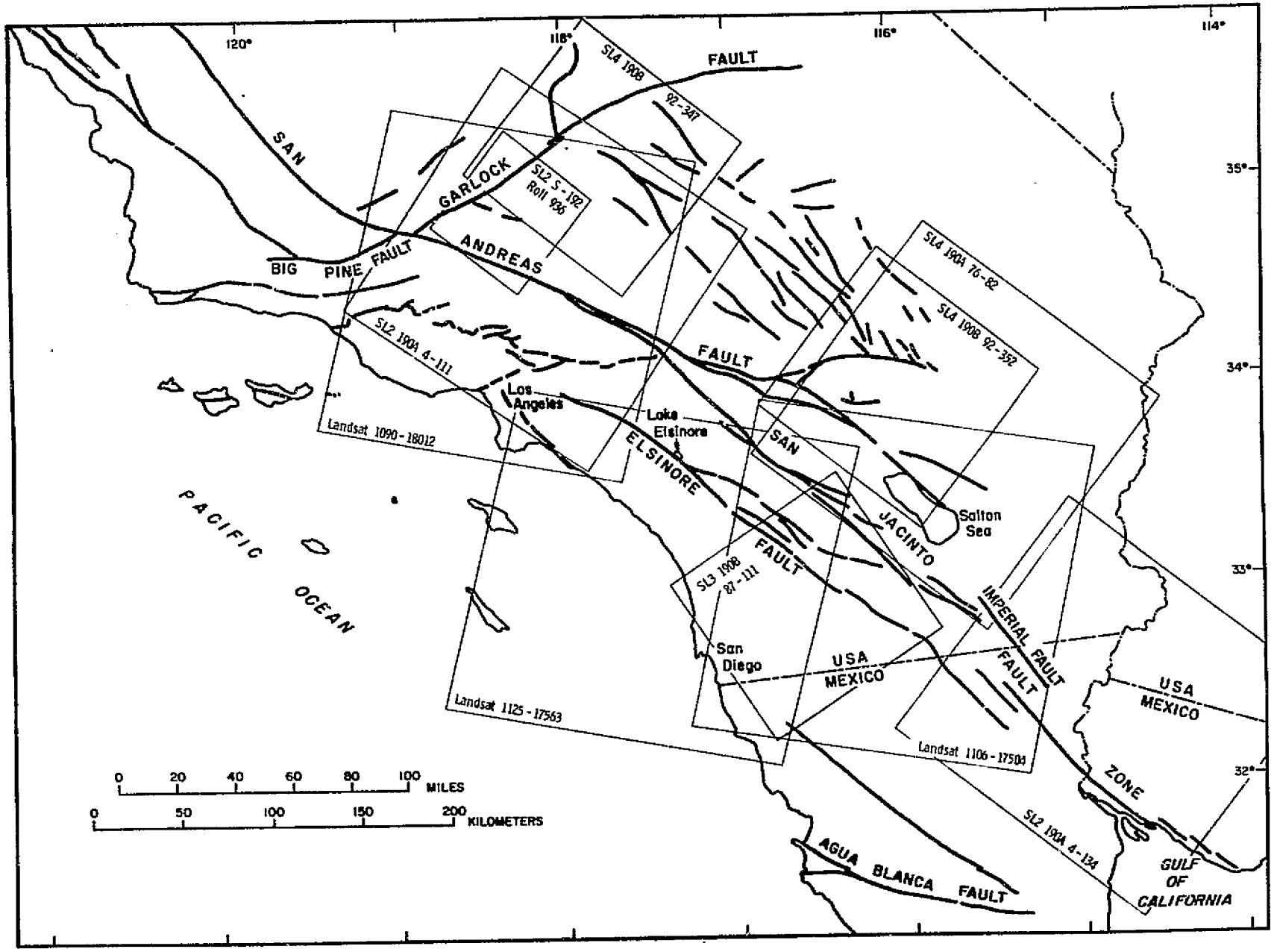

Fig. 2 - Map showing outlines of Skylab and Landsat images utilized in this report. Abbreviations: SL3: Skylab 3; 190B: 190B camera; 87-111: Roll 87, Frame 111.

included, owing to an orbit about 80 kilometers (50 miles) southwest of subsequent Skylab missions. Fig. 2 also shows the outlines of the Landsat images used in the study.

In addition to Skylab and Landsat imagery, aerial photographs from the following sources were used: NASA RB-57F, Mission 164, 1971, color IR; NASA U-2 photos, Flight 73-100, 1973, color IR; Army Map Service, Western United States Project 145, 1955, panchromatic; San Diego County, 1970, natural color; U. S. Department of Agriculture, 1953, panchromatic. Table I compares the scale and approximate spatial resolution of the imagery utilized. The aerial photography studied for each feature is identified in the appropriate parts of the report.

Sensor	Scale	Approximate Spatial Resolution (meters)	Swath Width (Km)
Landsat multispectral scanner	1:1,000,000	80	185
Skylab S-192 multispectral scanner	1:500,000	80	80
Skylab 190A camera	1:715,000	30 - 40	163
Skylab 190B camera	1:500,000	10 - 20	109
NASA U-2 and RB-57F aerial photographs	1:130,000	1.3 - 2.6	27
Army Map Service aerial photographs	1:63,000	0.6 - 1.3	14
San Diego County aerial photographs	1:24,000	0.3 - 0.5	5.5
U.S. Department of Agriculture aerial photographs	1:20,000	0.2 - 0.4	4.6

Table 1 - Scale, approximate spatial resolution and width of images used in investigation. The Landsat and Skylab multispectral scanner image scales are based on 18 x 18 centimeter (7 x 7 inch) format; all of the other scales are based on 23 x 23 centimeter (9 x 9 inch) format.

GENERAL CONCLUSIONS ON THE APPLICATION OF SATELLITE IMAGERY TO FAULT INVESTIGATIONS

In any geologic study it is desirable to obtain aerial photographs of as many different scales, times of the day and year and film types as are available, because variations in sun angle, seasonal variations in moisture and vegetation and spectral response will influence the recognition of individual features. However, Skylab and Landsat images add a new dimension to geologic investigations because the perspective afforded quickly focuses attention on prominent linears which are not obvious in larger scale imagery or on the ground. In our study of the Peninsular Ranges (Part II), it was found that linears of regional significance were immediately obvious on satellite images, but easily overlooked on conventional large-scale (1:20,000 to 1:63,000) aerial photographs.

Images at various scales, resolution and spectral response are superior to any single image; however, the single sensor most suitable for fault investigations, in our opinion, is the Skylab 190B camera. Using the study of a segment of the Garlock fault (Part III) as an example, a large number of topographic indicators of recent movement are resolved by the 190B camera with a spatial resolution of about 10-20 meters. Table II compares the ability to identify topographic indicators at resolutions of the Landsat or S-192 multispectral scanner, the 190A camera, and the 190B camera. This comparison is subjective and applies only to this specific study, because the scale of topographic indicators is variable and may differ significantly along other faults. Although the areal coverage of the 190B camera is

	Sensor and Spatial Resolution		
Topographic Feature	Landsat & S-192 80 meters	190A 30-40 meters	190B 10-20 meters
Scarp			X
Linear valley (in alluvium)			X
Offset channel			X
Linear ridge		X	X
Shutter ridge		X	X
Faceted ridge		X	X
Undrained depression	X	X	X

Table II - Recognition of topographic indicators of recent fault movement on a section of the Garlock fault (see Part III). An X indicates the feature can be recognized.

somewhat less than that of the 190A camera and Landsat, this is not a serious drawback. The combination of coverage and scale of the 190B camera is most desirable for regional fault studies and the recognition of topographic indicators of recent faulting.

Most of the indicators of faulting in the area are reflected in topographic rather than specular differences along or across faults. Thus, the multispectral capability of the 190A camera and the Landsat and S-192 multispectral scanners did not play a significant role in our fault investigations.

It must be emphasized that linears prominent on satellite images result from erosion along foliation and jointing, as well as faulting. The coincidental alignment of unrelated features may also give the appearance of faults. Detailed field investigations are required to establish the origin of any photo linears, and conclusions regarding the tectonic significance of linears whose origins have not been determined in the field are questionable. Table III summarizes our field investigations of twenty-five satellite photo linears not previously demonstrated to be faults.

The following paragraphs outline the approach, developed during this study, that proved to be the most efficient utilization of spacecraft imagery for fault investigations.

1. Latitude and longitude lines, corresponding to boundaries of U. S. Geological Survey topographic quadrangles (scales 1:24,000 and 1:62,500), to be used in field investigations are plotted on a plastic overlay of the satellite image. (Data given on coordinates of Landsat image corners were not sufficiently accurate.) The location of topographic map edges was determined by visual comparison of recognizable points common to maps and images.
2. Photo linears and other features of interest are plotted on the transparent plastic overlay of the satellite image.
3. Using the overlay plot of topographic map boundaries as a guide, the photo linears are plotted on the topographic maps. This was not difficult in most cases because the features were clearly reflected in the topography shown on the map. This and the following step were aided by using the intermediate scale (1:130,000) RB-57F and U-2 aircraft photographs.
4. Photo linears are studied on large-scale aerial photographs (scale 1:20,000 to 1:63,000), and more exact locations of photo linears

Feature	Reference
Previously unrecognized or unproven fault:	
Canyon City fault	Part II, p. 58-61
"L" fault west of Thing Valley	Part II, p. 48
San Diego River fault zone	Part II, p. 16-29
San Ysidro Creek fault	Part II, p. 10-15
Thing Valley fault	Part II, p. 39-48
Warren Canyon fault	Part II, p. 53
Probable fault - previously unrecognized or unproven:	
Otay Mountain linear	Part II, p. 56-58
Unnamed linear along southwest edge of Sand Hills	Part IV, p. 15-16
Unnamed linear, Mexicali Valley	Part IV, p. 17-18
Erosion along joints and/or foliation:	
Henderson Canyon linear	Part II, p. 52
Los Penasquitos Canyon linear	Part II, p. 33
Loveland Reservoir linear	Part II, p. 55
Pamo Valley linear (faulting along one segment)	Part II, p. 31-33
Pine Creek linear	Part II, p. 55
San Vicente Valley linear	Part II, p. 54
Sutherland Reservoir linear	Part II, p. 30-31
Sweetwater River linear	Part II, p. 36-39
Valle De Los Amigos linear	Part II, p. 31
Woodson Mountain linear	Part II, p. 54
Erosion along zone of weakness of unknown origin (not parallel to joints or foliation and faulting improbable):	
Himmel Canyon linear	Part II, p. 30
Witch Creek linear	Part II, p. 29-30
Erosion along zone of weakness of unknown origin (not parallel to joints or foliation, exposures not adequate to determine existence of fault):	
Hatfield Creek linear	Part II, p. 54-55
Previtt Canyon linear	Part II, p. 52-53
Apparent alignment of unconnected linear features:	
Porcupine Wash fault-Substation fault connection	Part IV, p. 20
Victory Pass fault-Pinkham Canyon connection	Part IV, p. 21

Table III - Summary of field evaluations of satellite photo linears described in this report.

are plotted on topographic maps. In many cases, photo linears seen in Landsat or Skylab images proved to be artifacts or the apparent alignment of unrelated features when studied on large-scale aerial photographs. Based on our experience, we conclude that the field investigation of features interpreted from satellite images should always be preceded by the study of large-scale aerial photographs.

5. Field investigations are planned and carried out subsequent to the study of existing geologic maps and large-scale aerial photographs, which facilitate selection of areas of good exposure and easy access.

Our field studies were focused on specific linears and other features interpreted from satellite imagery. Using this approach, remarkable exposures of breccia and fault gouge along previously unrecognized fault zones were discovered. Conventional areal geologic mapping would probably have revealed the same features but with considerably greater effort.

REFERENCES

Jennings, C. W., 1973, State of California, preliminary fault and geologic map, scale 1:750,000: Calif. Div. Mines and Geol., Preliminary Report 13.

Ziony, J. I., Wentworth, C. M., Buchanan-Banks, J. M. and Wagner, H. C., 1974, Preliminary map showing recency of fault movement in coastal Southern California: U. S. Geol. Survey, Misc. Inv. Map MF-585.

PART II

FAULTS AND LINEARS ON SKYLAB AND LANDSAT IMAGES OF PENINSULAR RANGES, SOUTHWESTERN CALIFORNIA

by

D. L. Lamar and P. M. Merifield

PREFACE

Linears in the Peninsular Ranges of southern California were studied as a portion of broader investigations to apply Skylab and Landsat images to the analysis of fault tectonics and earthquake hazards of southern California. Progress reports on a portion of the material in this report appear in CalESCO Technical Reports 74-1 (Merifield and Lamar, 1974) and 74-5 (Lamar and Merifield, 1974). Technical Report 74-1 was presented at the First International Conference on the New Basement Tectonics, Salt Lake City, Utah, June 1974, and is in press in the Proceedings Volume. A summary of the results was also presented at the NASA Earth Resources Survey Symposium, June 8-13, 1975, Houston, Texas, and appears in the Proceedings Volume (Merifield and Lamar, 1975a). This material was previously presented in preliminary form in CalESCO Technical Report 75-2 (Lamar and Merifield, 1975), and was summarized in Merifield and Lamar (1975b). It is planned to publish this material as a Special Report of the California Division of Mines and Geology.

CONTENTS

ILLUSTRATIONS

ABSTRACT

Prominent photo linears in basement terrane of the Peninsular Ranges, southwestern California, appear on Skylab and Landsat images. Among the most prominent are those formed by the active northwest trending Elsinore and San Jacinto fault zones. A distinctive photo linear appears along the northwestern segment of the Elsinore fault, where horizontal displacement of 30-40 kilometers (20-25 miles) has been inferred. However, to the southeast in the Vallecito Valley area, the fault is not well defined on the imagery, and horizontal displacements of only 1-3 kilometers (0.6-2 miles) have been reported, suggesting that distinctness of faults on the imagery may be related to the amount of horizontal slip. Field investigations, aided by study of large-scale aerial photos (NASA, Army Map Service, and U.S. Department of Agriculture), were accomplished to determine the geologic characteristics of other linears and the earthquake generating potential of previously unmapped faults. Several linears were found to mark previously unmapped faults, whereas others resulted from erosion along foliation, closely spaced joint sets, or the axes of shear (?) folds. These detailed field investigations proved necessary to distinguish linears due to faulting from those due to erosion along other zones of weakness. Previously unmapped faults fall into two distinct fault sets: one set trends northeast, and the other east-west. Right separation was demonstrated on two faults in the northeast set. The slip direction on the east-west trending faults has not been determined. The rakes of striations on slickensided shear surfaces associated with both sets suggest oblique movement. No indications of recent movement are present on these faults, which are restricted to pre-Tertiary basement rocks and are truncated by the active northwest trending faults as evident in both Skylab and Landsat images. The newly discovered faults may represent conjugate shears that formed in response to an earlier stress system involving west-southwest, east-northeast crustal shortening. The available data indicate that these faults are inactive and therefore are not likely to generate earthquakes. Skylab and Landsat images provided an efficient means of focusing on potential faults, and the synoptic view enabled regional fracture patterns and cross-cutting relations to be viewed in single images. Application of this imagery has contributed to a better understanding of the tectonic history and potential earthquake hazards in the area investigated.

INTRODUCTION

The Peninsular Ranges of southern California extend from the western edge of the continental borderland to the Salton Trough, and from the Transverse Ranges to the tip of Baja California. In southwestern California, the Peninsular Ranges province is composed principally of late Mesozoic plutonic rocks, which comprise the southern California batholith, and associated roof pendants of metamorphosed Paleozoic and Mesozoic rocks (Jahns, 1954a). Northwest trending faults, notably the San Jacinto and Elsinore faults (Figs. 1 and 2), are the dominant structural features of the Peninsular Ranges. Recently acquired small-scale images from Skylab (190A camera, scale: 1/700,000, 23 x 23 cm. or 9 x 9 inch format; 190B camera, scale: 1/500,000, 23 x 23 cm. or 9 x 9 inch format) and Landsat (scale: 1/1,000,000, 18 x 18 cm. or 7 x 7 inch format), as well as larger scale color aerial photos from RB-57 and U-2 aircraft (scale: 1/130,000, 23 x 23 cm. or 9 x 9 inch format), have provided a new look at this region. Lowman (1969) pointed out that unmapped northeast trending linear features, primarily straight valleys, are prominent on Gemini and Apollo photographs of the Peninsular Ranges of southwestern California. These features and the San Jacinto, Elsinore and other northwest trending faults are apparent in Skylab (Fig. 3) and Landsat (Figs. 4 and 5) images of the Peninsular Ranges. A number of west-northwest and north-south linears are also visible. Some of these linears have been previously mapped as faults, but many others have not. Linears apparent on the satellite images are identified on Fig. 2 and on detailed maps and enlarged images accompanying descriptions of individual features.

Using the perspective provided by small-scale imagery from Skylab and Landsat, we focused attention on conspicuous linears which were heretofore unmapped because they are not obvious in larger scale photography or on the ground. Aided by large-scale aerial photos, field investigations were accomplished to determine the nature of the linears not explained by previous detailed geologic mapping. Aerial photographs (23 x 23 cm. or 9 x 9 inch format) from the following sources were utilized in the investigation: NASA, RB-57 and U-2, scale: 1/130,000; Army Map Service, (AMS) scale: 1/63,000; U.S. Department of Agriculture (USDA), scale: 1/20,000; San Diego County, scale: 1/24,000, natural color. Specific photos which illustrate particular features are referred to or included in the descriptions of individual linears. Emphasis was placed on

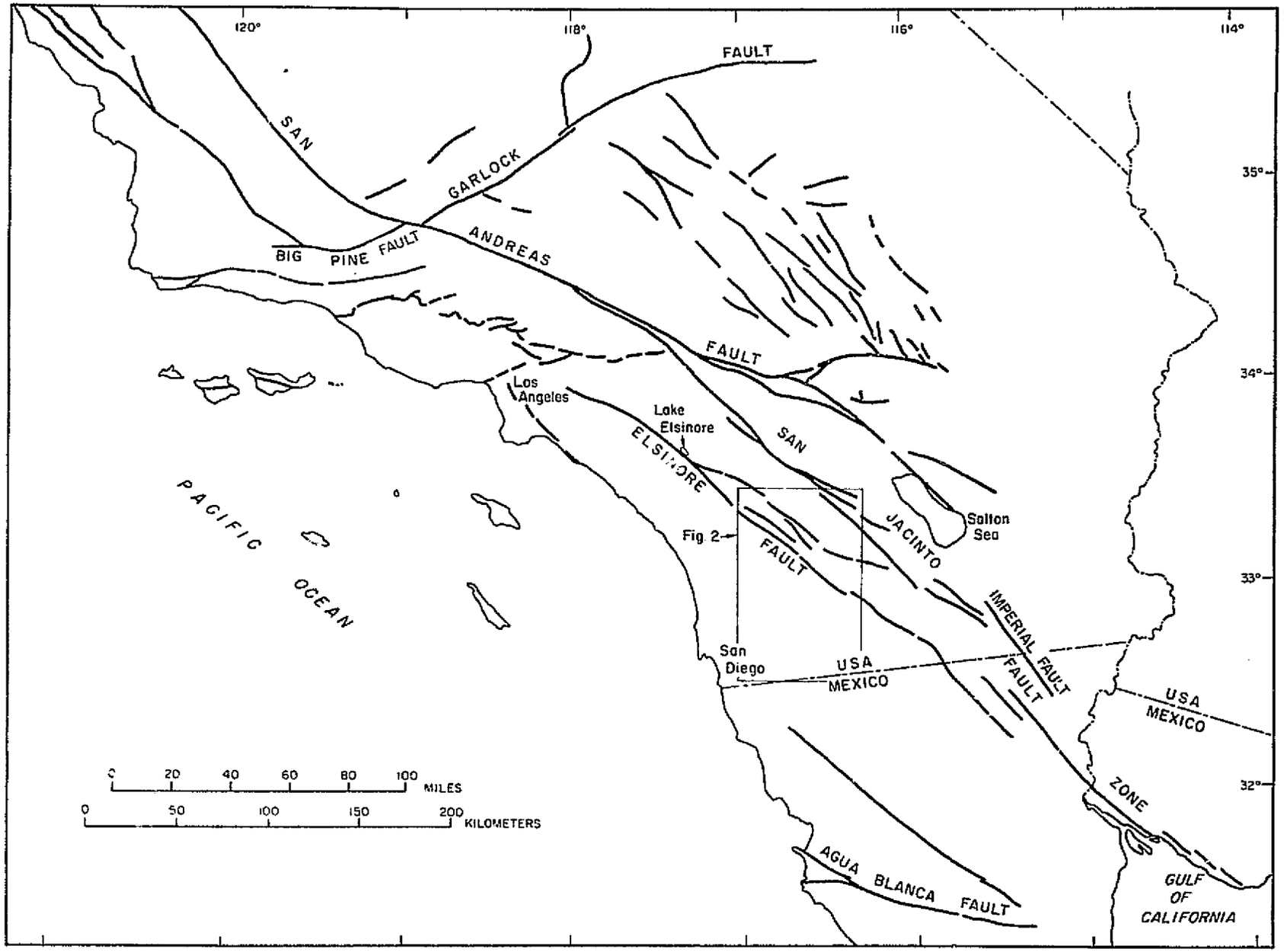

Fig. 1 - Index map showing major faults and area covered by generalized fault and linear map (Fig. 2). Redrawn from Proctor (1973).

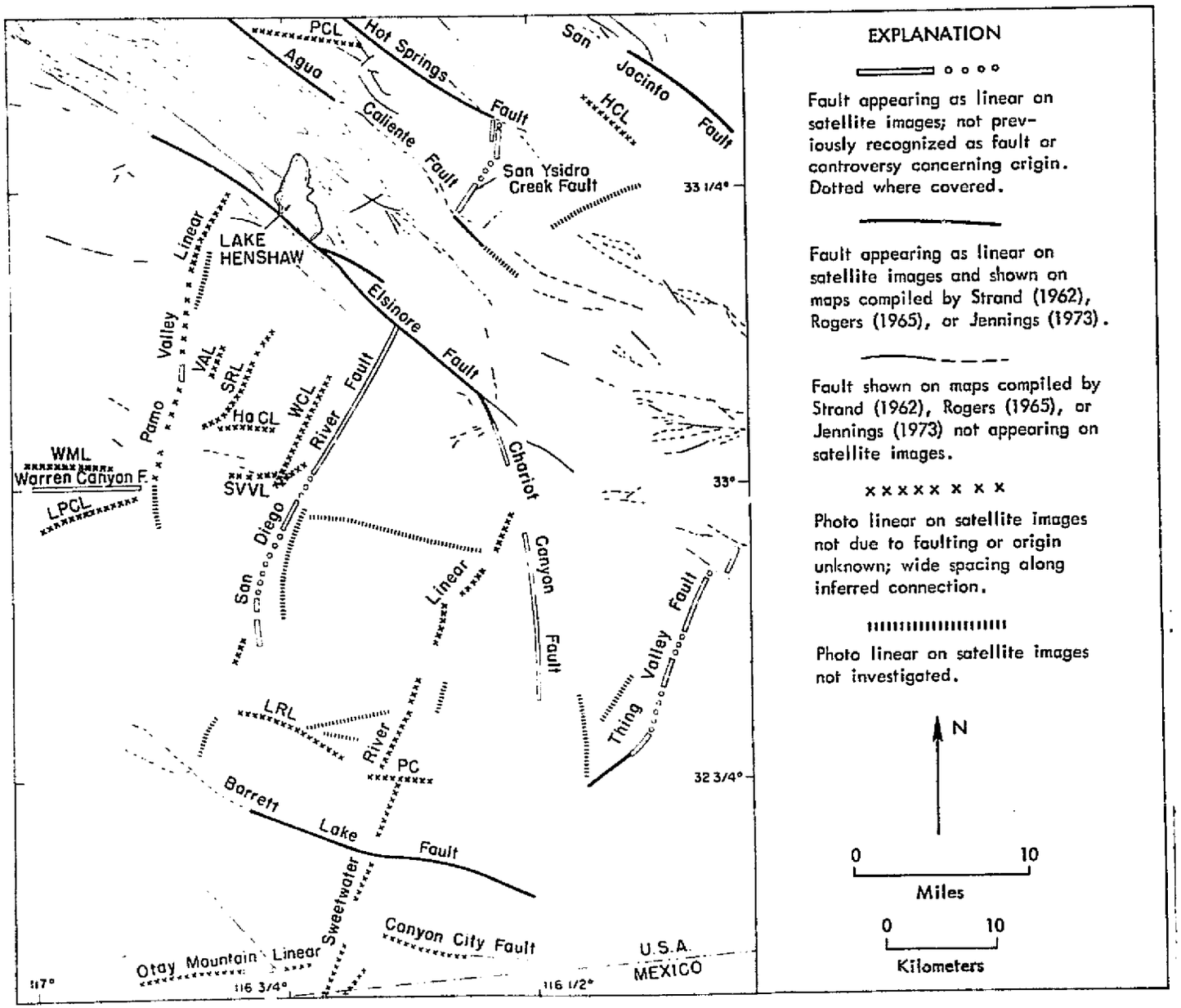

Fig. 2 - Faults and linears recognized on Skylab and Landsat images and previously mapped faults, southwestern California. Abbreviations: HaCL: Hatfield Creek linear; HCL: Henderson Canyon linear; LPCL: Los Penasquitos Canyon linear; LRL: Loveland Reservoir linear; PC: Pine Creek linear; PCL: Previtt Canyon linear; SRL: Sutherland Reservoir linear; SVVL: San Vicente Valley linear; VAL: Valle De Los Amigos linear, WCL: Witch Creek linear; WML: Woodson Mountain linear. See Fig. 1 for area covered.

Fig. 3 - Major faults and linears, Peninsular Ranges, southwestern California. Portion of Skylab 3, 190B camera, Roll 87, Frame 111 (original in color infrared). Abbreviations: BLF: Barrett Lake fault; CCF: Chariot Canyon fault; CaCF: Canyon City fault; EF: Elsinore fault; EVF: Earthquake Valley fault; HCL: Henderson Canyon linear; GV: Green Valley; OML: Otay Mountain linear; PVL: Pamo Valley linear; SDR: San Diego River fault zone; SMV: Santa Maria Valley; SR: Sweetwater River; SRL: Sweetwater River linear; SYC: San Ysidro Creek fault; TVF: Thing Valley fault; WCF: Warren Canyon fault.

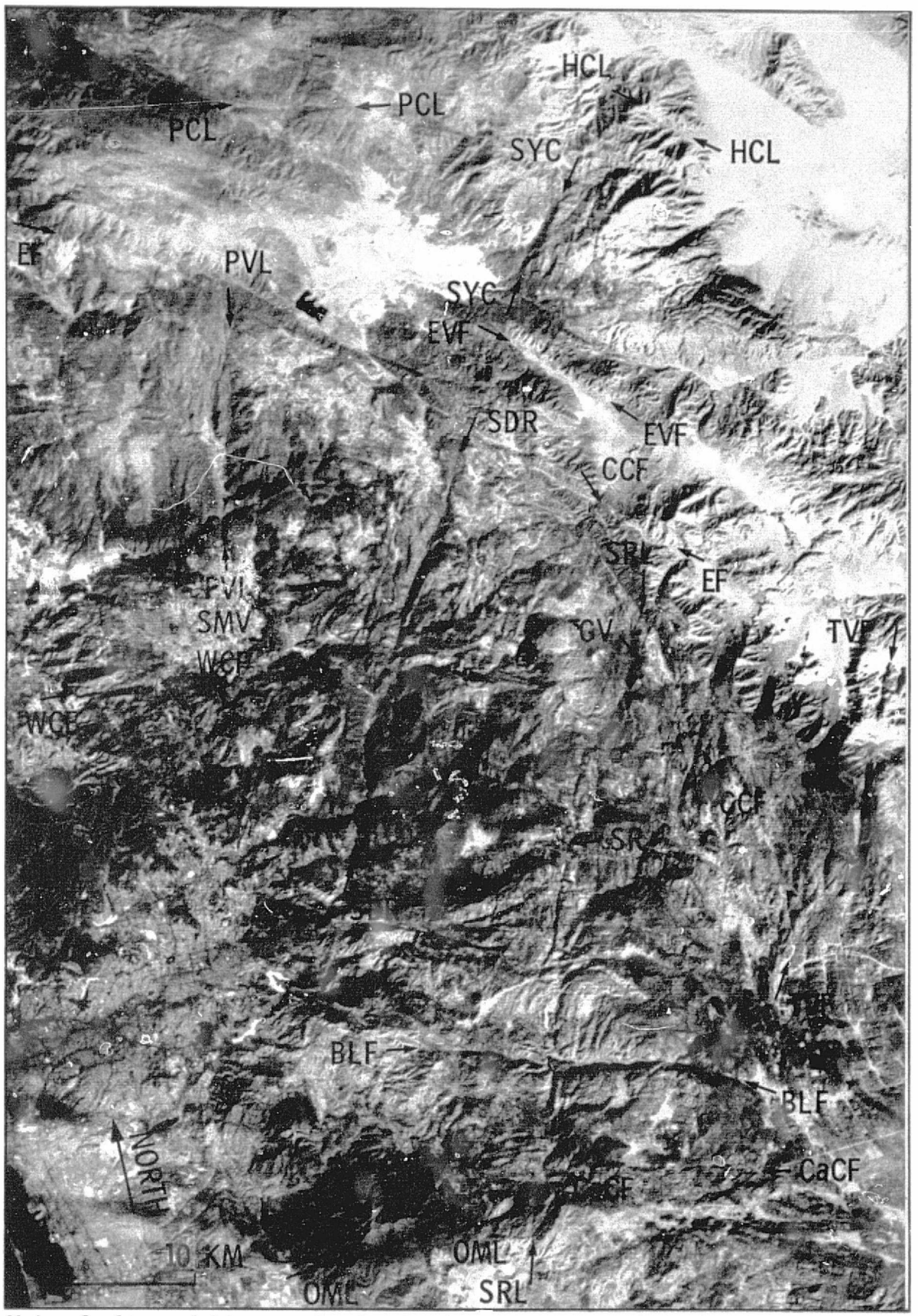

Fig. 4 - Major faults and linears, Peninsular Ranges, southwestern California. Portion of Landsat image 1106-17504. Abbreviations: BLF: Barrett Lake fault; CCF: Chariot Canyon fault; CaCF: Canyon City fault; EF: Elsinore fault; EVF: Earthquake Valley fault; HCL: Henderson Canyon linear; GV: Green Valley; OML: Otay Mountain linear; PCL: Previtt Canyon linear; PVL: Pamo Valley linear; SDR: San Diego River fault zone; SMV: Santa Maria Valley; SR: Sweetwater River; SRL: Sweetwater River linear; SYC: San Ysidro Creek fault; TVF: Thing Valley fault; WCF: Warren Canyon fault.

Fig. 5 - Major faults and linears, north central Peninsular Ranges, southwestern California. Portion of Landsat image 1125-17563. Abbreviations: ATM: Agua Tibia Mountains; EF: Elsinore fault; LE: Lake Elsinore; LH: Lake Henshaw; MP: Mount Palomar; PCL: Previtt Canyon linear; PVL: Pamo Valley linear; SDR: San Diego River fault zone; SMV: Santa Maria Valley; SYC: San Ysidro Creek fault; WCF: Warren Canyon fault.

identification of previously unmapped faults and assessment of their earthquake risk. Such information is applicable to land-use planning and to the siting of man-made structures. This paper summarizes the results of the field studies and discusses the appearance of faults on the satellite images.

Several of the linears have been identified as previously unrecognized faults as a result of our investigations. One or more of the following fault criteria were used for identification: (1) a well-developed cataclastic (breccia) zone, (2) slickensided shear surfaces or clay gouge zones, with the attitude of the shear surfaces or gouge zones parallel to the linear, and (3) displaced or terminated lithologic contacts and structures. Field investigation of the photo linears in southwestern California is hampered by a dense growth of chaparral which denies access to large areas. Moreover, zones of mixed rocks or gradational contacts are not easily proven to be displaced. Only in rare cases where abrupt contacts cross at a relatively high angle to the linear, or where a well-developed fault zone is exposed, can the presence or absence of a fault be determined. Persistent dikes are particularly useful in this regard but unfortunately are uncommon. Field studies revealed that a large percentage of the previously unmapped linears identified on the satellite photography are due to erosion along other planes of weakness such as joints and foliation; the origin of some linears could not be determined because of inadequate exposures.

Maps of Merriam (1946, 1955, 1958), Larson (1948), Everhard (1951), Gastil and Bushee (1961), Strand (1962), Weber (1963), Rogers (1965), Gastil et al (1971), and Jennings (1973) were invaluable. Most of the previous mapping was at scales of 1/62,500 or smaller, and some earlier studies were without the benefit of aerial photography (Richard Merriam, personal communication, 1975). Consequently, it is not surprising that some of the faults recognized in our investigation are not shown on existing geologic maps. Descriptions of the individual features studied during our investigation are presented in the following sections. Emphasis is placed on the geologic structure; petrologic descriptions are limited to rocks in, and adjacent to, photo linears. More complete descriptions of individual rock units may be found in the references. Fig. 6 is an index map which shows the outlines of the detailed geologic maps and enlarged Skylab and Landsat images accompanying the detailed descriptions.

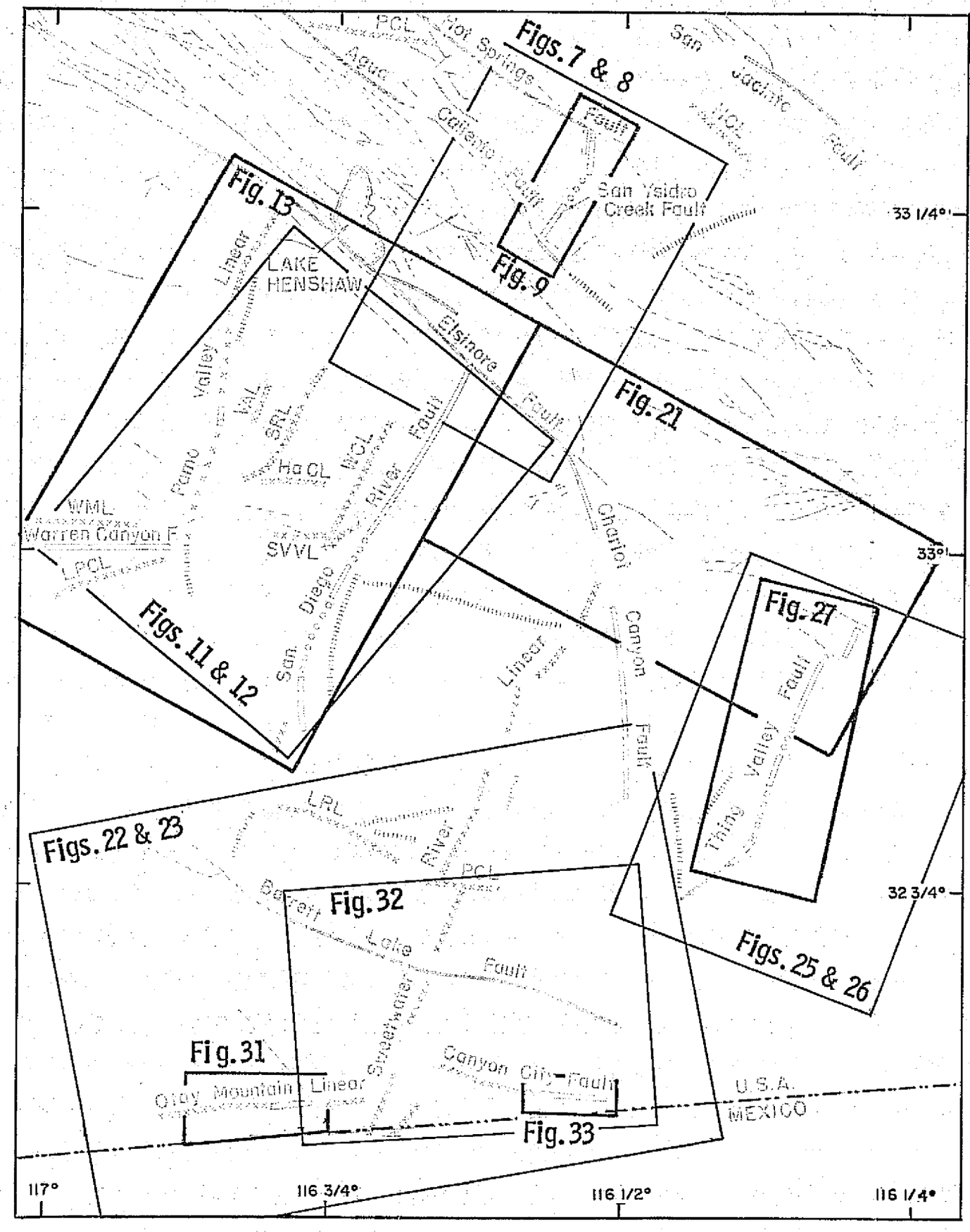

Fig. 6 - Index map showing outline of detailed maps (heavy lines) and enlarged satellite and RB-57 images (thin lines) of Peninsular Ranges, southwestern California.

NORTHEAST TO NORTH-SOUTH TRENDING FAULTS AND LINEARS

Several northeast to north-south trending linears are prominent on Skylab and Landsat images. The structural significance of some of these features has been a matter of controversy (Lowman, 1969) and little previous work has been done to determine their origin. Much of our field work was therefore directed to a study of these features.

San Ysidro Creek Fault

A segment of San Ysidro Creek and a stream canyon to the south form a prominent 7-kilometer (4-mile) long north-northeast trending linear visible on space imagery (Figs. 7 and 8). Fig. 9 is a geologic map of the San Ysidro Creek area. South of latitude 33°15', the area was mapped by Merriam (1958) and Scheliga (1963), and the entire area is shown on small-scale maps prepared by Weber (1963) and Rogers (1965). The northwest portion of the area is underlain by Lakeview Mountain Tonalite (Cretaceous), which is characterized by prominent, near-vertical east-west jointing. Julian Schist (Triassic) exposed to the southeast consists of biotite schist interlayered with gneiss and hornfels. Foliation in the metamorphic rocks generally trends north-northeast, parallel to the intrusive contact and the San Ysidro Creek linear. Locally, however, the foliation is undulatory and not parallel to the linear.

The steep slopes and dense brush limit access to areas underlain by bedrock. Alluvium in the stream valleys, as well as terrace deposits and thick soil in the southern portion of the area, further obscures the underlying structure. The faults shown on Fig. 9 appear as distinct linears on large-scale air photos (USDA, 1953, scale: 1/20,000; photo numbers: AXN-4N-162 to 164, AXN-11M-46 to 49, AXN-11M-128 to 132), but the fault zone is exposed only in roadcuts at the location of the dip symbol. A zone of crushed and sheared gouge up to 7 meters (23 feet) wide, with striations on shear surfaces, is present. The following attitudes and rakes of striations on shear surfaces were noted:

	Strike	Dip	Rake
	N3°W	85°W	1°S
	N4°W	62°E	3°S
	N50°E	90°	7°S
	N5°W	74°E	20°S
	N26°E	74°E	None
Average	N13°E	79°E	8°S

Fig. 7 - San Ysidro Creek and north end of San Diego River. Portion of Skylab 3, 190B camera, Roll 87, Frame 111 (original in color infrared). Abbreviations: EF: Elsinore fault; EVF; Earthquake Valley fault; HSF: Hot Springs fault; SYC: San Ysidro Creek; SDR: San Diego River.

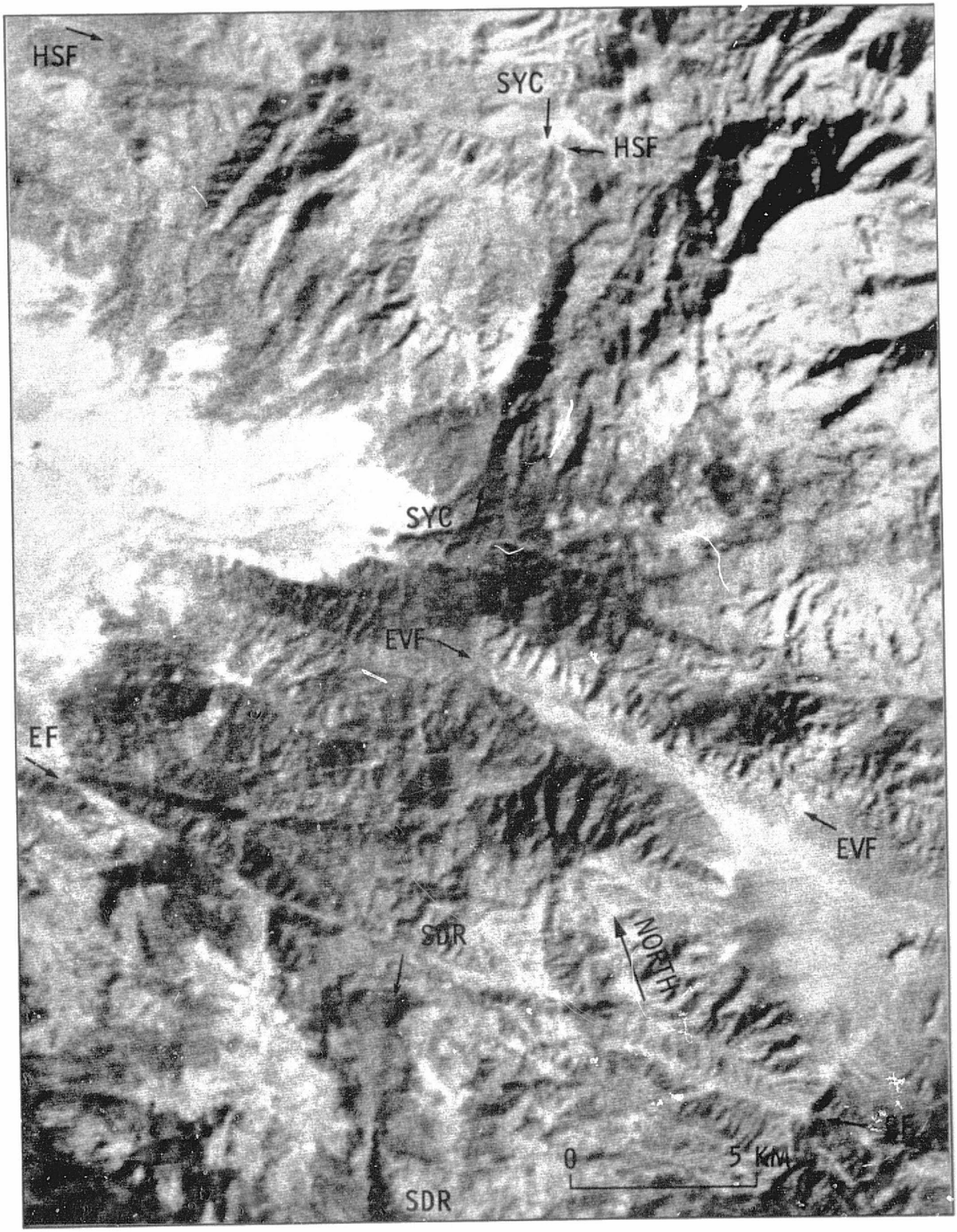

Fig. 8 - San Ysidro Creek and north end of San Diego River. Portion of Landsat image 1106-17504. Abbreviations: EF: Elsinore fault; EVF: Earthquake Valley fault; HSF: Hot Springs fault; SYC: San Ysidro Creek; SDR: San Diego River.

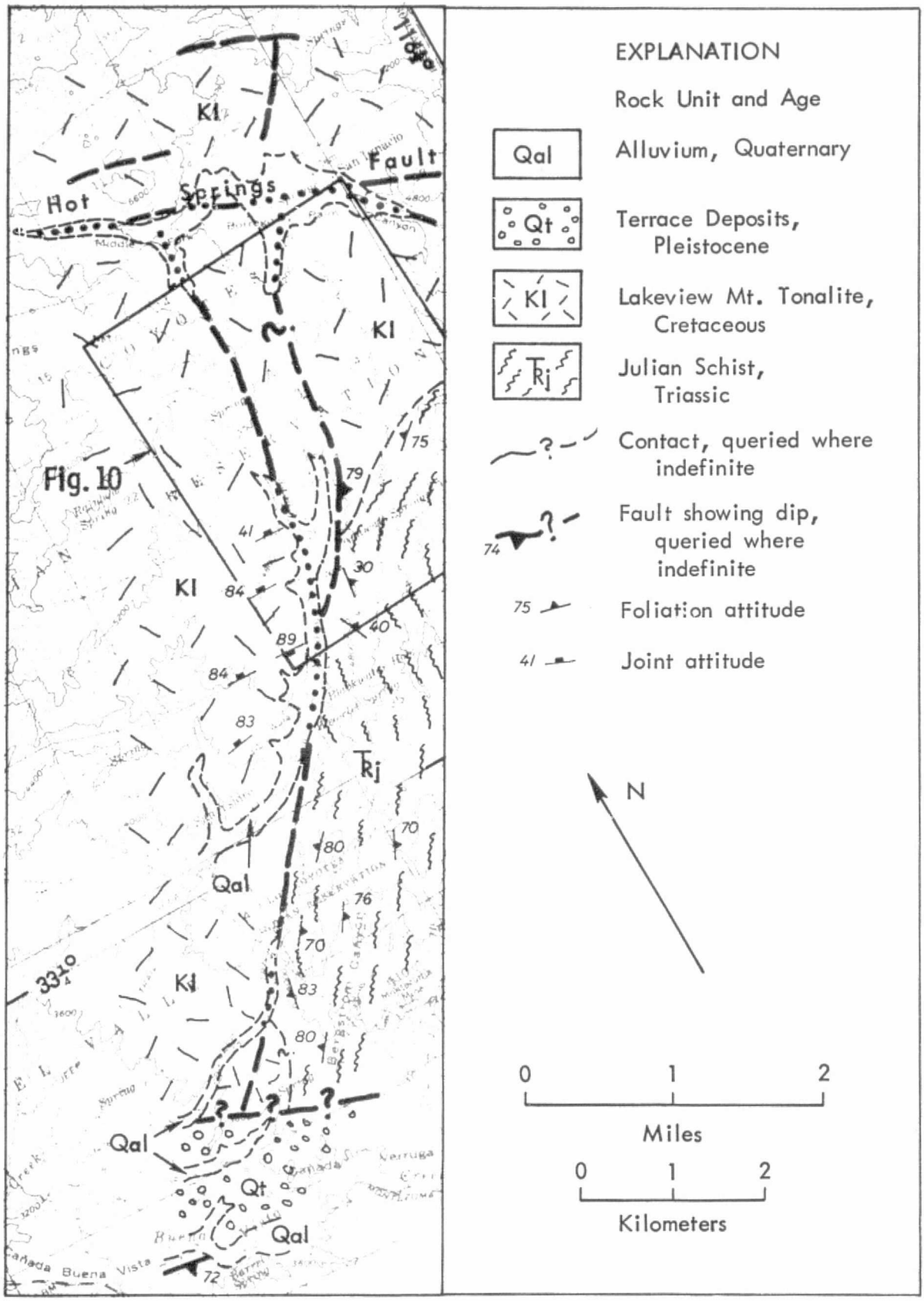

Fig. 9 - Geologic map of the San Ysidro Creek area. Hot Springs fault from Weber (1963); fault truncating south end of San Ysidro Creek fault from Merriam (1958) and Scheliga (1963). Topography from U.S. Geological Survey Santa Ysabel and Warner Springs Quadrangles. See Fig.6 for area covered.

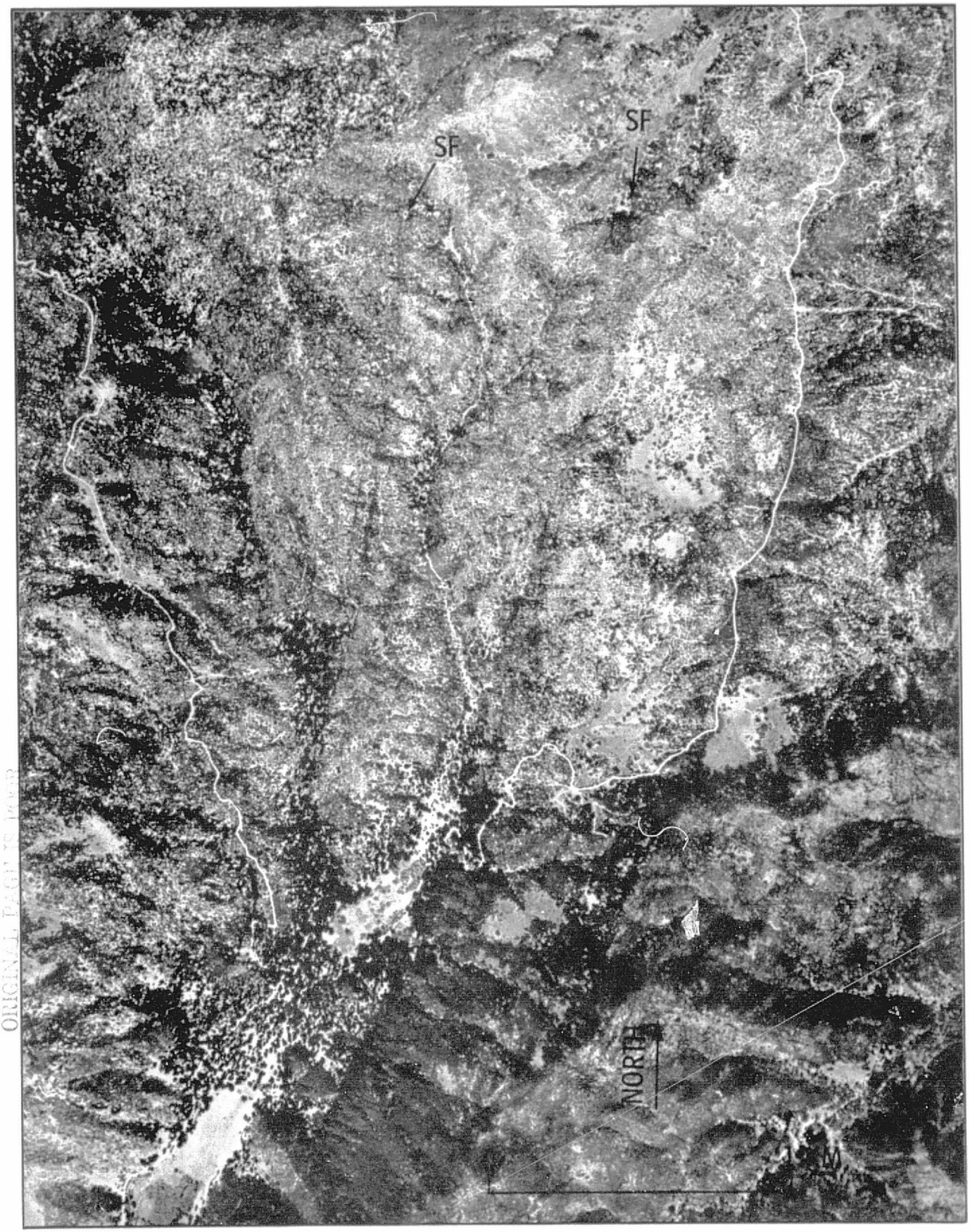

Fig. 10 - Portion of U.S. Department of Agriculture aerial photo number AXN-11M-130, April 24, 1953, showing branches of San Ysidro Creek fault (north ends labeled SF). See Fig. 9 for area covered and features identified.

The average value of N13°E lies between the N8°E trend of the linears branching to the north and the N37°E trend of the principal linear to the southwest. It is inferred from this exposure that the linears extending to the northeast and southwest on the air photos are faults. The striations on shear surfaces suggest predominantly horizontal movement. No data are available to determine the sense and cumulative displacement.

In the northern portion of the area, this probable fault splits into two branches which can be traced on large-scale air photos (Fig. 10 and USDA photo numbers AXN-11M-129 to 132) through massive tonalite to the Middle Fork of Borrego Palm Canyon. From our analysis of the air photos, we conclude that the San Ysidro fault abuts the northwest trending Hot Springs fault in the Middle Fork of Borrego Palm Canyon shown by Weber (1963) and Rogers (1965). Over most of its trace to the south, the fault parallels the average foliation in Julian Schist and may coincide with the intrusive contact. South of the roadcut fault exposure, a prominent line of denser vegetation can be traced for 1 kilometer (.6 mile) along the southeast side of San Ysidro Valley (Fig. 10). Additional alignments of straight canyon segments and intervening saddles to the south are believed to be a further extension of the San Ysidro Creek fault.

Structural relations near the south end of the San Ysidro Creek fault are obscured by thick brush and soil. The fault contact between basement rock and terrace deposits is based on mapping by Merriam (1958) and Scheliga (1963). Exposures within the area studied in the present investigation are not sufficient to verify the existence of this segment of the fault. One kilometer (.6 mile) farther southwest, Weber (1963) shows a northwest trending fault along the course of Buena Vista Creek. A fault zone with an attitude of N83°W, 72°S is exposed in the roadcut directly southwest of the San Ysidro Creek fault along the south side of Buena Vista Creek, and this may be a branch of the fault mapped by Weber (1963). Our study of large-scale air photos (USDA, photo numbers AXN-4M-162 and 163) reveals no evidence of a northeast trending fault south of Buena Vista Creek, and we conclude that the south end of the San Ysidro Creek fault is truncated by a northwest trending fault.

San Diego River Fault Zone

The northeast trending San Diego River Valley forms a prominent 30-kilometer (20-mile) long linear on space photography (Figs. 11 and 12). Although the San Diego River linear and the San Ysidro Creek fault are approximately aligned, enlarged satellite imagery (Figs. 7 and 8) as well as larger scale air photographs (NASA, RB-57, Mission 164, April 1971, scale: 1/130,000; photo numbers 49-3929 and 49-3954; USDA, 1953, scale: 1/20,000, photo numbers AXN-4M-162 and 163 at south end of San Ysidro Creek fault, AXN-7M-36 and 37 at north end of San Diego River fault) clearly show that these features are separated by 10 kilometers (6 miles) and do not connect. Some previous maps (Sauer, 1929; Miller, 1935; California Department of Water Resources, 1967; Jennings, 1973) show a fault or inferred fault along the San Diego River, while others (Everhart, 1951; Merriam, 1958; Strand, 1962; Rogers, 1965; Fitzurka, 1968) do not. Sauer (1929) and Miller (1935) appear to base the existence of a fault on the straight trend of the valley and differences in elevation between the relatively flat to gently rolling bedrock surfaces on opposite sides of the valley. Julian Mesa on the southeast side of the San Diego River lies about 150 meters (500 feet) higher than the northwest side (Sauer, 1929). None of the previous maps or reports indicating a fault describe any direct field observations of fault zone exposures or offset rock units. Everhart (1951) and Merriam (1958) suggest that prominent straight valleys in the region, such as the San Diego River Valley, have formed primarily as a result of erosion along joints or foliation. Merriam (1958, Fig. 2) shows the regional northwest trending foliation curving into a northeast trend, parallel to the San Diego River. Our mapping (Figs. 13, 14 and 15) suggests a similar change in trend of foliation along the San Diego River Valley.

Because the San Diego River Valley linear is one of the most prominent features on satellite photography of the Peninsular Ranges, a detailed field investigation was made to resolve disagreement concerning its origin. Fig. 13 is a generalized map showing the entire feature and other faults and linears to the north and west. In most cases, the joint and foliation directions shown on Fig. 13 are the average of several which were originally plotted on 1/24,000 scale U.S. Geological Survey Quadrangles. Descriptions of the petrology and maps showing the distribution of rock units along most of the San Diego River

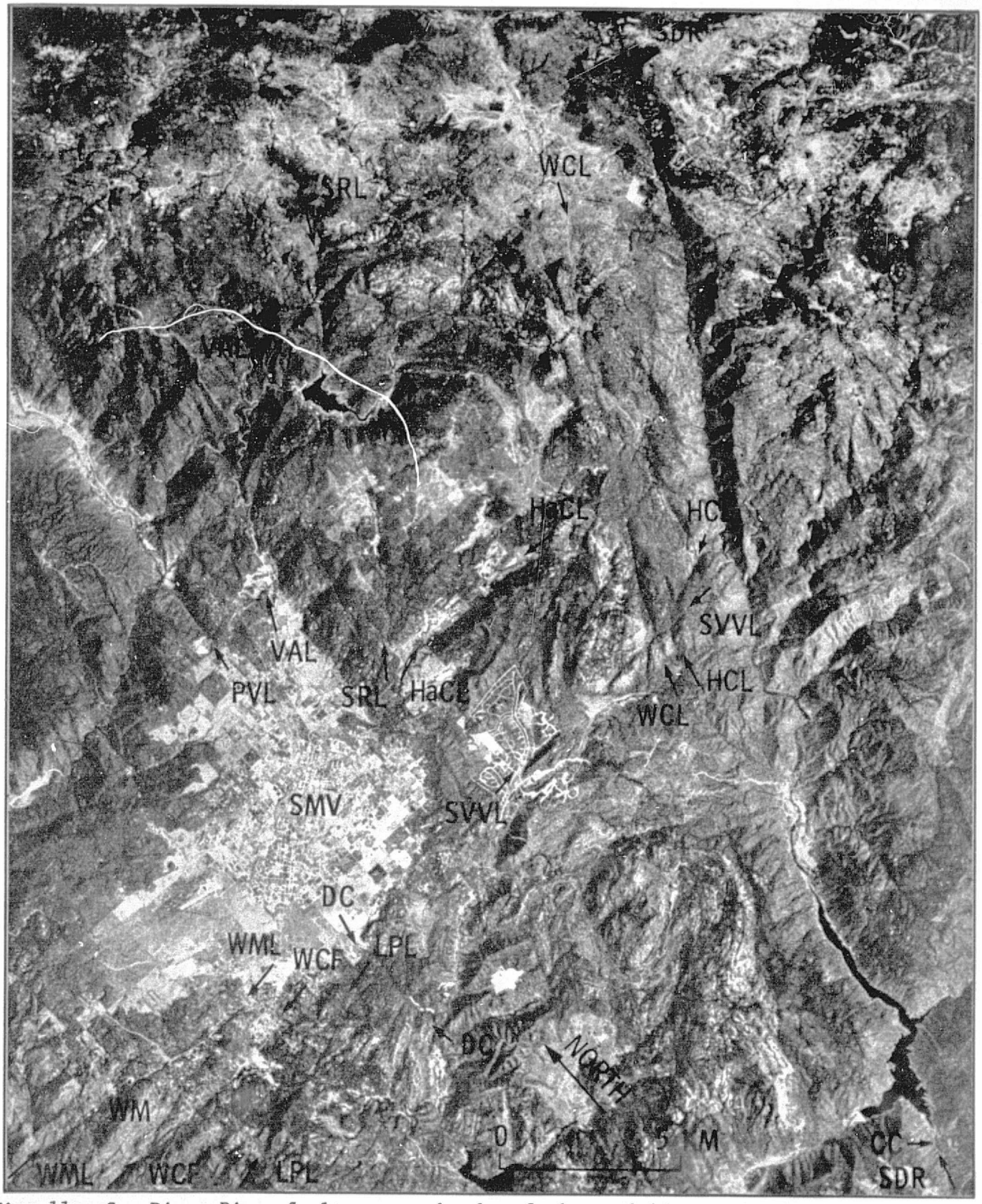

Fig. 11 - San Diego River fault zone and other faults and linears in the Santa Maria Valley area. Portion of Skylab 3, 190B camera, Roll 87, Frame 111 (original in color infrared). Abbreviations: CC: Chocolate Canyon; DC: Daney Canyon; HaCL: Hatfield Creek linear; HCL: Himmel Canyon linear; LPL: Los Penasquitos Canyon linear; PVL: Pamo Valley linear; SDR: San Diego River fault zone; SMV: Santa Maria Valley; SRL: Sutherland Reservoir linear; SVVL: San Vicente Valley linear; VAL: Valle De Los Amigos linear; WCF: Warren Canyon fault; WCL: Witch Creek linear; WM: Woodson Mountain; WML: Woodson Mountain linear.

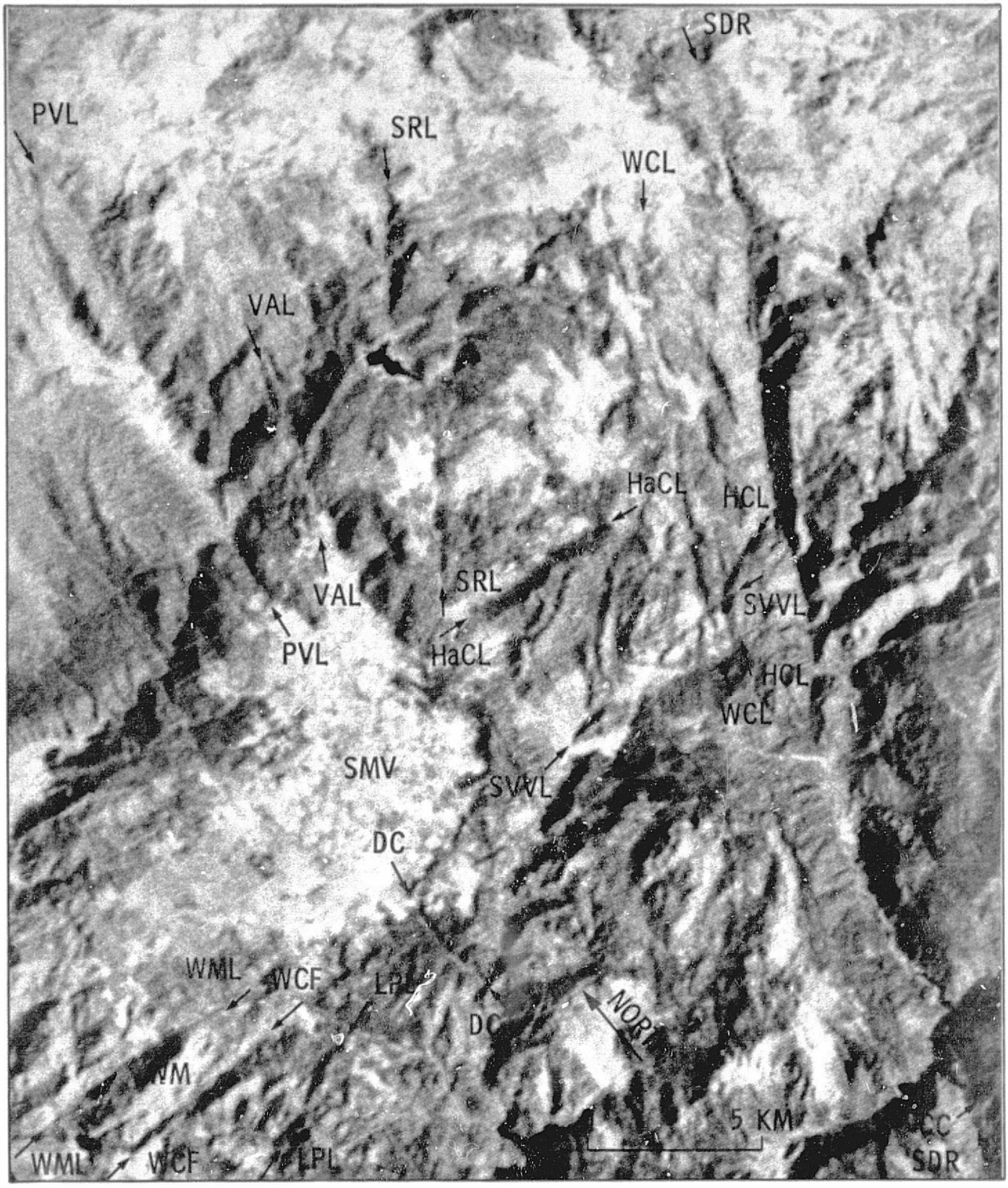

Fig. 12 - San Diego River fault zone and other faults and linears in the Santa Maria Valley area. Portion of Landsat image 1106-17504. Abbreviations: CC: Chocolate Canyon; DC: Daney Canyon; HaCL: Hatfield Creek Linear; HCL: Himmel Canyon linear; LPL: Los Penasquitos Canyon linear; PVL: Pamo Valley linear; SDR: San Diego River fault zone; SMV: Santa Maria Valley; SRL: Sutherland Reservoir linear; SVVL: San Vicente Valley linear; VAL: Valle De Los Amigos linear; WCF: Warren Canyon fault; WCL: Witch Creek linear; WM: Woodson Mountain; WML: Woodson Mountain linear.

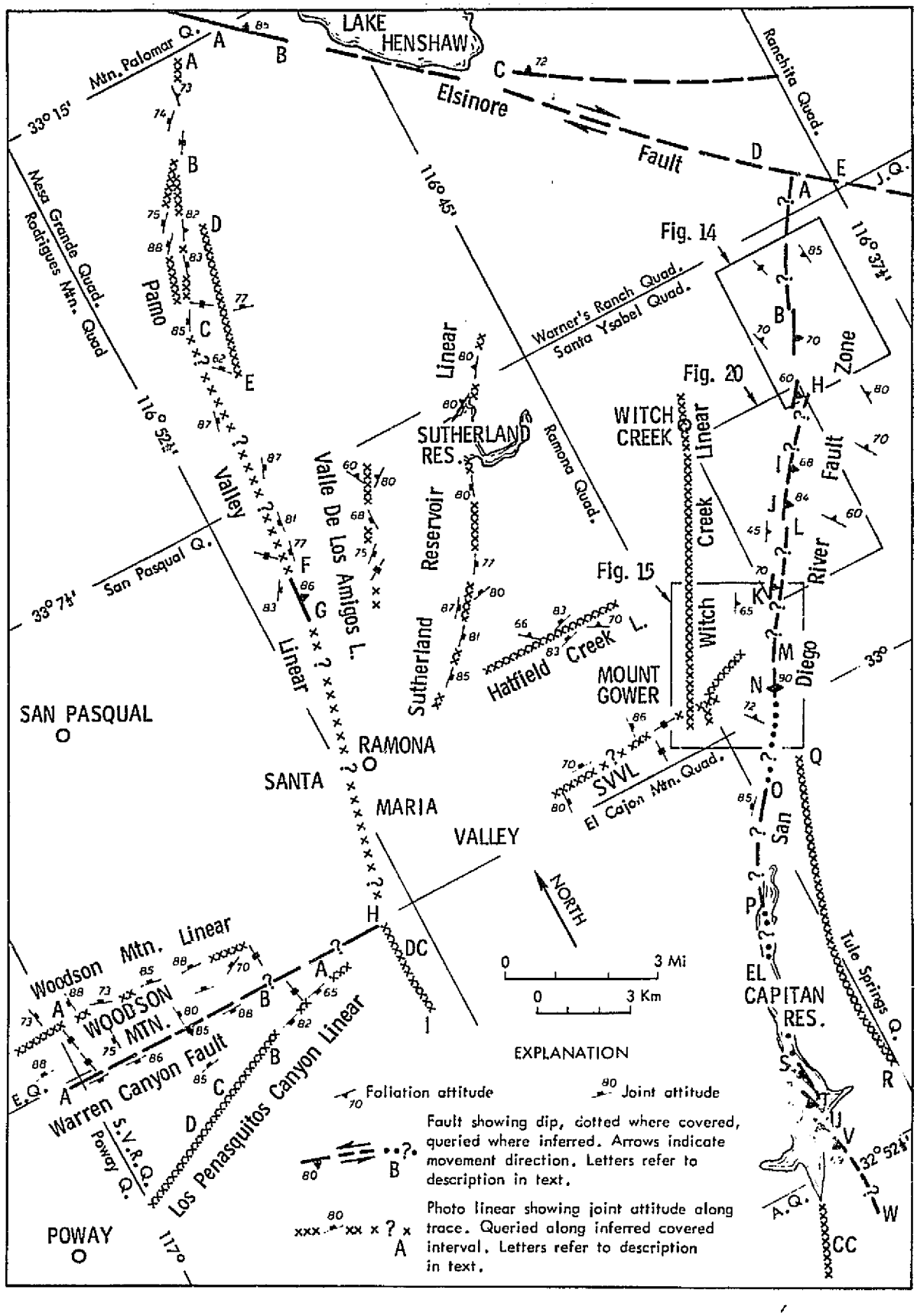

Fig. 13 - Map showing faults and linears in the Santa Maria Valley area. Joint and foliation attitudes are usually the average of several which were originally plotted on 1:24,000 scale U.S. Geological Survey Quadrangles. Abbreviations: AQ: Alpine Quad.; CC: Chocolate Canyon; DC: Daney Canyon; EQ: Escondido Quad.; JQ: Julian Quad.; SVRQ: San Vicente Reservoir Quad.; SVVL: San Vicente Valley linear. See Fig. 6 for area covered.

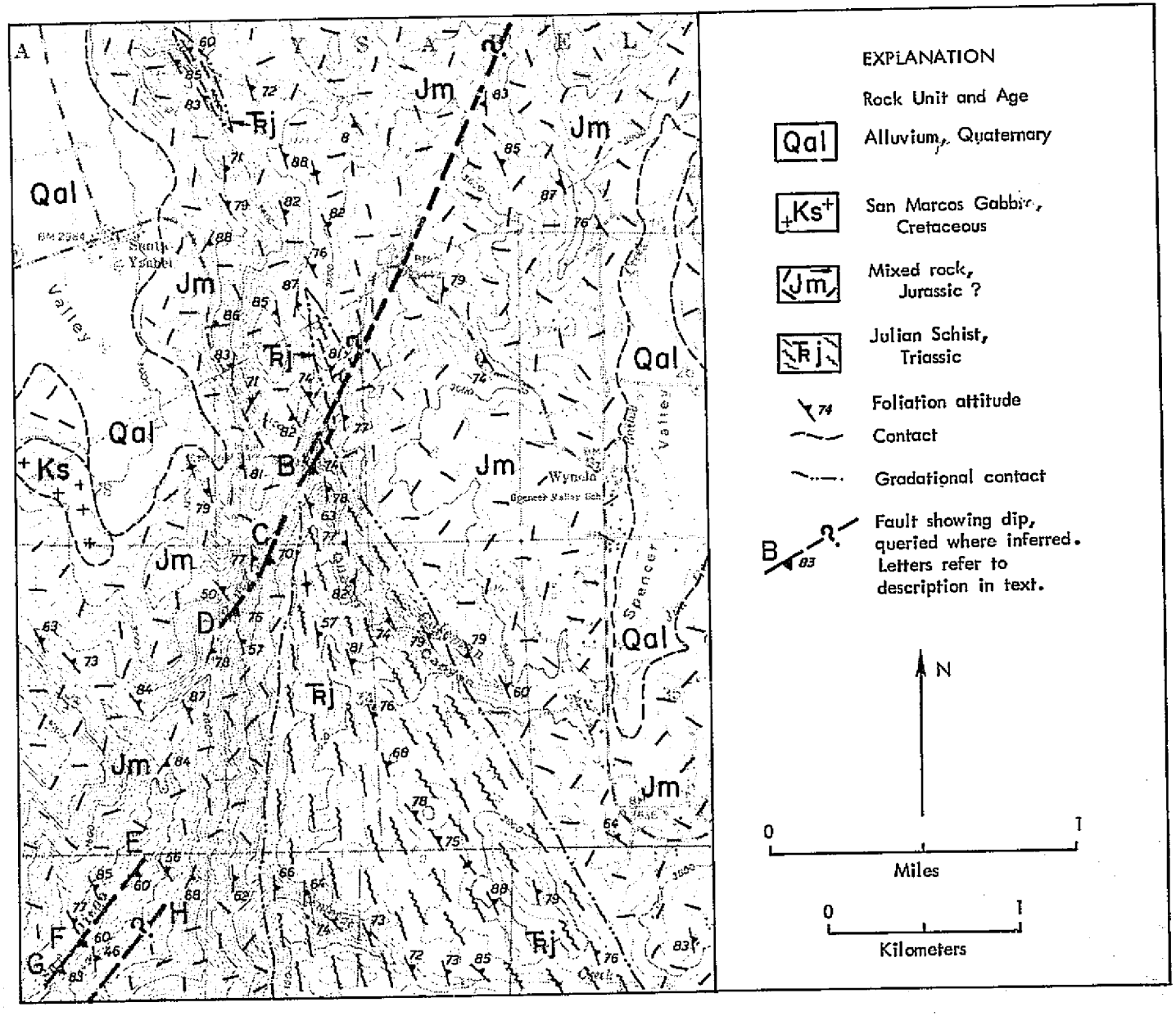

Fig. 14 - Geologic map of portion of north end of San Diego River fault zone. Topography from U.S. Geological Survey Santa Ysabel Quadrangle. See Fig. 13 for area covered.

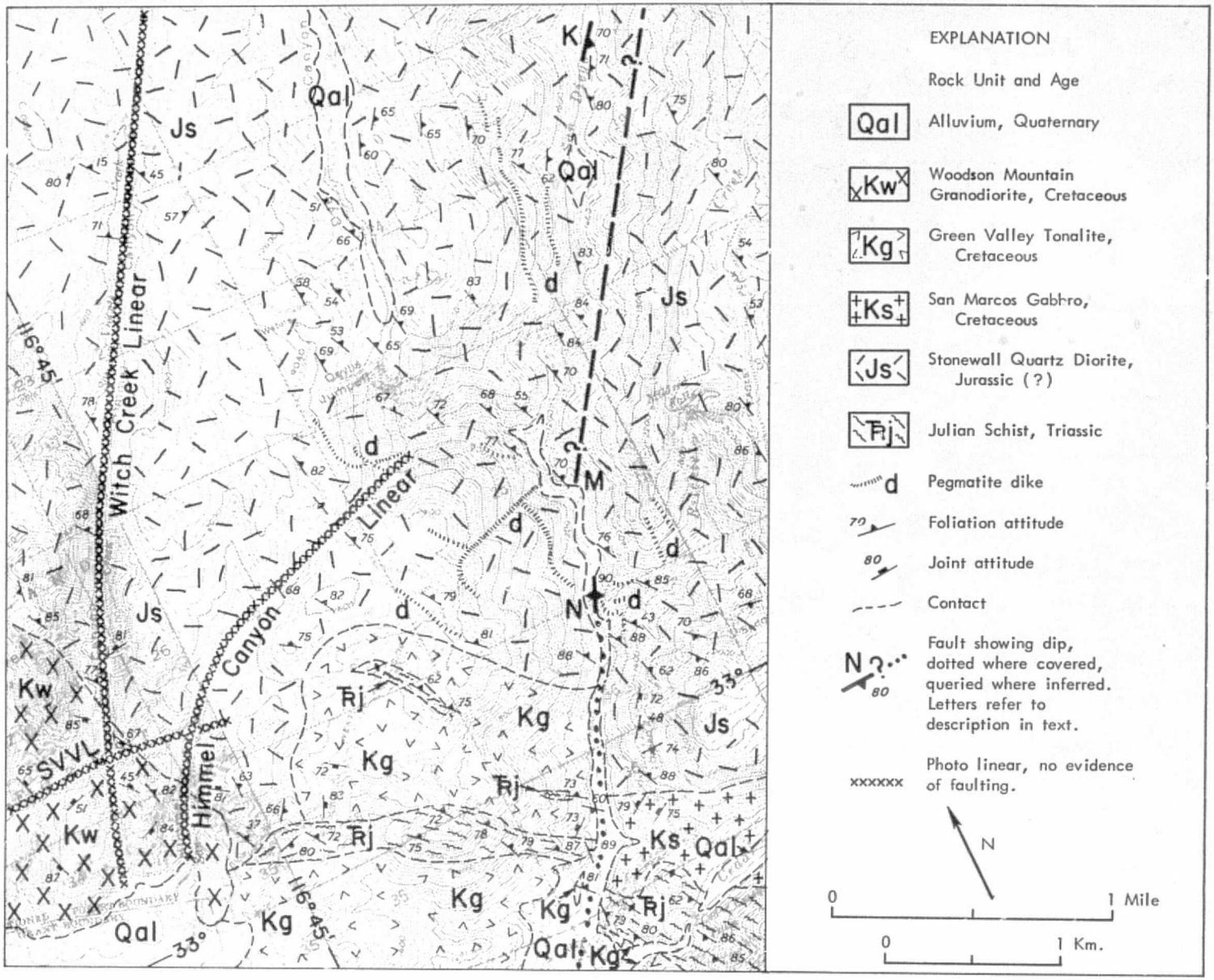

Fig. 15 - Geologic map of central portion San Diego River fault zone. Topography from U.S. Geological Survey Quadrangles. See Fig. 13 for area covered and quadrangle names. Abbreviation: SVVL: San Vicente Valley linear.

have been prepared by Everhart (1951), Merriam (1958), Gastil and Bushee (1961), Strand (1962), Weber (1963), Rogers (1965) and Fitzurka (1968). The oldest rock unit exposed along the San Diego River is the Julian Schist (Triassic) which consists of quartzite, quartz-mica schist and gneiss. Stonewall Quartz Diorite (Jurassic) and mixed rocks consisting of intimately mixed Stonewall Quartz Diorite and Julian Schist are the next youngest rock units exposed. Bedrock exposed in the area covered by Fig. 14 consists of mixed rocks and a small area of San Marcos Gabbro; gradational contacts have been mapped between areas underlain predominantly by gneissic Stonewall Quartz Diorite and Julian Schist. In the area covered by Fig. 15, Julian Schist and Stonewall Quartz Diorite are intruded by massive plutonic rocks of Cretaceous age designated as the San Marcos Gabbro (Cuyamaca Gabbro of Everhart, 1951), Green Valley Tonalite, and Woodson Mountain Granodiorite. Light-colored pegmatite dikes intruding Stonewall Quartz Diorite were also mapped in the area covered by Fig. 15.

Zones of altered rocks with smooth fracture surfaces parallel to the axis of the canyon are exposed at several locations along the San Diego River. Because the texture is usually not clearly revealed in hand specimen, several samples were studied in thin section. Figs. 16 and 17 are representative photomicrographs of fault breccia exposed along the San Diego River fault zone. Fracturing of mineral grains, inferred to be caused by displacement along the fracture surfaces, was observed in some thin sections. Attitudes of the fracture surfaces and other descriptive remarks are listed in Table 1. These features are described in sequence from north to south, and letters on the maps (Figs. 13, 14 and 15) are keyed to the descriptions.

Topographic maps and large-scale air photographs (USDA, 1953, photo numbers AXN-7M-36 to 40) show a subtle alignment of saddles and straight canyon segments between point A (Fig. 13) next to the Elsinore fault, and point B (Fig. 14). There are no exposures of bedrock along this linear; however, the southeast end of a body of Julian Schist appears to terminate abruptly against the mixed rocks along this trend (Fig. 14). A shear zone dipping 75°SE within Julian Schist is exposed close to the southeast end of the photo linear at point B. The distribution of bedrock indicates the shear zone at point B and the A-B photo linear are not continuous but are arranged

Fig. 16 - Photomicrograph of fault breccia exposed along San Diego River fault zone at point F, Fig. 14; 5 x enlargement.

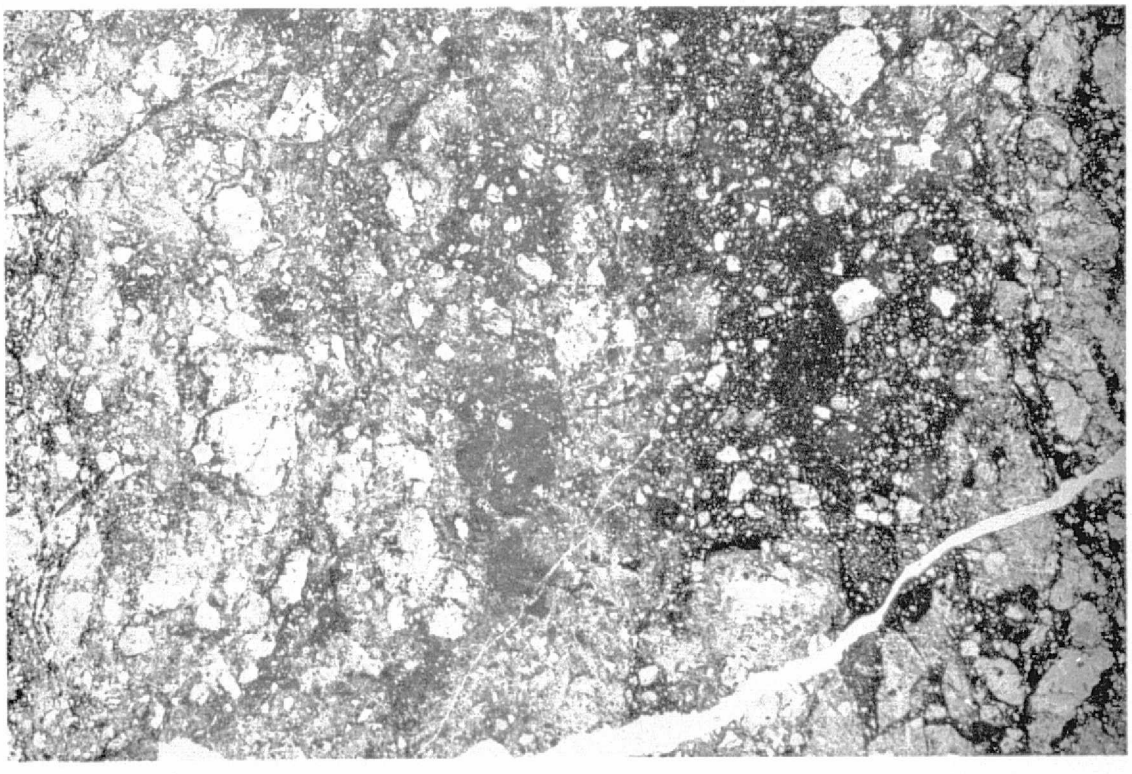

Fig. 17 - Photomicrograph of fault breccia exposed along San Diego River fault zone at point N, Figs. 13 and 15; 5 x enlargement.

Station	Attitude of Fracture Surfaces	Remarks
B	N42°E, 58°SE N24°E, 82°E N34°E, 81°E	Zone of sheared and brecciated Julian Schist with smooth fracture surfaces; 1 meter (3 feet) wide.
C	N22°E, 70°E	Zone of brecciated Stonewall Quartz Diorite with smooth fracture surfaces; 5 meters (16 feet) wide.
D	N43°E, 75°E	Two parallel fracture surfaces, in mixed rocks; 0.3-0.6 meters (1-2 feet) apart.
E	N40°E, 60°SE	Parallel fracture surfaces in brecciated Stonewall Quartz Diorite.
F	N40°E, 60°SE N26°E, 58°SE N37°E, 73°E	Zone of sheared and brecciated mixed rocks 1-2 meters (3-6 feet) wide; elongate pond eroded along axis of river. Appears highly fractured in thin section (Fig. 16); fractures form an anastamosing pattern. Quartz and potassium feldspar show undulose extinction.
G	N40°E, 63°SE	Zone of sheared and brecciated rocks, 1-2 meters (3-6 feet) wide; elongate pond eroded along axis of river.
I	N42°E, 68°SE	Smooth fracture surfaces. No evidence of granulation observed in thin section. Moderately altered.
J	N30°E, 84°E	Similar to I.
K	N38°E, 70°E	Smooth fracture surfaces in zone of fractured rock 1 meter (3 feet) wide. In thin section, bands of chlorite and opaque minerals concentrated along fractures form an anastomosing pattern around augen of quartz and feldspar.
N	N24°E, 90°	Tabular body, 1 meter (3 feet) wide, 12 meters (40 feet) long. Olive green, fine-grained. In thin section (Fig. 17), fine-grained quartz, plagioclase and alteration material. Some of the larger fragments appear to have spalled off fragments around their edges.
S	N1°W, 78°W	Fault gouge of fine-grained, friable, pulverized rock; 1 meter (3 feet) wide.
T	N13°W, 57°W N25°W, 67°W	Fault gouge of fine-grained friable fractured rock 2 meters (6 feet) wide. In thin section patches of mica are bent and distorted. Rake of striae on slickensided shear surface: 7°S.
U	N27°W, 75°W N33°W, 66°W N2°E, 87° W	Fault gouge of fractured rock .1-1 meter (.3-3 feet) wide. In thin section grains are fractured but unstrained.
V	N11°W, 69°W	Zone of clay gouge (?), 10 centimeters (4 inches) wide.

Table 1 - Data on fracture zones along San Diego River fault zone.
See Figs. 13, 14 and 15 for station locations.

en echelon. Approximately 420 meters (1400 feet) of right separation of a body of Julian Schist is indicated by the mapped relations. The en echelon arrangement of the A-B photo linear and shear zone near point B is compatible with right-slip faulting (Harding, 1974).

Exposures of fracture surfaces at C and D (Fig. 18) are inferred to be continuous with the shear zone exposed near B. A possible right separation of 6 meters (20 feet) of a contact between schist and coarse-grained quartz diorite was observed along the end of the shear zone exposed at point D. No other sheared or brecciated rock is exposed on line to the southwest of the shear zone at D, and no linear appears on large-scale air photographs (USDA, 1953, photo numbers AXN-7M-39 and 40).

Another en echelon zone of fractures appears in discontinuous exposures at E, F, and G. Exceptionally straight stretches of the canyon occur at points F (Fig. 19) and G. This fracture zone cannot be traced southwest of G, and continuous exposures of bedrock in the canyon bottom 700 meters (2400 feet) to the southwest of G are unfractured. Between H and I an alignment of saddles and subtle differences in vegetation can be traced on the large-scale air photographs (Fig. 20 and USDA, 1953, photo numbers AXN-6M-5 and 6, AXN-7M-40 and 41) to the southeast and en echelon with the E-F-G fracture zone (Figs. 13 and 14). Fracture surfaces aligned with the H-I photo linear are exposed in the canyon bottom at I and J (Fig. 13). No exposures of fractured rocks were observed in almost continuous exposures in the canyon bottom between points J and K. As previously noted by Merriam (1958, Fig. 2), along this portion of the river the average trend of foliation is parallel to the river as compared to the regional northwest trend (Figs. 13 and 15). The linear in this area may parallel the axis of a shear fold. The rocks at K appear fractured in thin section and smooth fracture surfaces are aligned with the canyon axis. Another photo linear (Fig. 20 and USDA, 1953, photo numbers AXN-6M-6 to 8, AXN-5M-76 and 77) similar to the H-I linear is located between L and M, en echelon and to the southeast of the H-I linear. A tabular body of olive green, very fine-grained rock aligned with the canyon bottom and en echelon with the L-M photo linear is exposed at N (Fig. 15). Individual grains seen in thin section (Fig. 17) are fractured. This rock is interpreted to be a zone of altered fault breccia.

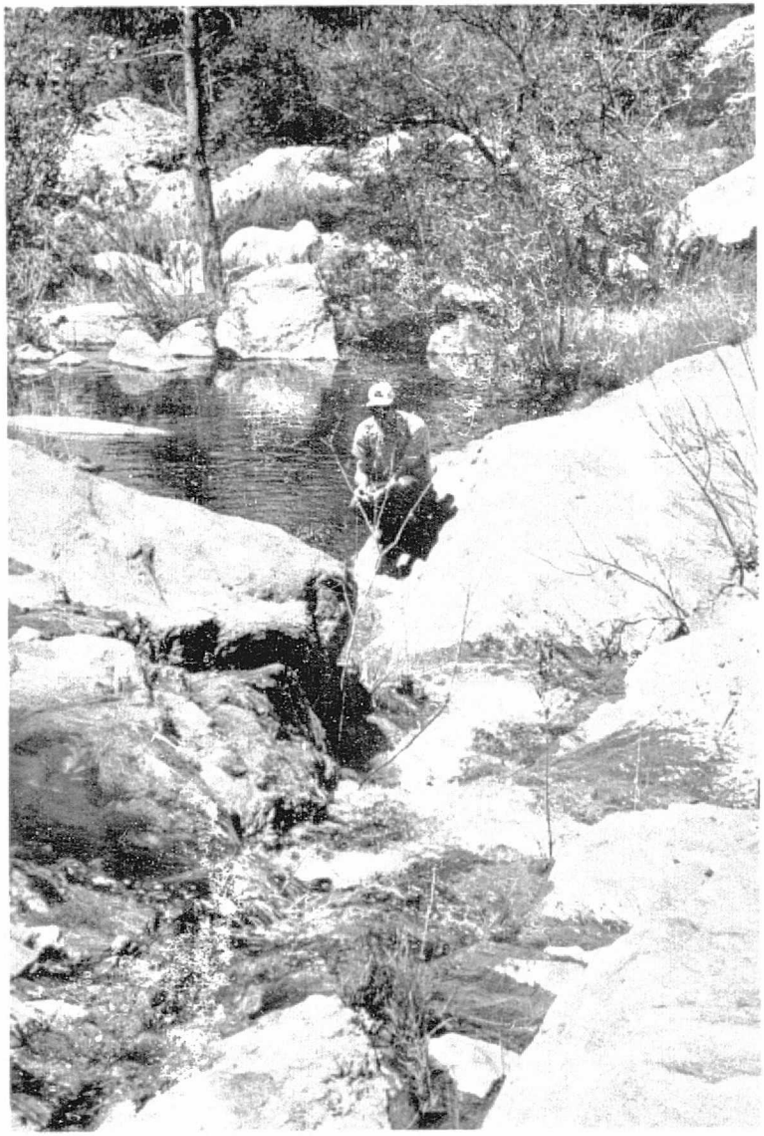

Fig.18 - Exposure of fault surface along San Diego River fault zone at point D, Fig. 14.

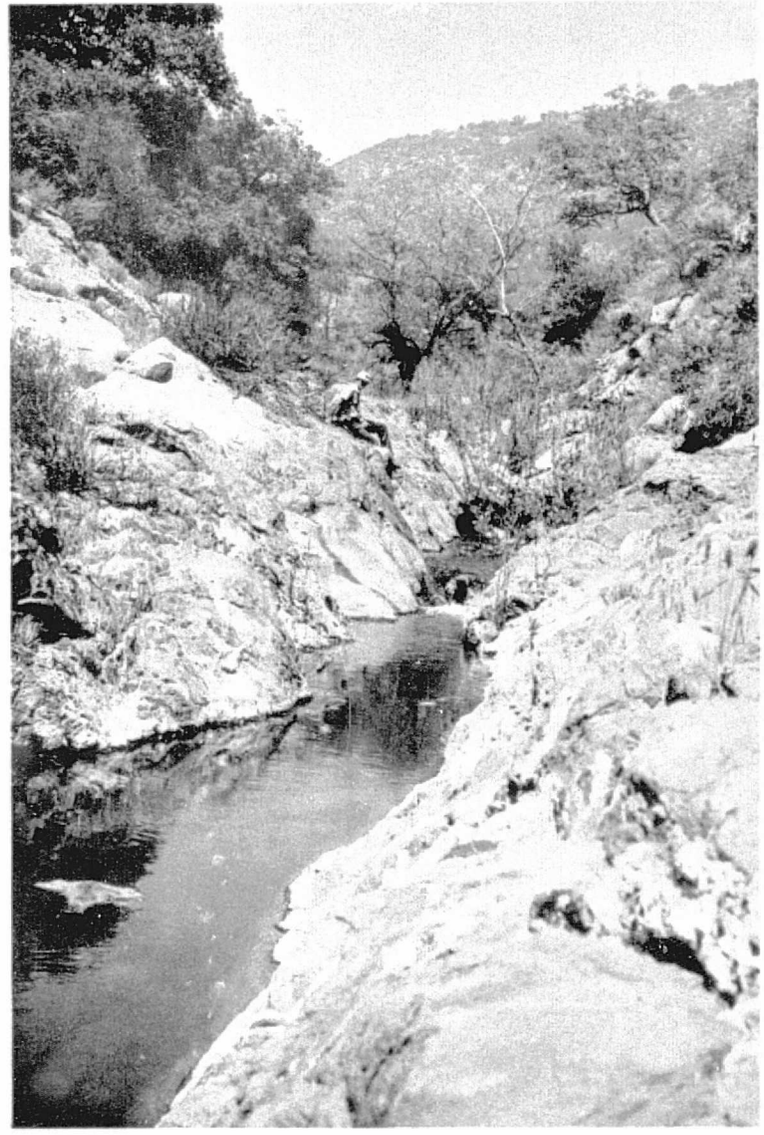

Fig.19 - View of straight pond eroded along San Diego River fault zone at point F, Fig. 14.

Fig. 20 - Portion of U.S. Department of Agriculture aerial photo number AXN-6M-6, April 2, 1953, showing linears along San Diego River fault zone. Arrows indicate ends of linears and letters keyed to Fig. 13. See Fig. 13 for area covered.

Alluvium in the valley between N and O (Fig. 13) would obscure any evidence of faulting; however, the distribution of bedrock in the area covered by Fig. 15 could be explained by right separation along a fault coincident with the canyon axis. The southeast portion of the area covered by Fig. 15 was also mapped by Fitzurka (1968), who shows a similar distribution of rock units. Right separation of approximately 630 meters (2100 feet) is indicated along the south edge of the Stonewall Quartz Diorite. The distribution of irregular masses of Julian Schist in the southern portion of the area also suggests about 320 meters (1050 feet) of right separation along the valley.

San Diego River curves eastward so that a southern continuation of the inferred fault along the valley would pass through bedrock between points O and P (Fig. 13). An alignment of straight canyon segments and saddles can be seen on the satellite imagery (Figs. 11 and 12) and large-scale air photos (Army Map Service (AMS), 1955, scale: 1/63,000, photo numbers 6065 and 6066; USDA, photo numbers AXN-6M-50 and 51) along O-P. Green Valley Tonalite is exposed in an area of heavy brush and thick soil on both sides of the O-P photo linear. Joints are parallel to the linear, and no prominent fracture surfaces, breccia, slickensided shear surfaces or other evidence of faulting were found. However, the exposures are not adequate to prove or disprove the presence of a fault.

An alignment of straight canyon segments and saddles appears on the satellite images, large-scale air photos (AMS, 1955, photo numbers 6066 and 6067), and topographic maps between Q and R. Exposures are lacking, and heavy brush and rugged terrain deny access to the northern end of this feature. Possible exposures along canyons and fire roads which cross the central and southern segments of this feature were not investigated. The Q-R linear is located en echelon with the faults to the north so that right-slip along a southern continuation of the San Diego River fault zone could be accommodated. However, San Diego River Valley is the more prominent linear topographic feature. Alluvium and El Capitan Reservoir obscure any exposures in the valley between points P and S (Fig. 13).

The reservoir curves eastward between points S and T so that bedrock crops out in the area south of the principal axis of the valley between P and S. A continuous linear cannot be seen along S-T on satellite images or

large-scale air photos (AMS, 1955, photo numbers 6066 and 6067). However, fault gouge was exposed at points S and T along the shore of the reservoir during the low water level of January 1975. An 800-meter (2600-foot) long, straight canyon occurs to the north along the trend of the fault zone exposed at T. The fault zones at S and T are arranged en echelon. En echelon and south of S-T, a 2.6-kilometer (1.6-mile) long alignment of straight canyons can be seen on large-scale air photographs (AMS, 1955, photo numbers 6067 and 6068) along U-V-W; fault gouge is exposed at points U and V (Fig. 13).

The faults around the southern portion of El Capitan Reservoir trend north-south to north-northwest and dip west as compared to the faults to the north between A and N which strike north-northeast and dip east, with the exception of the vertical dip at point N. This change in strike is reflected in a similar curve in the trend of the San Diego River Canyon. On the basis of this regional change in physiographic trend, which is well displayed on the satellite images, a continuous zone of en echelon faults has been inferred along the poorly exposed section of the canyon between N and S. It should be noted that the only evidence of the amount or direction of displacement on the faults around El Capitan Reservoir is the nearly horizontal striae on a slickensided surface observed at point T. Also, the en echelon pattern in this area is consistent with left-slip, rather than the right-slip pattern along the northern segment of the San Diego River fault zone. Green Valley Tonalite is exposed on both sides of the linear from the south edge of Fig. 15 southward, so it is doubtful that additional detailed mapping would reveal any additional information concerning displacement.

The south arm of the El Capitan Reservoir along Chocolate Canyon appears as a fairly straight feature on the satellite imagery. The canyon is fairly sinuous on large-scale air photographs (AMS, 1955, photo numbers 6067 and 6068), and there are no exposures in the canyon to prove or disprove a fault. 5.2 kilometers (3.2 miles) south of Chocolate Canyon, a straight 3.5-kilometer (2.2-mile) long segment of the North Fork of the Sweetwater River appears on satellite imagery (Figs. 3 and 4) aligned with Chocolate Canyon and San Diego River Valley; this feature was not investigated.

Witch Creek Linear

The Witch Creek linear appears on satellite images (Figs. 11 and 12) as

an alignment of remarkably straight canyons 12.2 kilometers (7.6 miles) long. The feature trends north-northeast parallel to the San Diego River fault zone through the community of Witch Creek (Fig. 13). Maps prepared by Merriam (1946, 1958) and Rogers (1965) do not show a fault along this feature; Weber (1963) and Jennings (1973) show a fault. Mixed rock consisting of Stonewall Quartz Diorite and Julian Schist are exposed along most of the Witch Creek linear (Merriam, 1946, 1958). A body of Woodson Mountain Granodiorite intrusive into mixed rocks is exposed at the south end of the linear in the area of Mount Gower (Merriam, 1946). As shown on Fig. 15, the San Vicente Valley linear and the contact between Woodson Mountain Granodiorite and mixed rock are apparently undisplaced across the trace of the linear. Soil and vegetation occur in the canyons eroded along the Witch Creek linear and exposures of bedrock are infrequent; no evidence of faulting was detected in the few exposures observed. Jointing and foliation do not appear to be aligned with the linear (Fig. 15). The origin of the Witch Creek linear is unknown, although it apparently did not originate as a result of erosion along a fault zone.

Himmel Canyon Linear

A straight segment of Himmel Canyon and canyons to the northeast appear as a prominent, curving 2.8-kilometer (1.7-mile) long linear on satellite images (Figs. 11 and 12). The Himmel Canyon linear crosses and does not displace the east end of the San Vicente Valley linear and the contact between Woodson Mountain Granodiorite and Stonewall Quartz Diorite; neither jointing nor foliation appears to be parallel to the linear (Fig. 15). Rare exposures of bedrock along the linear show no evidence of faulting. The origin of the Himmel Canyon linear is unknown.

Sutherland Reservoir Linear

The Sutherland Reservoir linear trends north-northeast for 9.3 kilometers (5.8 miles) along a gently curving path through Sutherland Reservoir (Figs. 11 and 12). Bedrock exposed along the southern portion of the linear, south of the reservoir, consists of Lakeview and Green Valley Tonalite; Julian Schist is exposed north of the reservoir (Merriam, 1946). No evidence of faulting was observed in bedrock exposures along this linear. The average of several measurements of joints and foliation is shown on Fig. 13. South of the

reservoir the average joint direction in tonalite is parallel to the linear, and north of the reservoir the foliation in Julian Schist is parallel to the linear.

Valle De Los Amigos Linear

A photo linear represented by an alignment of straight canyons and saddles appears on satellite images (Figs. 11 and 12) north-northeast of the Valle De Los Amigos (Fig. 13). Bonsall and Lakeview Tonalite are exposed along the southern portion of this linear and Julian Schist along the northern segment (Merriam, 1946). The average trend of jointing along the southern portion is parallel to the linear. Foliation in Julian Schist changes trend across the north end of the linear; a fault or fold axis may be coincident with the linear. Exposures are not adequate to prove or disprove the presence of a fault along this linear. The available evidence indicates that jointing in tonalite is primarily responsible for the north-northeast trend of the Valle De Los Amigos linear.

Pamo Valley Linear

Pamo Valley and an alignment of north-south to north-northeast trending straight canyon segments and saddles to the north and south form a prominent linear on satellite images (Figs. 11 and 12); this feature can be traced for 18.5 kilometers (11.5 miles) from the north end of Santa Maria Valley to a saddle on the southwest side of San Luis Rey River, almost to the Elsinore fault (Fig. 13). Merriam (1946) does not indicate any faulting along this feature. Jennings (1973) shows a fault along the entire linear and extending 12.9 kilometers (8.0 miles) farther south beneath the alluvium of Santa Maria Valley and along a straight north-south trending canyon. Bedrock exposed along this feature consists of Bonsall, Ramona, and Green Valley Tonalite and, along the possible extension south of Santa Maria Valley, Woodson Mountain Granodiorite (Merriam, 1946, 1954). Features along the Pamo Valley linear are described from north to south and letters on Fig. 13 are keyed to the descriptions.

A distinctive alignment of saddles and straight canyons can be seen on large-scale aerial photos (USDA, 1953, photo numbers AXN-6M-94 to 96) and the topographic map between points A and B. Heavy brush prevented access to

the northern portion of this feature. Jointing in tonalite trends parallel to the canyon at the south end, and no evidence of faulting could be seen in exposures in the canyon bottom. Between B and C, two parallel linears (USDA, 1953, photo numbers AXN-6M-171 to 174) follow straight canyons. Heavy brush and rugged terrain denied access to much of this feature, and no evidence of faulting was seen in the few exposures of bedrock along the linear. As indicated on Fig. 13, jointing and foliation in tonalite are parallel to the linear. The exposures studied during the present investigation indicate that the A-C segment of the linear formed primarily as a result of erosion along the joint direction in tonalite; erosion along foliation may also have been important. Most previous workers (Weber, 1963; Rogers, 1965; Jennings, 1973) show a branching fault corresponding to the linear on Fig. 13.

A prominent north-south trending linear between D and E can be seen on satellite imagery and a straight canyon segment appears in Section 36, T11S, R1E. Large-scale photos (USDA, 1953, photo numbers AXN-6M-169 to 172) do not show a sharp, straight linear along this feature, and heavy brush prevented access. The origin of the D-E linear is unknown. Between C and F, Pamo Valley is straight and trends north-south. Alluvium in the valley obscures this portion of the linear, but joint directions measured in tonalite along the sides of the valley (Fig. 13) are predominantly parallel to the linear.

Evidence of faulting was observed along a straight canyon (northwest corner, Sect. 34, T12S, R1E) eroded in bedrock between points F and G directly south of Pamo Valley. The following attitudes of fault gouge zones were measured from north to south along the axis of the canyon:

	Strike	Dip
	N12°E	85°W
	N5°E	78°E
	N10°E	87°E
	NS	83°E
Average	N7°E	86°E

The canyon trends N4°E, within 3° of the average direction of the gouge zone. The width of the gouge zone varies from 2 centimeters (1 inch) to 10 centimeters (4 inches). In hand specimen and thin section the fault gouge consists of fine-grained, fractured and altered tonalite. Striations on a slickensided shear surface at the south end of the F-G linear have a rake of 72°S.

Bedrock is similar on both sides of the linear, and there is no other evidence of the direction or sense of fault displacement.

Between G and H, bedrock is obscured by alluvium beneath Santa Maria Valley. To the south, a 3.2-kilometer (2.0-mile) long, straight segment of Daney Canyon can be seen on satellite imagery and on the topographic map between H and I. Jennings (1973) indicates that the H-I linear is a fault; this feature was not studied during the present investigation. The only evidence of faulting observed on the Pamo Valley linear during the present investigation was along the canyon at F-G. The origin of the remainder of the linear is either indeterminant or due to erosion along the joint and foliation directions in bedrock.

Los Penasquitos Canyon Linear

A straight segment of Los Penasquitos Canyon and an alignment of saddles and straight canyons form a fairly distinct 10.1-kilometer (6.3-mile) long, N67°E trending linear on satellite images (Figs. 11 and 12). Only the segment at the northeast end, between points A and B (Fig. 13), appears as a sharp linear on large-scale air photos (USDA, 1953, photo numbers AXN-5M-181 and 182, AXN-9M-31 and 32); to the southwest of point B, a linear feature is not apparent on large-scale aerial photographs (USDA, 1953, photo numbers AXN-9M-78 and 79). Bedrock exposed along the Los Penasquitos Canyon linear consists of Woodson Mountain Granodiorite, Bonsall Tonalite (Gastil and Bushee, 1961), and Black Mountain Volcanics (Jurassic and/or Triassic) (Strand, 1962). Joint directions in granodiorite at the northeast end are predominantly parallel or orthogonal to the trace of the linear; the segment to the southwest of point B was not studied on the ground. Erosion along joints may be the principal cause of this linear. No exposures of bedrock were observed along the linear trace. It is doubtful that faulting has occurred, because a north-south trending body of Black Mountain Volcanic rocks (Gastil and Bushee, 1961) crosses the linear between points C and D and is not displaced, nor could any evidence of displacement be seen on large-scale air photographs (USDA, 1953, photo numbers AXN-9M-78 and 79).

Chariot Canyon Fault

The Chariot Canyon fault branches from the Elsinore fault at the town of Banner and follows the trend of Chariot Canyon to the south-southeast.

A short segment at the mouth of Chariot Canyon was originally mapped by Hart (1964) and is shown by Rogers (1965). Based on the study of Landsat images and field studies, Allison (1974bc) suggested that the Chariot Canyon fault continues south into Mexico. Allison (1974abc) reports 8 kilometers (5 miles) of right separation based on the distribution of Julian Schist and plutonic rock along the fault. We were unable to recognize a continuous linear on satellite images (Figs. 3 and 4) extending from Chariot Canyon into Mexico; our interpretation of the images is shown on Figs. 2 and 21. The prominent light line on the satellite images paralleling the Chariot Canyon fault to the southwest is an area cleared of vegetation.

Our examination of a number of exposures in Chariot Canyon did not reveal a single fault separating Julian Schist on the west from granitic rocks on the east, but a broad shear zone appears to occupy the width of the canyon. Steeply dipping, slickensided shear surfaces were observed to strike between north-south and N30°W. The foliation in schist and gneiss is locally undulatory but has a general strike conformable with the shear surfaces and the trend of the canyon. According to Allison (1974b), south of Chariot Canyon (between points A and B, Fig. 21), "....the fault can be followed by topographic evidence." We did not study large-scale air photos or accomplish detailed field studies along the trace of the linear south of Chariot Canyon. However, at point B (Fig. 21), we were unable to find a shear zone aligned with the linear in excellent exposures of bedrock across the trace of the linear along Sunrise Highway (Sect. 12, T14S; R4E).

A 16-kilometer (10-mile) long alignment of straight canyons and saddles on satellite images (Figs. 3 and 4) extends south of point B (Fig. 21). A shear surface on the trace of the linear 10.7 kilometers (6.6 miles) south of point B (Fig. 21) along Sunrise Highway (Mount Laguna Quadrangle; Sect. 32, T15S; R5E) was visited in December 1974 on a San Diego Association of Geologists field trip. At this location, a sinuous wall of igneous rock in a borrow pit marks the probable western edge of the Chariot Canyon fault zone (Allison, 1974c). The average attitude of the shear surface is N20°W, 82°E. Striae on slickensided shear surfaces have rakes of 3°S and 6°S. The average trend of the linear between this exposure and its topographic expression to the north is N6°W. The difference in strike and the apparent lack of a continuous shear zone could perhaps be explained if the Chariot Canyon linear

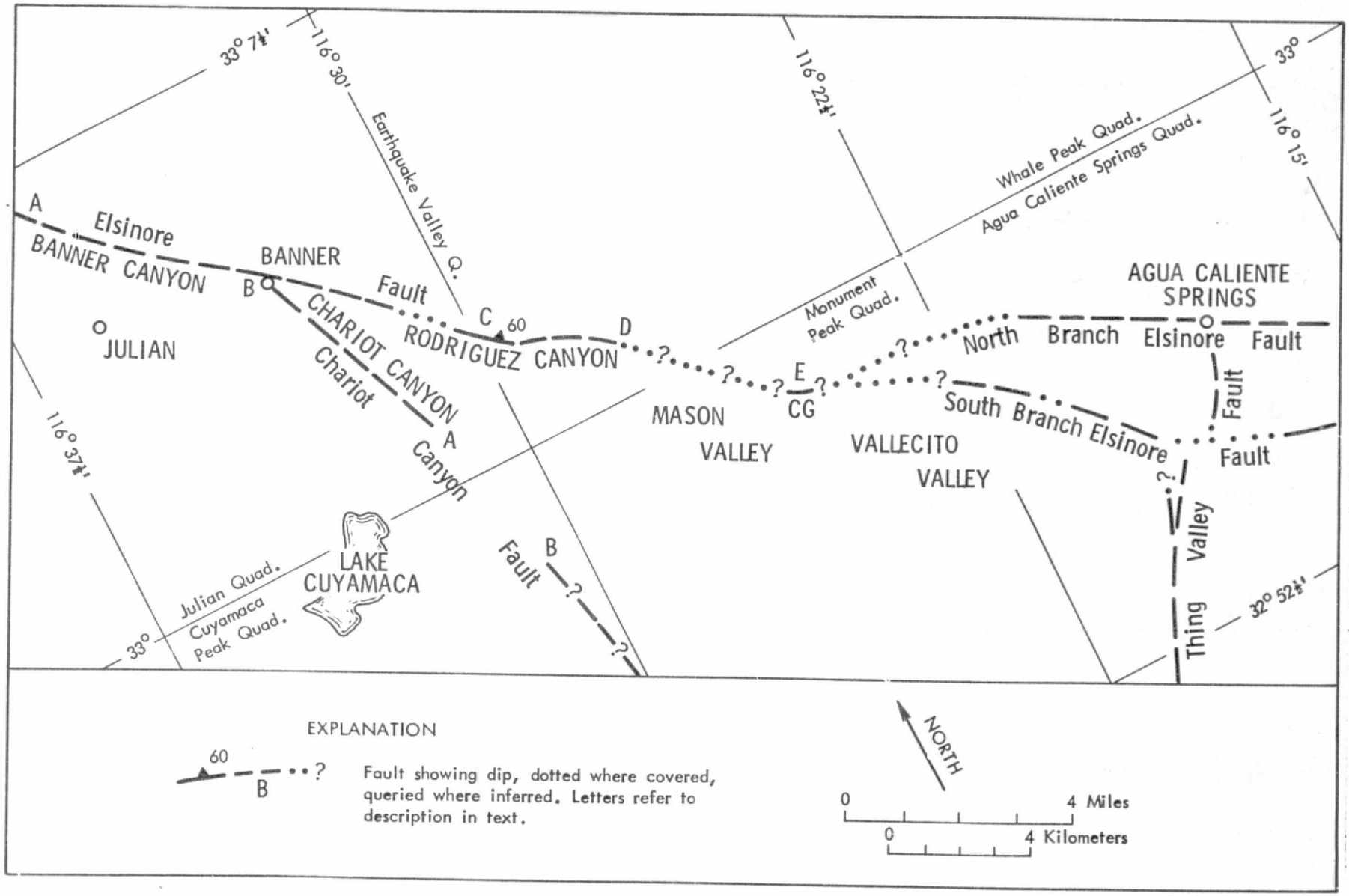

Fig. 21 - Map showing southeastern portion of Elsinore and Chariot Canyon faults in Julian-Vallecito Valley area. See Fig. 6 for area covered. Abbreviation: CG: Campbell Grade.

formed as a result of erosion along a series of en echelon faults similar to the San Diego River fault zone. Additional detailed mapping is required for a better understanding of the Chariot Canyon fault zone.

Sweetwater River Linear

The linear stretching over 50 kilometers (30 miles) from the United States-Mexico border northeastward nearly to the Elsinore fault zone is second only to the San Diego River linear in prominence on spacecraft photography of the Peninsular Ranges (Figs. 3 and 4). It is herein referred to as the Sweetwater River linear after the Sweetwater River (Figs. 3 and 4). The linear consists primarily of nearly linear stream valleys which, at first glance, appear to be aligned, but upon closer inspection are seen to be discontinuous or en echelon. The largest stream valleys, beginning at the northeast end of the linear, are Green Valley, Sweetwater River (Figs. 3 and 4), Horsethief Canyon, Pine Valley Creek, and Cottonwood Creek (Figs. 22 and 23). The distribution of bedrock along the northern portion of the linear is shown by Everhart (1951) and, in less detail along the entire linear, by Strand (1962) and Weber (1963).

The north end of the linear along Green Valley is under study by the U.S. Geological Survey; no evidence for faulting has been found during their investigation (Victoria Todd, U.S. Geological Survey, personal communication, 1974). To the southeast, contacts on the margin of a body of Bonsall Tonalite bend to the right as they cross the Sweetwater River (directly east of Sects. 6 and 7, T15S; R4E, Everhart, 1951) and no distinct break is evident. The linear in this area may correspond to the axis of a small flexure, or perhaps shear fold. Southwest of Descanso Junction, the regional trend in foliation shown by Everhart (1951) is east-west to northwest. The margins of a body of Green Valley Tonalite also mapped by Everhart (1951) bend to the right 400 to 700 meters (1300 to 2300 feet) where they cross the linear (Sects. 25 and 36, T15S; R3E), which suggests that this portion of the linear may also be the result of erosion along a shear fold.

To the southwest, Horsethief Canyon follows foliation in Woodson Mountain Granodiorite and Bonsall Tonalite. Some slickensided shear surfaces parallel to Horsethief Canyon were observed in roadcuts, but because the shear surfaces are parallel to foliation in bedrock, no displacement could be determined.

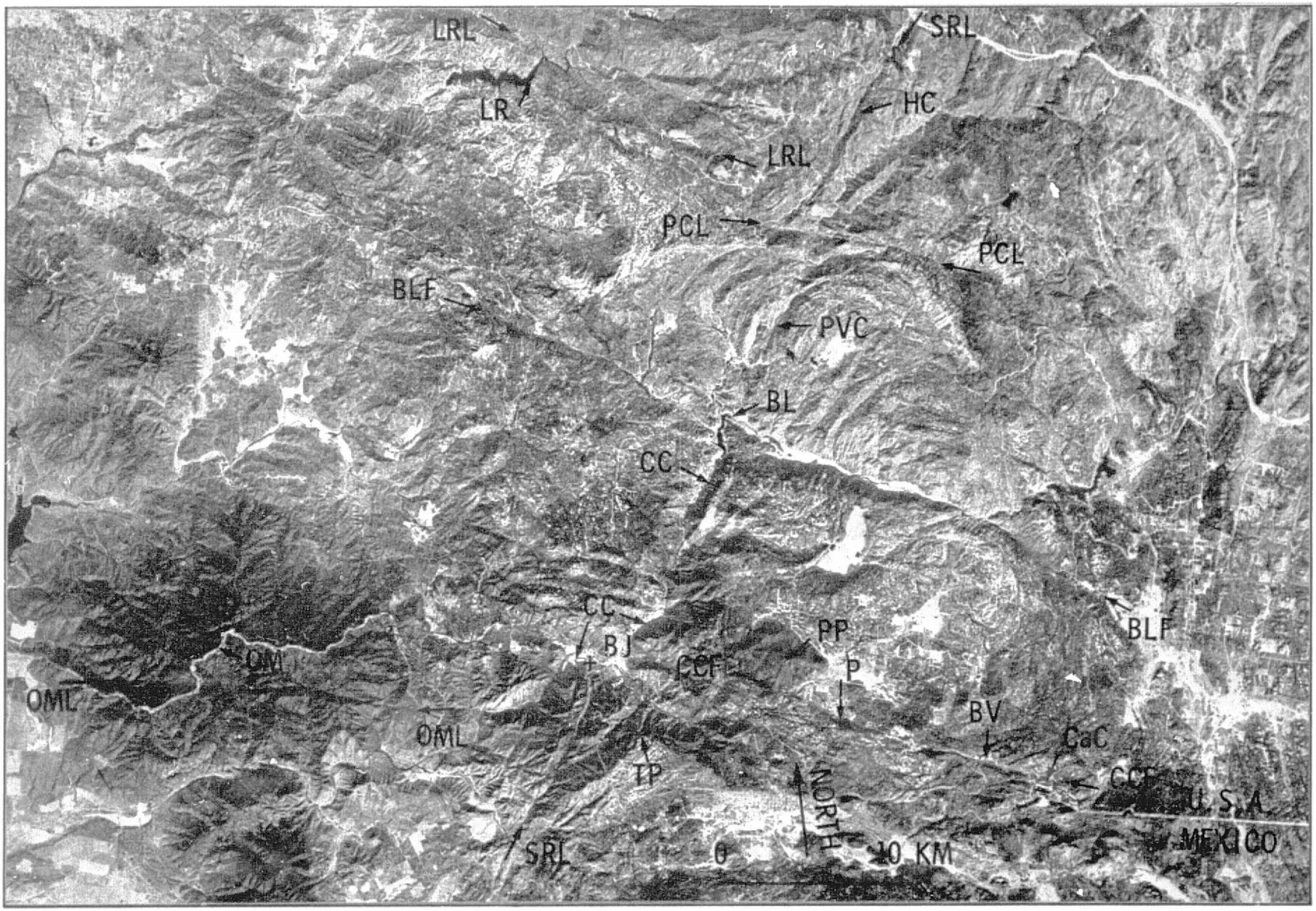

Fig. 22 - Barrett Lake fault and other faults and linears in Peninsular Ranges, southernmost California. Portion of Skylab 3, 190B camera, Roll 87, Frame 111 (original in color infrared). Abbreviations: BJ: Barrett Junction; BL: Barrett Lake; BLF: Barrett Lake fault; BV: Bell Valley; CaC: Canyon City; CC: Cottonwood Creek; CCF: Canyon City fault; HC: Horsethief Canyon; LR: Loveland Reservoir; LRL: Loveland Reservoir linear; OM: Otay Mountain; OML: Otay Mountain linear; P: Potrero; PCL: Pine Creek linear; PP: Potrero Peak; PVC: Pine Valley Creek; SRL: Sweetwater River linear; TP: Tecate Peak.

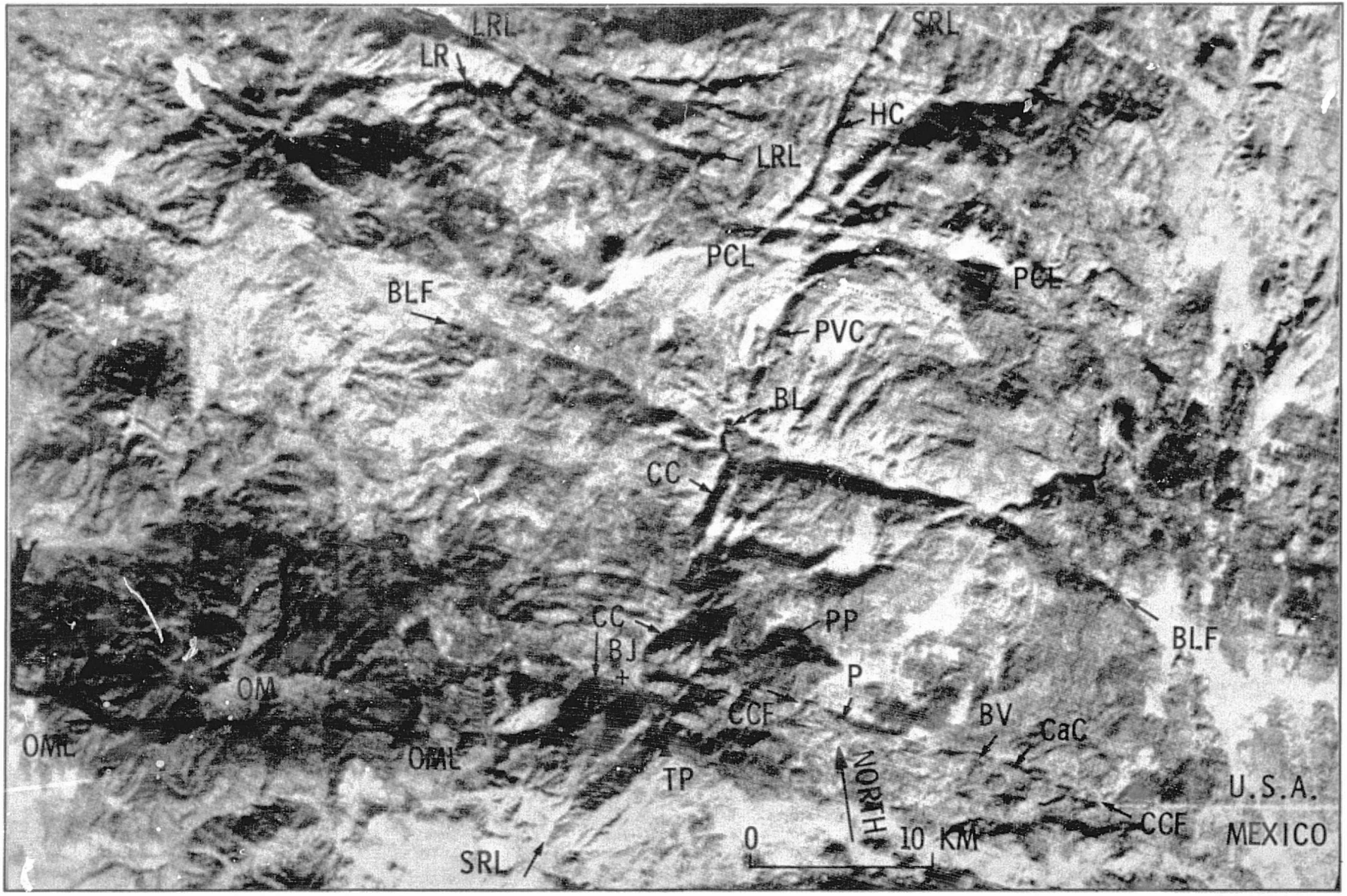

Fig. 23 - Barrett Lake fault and other faults and linears in Peninsular Ranges, southernmost California. Portion of Landsat image 1106-17504. Abbreviations: BJ: Barrett Junction; BL: Barrett Lake; BLF: Barret Lake fault; BV: Bell Valley; CaC: Canyon City: CC: Cottonwood Creek; CCF: Canyon City fault; HC: Horsethief Canyon; LR: Loveland Reservoir; LRL: Loveland Reservoir linear; OM: Otay Mountain; OML: Otay Mountain linear; P: Potrero; PCL: Pine Creek linear; PP: Potrero Peak; PVC: Pine Valley Creek; SRL: Sweetwater River linear; TP: Tecate Peak.

Farther southwest, the apparent trace of the linear is offset to the left 1.2 kilometers (.75 mile) along the Pine Creek linear and an en echelon linear continues south-southwest along Pine Valley Creek to Barrett Lake. (Figs. 22 and 23). Foliation along Pine Valley Creek trends north-northeast, parallel to the linear and the margins of a pluton which can be seen on the satellite images. Immediately south of Barrett Lake a deep, straight, 3-kilometer (2-mile) long section of Cottonwood Creek is aligned with Pine Valley Creek. The origin of this prominent segment of the linear is unknown; Woodson Mountain Granodiorite (Strand, 1962) exposed along Cottonwood Creek is massive, and no evidence of faulting or foliation and jointing parallel to the linear was observed.

To the southwest the course of Cottonwood Creek is sinuous and a 4.0-kilometer (2.4-mile) gap occurs in the Sweetwater River linear. South of Barrett Junction (Figs. 22 and 23), the linear is represented for about 5 kilometers (3 miles) by an alignment of tributary valleys and saddles. Several shorter, less prominent linears run parallel to the principal linear between Cottonwood Creek and Tecate Peak. Bedrock consists of massive Woodson Mountain Granodiorite; distinctive lithologic contacts or layering are absent. However, the strikes of prominent joint sets are particularly well developed in the northeast quadrant (Fig. 24). In the absence of layering and evidence for faulting, control of the linear in this area by jointing is the most plausible explanation.

Although minor shearing may have occurred along portions of it, the Sweetwater River linear clearly does not represent a fault but appears to result from the approximate and perhaps fortuitous alignment of linear segments of diverse origin.

Thing Valley Fault

Thing Valley and several straight segments of stream canyons to the northeast appear as a prominent north-northeast trending, 20-kilometer (12-mile) long linear on satellite images of southeastern San Diego County (Figs. 25 and 26). A conventional air photo (USDA, 1953, photo numbers AXN-12M-99 to 102, -13M-10 to 14, -14M-191 to 194, -16M-20 and 21, -17M-58 to 66) and field study was pursued to determine the nature and extent of this feature; a geologic map (Fig. 27) is the result of that investigation. The distribution of rock units has been modified from an unpublished

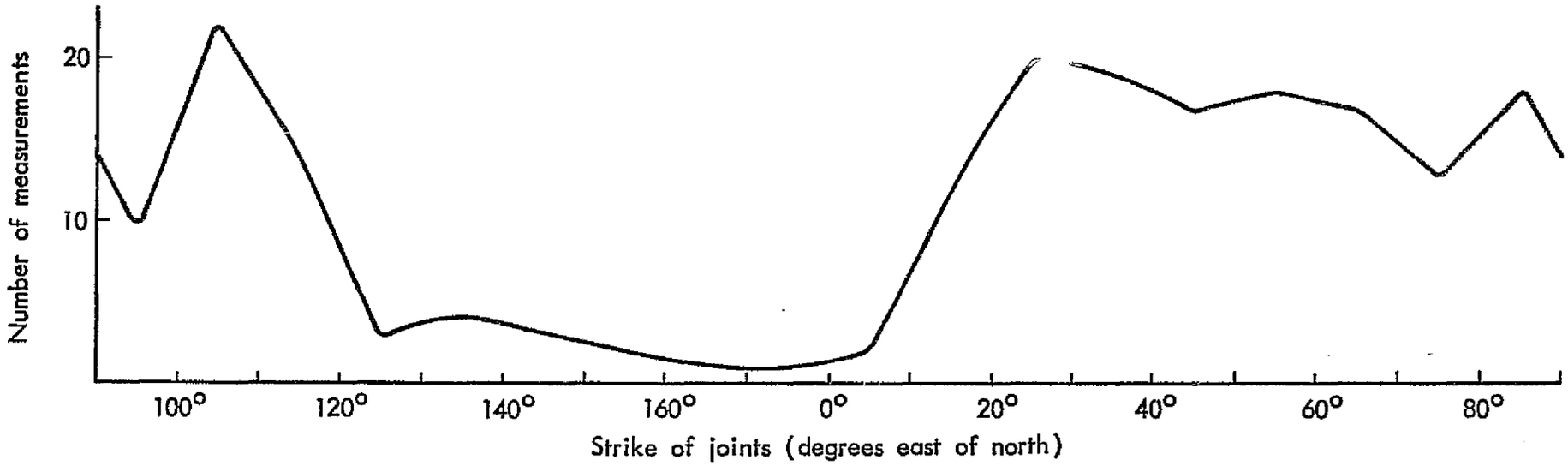

Fig. 24 - Strikes of jointing, Tecate Quadrangle, sections 23, 24, 25, and 26, T18S, R2E and sections 19 and 30, T18S, R3E; 196 measurements. 10° intervals.

Fig. 25 - Thing Valley and vicinity. Portion of Skylab 3, 190B camera, Roll 87, Frame 111 (original in color infrared). Abbreviations: AC: Agua Caliente Hot Springs; NBEF: North Branch Elsinore fault; SBEF: South Branch Elsinore fault; TV: Thing Valley; TVF: Thing Valley fault. Points G and H are keyed to the geologic map of Thing Valley area.

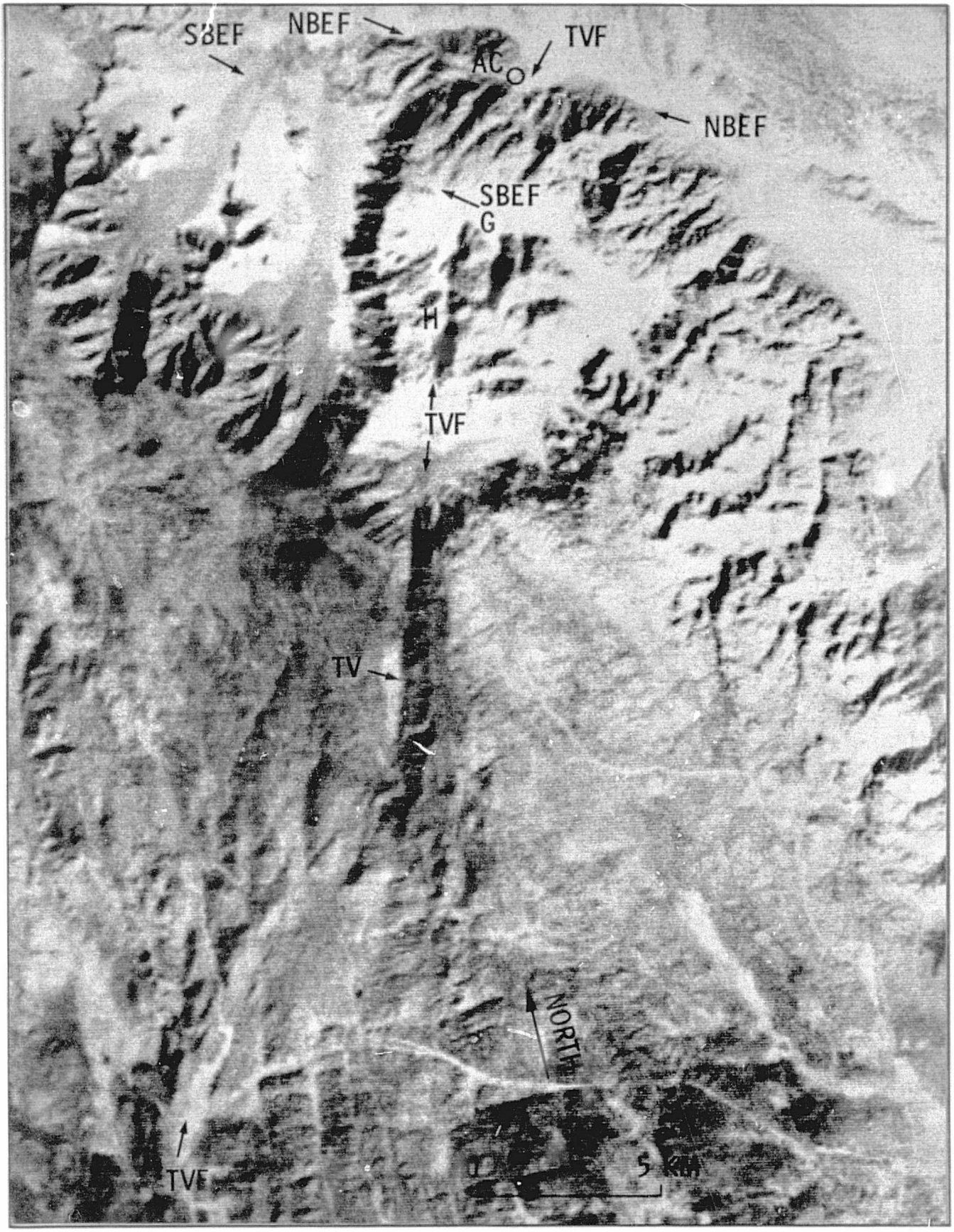

Fig. 26 - Thing Valley and vicinity. Portion of Landsat image 1106-17504. Abbreviations: AC: Agua Caliente Hot Springs; NBEF: North Branch Elsinore fault; SBEF: South Branch Elsinore fault; TV: Thing Valley; TVF: Thing Valley fault. Points G and H are keyed to the geologic map of Thing Valley area.

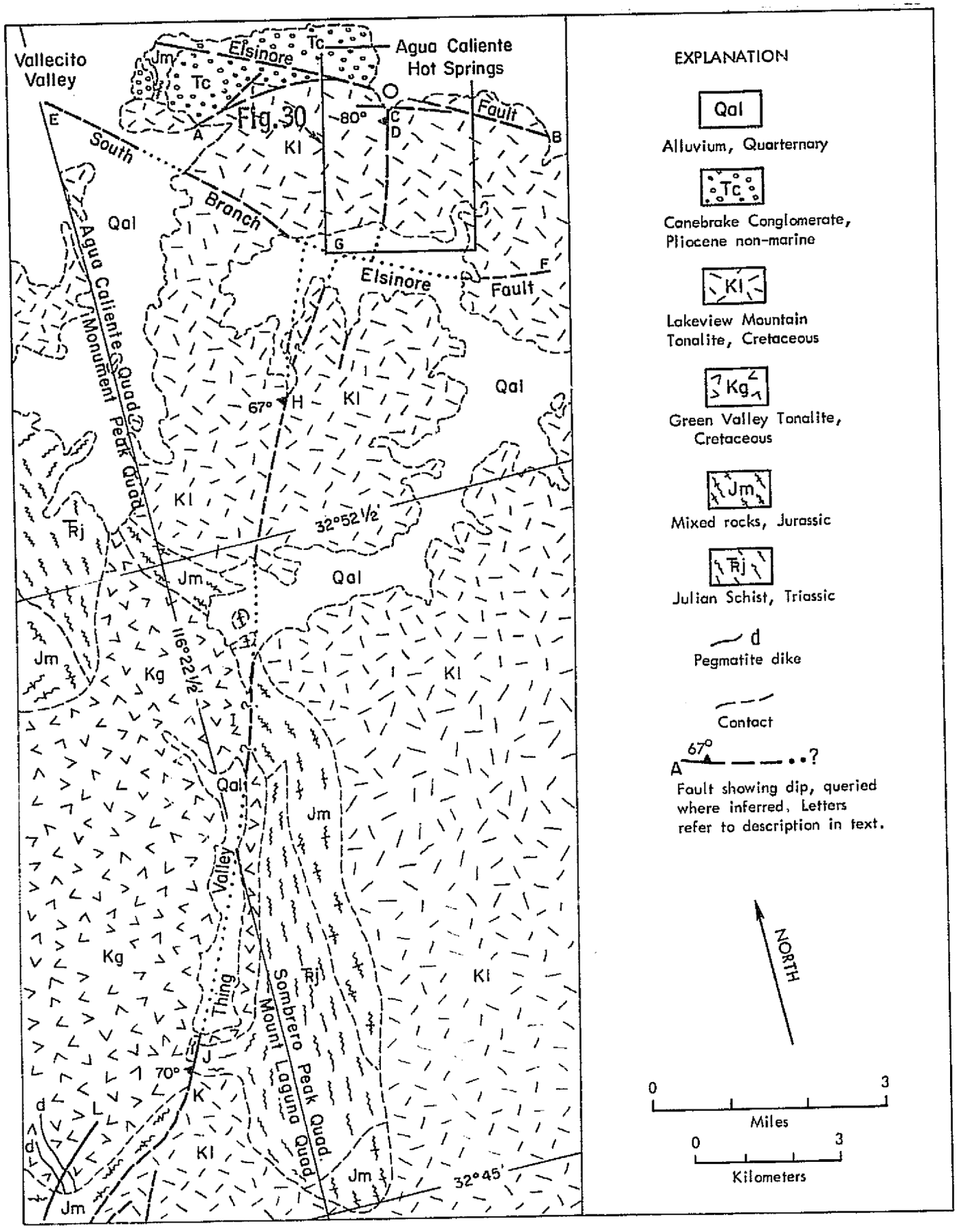

Fig. 27 - Geologic map of Thing Valley area. Geology modified from Merriam (1955) and Buttram (1962); northeast trending faults mapped by authors. See Fig. 6 for area covered.

map prepared by Dr. Richard Merriam (1955). The oldest rock unit is the Julian Schist, which consists of quartzite, gneiss, and quartz-mica schist. Mixed rocks consisting of schist and gneissoid quartz diorite of Mesozoic age are also present. These metamorphic and mixed rocks are intruded by Lakeview Mountain and Green Valley Tonalite.

Letter symbols on Fig. 27 are keyed to descriptions of individual fault segments. The north branch of the Elsinore fault and other west-northwest to northwest trending faults in the area between A and B were mapped by Merriam (1955) and Buttram (1962). Bedrock in the area to the south consists of Lakeview Mountain Tonalite, which crops out as scattered light-gray weathering residual blocks. Faults in Lakeview Mountain Tonalite appear on large-scale air photos as straight canyon segments (Fig. 28), aligned saddles, linear depressions, and lines of denser vegetation. Over most of their length, the fault zones are covered by boulders; these have apparently accumulated in the low areas eroded in brecciated rock along the fault zone.

A 300-meter (1000-foot) long zone of breccia and fault gouge with grooved and slickensided shear surfaces is exposed at point C. The zone is approximately 7 meters (23 feet) wide at the south end of the exposed fault segment and widens to 35 meters (115 feet) at the northeast end. The relationship with the Elsinore fault to the north is obscured by spring deposits and alluvium in the area of Agua Caliente Springs. A concentration of breccia at the fault intersection may provide a conduit for the hot water. A fault zone is exposed 200 meters (650 feet) to the southwest at point D; at this location shear surfaces spaced 2 to 30 centimeters (1 to 12 inches) occur in a 3-meter (10-foot) wide, 30-meter (100-foot) long zone of unbroken tonalite. The following attitudes of shear surfaces and rakes of striations were measured at points C and D:

	Strike	Dip	Rake
C	N2°E	87°E	52°S, 83°S
	N3°E	68°W	None
	N18°E	78°W	47°S
D	N20°E	81°W	85°S
Average	N11°E	80°W	67°S

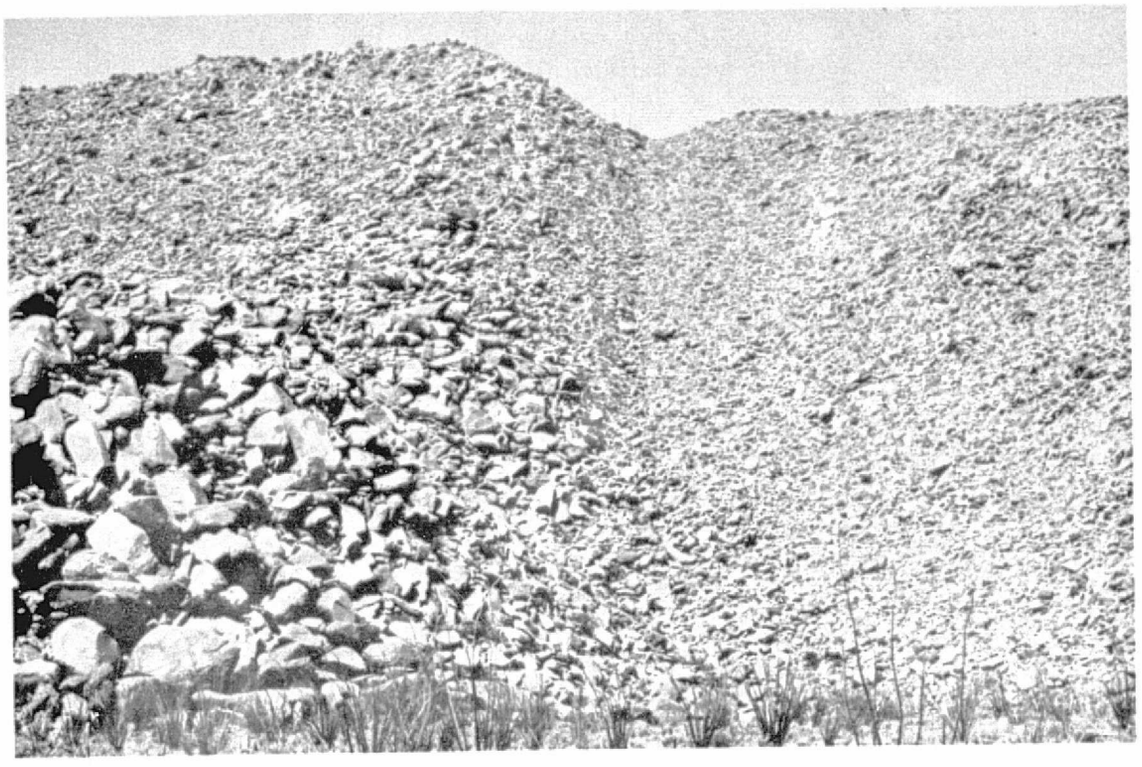

Fig. 28 - View southwest along straight canyon eroded in branch of Thing Valley fault directly southwest of point G, Fig. 27.

Fig. 29 - Exposure of fault gouge within a brecciated zone along Thing Valley fault at point H, Fig. 27. View to north, hammer for scale.

The linear on large-scale air photos (Fig. 30 and USDA, photo numbers AXN-16M-21 and 22) in this area has a trend of N15°E.

The location of the northwest to east-west trending south branch of the Elsinore fault between points E and F has been modified from previous mapping by Merriam (1955) and Buttram (1962). A search for breccia and gouge along the trace observed on air photos (USDA, photo numbers AXN-14M-190 and 191, AXN-17M-68 and 69, AXN-16M-20 and 21) was not accomplished during the present investigation. This fault is inferred to continue northwest to join the north branch of the Elsinore fault (Merriam, 1955). In Vallecito Valley, the fault is reflected as a line of vegetation apparently caused by ground water blockage upstream of the fault; Buttram (1962) has reported a fault scarp in alluvium at this location. At point G, traces of the Thing Valley fault appear to be displaced 700 to 1300 meters (2300-4300 feet) in a right lateral sense by the south branch of the Elsinore fault. It is impossible to prove that any of the faults between H and D were ever continuous across this branch of the Elsinore fault; however, previous alignment is suggested by similar attitudes of the fault segments, and fault offset is in the expected right-lateral sense.

A 25-meter (80-foot) wide zone of light gray breccia and red-brown fault gouge is exposed in two east-west trending gullies at point H (Fig. 29). Slickensided shear surfaces in the fault zone strike between N32°E and N54°E and dip 59° to 78° to the northwest; the representative dip is 67°. The linear observed on air photos (USDA, photo numbers AXN-14M-192 to 194, AXN-17M-65 and 66) in this area strikes approximately N24°E. Striations observed on one slickensided surface in the fault zone have a rake of 4°S.

A straight, deep canyon aligned with the fault zone is present at I, and Thing Valley to the south-southwest is a narrow, straight feature along the same alignment. We infer that Thing Valley and canyon I developed as a result of erosion of fault gouge and breccia within the fault zone. Alluvium within Thing Valley and alluvium, talus, and dense brush in canyon I obscure the geologic relations, and the existence of a fault zone cannot be confirmed. Field mapping and the study of large-scale air photos (USDA, photo numbers AXN-17M-61 to 63) suggest as much as 1 kilometer (.6 mile) of right separation

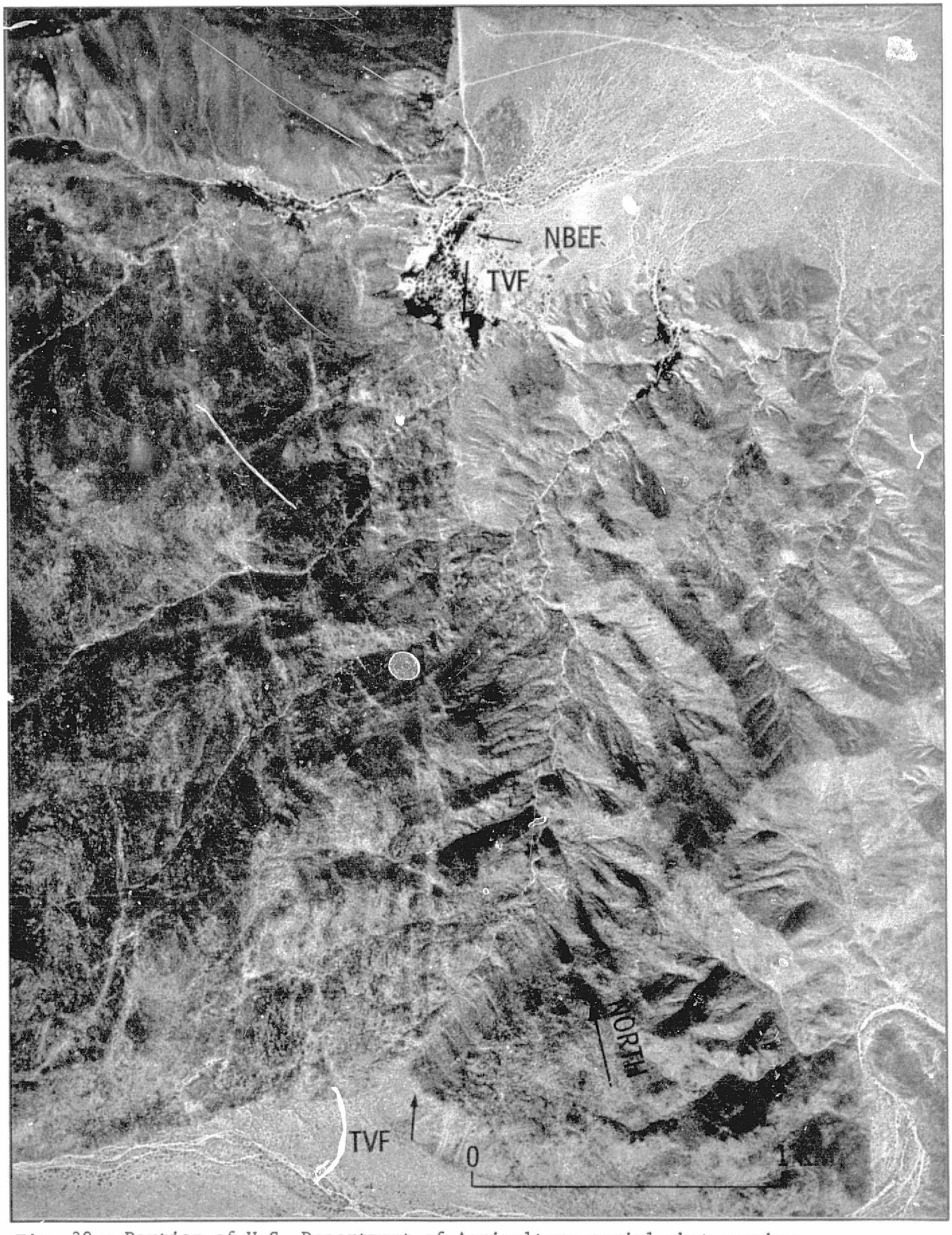

Fig. 30 - Portion of U.S. Department of Agriculture aerial photo number AXN-16M-22, April 2, 1953, showing Thing Valley fault between north and south branches of Elsinore fault. Abbreviations: NBEF: north branch Elsinore fault; TVF: Thing Valley fault. See Fig. 27 for area covered.

of the zone of mixed rock along canyon I. However, the steeply dipping foliation trends in these rocks vary from N36°E to N26°W; consequently, the apparent displacement could be explained by contacts curving nearly parallel into the fault along the axis of a shear fold.

Southwest of Thing Valley, exposures are much poorer than in the desert northeast of Thing Valley. However, a fault is exposed in a roadcut crossing a north-northeast trending saddle (J on Fig. 27) which separates Julian Schist on the east from Green Valley Tonalite on the west. Twelve meters (39 feet) of brecciated schist lies east of an 8-10 centimeter (3-4 inch) wide gouge zone with a strike of N30° to 35°E and a dip of 70°W. The breccia zone west of the gouge may be as much as 18 meters (59 feet) wide, but the zone is largely covered by colluvium. The northwest trending contact between schist and intrusive rocks has a right separation of about 100 meters (300 feet); the dip of the contact is not known. Southwest of the roadcut, the relations are obscure owing to dense brush, but air photos suggest the fault splays out into several branches, one of which (K on Fig. 27) is shown on Merriam's (1955) map.

Another fault to the west (L on Fig. 27) follows a northeast trending valley parallel to the faults discussed above. A left separation of 73 meters (240 feet) is clearly evidenced by offset granite pegmatite dikes; the attitude of the dikes is N13°W, 42°W. Insufficient data are available to determine the sense of slip along this fault.

We conclude that the Thing Valley linear is the expression of a fault over 20 kilometers (12 miles) in length. Rakes of striations within the fault zone suggest oblique movement with the west block moving upward and northeastward relative to the east block (reverse right-slip fault). Possible right separation varies from 100 meters (300 feet) near the southwest end to as much as 1 kilometer (.6 mile) along the central portion of the fault.

NORTHWEST TRENDING FAULTS AND LINEARS

Several northwest trending faults and linears, related and unrelated to known faults, are prominent on satellite images of the Peninsular Ranges (Figs. 3, 4 and 5). Most of the northwest trending faults between the San Jacinto and Elsinore faults (Fig. 2) are shown on existing geologic maps

(Weber, 1963; Rogers, 1965; Sharp, 1967; Jennings, 1973) and were not studied during the present investigation. Strands of the San Jacinto fault zone appearing on Skylab images are discussed elsewhere (Merifield and Lamar, 1975ac).

Elsinore Fault

The Elsinore fault was studied because it appears to truncate or displace some of the faults and linears identified in the present study; other significant faults branch from the Elsinore fault, and discrepancies exist concerning the amount of displacement suggested for different segments of the Elsinore fault. The northwest trending Elsinore fault zone extends a distance of 200 kilometers (125 miles) from just north of the Mexican border to the northern end of the Santa Ana Mountains (Strand, 1962; Rogers, 1965). Apparent offset of facies and thicknesses within Paleocene sediments along the Elsinore fault in the area northwest of Lake Elsinore (Fig. 1) suggests 30 to 40 kilometers (20 to 25 miles) of right-slip (Lamar, 1961; Yerkes and Cambell, 1971; Sage 1973). Much smaller displacements have been reported along the southeast segment of the Elsinore fault shown on Fig. 21.

Weber (1963) has noted that basement rocks in the Julian area (Fig. 21) display only about 600 meters (2000 feet) of right separation. To the southeast, Gastil and Bushee (1961) and Hart (1964, 1974) show right separations of 760 to 2400 meters (2500 to 8000 feet) on the margins of a Bonsall Tonalite body exposed in Rodriquez Canyon (Fig. 21). Farther southeast, Dr. Robert V. Sharp (1968; personal communication, 1972) reported that displaced cataclastic zones within plutonic rocks along the margins of Vallecito Valley (Figs. 21 and 27) limit the amount of right-slip on the Elsinore fault to about 5 kilometers (3 miles) or less. The cataclastic zones are probably at least as old as Middle Cretaceous (Sharp, 1967). The possible right separation of 700-1300 meters (2300-4300 feet) on the Thing Valley fault by the south branch of the Elsinore fault (Fig. 27) is consistent with relatively small right-slip on the Elsinore fault in the Vallecito Valley area.

The discrepancy between the pre-Pliocene displacement northwest of Lake Elsinore and in the Julian-Vallecito Valley area (Fig. 21) could easily be accounted for in the 100 kilometers (60 miles) which separate the areas. Allison (1974abc) has suggested that a portion of the right-slip could be distributed on the Chariot Canyon fault which branches from the Elsinore

fault (Fig. 21). Several northwest to east-west trending faults also appear to splay off from the Elsinore fault southeast of Lake Elsinore (Fig. 1) (Mann, 1955; Rogers, 1965). Mann (1955) described stream offsets and horizontal striae on slickensided surfaces along these faults in the Temecula area. The faults studied by Mann, and other faults, continue for a number of kilometers to the southeast (Rogers, 1965); additional right-slip on the northwest portion of the Elsinore fault zone could be distributed on these faults. Detailed published maps of the area directly southeast of that described by Mann are not available. However, Rogers (1965) shows abrupt changes in basement rock type across the Agua Caliente, Lancaster, and Aguanga faults.

The topographic reflection of the Elsinore fault zone is conspicuous along the steep northeast slope of the Santa Ana Mountains to the north end of the Agua Tibia Mountains on Landsat images (Fig. 5). As seen on the Landsat images, two sharp bends or en echelon breaks occur along this segment of the fault; the most prominent is directly northwest of Lake Elsinore (see also Rogers, 1965). The trace along the southwest slope of the Agua Tibia Mountains appears as a prominent curving alignment of straight canyons and saddles. A sharp change in trend occurs at the southwest edge of the Agua Tibia Mountains, and the fault zone continues southeast along the southwest slope of the Agua Tibia Mountains and Palomar Mountain (Figs. 3, 4 and 5).

Points along the trace of the Elsinore fault to the southeast are indicated by letters on Figs. 13 and 21. The San Luis Rey River has eroded a straight canyon along the fault zone directly northwest of Lake Henshaw (Jahns, 1954b); shear surfaces and fault gouge are exposed in cuts along Highway 76 which follows the river valley (between points A and B, Fig. 13; Sects. 4 and 5, T11S; R2E). The following attitudes and rakes of striations on shear surfaces were noted from northwest to southeast:

	Strike	Dip	Rake
	N34°W	90°	0°
	N45°W	90°	8°NW
	N38°W	80°NE	11°NW
	N49°W	67°NE	23°NW
	N47°W	73°NE	None
	N38°W	87°SW	None
	N20°W	79°W	None
Average	N39°W	85°NE	11°NW

The river valley trends N51°W. Striae and grooves on shear surfaces indicate predominantly horizontal displacement.

The steep, straight, northeast facing slope along the southwest shore of Lake Henshaw trends southeast to point C. No exposures of faulted bedrock were observed along this segment of the fault zone northwest of C. Another fault (Rogers, 1965) branches from the Elsinore fault at point C and follows a straight canyon for 8.7 kilometers (5.4 miles) to the southeast (Figs. 3 and 4). Gouge 0.3 meters (1 foot) wide in this fault zone, striking N62°W and dipping 72°NE was observed in a roadcut (east side of Highway 79 directly east of point C, Fig. 13).

The Elsinore fault zone continues to the southeast along a series of straight canyon segments to point D (Fig. 13). Between points D (Fig. 13) and A (Fig. 21), the trace is less distinct on satellite images. Large-scale air photos (USDA, 1953, photo numbers AXN-7M-36 and 37) and topographic maps show a series of right-lateral stream offsets along this segment of the fault. The maximum offset observed is 600 meters (2000 feet) (Point E, Fig. 13; Sects. 13 and 14, T12S; R3E). Horizontal movement along the Elsinore fault to the northwest and southeast would not be reflected in displaced minor drainage courses because the fault underlies long straight canyons.

To the southeast, the fault zone follows the straight course of Banner Canyon to Banner (Fig. 21). A row of small offset spurs on the northeast side of Banner Canyon mark the position of one branch of the fault (Merriam, 1958). Another branch may lie beneath Banner Canyon. Hart (1964) has mapped the Elsinore fault along Rodriguez Canyon and the north side of Mason Valley to Point D (Fig. 21). Rodriguez Canyon has a more sinuous course than Banner Canyon, and the trace of this segment of the Elsinore fault is not obvious on satellite images. The Elsinore fault is well exposed at the mouth of Rodriguez Canyon (point C, Fig. 21; Sect. 20, T13S; R5E) as a 60-meter (200-foot) wide zone of shattered and slickensided blocks of schist and pegmatite dikes; striae plunging 43°S have been reported on a fault plane at this location with an attitude of N42°W, 60°N (Hart, 1974).

The trace of a southeast continuation of the Elsinore fault to Vallecito Valley (Figs. 21 and 27) would be almost entirely covered by alluvium. Moyle (1968), Hart (1974) and Lowman (1975) question whether the Elsinore fault

can be a continuous feature between Mason and Vallecito Valleys. A continuous fault would have to cut bedrock on a ridge between the valleys at Campbell Grade (E, Fig. 21, NW corner Sect. 1, T14S; R5E). Lowman (1975) shows that foliation in metamorphic rocks exposed along this ridge is uninterrupted across the inferred Elsinore fault trace as shown on existing maps (Merriam, 1955; Strand, 1962; Weber, 1963).

The branches of the Elsinore fault to the southeast in the vicinity of Agua Caliente Springs, and their relationship to the Thing Valley fault, were previously discussed. No linears are evident on satellite photographs of branches of the Elsinore fault in this area. The abrupt termination of the Elsinore fault zone as a prominent photo linear near Banner may be related to a change in the magnitude of horizontal slip along the fault at this location, as suggested by recent studies.

Henderson Canyon Linear

Henderson Canyon northwest of Borrego Springs appears as a prominent linear on satellite images (Figs. 3 and 4). However, field investigation of this feature provided no evidence of faulting. Foliation in banded gneiss (Henderson Canyon Complex of Sharp, 1967) along the central segment of Henderson Canyon trends northwest, parallel to the canyon axis; thus, it is concluded that the Henderson Canyon linear formed as a result of erosion parallel to the foliation direction.

WEST TO WEST-NORTHWEST TRENDING FAULTS AND LINEARS

In addition to the northeast to north-south trending linears, several west to west-northwest trending linears are prominent on satellite images. Most of these features do not appear on existing geologic maps; field studies were directed to a determination of their origin.

Previtt Canyon Linear

Previtt Canyon and a straight segment of Dodge Valley to the west appear as a prominent 13-kilometer (9-mile) long linear on satellite imagery (Figs. 4 and 5). The average trend of the Previtt Canyon linear is N78^{o}W. A fault with a 2-meter (6-foot) breccia zone striking N75^{o}W and dipping 60^{o}S is exposed about 50 meters (160 feet) northwest of the intersection of Chihuahua Valley Road and the stream channel in Previtt Canyon (Warner Springs Quadrangle, Sect. 19. T9S; R3E). Identical granitic rocks occur on either

side of the linear in Previtt Canyon, and a number of small faults with variable attitudes were observed in nearby roadcuts. No dominant joint directions were noted, and foliation is not consistent with the linear. Insufficient data are available to determine the origin of this linear.

Warren Canyon Fault

A straight, east-west trending segment of Warren Canyon and an alignment of canyons and saddles to the east form a prominent 10.7-kilometer (6.6-mile) long linear appearing on Skylab (Fig. 11) and Landsat (Fig. 12) images along the south sides of Woodson Mountain and Santa Maria Valley (Fig. 13). This feature was previously called the Ramona fault (Merifield and Lamar, 1974). The western end, between points A and B (Fig. 13), appears as a prominent linear on large-scale air photos (USDA, 1953, photo numbers AXN-9M-31 and 32, 79 and 80, 143 and 144); the eastern portion, between points B and H, is indistinct on large-scale air photos (USDA, 1953, photo numbers AXN-5M-181 and 182, AXN-9M-31 and 32). The east end of the linear appears to terminate against the possible southern extension of the Pamo Valley linear at Daney Canyon (Fig. 13).

Bedrock exposed along the Warren Canyon linear consists of Woodson Mountain and Wolford Granodiorite (Gastil and Bushee, 1961). Joint directions in granodiorite along the western half of the linear are predominantly parallel and orthogonal to the linear. Because of heavy brush and soil, natural exposures are lacking in the canyons along the linear. The only exposure of bedrock observed is located in a roadcut at the head of Warren Canyon on the south side of Highway 67 (west edge Sect. 35, T13S; R1W). A 3-meter (10-foot) wide, gray clay gouge zone is present about midway in a zone of breccia and shear surfaces at least 30 meters (100 feet) wide. The surfaces are spaced .3 to 1 meter (1 to 3 feet) apart and trend N80°E; striae on one shear surface have a rake of 88° east. Based on this exposure, we conclude that the Warren Canyon linear is predominantly fault-controlled; erosion along joints may have also contributed to its origin. There are no bedrock contacts in the vicinity to determine the sense and direction of possible fault displacement; however, the total displacement is probably not large because similar rocks are exposed on both sides of the fault.

Woodson Mountain Linear

An 8.8-kilometer (5.5-mile) long east-west alignment of straight canyons and saddles can be seen on Skylab (Fig. 11) and Landsat (Fig. 12) images and on large-scale air photographs (USDA, 1953, photo numbers AXN-9M-30 and 31, 80 and 81, 142 and 143) along the north side of Woodson Mountain. Bedrock exposed on both sides of the linear consists of Woodson Mountain Granodiorite (Merriam, 1946). Woodson Mountain is a prominent, elongated topographic high with east-west trending linears along the north and south flanks; evidence of faulting was observed along the Warren Canyon linear on the south flank. No evidence of faulting was observed in exposures in the canyon along the trace of the Woodson Mountain linear at point A (Fig. 13) (Sect. 28, T13S; R1W). Because of heavy brush and soil cover, there are no exposures of bedrock along the remainder of the linear trace. Joint directions in granodiorite are predominantly parallel and orthogonal to the linear (Fig. 13), and erosion along joints may have been the principal cause of this feature.

San Vicente Valley Linear

An east-west trending break in slope on the north flank of a hill directly north of San Vicente Valley, aligned with a series of straight canyon segments and saddles to the east, appears as a prominent linear on satellite images (Figs. 11 and 12). Bedrock exposed along the western segment of the linear consists of Wolford Granodiorite and Stonewall Quartz Diorite (Merriam, 1946). Weber (1963) and Rogers (1965) show a fault along the western portion of this feature. Exposures are not adequate to confirm faulting at this location. The east end of the San Vicente Valley linear crosses and does not displace the Witch Creek and Himmel Canyon linears and the contact between Woodson Mountain Granodiorite and Stonewall Quartz Diorite (Fig. 15). Although the San Vicente Valley linear is aligned with the Warren Canyon fault to the west (Fig. 13), no evidence of faulting was observed. The average joint directions are parallel and orthogonal to the linear, and this linear probably formed as a result of erosion along joints.

Hatfield Creek Linear

A fairly straight, east-west trending, 6.1-kilometer (3.8-mile) long change in tone from dark gray on the south to light gray on the north can

be seen on space photographs (Figs. 11 and 12) along the south side of Hatfield Creek (Fig. 13). Bedrock along the Hatfield Creek linear consists of Lakeview Tonalite (Merriam, 1946). Bedrock is covered by soil and vegetation along the linear trace. Neither foliation nor joint directions are parallel to the linear (Fig. 13). The straightness of the canyon side appearing on satellite imagery has been accentuated by a boundary between cultivated fields on the north and natural vegetation on the south. Although the origin of the straight, south side of the canyon is unknown, there is no evidence for fault control.

Loveland Reservoir and Pine Creek Linears

The Loveland Reservoir linear is expressed by gently curving valleys continuing for about 10 kilometers (6 miles) in a west-northwest direction. Roughly parallel to this linear, but beginning 3 kilometers (2 miles) southeast of its eastern termination, is a 5-kilometer (3-mile) linear along Pine Creek (Figs. 22 and 23). Both of these linears are parallel to well-developed foliation and intrusive contacts between Woodson Mountain Granodiorite and Green Valley Tonalite (Everhart, 1951). The linears are covered over most of their length, but available exposures were examined where the linears cross ridge crests; no evidence of faulting was observed. The possibility of faulting cannot be excluded. However, when intrusive contacts are parallel to the linear, faulting is difficult to confirm; additional field study might produce evidence for, or against, faulting.

Barrett Lake Fault

The most prominent west-northwest trending linear on Skylab and Landsat photos is a 40-kilometer (25-mile) long fault mapped by Weber (1963); the central portion of the fault passes through Barrett Lake (Figs. 22 and 23). Weber (personal communication, 1975) did not determine the amount and sense of slip. Color aerial photos at a scale of 1/24,000 (San Diego County, 1970, photo numbers 18-7 to 18-9) were studied in an attempt to establish the sense of slip and select areas where field work would be most useful. The fault was found exposed at two locations along the linear: 0.5 kilometer (0.3 mile), and 2 kilometers (1.2 miles) west of Barrett Lake. In roadcuts at the first location, the fault zone consists of gouge and breccia

7 meters (23 feet) wide containing slickensided shear surfaces. The following attitudes of shear surfaces and rakes of striations were measured:

	Strike	Dip	Rake
	N65°E	90°	18°W
	N45°W	70°S	50°W
	N75°W	70°S	9°W
	N35°W	60°S	75°W
	N55°W	60°S	30°E
	EW	75°S	4°W
	N75°W	37°S	0°
Average	N66°W	60°S	18°W

The striae suggest oblique movement; however, owing to the lack of distinctive lithologic contacts, the sense of slip and cumulative displacement are indeterminate.

Otay Mountain Linear

The Otay Mountain linear appears as a remarkably straight series of aligned tributary drainage courses and saddles across the south slope of Otay Mountain (Figs. 22 and 23). The 9.7-kilometer (6.0-mile) long linear trends east-west, perpendicular to the principal south flowing drainage courses. Pre-batholitic volcanic rocks exposed along the linear consist of mildly metamorphosed flows, tuffs, and volcanic breccias designated the Black Mountain Volcanics (Jurassic and/or Triassic) (Strand, 1962).

Owing to extremely dense chaparral and rugged terrain, access to the Otay Mountain linear is practically limited to exposures near the two dirt roads at the east and west ends (Fig. 31). Along the east end of the linear, a fault is inferred by an apparent 200-meter (600-foot) left separation of a greenish-gray volcanic agglomerate (location A on Fig. 31). In the prominent saddle (location B) on the ridge immediately to the west, thin-bedded, slaty, gray andesite (?) with a thinly banded wavy flow structure appears to strike abruptly into thick-bedded massive gray andesite (?) north of the linear. On the slope west of the saddle, an exposure of highly fragmented, bleached volcanics may represent fault breccia. However, because of the irregularities of contacts within volcanic rocks and abrupt vertical and lateral changes in texture and structure within flows, the existence of a fault cannot be positively established.

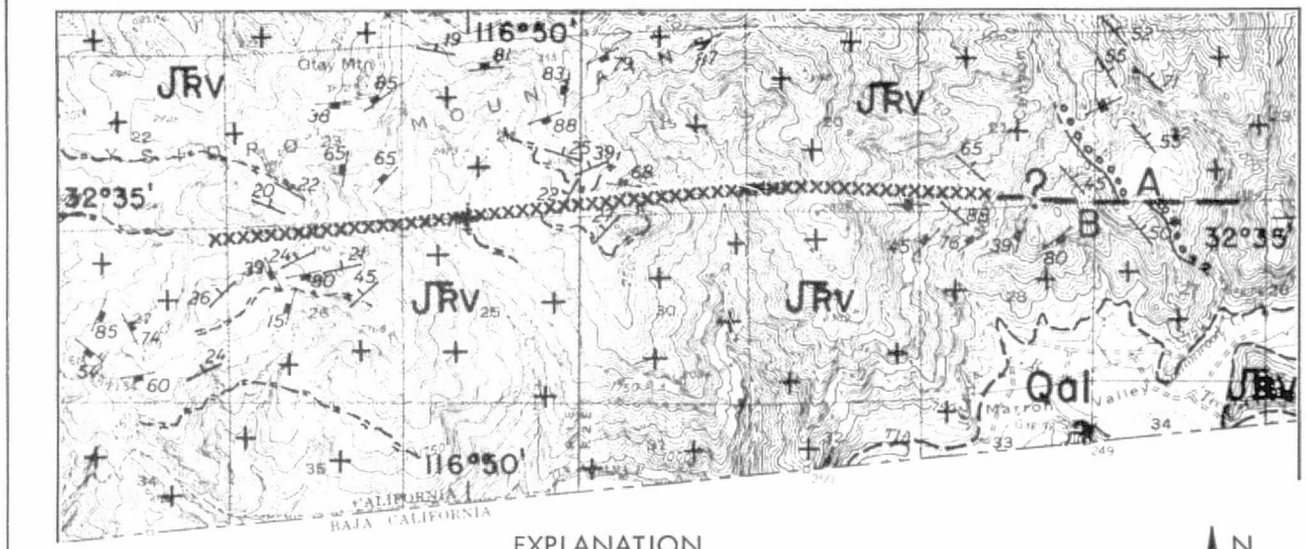

EXPLANATION

Rock Unit and Age

Qal — Alluvium, Quaternary

JRV — Black Mountain Volcanics, Jurassic and/or Triassic

Resistant volcanic flow mappable on 1:20,000 scale aerial photos

Base of greenish-gray agglomerate

Contact

70 — Attitude of bedding

80 — Attitude of jointing

Vertical jointing

?/A — Inferred fault, letters refer to description in text

xxxxxx — Photo linear

N

0 1 Miles

0 1 Kilometers

Fig. 31 - Geologic map of Otay Mountain linear. Topography from U.S. Geological Survey Jamul Quadrangle. See Fig. 6 for area covered.

West of these exposures, study of large-scale aerial photos (USDA, 1953, photo numbers AXN-3M-18 to 22) suggests the offset or truncation of several resistant flows, but poor access and lack of distinctive marker beds make substantiating field evidence difficult to obtain. The Otay Mountain linear is not parallel to foliation. Although east-west jointing is present in the Black Mountain Volcanics, it is not the dominant direction. Because the Otay Mountain linear is a remarkably straight feature, it is unlikely that it originated simply as a result of the coincidental alignment of canyon segments and saddles. However, field data are insufficient to establish a fault origin.

Canyon City Fault

A prominent linear on Skylab and Landsat images extends for about 11 kilometers (7 miles) through the towns of Potrero and Canyon City (Figs. 22 and 23). The linear, which consists of a series of valleys, has a trend of N70-80°W and is essentially parallel with the Barrett Lake fault mapped by Weber (1963). For comparison, an RB-57 photo is reproduced in Fig. 32. The prominent Barrett Lake fault is readily apparent in the Landsat image (Fig. 23), as well as the Skylab (Fig. 22) and RB-57 images. The less prominent Canyon City linear can be seen about as well in the Skylab and RB-57 images, but is much less apparent in the Landsat image. Bedrock consists entirely of plutonic rocks of the southern California batholith, including Bonsall Tonalite, Woodson Mountain Granodiorite, small bodies of San Marcos Gabbro (Rogers, 1965), and granitic pegmatite dikes. Consistent foliation north of the linear trends northeast to east-northeast. Two conspicuous valleys eroded along the foliation north of the linear are visible on the satellite images and are indicated on the geologic map (Fig. 33). South of the linear, foliation is mostly east-west and forms discontinuous ridges and valleys. The most prominent joints trend north and northeast.

Fault gouge and breccia in a zone up to 4 meters (13 feet) wide are exposed along the solid line on Fig. 33 in roadcuts on the north side of Highway 94. This fault was previously referred to as the Potrero fault (Merifield and Lamar, 1974, 1975a; Lamar and Merifield, 1974) and has been renamed because of prior use of "Potrero fault" in the Newport-Inglewood structural zone (Barrows, 1974). Slickensided shear surfaces in the fault

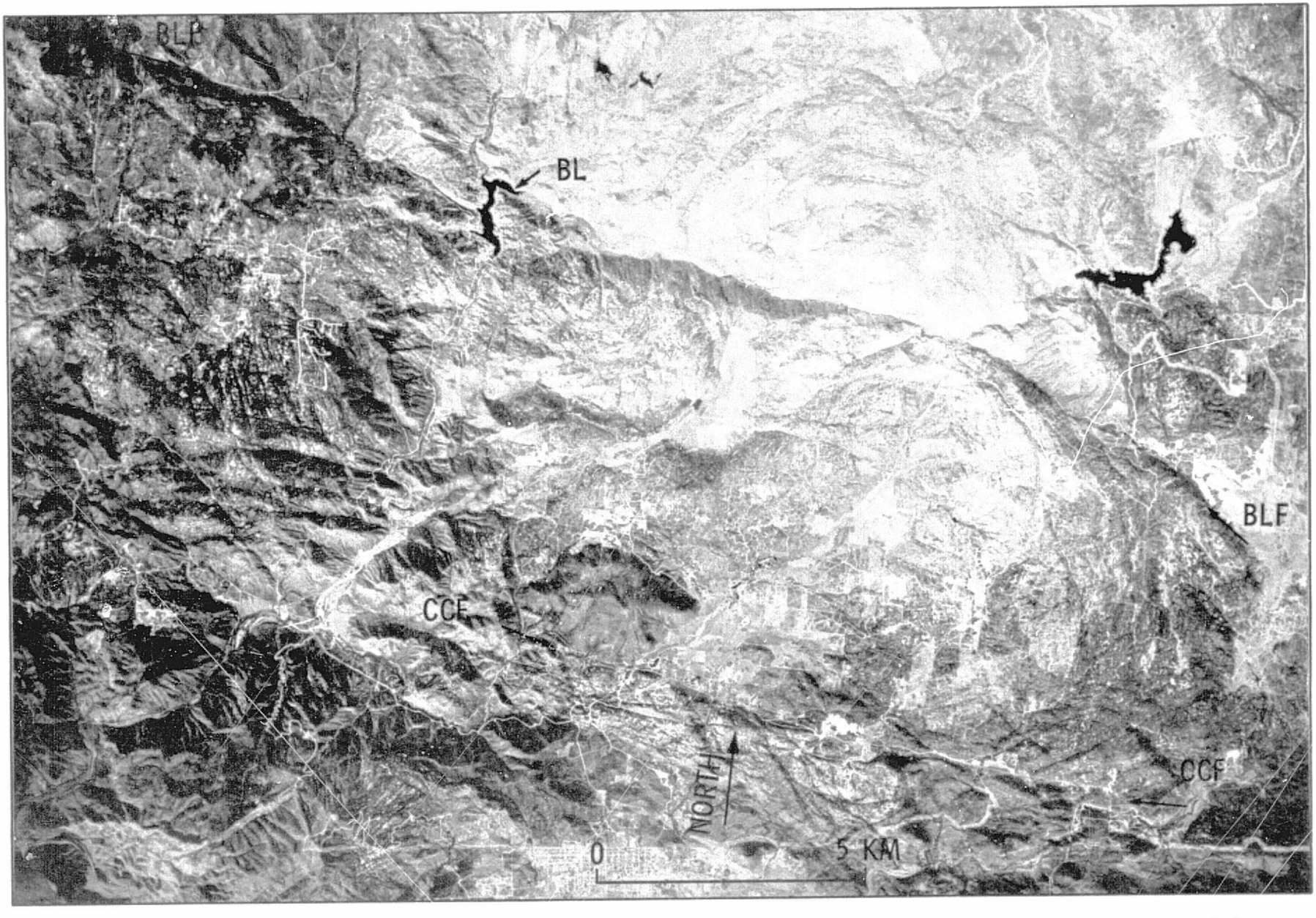

Fig. 32 - Portion of NASA/MSC aerial photo number 49-4013, Mission 164, April, 1971, showing the Barrett Lake and Canyon City faults. Abbreviations: BL: Barrett Lake; BLF: Barrett Lake fault; CCF: Canyon City fault. See Fig. 6 for area covered.

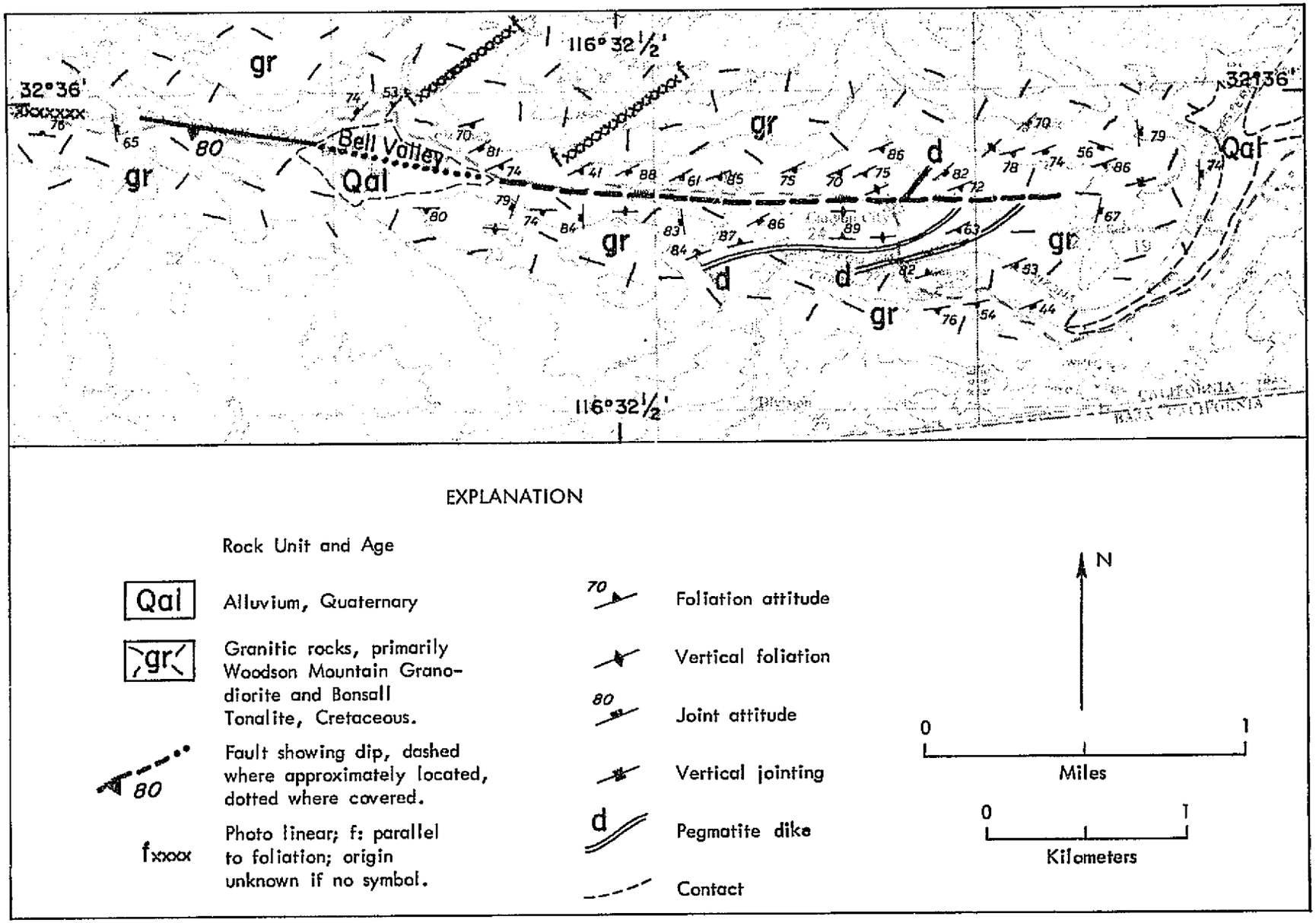

Fig. 33 - Geologic map of Canyon City fault. Topography from U.S. Geological Survey Potrero Quadrangle. See Fig. 6 for area covered.

zone strike N70°W and dip 80°S; rakes of 75°E and 10°E were measured on striations on shear surfaces. The fault could not be traced west of the solid line on Fig. 33, but a linear valley approximately aligned with the fault extends about 3 kilometers (2 miles) west of the area shown. Bedrock exposures along the linear to the west are obscured by valley alluvium and thick soil cover. The westernmost segment of the linear coincides with the straight contact between San Marcos Gabbro exposed on Potrero Peak and Woodson Mountain Granodiorite to the south (Strand, 1962). No exposures of the contact were observed, although color difference between deep red-brown clay soil on gabbro and light gray granular soil on granodiorite appears at the surface.

In the vicinity of Canyon City, at the east end of the fault, a number of granitic pegmatite dikes parallel foliation. Two of these dikes, varying in thickness from 0.3-1.0 meters (1-3 feet), can be mapped for a distance of greater than one kilometer. To the east, these dikes appear to terminate at the fault (Fig. 33).

Evidence for the Canyon City fault can be summarized as follows: (1) exposures of gouge, breccia and slickensided shear surfaces parallel to the linear directly west of Bell Valley; (2) twenty to thirty degrees difference in the strike of foliation in granitic rocks on either side of the fault; and (3) the apparent truncation of two granitic pegmatite dikes 0.5 kilometer (0.3 miles) east of Canyon City. Correlation of lithologic units across the fault has not been possible; hence, the amount and sense of slip is unknown.

STRIKE OF FAULTS EXPOSED IN ROADCUTS

Roadcuts in basement rock throughout the portion of the Peninsular Ranges covered by Fig. 2 were examined to determine the attitude of fault zones and the rake of striations on slickensided shear surfaces. The exposures were selected for their well-developed fault zones rather than for any relation to linears on the Landsat and Skylab images. These observations were combined with measurements on the specifically studied individual faults and are summarized on Fig. 34. The observations were made to determine if there is any relationship between the directions of individual fault zones and the linear trends (Fig. 35). With the exception of the northeast trend, no close relationships are apparent.

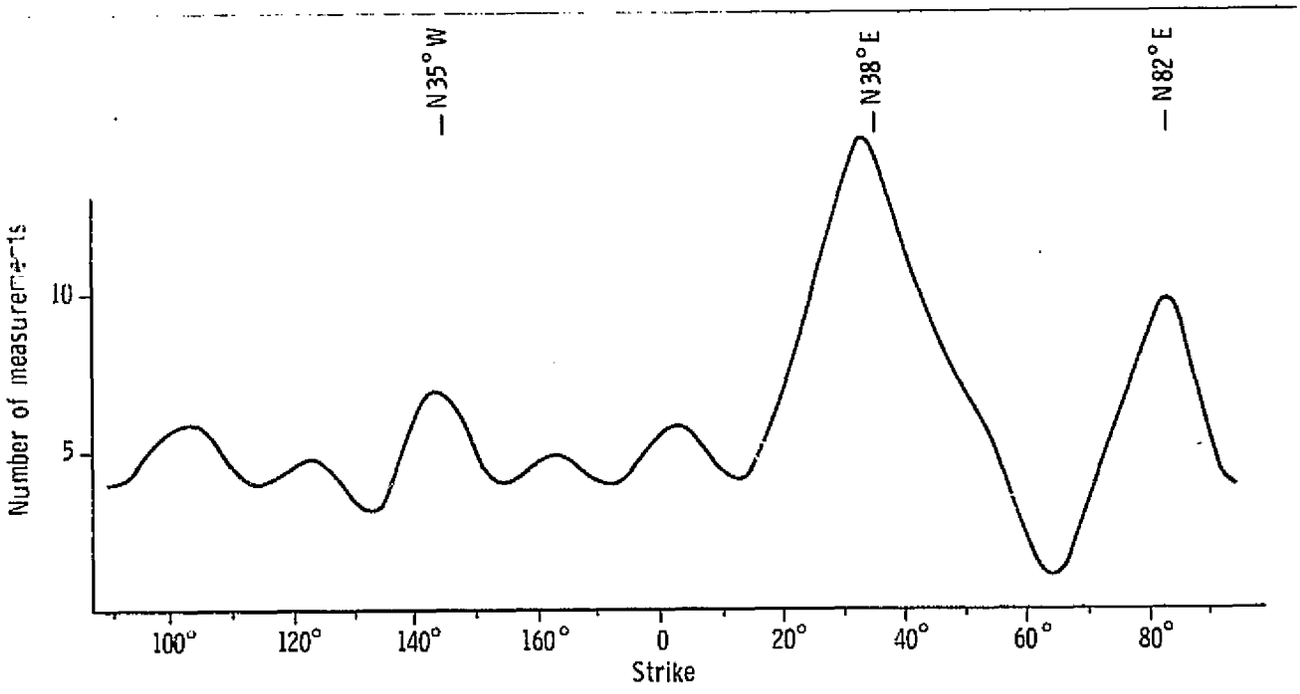

Fig. 34 - Shear zone directions, Peninsular Ranges of southern California, 109 strikes, 10° intervals.

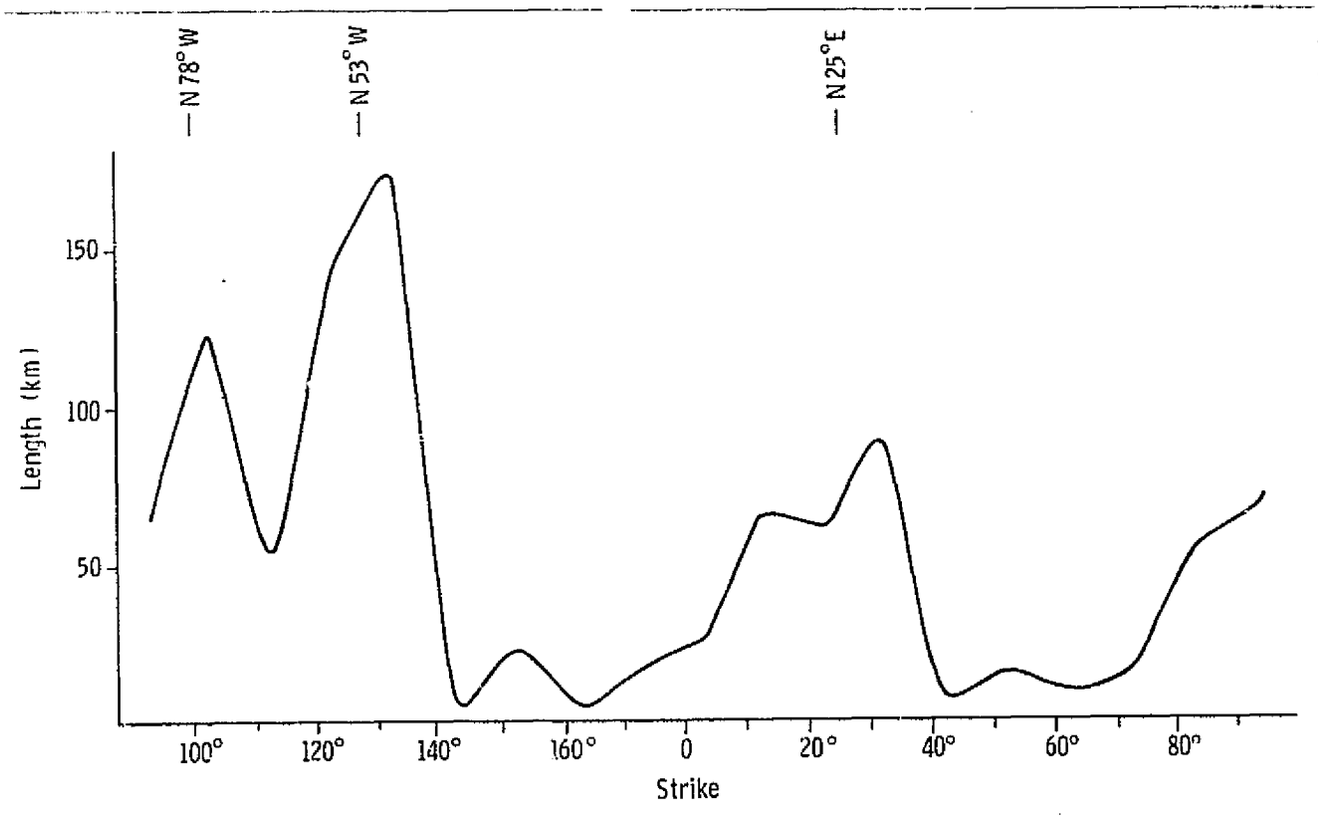

Fig. 35 - Directions of linears shown in Fig. 3 (Merifield and Lamar, 1974) length vs. strike, 10° intervals.

EARTHQUAKE RISK IN PENINSULAR RANGES, SOUTHWESTERN CALIFORNIA

A practical objective of this investigation is to contribute to a better understanding of the earthquake risk in southwestern California by analysis of satellite imagery. The northwest trending faults in the northeast portion of the area studied show geomorphic evidence of recent movement, and destructive earthquakes have occurred on the San Jacinto fault in historic time. Estimated earthquake recurrence intervals on the Elsinore and San Jacinto faults (Lamar, Merifield and Proctor, 1973) are based in part on the average slip rate from data on offset geologic units. However, owing to inconsistencies in reported displacement for different segments, estimates of the earthquake recurrence interval on the Elsinore fault are especially questionable.

The relatively small displacement reported on the southern portion of the Elsinore fault appears to be inconsistent with the large displacement reported on the northern portion. However, north of Lake Elsinore, the fault zone is comparatively narrow. South of Lake Elsinore, displacement is very likely spread over the broad zone of sub-parallel faults in the Lake Henshaw region, notably the Agua Caliente, Aguanga and Agua Tibia faults. Furthermore, if additional right-slip can be attributed to the recently investigated Chariot Canyon fault, small displacement on the Elsinore fault in Vallecito Valley is understandable.

The large right-slip reported along the northwestern segment of the Elsinore fault may be distributed on several branching faults to the southeast. We conclude that the risk of a damaging eathquake is greater along the northwestern portion of the Elsinore fault. Here strain may be accumulating within a narrow zone and may be released in the form of large, infrequent earthquakes, whereas to the southeast, strain may be accumulating on several faults branching over a wide area. The epicenter map (Fig. 36) indicates that strain is being released as frequent small earthquakes over a wide area east of the southeastern segment of the main fault. During the same period, the northwestern segment has been relatively quiescent.

The northeast and east-west trending faults and linears conspicuous on satellite images appear to be the most significant tectonic features of the Peninsular Ranges between the Elsinore fault and the post-batholithic sedimentary rocks to the southwest. Information on the amount and sense of

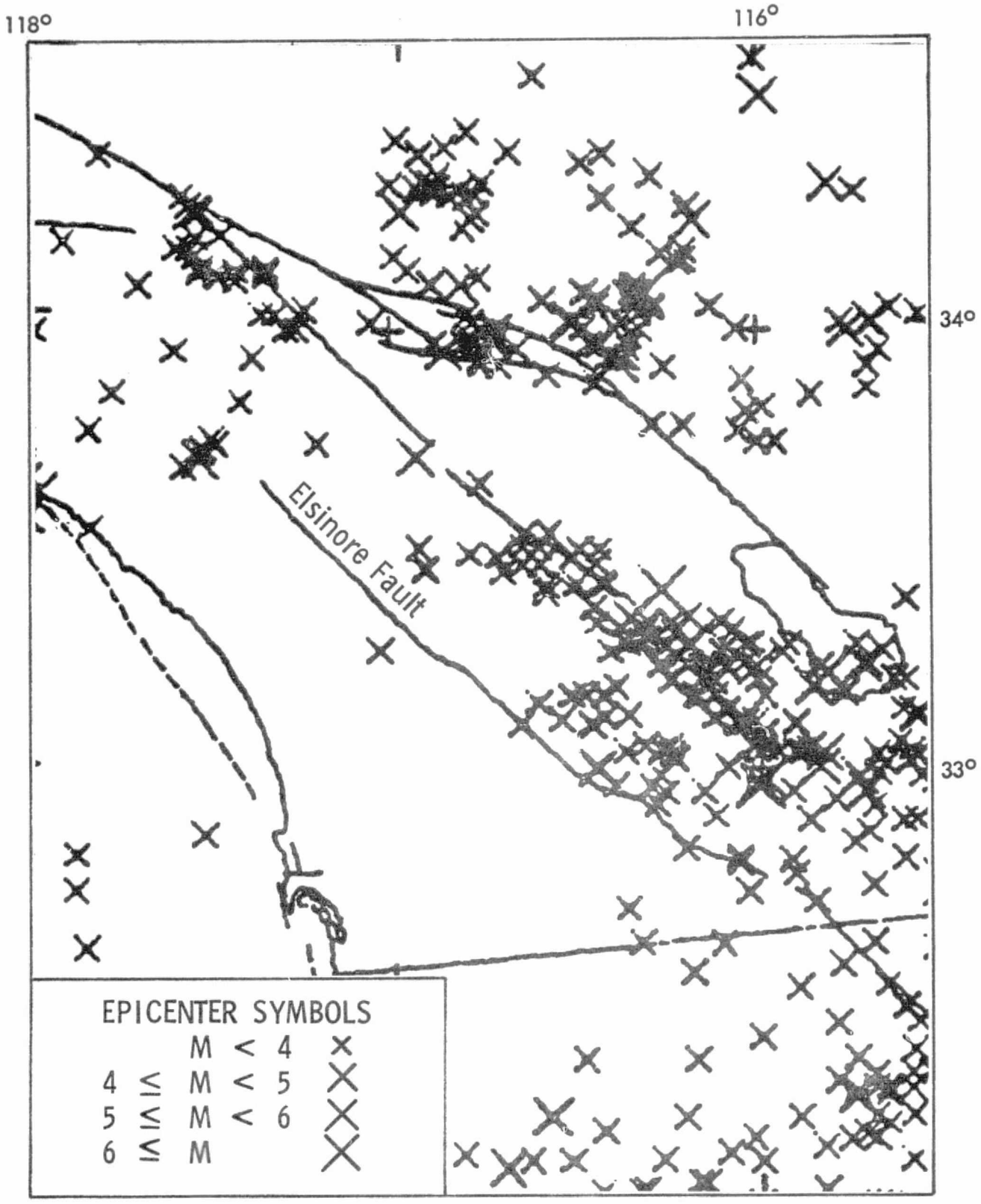

Fig. 36 - Seismic events equal to or greater than Magnitude 4, 1932-1972 (from Hileman, et al, 1973).

displacement on these faults is incomplete, but speculation on their history and tectonic significance is justified in order to evaluate their earthquake generating potential and seismic risk.

The northeast and east-west trending faults are steeply dipping and possess well-developed breccia zones and slickensided shear surfaces. Rakes of striations on shear surfaces suggest oblique movement. Offsets of steeply dipping contacts by the northeast trending Thing Valley and San Diego River faults suggest right-slip, and deformation may also have occurred in the form of flexuring or shear folding in a right-slip sense on the Sweetwater River linear and across portions of the San Diego River and Thing Valley faults. The sense of slip on the east-west trending faults has not been established. The apparent left separation of a volcanic unit on the Otay Mountain linear could be due to left-slip or vertical slip. The Sweetwater River linear appears to be displaced in a left sense by the Pine Creek linear. But faulting has not been demonstrated on the Pine Creek linear, nor can it be shown that the Sweetwater River linear was ever a continuous feature. Additional detailed mapping in the Pine Creek area, and along the Barrett Lake fault, could provide information on the sense of slip along the east-west faults.

The northeast trending faults are truncated by the active northwest trending faults, and the Thing Valley fault appears to be offset in a right lateral sense 700-1300 meters (2300-4300 feet) by the south branch of the Elsinore fault. Right slip on the northeast trending faults is in the wrong sense for these features to be related to right-slip on the active northwest trending faults. We found no geomorphic evidence of recent displacement on the northeast and east-west faults, and the epicenter map (Fig. 36) shows no seismic activity during the past 40 years in the area cut by these faults. The lack of recent activity and limited data on the slip direction could be explained if the northeast and east-west faults represent conjugate shears related to an older stress system. East-northeast, west-southwest crustal shortening is consistent with the fault pattern, right slip on the Thing Valley and San Diego River faults, and conjectural left-slip on the Otay Mountain and Pine Creek linears. On the basis of north-south trending thrust faults and mylonitic zones, Sharp (1968) has also suggested an earlier period (Middle Cretaceous to Eocene?) of east-west crustal shortening in the

eastern Peninsular Ranges. The plate tectonic model of a subduction zone parallel to the continental margin during the Mesozoic (Hamilton, 1969; Hill, 1971) is also consistent with earlier east-west crustal shortening. Based on these arguments, we conclude that the northeast and east-west trending faults are inactive and not likely to generate earthquakes.

APPLICABILITY OF SATELLITE IMAGERY TO FAULT AND EARTHQUAKE HAZARDS STUDIES

The perspective afforded by satellite images quickly focuses attention on prominent linears which are not obvious in larger scale photography or on the ground. Our study has concentrated only on the most prominent linears which are here represented, for the most part, by deeply eroded valleys. Consequently, they are equally apparent on the lower resolution Landsat images and on Skylab photos. The utility of the higher resolution Skylab imagery in distinguishing active from inactive faults has been described elsewhere (Merifield and Lamar, 1975ac). There may be a general relationship between the distinctness of recently active strike-slip faults in the images and the amount of horizontal slip. The northwestern segment of the Elsinore fault, where 30-40 kilometers (20-25 miles) of right slip has been reported, is very distinct on the images, whereas the southeastern segment with 1-3- kilometers (0.6-2 miles) of right-slip is not well defined. Additional research is required to determine if this relationship has general application.

It should be emphasized that linears prominent on satellite photos result from erosion along foliation and joints as well as faults. The coincidental alignment of unrelated features may also give the appearance of faults. Care must be taken to distinguish between linears of fault and non-fault origin and to avoid unsubstantiated extensions of faults and connections between discontinuous fault segments. Detailed field investigations are required to establish the origin of any linears. The nature of the evidence for the origin of the linear should be documented so that subsequent investigators can more intelligently plan detailed studies. This is particularly important because of the current stringent requirements of seismic risk evaluations for critical structures.

The perspective also enables fault patterns to be viewed in a single image; this is useful in understanding regional relationships and the relative ages of faults. The truncation of the east-west and northeast trending fault sets by the active northwest trending right-slip faults in the Peninsular Ranges is evident in Skylab and Landsat imagery. This relationship, along with the lack of seismicity and geomorphic indications of recent movement, has led to the inference that the northeast and east-west faults belong to an inactive strain system. We conclude that in areas such as southwestern California, where the geology has been previously mapped on a reconnaissance scale, Skylab and Landsat imagery can reveal unrecognized faults and clarify regional fault relationships. Several unreported faults were identified during our investigation, and new information relating to the tectonic history of the Peninsular Ranges was acquired. These faults will be plotted on updated versions of the "Fault Map of California", compiled by the California Division of Mines and Geology (C. W. Jennings, personal communication, October 29, 1975). Study of Skylab and Landsat images can greatly increase the efficiency of fault investigations and should precede the study of larger scale imagery and detailed field investigations.

SUGGESTIONS FOR FUTURE WORK

Our investigation of linears on Skylab and Landsat images covered a large area, and insufficient time was available to obtain all of the data necessary for a complete evaluation of satellite images of the region. Such an analysis would contribute to a data base for estimating the percentage of linears due to faulting, foliation, jointing and other origins. Our field work was necessarily concentrated on the most accessible segments of the most prominent linears, and time considerations prevented a thorough investigation of the features which were studied. Several less prominent linears in the study area were not investigated (Fig. 2). We believe, however, that our investigation demonstrates the usefulness of satellite imagery to the analysis of fault tectonics and earthquake hazards of the region, and our experience thus far will permit more efficient investigation of the unstudied features.

Additional field work and study of large-scale aerial photos of the following features should be accomplished:

1. Study of linears shown on Fig. 2 as not investigated to determine their geologic characteristics and origin.

2. Detailed investigation of the intersection of the Pine Creek and Sweetwater River linears for evidence of faulting and possible left displacement of Sweetwater River linear by Pine Creek linear.

3. Additional investigation of Barrett Lake fault to determine sense of slip. This study and item 2 are important in determining the probable age and earthquake generating potential of the east-west faults in the area.

4. Additional work along the Thing Valley and Chariot Canyon faults and Loveland Reservoir and Otay Mountain linears to more fully determine their characteristics.

Our investigations have provided information on the origin and significance of prominent linears in the basement terrane of the Peninsular Ranges, southwestern California. Conspicuous linears also appear on satellite images of similar terrane in the Sierra Nevada and Transverse Ranges to the north, and on the southern extension of the Peninsular Ranges into Baja California. Regional tectonics and seismic hazards would be better understood if linears in the basement terranes of these areas were investigated by the methods pursued in this study.

ACKNOWLEDGMENTS

The work reported herein was accomplished under NASA Contract NAS 2-7698 and U.S. Geological Survey Contract 14-08-0001-13911. Technical monitoring was provided by David Amsbury of NASA and Ernest Lathram of the U.S. Geological Survey whose interest and helpful suggestions are gratefully acknowedged. The project grew out of discussions with Paul Lowman, NASA-Goddard Space Flight Center. We wish to acknowledge valuable discussions with Richard Merriam, Harold Weber, Victoria Todd, Gordon Gastil, and Mason Hill; David Amsbury and Mason Hill critically read the manuscript, and Richard Merriam kindly loaned us his unpublished field maps of the Thing Valley area. Mac Parkins of the Soil Conservation Service loaned USDA air photographs of the region. The assistance of several students at the University of California is also acknowledged, particularly that of Thomas Troutman, Thomas Davis and Jerry Treiman. Photographs for this report were prepared by Roy Stratton,

and negatives of the Landsat images were generated from digital tapes by Jeannine Lamar at the Jet Propulsion Laboratory. The manuscript was typed by Velma Furchner and edited by Ruth Merifield. The drafting was done by Helen Cushman.

REFERENCES

Allison, M. L., 1974a, Geophysical studies along the southern portion of the Elsinore fault: M.S. thesis, San Diego State University, 229 p.

Allison, M. L., 1974b, Tectonic relationship of the Elsinore fault zone and the Chariot Canyon fault, San Diego County, California: Abstracts with program, Geol. Soc. Amer., Cordilleran Section, p. 138.

Allison, M. L., 1974c, Geologic and geophysical reconnaissance of the Elsinore-Chariot Canyon fault systems: in Guidebook prepared for the December 14 and 15, 1974, field trip of the San Diego Association of Geologists, p. 21-35.

Darrows, A. G., 1974, A review of the geology and earthquake history of the Newport-Inglewood structural zone, southern California: Calif. Div. Mines and Geol., Spec. Report 114, 115 p.

Buttram, G. N., 1962, The geology of the Agua Caliente Quadrangle, California: M.S. thesis, Univ. of Southern Calif.

California Department of Water Resources, 1967, Ground water occurrence and quality: San Diego Region: Calif. Dept. Water Res. Bull. 106-2, 233 p.

Everhart, D. L., 1951, Geology of the Cuyamaca Peak Quadrangle, San Diego County, California: Calif. Div. Mines and Geol., Bull. 159, p. 51-115.

Fitzurka, M., 1968, Geology of a portion of the San Diego River Valley, California: Senior thesis, San Diego State Univ.

Gastil, R. G. and Bushee, J., 1961, Geology and geomorphology of eastern San Diego County: in Guidebook for Field Trips, Geol. Soc. Amer., Cordilleran Section, p. 8-22.

Gastil, R. G., Phillips, R. P., and Allison, E. C., 1971, Reconnaissance Geologic Map of the State of Baja California: Geol. Soc. Amer., scale 1:250,000.

Hamilton, W., 1969, Mesozoic California and the underflow of Pacific mantle: Geol. Soc. Amer., Bull., v. 80, p. 2409-2430.

Harding, T. P., 1974, Petroleum traps associated with wrench faults: Amer. Assoc. Petrol Geol. Bull., v. 58, p. 1290-1304.

Hart, M. W., 1964, The Elsinore fault between Banner Grade and Vallecito Valley, San Diego County, California: San Diego State Univ. Geol. Dept. Undergraduate Research Reports, v. 8, pt. 3, 14 p.

Hart, M. W., 1974, Field guide road log: in Guidebook prepared for the December 14 and 15, 1974 field trip of the San Diego Association of Geologists, p. 5-9.

Hileman, J. A., Allen, C. R., and Nordquist, J. M., 1973, Seismicity of the southern California region, 1 January 1932 to 31 December 1972: Seismological Lab., Calif. Inst. Technology.

Hill, M. L., 1971, Newport-Inglewood zone and Mesozoic subduction, California: Geol. Soc. Amer., Bull., v. 82, p. 2957-2962.

Jahns, R. H., 1954a, Geology of the Peninsular Ranges Province, Southern California and Baja California: in Calif. Div. Mines and Geol., Bull. 170, Ch. 2, p. 29-52.

Jahns, R. H., 1954b, Geologic guide to northern part of the Peninsular Range Province: in Calif. Div. Mines and Geol. Bull. 170, 59 p.

Jennings, C. W., 1973, State of California preliminary fault and geologic map, scale 1:750,000: Calif. Div. Mines and Geol., Preliminary Report 13.

Lamar, D. L., 1961, Structural evolution of the northern margin of the Los Angeles basin: Ph.D. thesis, Univ. Calif., Los Angeles, 142 p.

Lamar, D. L. and Merifield, P. M., 1974, Investigation of lineaments on Skylab and ERTS images of Peninsular Ranges, southwestern California: CalESCO Technical Report 74-5, 13 p.

Lamar, D. L. and Merifield, P. M., 1975, Application of Skylab and ERTS imagery to fault tectonics and earthquake hazards of Peninsular Ranges, southwestern California: CalESCO Technical Report 75-2.

Lamar, D. L., Merifield, P. M., and Proctor, R. J., 1973, Earthquake recurrence intervals on major faults in southern California: in Geology, Seismicity and Environmental Impact, Assoc. Eng. Geol., Spec. Publ., p. 265-276.

Larsen, E. S., Jr., 1948, Batholith and Associated Rocks of Corona, Elsinore, and San Luis Rey Quadrangles, Southern California: Geol. Soc. Amer. Memoir 29.

Lowman, P. D., 1969, Apollo 9 multispectral photography: geologic analysis: NASA Goddard Space Flight Center, Greenbelt, Md., X-644-69-423.

Lowman, P. D., 1975, The Elsinore fault of southern California: evidence against strike-slip displacement: Jour. of Geology, in press.

Mann, J. F., 1955, Geology of a portion of the Elsinore fault zone, California: Calif. Div. Mines and Geol., Spec. Report 43, 22 p.

Merifield, P. M., and Lamar, D. L., 1974, Lineaments in basement terrane of the Peninsular Ranges, southern California: presented at First International Conference on New Basement Tectonics, in press in Proceedings volume, also CalESCO Technical Report 74-1.

Merifield, P. M. and Lamar, D. L., 1975a, Active and inactive faults in southern California viewed from Skylab: presented at the NASA Earth Resources Survey Symposium June 8-13, 1975, Houston, Texas, in: Proceedings Volume, NASA TM X-58168, JSC-09930, p. 779-797.

Merifield, P. M. and Lamar, D. L., 1975b, Faulting in basement terrane, San Diego County, California: in Studies on the Geology of Camp Pendleton and Western San Diego County, California, San Diego Association of Geologists, p. 51-55.

Merifield, P. M. and Lamar, D. L., 1975c, Faults on Skylab imagery of the Salton Trough area, Southern California: CalESCO Technical Report 75-1.

Merriam, R., 1946, Igneous and metamorphic rocks of the southwestern part of the Ramona Quadrangle, San Diego County, California: Geol. Soc. Amer. Bull., v. 57, p. 223-260.

Merriam, R., 1954, Geologic map 10: in Geologic guide to northern part of the Peninsular Range Province: in Calif. Div. Mines and Geol. Bull. 170, 59 p.

Merriam, R., 1955, Geologic map of Cuyapaipe Quadrangle, California, scale 1:62,500: unpublished map (Cuyapaipe Quad. presently designated Mt. Laguna Quad.).

Merriam, R., 1958, Geology and mineral resources of Santa Ysabel quadrangle, San Diego County, California: Calif. Div. Mines and Geol., Bull. 177, 42 p.

Miller, W. J., 1935, Geomorphology of the southern Peninsular Range of California: Geol. Soc. Amer., Bull., v. 46, p. 1535-1562.

Moyle, W. R., Jr., 1968, Water wells and springs in Borrego, Carrizo, and San Felipe Valley areas: Calif. Dept. Water Res., Bull. 91-15, 76 p.

Proctor, R. J., 1973, Map showing major earthquakes and recently active faults in the southern California region: in Geology, Seismicity and Environmental Impact, Assoc. Eng. Geol., Special Publ.

Rogers, T. H., 1965, Geologic map of California, Santa Ana Sheet: Calif. Div. of Mines and Geol.

Sage, O. G., Jr., 1973, Paleocene geography of the Los Angeles region: in Proc. Conf. on Tectonic problems of the San Andreas Fault System, Stanford Univ. Publ., Geol. Sci. v. XIII, p. 348-357.

Sauer, C., 1929, Land forms in the Peninsular Range of California as developed about Warner's Hot Springs and Mesa Grande: Univ. Calif., Pubs. in Geography, v. 3, p. 199-290.

Scheliga, J. T., Jr., 1963, Geology and water resources of Warner Basin, San Diego County, California: M.S. thesis, Univ. of Southern Calif.

Sharp, R. V., 1967, San Jacinto fault zone in the Peninsular Ranges of southern California: Geol. Soc. Amer., Bull., v. 78, p. 705-730.

Sharp, R. V., 1968, The San Andreas fault system and contrasting pre-San Andreas structures in the Peninsular Ranges of southern California: in Proc. Conf. on Geologic Problems of the San Andreas Fault System, Stanford Univ. Publ., Geol. Sci., v. XI, p. 292-293.

Strand, R. G., 1962, Geologic map of California, San Diego-El Centro Sheet: Calif. Div. of Mines and Geol.

Weber, F. H., 1963, Geology and mineral resources of San Diego County, California: Calif. Div. Mines and Geol., county report 3, 309 p.

Yerkes, R. F., and Campbell, R. H., 1971, Cenozoic evolution of the Santa Monica Mountains-Los Angeles basin area: U.S. Geol. Survey, open file report.

PART III

THE GARLOCK FAULT: AN EXAMPLE OF THE ABILITY OF EREP IMAGERY TO RESOLVE INDICATORS OF ACTIVE FAULTS

by

P. M. Merifield and D. L. Lamar

PREFACE

The appearance of the Garlock fault on Skylab 190B imagery was studied as a part of a broader investigation to apply Skylab images to the analysis of fault tectonics and earthquake hazards of southern California. Although the Garlock fault is outside the original test area (Fig. 1, Part I), it was chosen for study because a variety of indicators of recent fault movement are prominently displayed. This report was presented at the NASA Earth Resources Survey Symposium, June 8-13, 1975, Houston, Texas, and appears in the Proceedings Volume (Merifield and Lamar, 1975).

CONTENTS

ILLUSTRATIONS

INTRODUCTION

It is generally assumed that future movement will occur on faults that have been active in the recent past. Movement in Holocene time (past 11,000 years) is a commonly accepted criterion for classifying a fault as active although faults showing displacement since late Quaternary time should probably also be considered active for some purposes (Wentworth and Yerkes, 1971). In addition to the historic record and stratigraphic relationships, certain topographic features are useful indicators of recent movement. These include scarps, benches, linear ridges, shutter ridges, linear valleys (in recent sediments), undrained depressions, ponded alluvium and offset drainage; these features are illustrated in Fig. 1. Although their preservation will vary depending on climatic conditions and rock type, at most locations these features probably would be obliterated by erosion or deposition in 11,000 years. They need to be evaluated with care in order to differentiate them from fault-line scarps, fault-line valleys, notches and apparent offset streams (trellis drainage), all of which could have been formed along ancient faults by differential erosion.

S-190B IMAGE OF GARLOCK FAULT

The ability of the Skylab 190B camera to resolve indicators of recent movement is examined along the section of the Garlock fault shown on the index map in the Introduction and Summary Section of this report (Part I, Fig. 1). Although movement on the Garlock fault has not occurred in historic time, it should be considered active because of physiographic evidence of recent displacement. The following features previously described by Clark (1973) are visible on the enlarged Skylab image (Fig. 2): offset drainage, depressions, linear valleys, linear ridges, shutter ridges and faceted ridges. Other features with relief on the order of one meter are not visible. Comparison with Clark's map indicates that scarps and ridges down to perhaps 5 meters or less in height can be seen when aided by shadow. Topographic indicators of recent faulting possess a wide range in scale; depressions may be measured in kilometers and scarps in centimeters. But a large proportion of them fall into the range of meters to tens of meters and are, therefore,

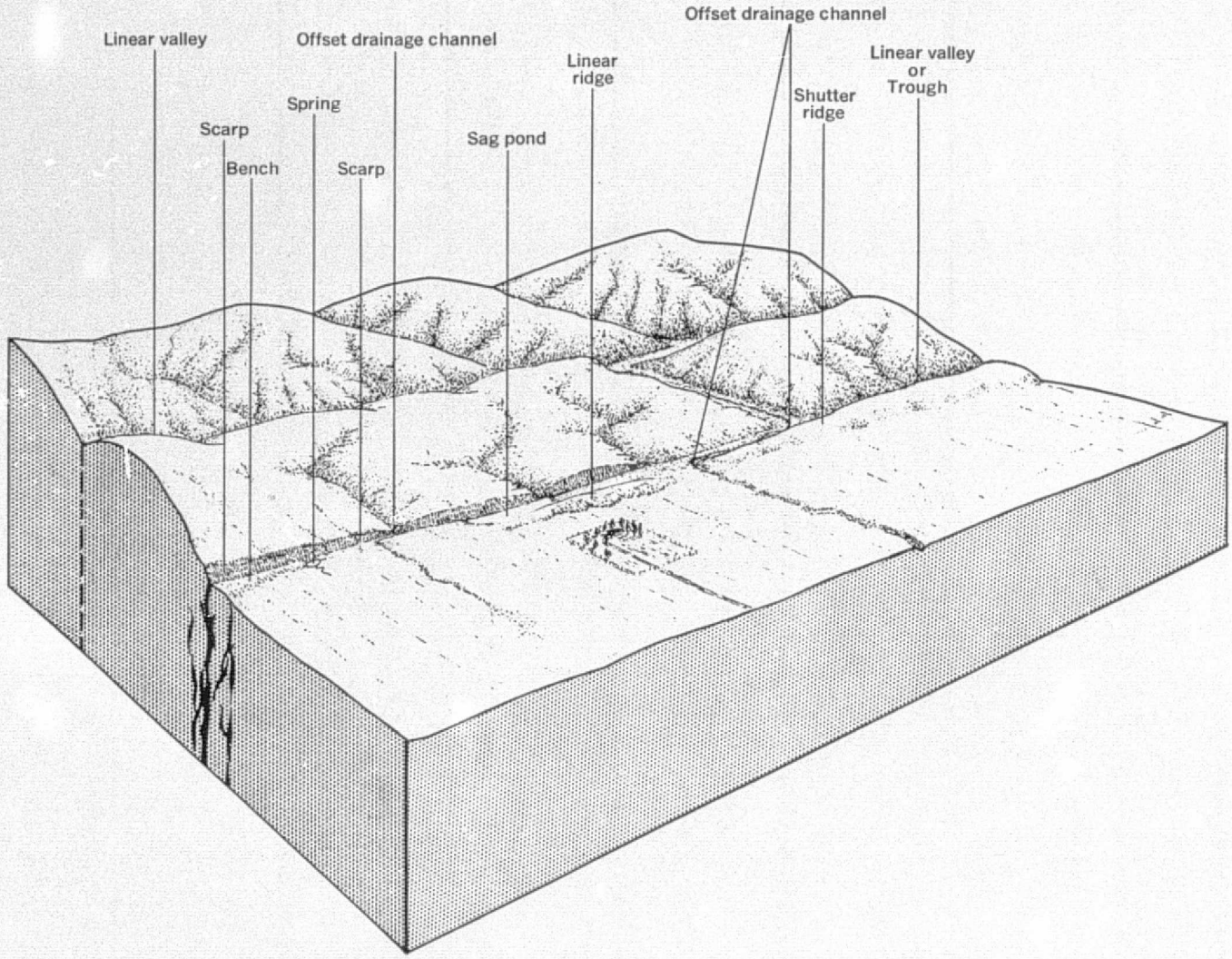

Fig. 1 - Block diagram showing landforms produced along recently active faults, from Vedder and Wallace (1970).

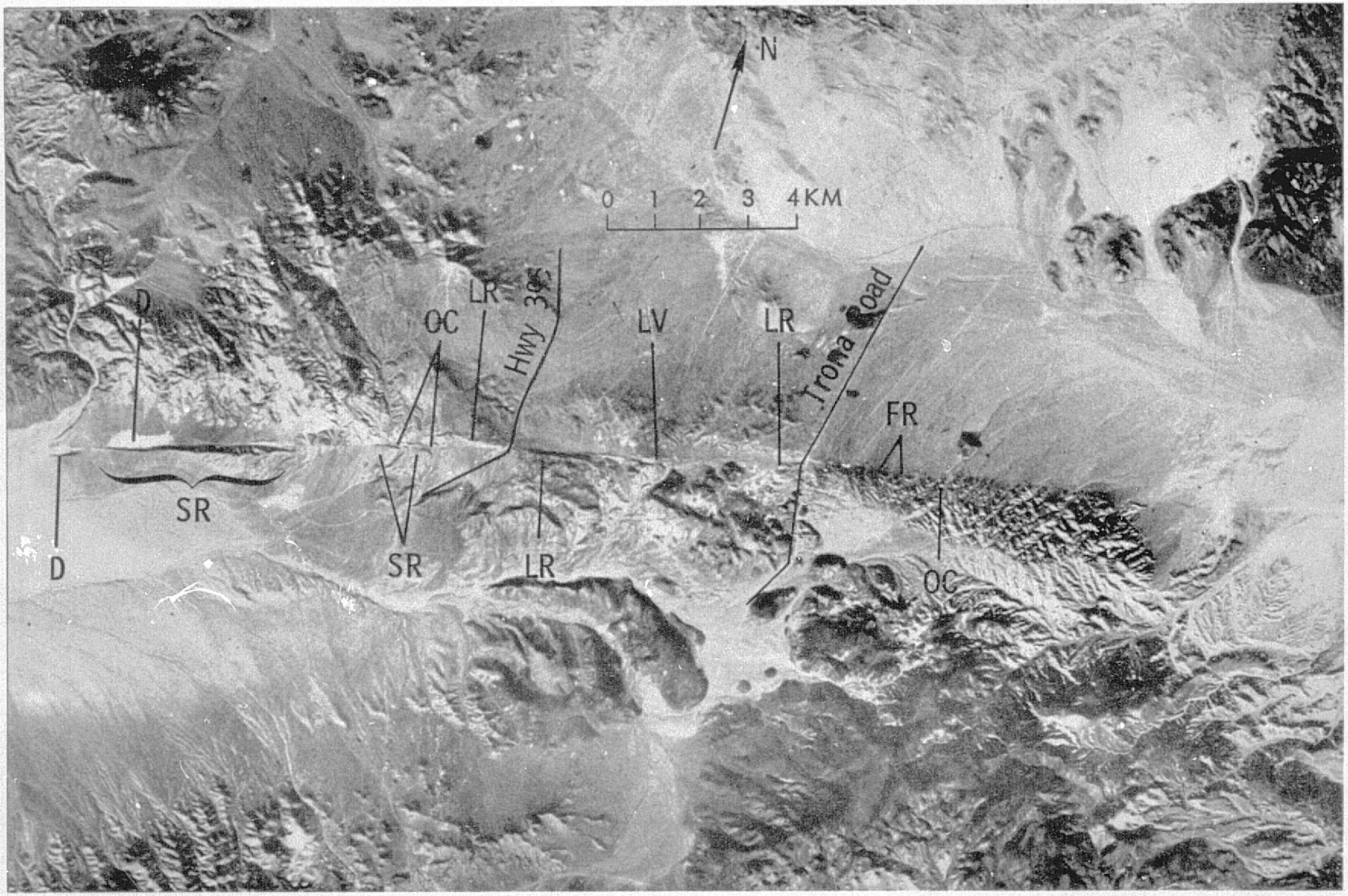

Fig. 2 - Portion of Skylab 4, 190B camera, Roll 92, Frame 347 (original in natural color) showing geomorphic indicators of recent movement on Garlock fault south of Trona, California. Abbreviations: D: depression; FR: faceted ridges; LR: linear ridge; LV: linear valley; OC: offset channel; SR: shutter ridge.

resolved by the 190B camera with an estimated spatial resolution of about 10-20 meters (ca. 30-60 feet). The 190A camera, with a resolution of around 30 meters (ca. 100 feet), resolves a large percentage of these features, but is less suitable for this purpose.

REFERENCES

Clark, M. M., 1973, Map showing recently active breaks along the Garlock and associated faults, California: U. S. Geol. Survey Misc. Inv. Map I-741.

Merifield, P. M., and Lamar, D. L., 1975, Active and inactive faults in southern California viewed from Skylab: presented at the NASA Earth Resources Survey Symposium, June 8-13, 1975, Houston, Texas, in Proceedings Volume, NASA TM X-58163, JSC-09930, p.779-797.

Vedder, J. G., and Wallace, R. E., 1970, Map showing recently active breaks along the San Andreas and related faults between Cholame Valley and Tejon Pass, California: U. S. Geol. Survey, Misc. Geol. Inv., Map I-574.

Wentworth, L. M., and Yerkes, R. F., 1971, Geologic setting and activity of faults in the San Fernando area, California: in San Fernando, California, earthquake of February 9, 1971; U. S. Geol. Survey Prof. Paper 733, p. 6-16.

PART IV

FAULTS ON SKYLAB IMAGERY OF THE SALTON TROUGH AREA, SOUTHERN CALIFORNIA

by

P. M. Merifield and D. L. Lamar

PREFACE

The regional geologic structure displayed on Skylab photos of the Salton Trough area was studied as part of a broader investigation to apply Skylab images to the analysis of fault tectonics and earthquake hazards of southern California. This research was sponsored by the NASA Lyndon B. Johnson Space Center. A portion of this report was presented at the NASA Earth Resources Survey Symposium, June 8-13, 1975, Houston, Texas and appears in the Proceedings Volume (Merifield and Lamar, 1975a). This material was previously presented in preliminary form in CalESCO Technical Report 75-1 (Merifield and Lamar, 1975b).

CONTENTS

ILLUSTRATIONS

ABSTRACT

Long segments of previously mapped major high-angle faults in the Salton Trough area are readily identifiable on Skylab images. Along active faults, distinctive topographic features such as scarps and offset drainage, and vegetation differences due to ground water barriers in alluvium are visible. Other fault-controlled features along inactive as well as active faults visible in Skylab photography include straight mountain fronts, linear valleys, alignment of saddles and lithologic differences producing contrasting tone, color or texture. A fault in the San Andreas set, inferred by recent geophysical work in northwest Sonora, may be indicated by the regional alignment of possible fault-controlled features. This postulated fault is largely covered by Holocene deposits, principally windblown sand; therefore, subsurface exploration would be necessary to verify its existence. Another northwest trending fault is suggested on Skylab photos by tonal change in cultivated fields across Mexicali Valley. Surface evidence for this fault has not been observed; however, the linear may be caused by differences in soil conditions along an extension of a segment of the San Jacinto fault zone. No field evidence of faulting could be found along linears which appear as possible extensions of the Substation and Victory Pass faults, demonstrating that the interpretation of linears as faults in small-scale photography must be confirmed or disproved by field investigations. The principal advantage of Skylab images for regional fault studies is the synoptic view which makes regional alignments of structural features apparent. The high resolution is an additional advantage because many distinctive fault-controlled topographic features can be identified.

INTRODUCTION

The Salton Trough extends from the upper Coachella Valley north of the Salton Sea to the Gulf of California; the regional structure is dominated by the northwest trending San Andreas and San Jacinto fault zones (Fig. 1). The structure of the Salton Trough is of considerable current interest partially because of the region's potential for geothermal energy and the uncertainty concerning southeastern extension of the San Andreas fault zone. The objective of this paper is to describe the application of Skylab imagery to improved knowledge of the location and history of movement on faults in the Salton Trough area.

Photos of the Salton Trough taken from Skylab provide a remarkable overview which aids in the interpretation of the regional relationship between structural features. Each frame from the 190A camera covers 163 km x 163 km (100 mi x 100 mi); 23 cm x 23 cm (9 in x 9 in) enlarged transparencies used in interpretation have a scale of about 1:7,000. A photo interpretation of faults and linears appearing on Skylab images of the region between the north end of the Salton Trough and the Gulf of California was accomplished. Features identified in this study, and the areas covered by the Skylab images utilized, are shown in Fig. 2, and the individual Skylab images and overlays are reproduced as Figs. 3, 4, and 5. Detailed investigations consisting of field studies and aircraft overflights of critical locations were concentrated in the area north of the Salton Sea covered by Figs. 3 and 5. South of the Salton Sea, reconnaissance studies were made of linears which may represent previously unrecognized fault segments along the trends of the San Andreas and San Jacinto fault zones.

SAN ANDREAS FAULT

The San Andreas fault, the major tectonic feature of California, extends for nearly 1000 kilometers (600 miles) southeasterly from the Pacific Ocean near Cape Mendocino to at least a point approximately midway along the eastern shore of the Salton Sea (Fig. 1). The fault is the most recent surface rupture within a zone of roughly parallel fractures that branch and interlace within a zone as much as 10 kilometers (6 miles) wide (Crowell, 1962). The group of major faults roughly parallel to the San Andreas fault in southern California, such as the San Jacinto and Elsinore, are included in the San Andreas fault

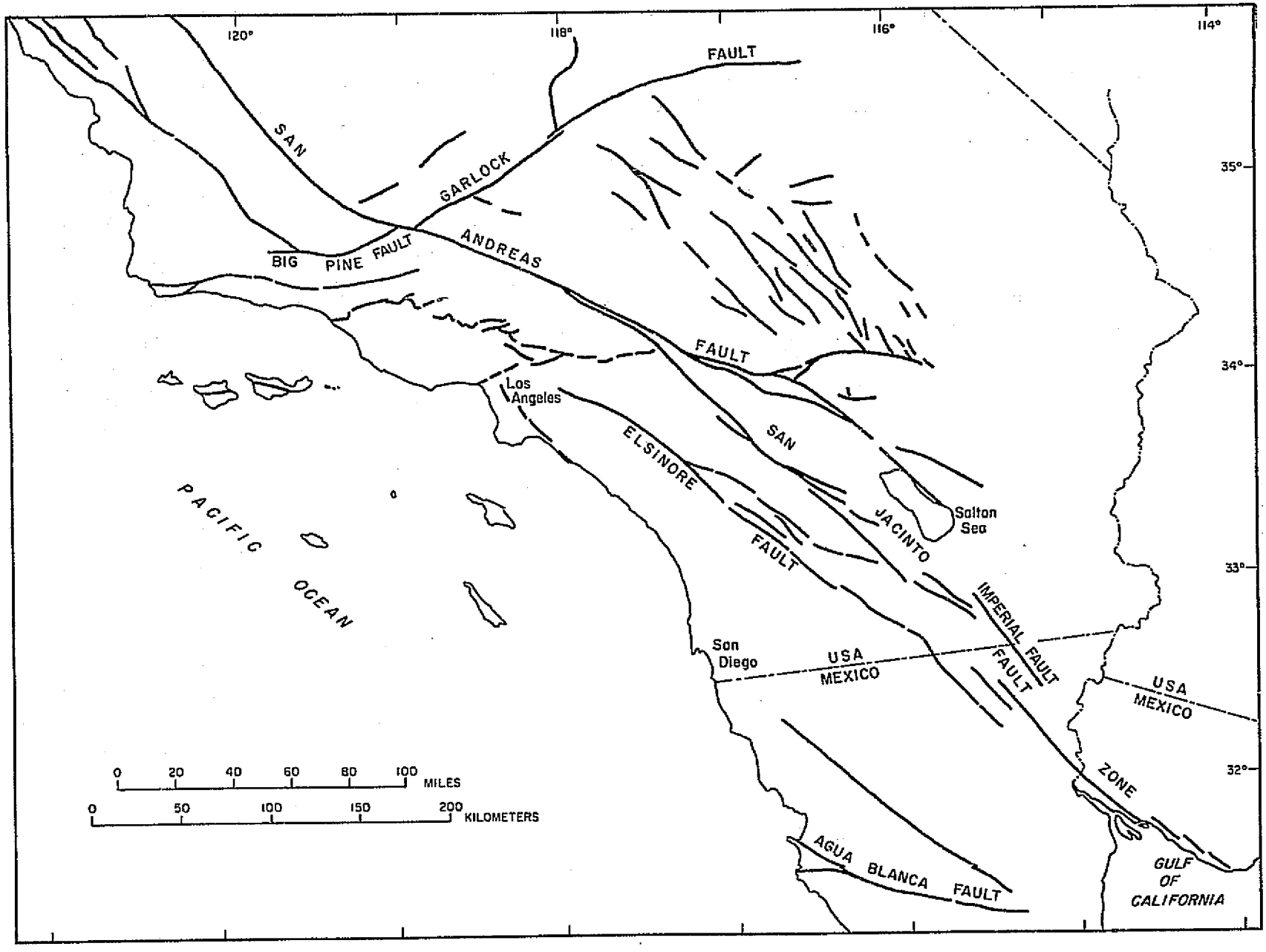

Fig. 1 - Map showing major faults in southern California and northern Mexico. Redrawn from Proctor (1973).

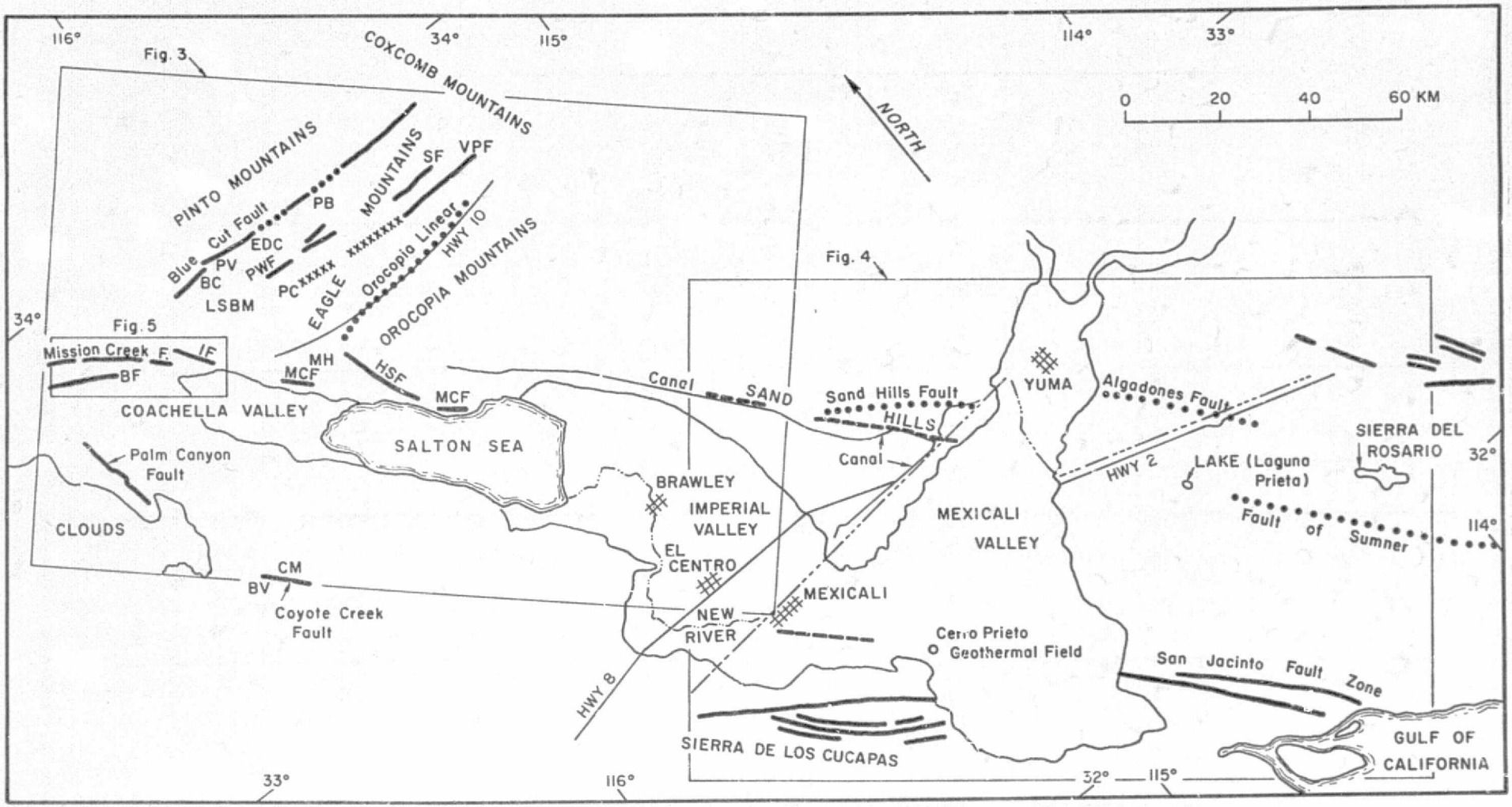

Fig. 2 -- Map of Salton Trough and vicinity showing faults and linears seen on Skylab images or discussed in text. The outlines of Skylab images included in this report are indicated. Explanation: solid line: photo linear coincident with known fault or fault line scarp; dashed line: photo linear related to possible surface expression of fault; dotted line: covered fault; xxx: photo linear with no evidence of faulting. Abbreviations: BC: Blue Cut; BF: Banning fault; BV: Borrego Valley; CM: Coyote Mountain; EDC: El Dorado Canyon; HSF: Hidden Springs fault; IF: Indio fault; LSBM: Little San Bernardino Mountains; MCF: Mission Creek fault; MH: Mecca Hills; PB: Pinto Basin; PC: Pinkham Canyon; PV: Pleasant Valley, PWF: Porcupine Wash fault; SF: Substation fault; VPF: Victory Pass fault.

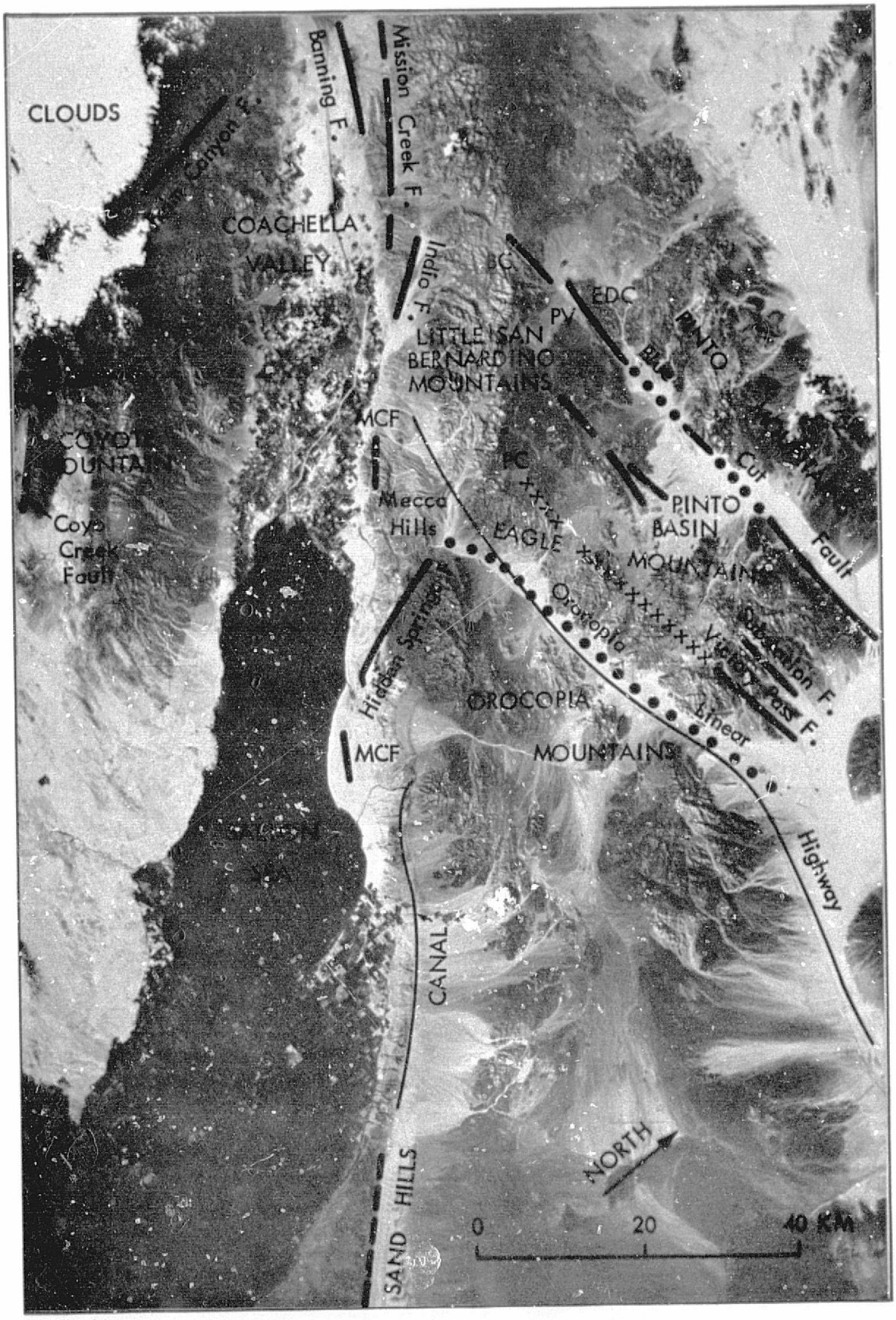

Fig. 3 - Salton Sea and vicinity. Portion of Skylab 4, 190A camera, Roll 76, Frame 82 (original in natural color). Abbreviations: BC: Blue Cut; BV: Borrego Valley; EDC: El Dorado Canyon; MCF: Mission Creek fault; PC: Pinkham Canyon; PV: Pleasant Valley.

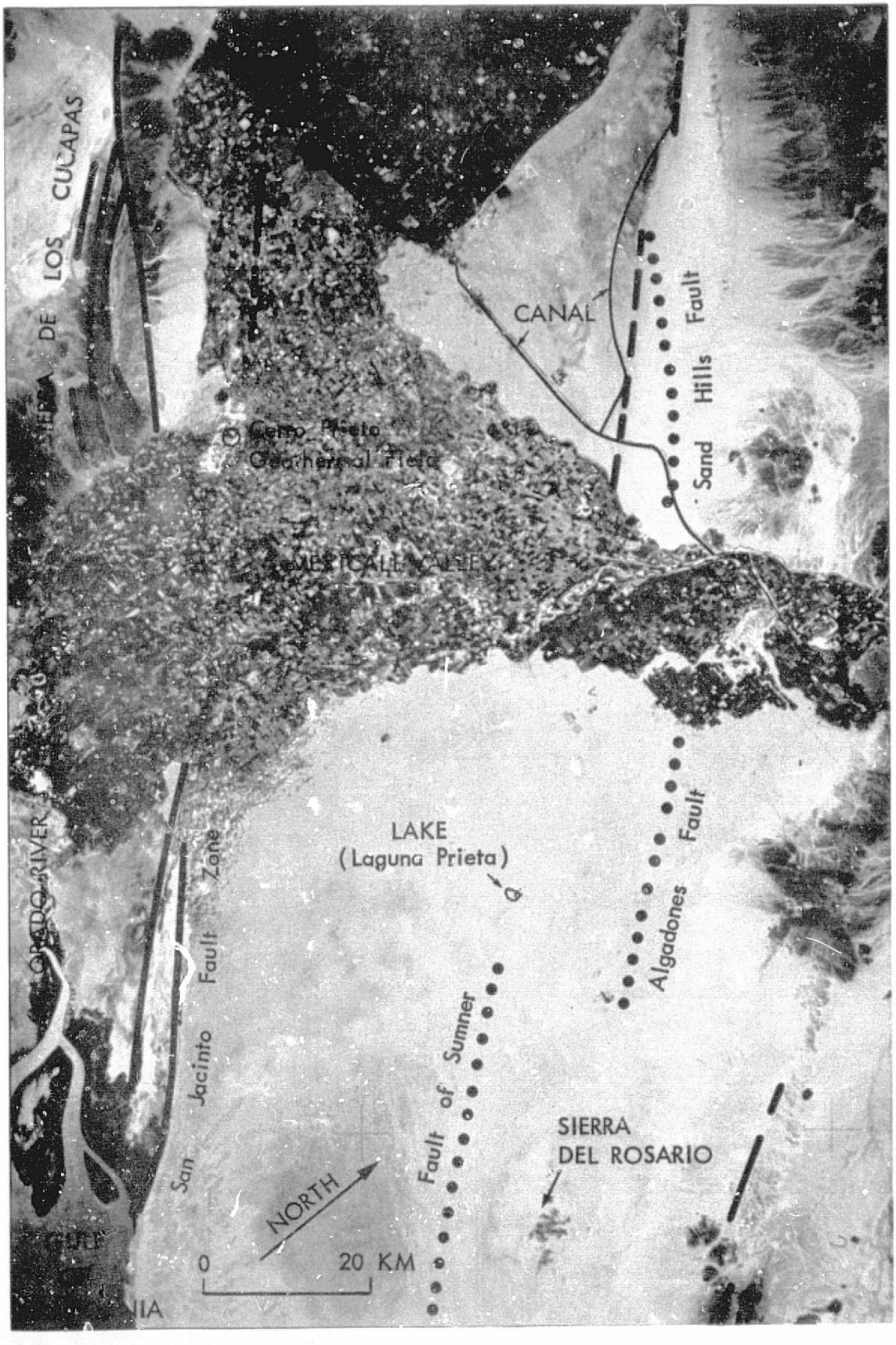

Fig.4 - Salton Trough between Gulf of California and Imperial Valley. Portion of Skylab 2, 190A camera, Roll 4 Frame 134 (original in natural color). See Fig. 2 for features identified.

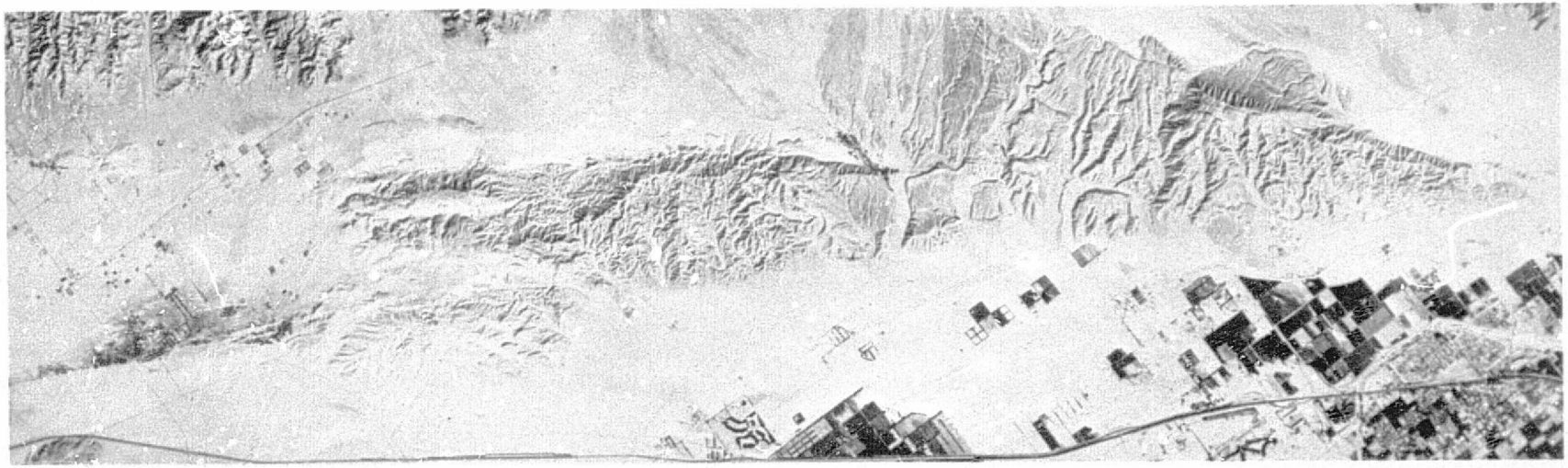

Fig.5 - Indio Hills and vicinity. Enlarged portion of Skylab 4 image, 190B camera, Roll 92, Frame 352 (original in natural color) See Fig.6 for features identified.

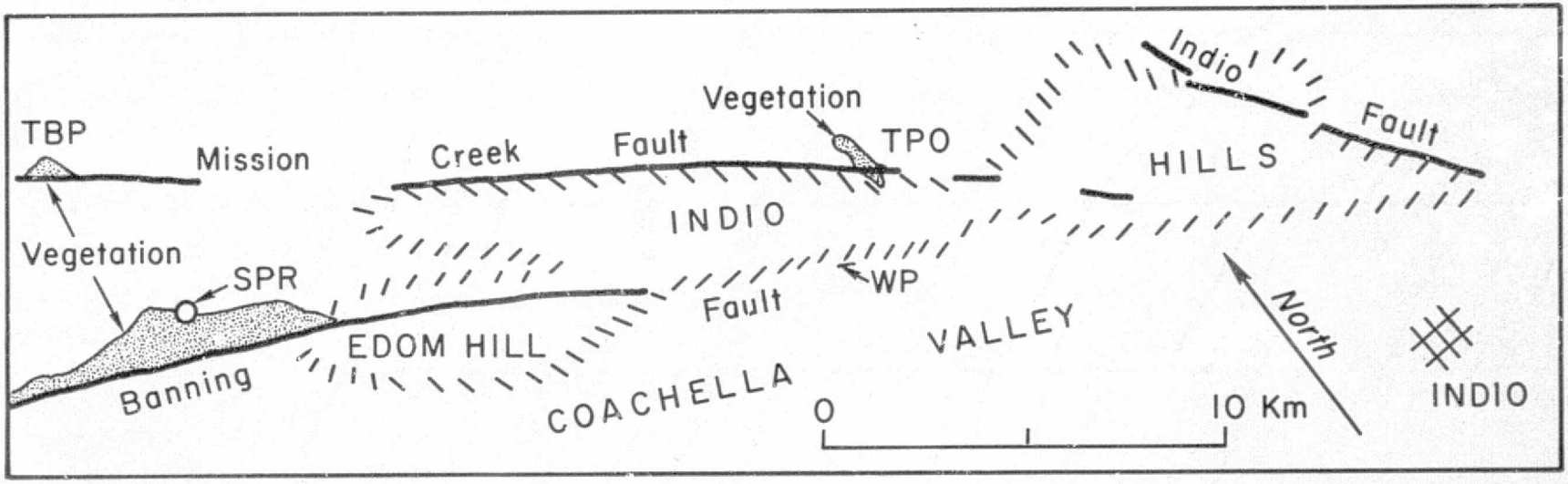

Fig.6 - Map of Indio Hills and vicinity showing features identified on Fig.5. Solid lines indicate prominent linear features along faults discussed in text. Hachured lines indicate boundaries of physiographic features. Abbreviations: SPR: Seven Palms Ranch; TBP: Two Bunch Palms; TPO: Thousand Palms Oasis; WP: Willis Palms.

system by Crowell (1962) and Dibblee (1968) and in the San Andreas set by Hill (1965).

Southeast of the Salton Sea, surface evidence of faulting in late Quaternary sediments and seismic activity are lacking; and on the basis of subsurface investigations, Biehler et al (1964) conclude that a southeastern extension of the San Andreas fault cannot be justified. Allen et al (1972) have suggested that the San Andreas fault is a right-lateral transform fault and that activity at the southeast end may terminate at a spreading center. The spreading center could lie between the San Andreas and San Jacinto faults beneath Quaternary volcanic rocks and geothermal anomalies on the southeast shore of the Salton Sea (Elders et al, 1972). According to this hypothesis, northwest trending faults southeast of the termination of the active San Andreas fault would have little or no horizontal displacement but would bring crusts of different age and character into juxtaposition. The eastern edge of the Salton Trough sedimentary basin is possibly delineated by such faults, with abrupt differences in depth to basement. The active San Andreas fault zone in Coachella Valley northwest of the hypothetical spreading center and other known and inferred faults with the same trend to the southeast are described below.

Coachella Valley Area

At the northwest end of Coachella Valley, the Banning and Mission Creek faults comprise the principal segments of the San Andreas fault zone (Figs. 2 and 6). East of its juncture with the south branch of the San Andreas in San Gorgonio Pass, on the south slope of the San Bernardino Mountains, the Banning fault is a north-dipping thrust fault with basement rocks thrust over Tertiary sediments and Pleistocene gravels (Allen, 1957). To the southeast in Coachella Valley, the Banning fault becomes a "high-angle fault characteristic of the San Andreas with right-slip movements that involve Pleistocene and Recent alluvial sediments" (Dibblee, 1968).

The Mission Creek fault dips steeply (62°-90°) to the northeast. Recent movement is indicated by trenches and scarplets in alluvium, offset streams and dammed ground water, which is hot and shallow on the northeast side of the fault and cold and deep on the southwest side (Proctor, 1958). The Cabazon Fanglomerate (Holocene) shows a minimum of 330 meters (1100 feet)

of vertical separation (north side up), and right-lateral stream offsets up to 240 meters (800 feet) are present in the Indio Hills. The 1948 Desert Hot Springs earthquake may have occurred on the Mission Creek fault (Proctor, 1958).

The Banning fault and Mission Creek fault join directly north of Indio; from this point the San Andreas fault zone trends about S45°E to the possible spreading center southeast of the Salton Sea (Fig. 1). A zone of tightly folded and sheared Cenozoic sediments that form spectacular linear valleys occurs along this portion of the fault (Allen et al, 1972). Displacements up to 1.3 centimeters (.5 inch) and creep along the San Andreas from the Mecca Hills to its terminus east of the Salton Sea were apparently triggered by the 1968 Borrego Mountain earthquake (Allen et al, 1972). These breaks coincide with recently active segments of the San Andreas fault zone mapped by Hope (1969a).

Fig. 5 is an enlarged portion of a Skylab image of the north end of Coachella Valley which shows strands of the San Andreas fault zone and other faults in greater detail. The locations of individual features on Fig. 5 are shown on the sketch map (Fig. 6). Unless otherwise indicated, the faults are most distinct in the aerial color photography. Of the black and white bands, the red (.6-.7 μm) is superior for topographic detail, and vegetated areas are most apparent in the color IR (.5-.88 μm).

Upper Coachella Valley constitutes an important ground water basin. The following description of the geohydrologic conditions is summarized from Tyley (1971). Unconsolidated late Pleistocene and Holocene valley fill deposits serve as the main water-bearing units. These deposits reach a thickness in excess of 1000 meters (3000 feet) in the deeper parts of the valley (Biehler, 1964). Ground water movement is affected by the Mission Creek, Banning, Garnet Hill and Indio faults which divide the valley into a series of subbasins (Fig. 7). Blockage by the Mission Creek fault results in a 46- to 76-meter (150- to 250-foot) decrease in the water level between the Desert Hot Springs subbasin and the Mission Creek subbasin (Fig. 8). The Banning fault is also an effective ground water barrier to ground water movement as evidenced by the 30- to 60-meter (100- to 200-foot) water level drop between the Mission Creek subbasin and the Garnet Hill subbasin. The

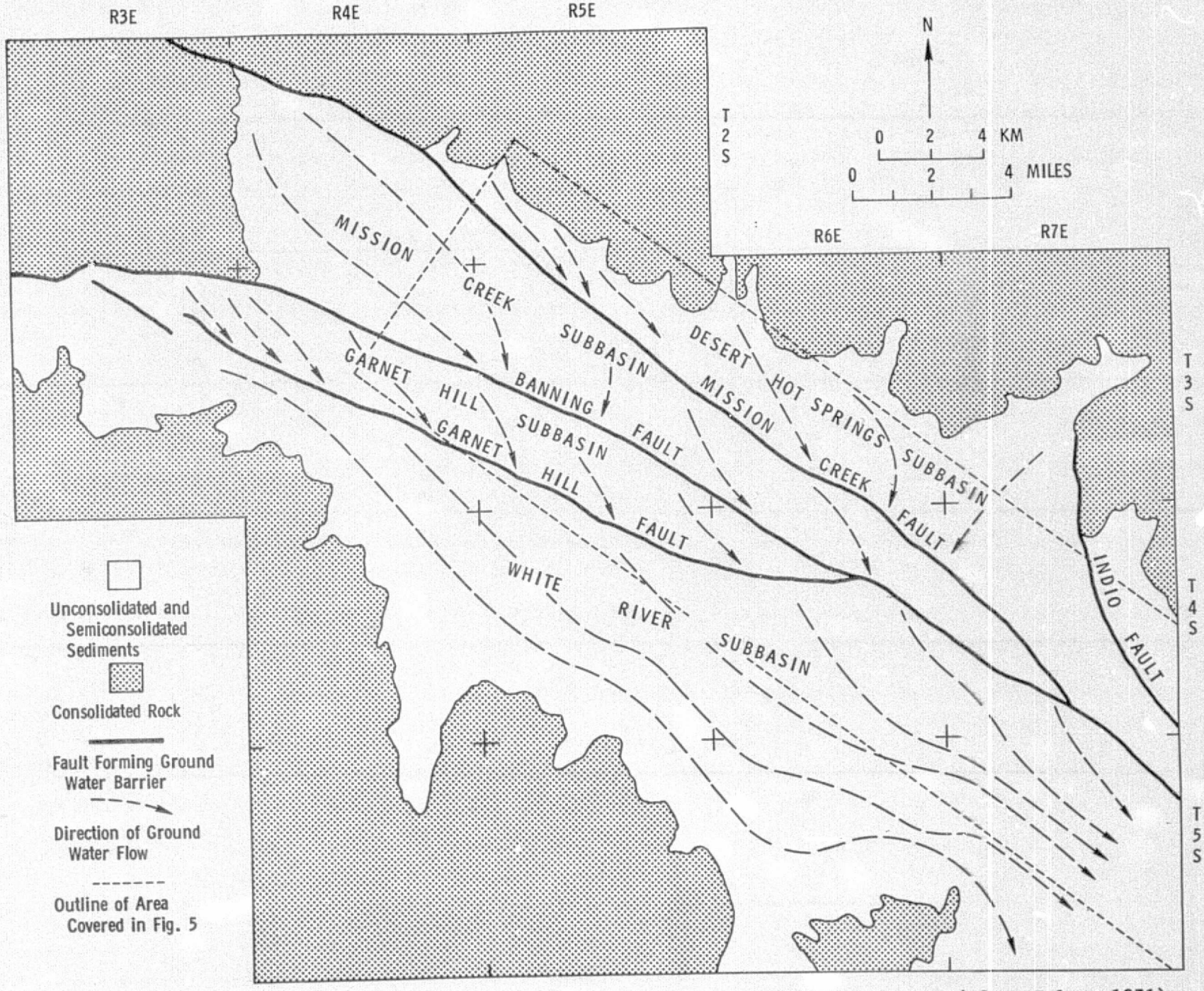

Fig. 7 - Ground water subbasins and generalized flow lines, Upper Coachella Valley (after Tyley, 1971)

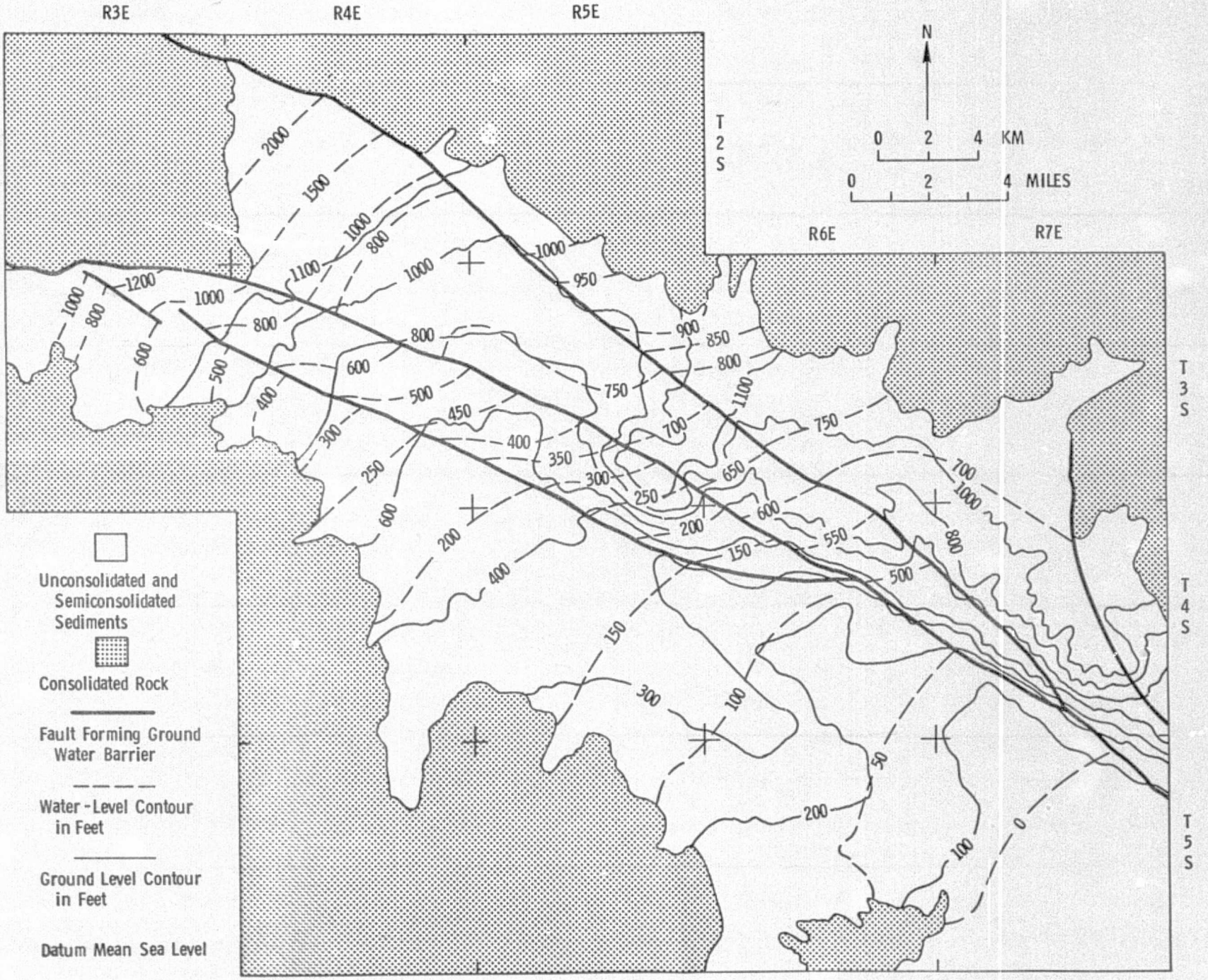

Fig. 8 - Water-level contours, Upper Coachella Valley, 1967 (after Tyley, 1971)

Garnet Hill fault creates about a 30-meter (100-foot) water-level decrease between the Garnet Hill subbasin and the Whitewater River subbasin. This fault is difficult to locate accurately owing to its lack of surface expression. The Indio fault also acts as a partial barrier to ground water movement in valley fill between the Indio Hills and the Little San Bernardino Mountains. Sparse data indicate that a water-level drop of 10-15 meters (30 to 50 feet) is probable from the west to the east side of the fault.

The Banning fault is visible on Skylab imagery for most of the interval from its convergence with the Mission Creek fault directly north of Indio, to the north end of Coachella Valley. The fault is most prominently delineated as an abrupt break in vegetation for 8 kilometers (5 miles) across the desert surface directly northwest of the Indio Hills (Fig. 9). This is an excellent example of surface evidence of a buried fault. Thick vegetation, consisting mostly of mesquite but also large trees, is only present on the northeast side of the fault. Southwest of the fault, the desert surface consists mostly of light-colored medium to coarse-grained sand with occasional pebbles. Brown sage bushes are spaced 3-6 meters (10-20 feet) apart. More vegetation is present on the north side of the fault because the fault acts as a barrier to ground water flowing from the north. Tyley (1971) has estimated that these phreatophytes extract about 4000 acre-feet per year from the ground water basin. Northeast of the fault, static water levels are at depths averaging about 10 meters (30 feet); south of the fault the water level is around 100 meters (300 feet) below the surface (Tyley, 1971). Artesian springs are present north of the fault at Seven Palms Ranch.

To the southeast between Edom Hill and the Indio Hills, the trace of the Banning fault is marked by a prominent linear valley and faint differences in ground color. The trace along the southwest edge of the Indio Hills is evidenced by the tonal contrast between the desert surface, described above, on the southwest and tan colored Ocotillo Conglomerates of Quaternary age uplifted along the northeast side of the fault. Although the southwest edge of the Indio Hills is relatively straight, no direct geomorphic evidence of faulting can be seen on Skylab images. Willis Palms, an oasis along the southwest edge of the Indio Hills, is visible in the Skylab images as a small dark

Fig. 9 - Low-altitude aerial view looking northwestward along Banning Fault. San Bernardino Mountains in background.

Fig. 10 - Low-altitude aerial view looking eastward along Blue Cut Fault. Blue Cut is in the middle view and Pleasant Valley is in the background.

area of vegetation. This is another locality of near-surface ground water caused by subsurface blockage of ground water flow by the Banning fault.

The Mission Creek fault can be traced on the enlarged Skylab image (Fig. 5) over most of its length from Two Bunch Palms to the southeast end of the Indio Hills. Like the Banning fault, the Mission Creek fault dams ground water and creates a high water table on its northeast side. The most prominent areas of vegetation along the fault are located at Two Bunch Palms and Thousand Palms Oasis. The water table is located within 5 meters (16 feet) of the surface at Two Bunch Palms (Proctor, 1958). Several other oases supporting palm trees and mesquite appear along the fault as small dots on the imagery. An alignment of cultivated plots, owing to the availability of near-surface ground water, can be seen along the north side of the fault between Two Bunch Palms and the northwest end of the Indio Hills.

To the southeast, the fault can be traced to Thousand Palms Oasis as an almost continuous alignment of linear valleys and ridges along the straight northeast edge of the Indio Hills. Within the Indio Hills, stream courses at three locations along the fault southeast of Thousand Palms Oasis appear to be deflected to the right an average of about 2 kilometers (1.2 miles). A shutter ridge (displaced ridge shutting off an adjacent canyon) appears along the central stream offset, and a prominent linear valley with a parallel linear ridge uplifted along the southwest side of the fault can be seen along the southeastern stream offset.

A linear valley along the Mission Creek fault zone appears on the Skylab image (Fig. 3) on the southwest edge of the Mecca Hills. The fault is covered for about 16 kilometers (10 miles) southeast of the Mecca Hills and reappears along the east shore of the Salton Sea. Two linear, dark areas are produced by juxtaposed formations of contrasting color along the fault. Upturned, red-brown continental sediments of Quaternary age occur on the northeast side, and younger lake sediments (Late Pleistocene or Recent), consisting of tan mudstone and tan fine-grained sandstone, occur on the southwest side. The Mission Creek fault and uplifted and deformed Quaternary sediments are not in evidence on Skylab imagery southeast of these exposures. Thus, our interpretation of Skylab imagery is in accord with previous surface mapping and geophysical studies that suggest the San Andreas fault terminates near the

southeast end of the Salton Sea, possibly at a spreading center (Allen, et al, 1972).

Southeastern Imperial Valley and Sonora, Mexico

Faults along the trend of the San Andreas southeast of the suggested spreading center would be comparatively inactive under the hypothesis that the San Andreas is a transform fault. However, significant vertical separation on the top of basement rocks could occur as a result of isostatic adjustment of crustal blocks of different thicknesses. East of the Salton Trough, deposits similar to or correlative with the Imperial Formation (Pliocene) are exposed at an altitude of about 320 meters (1050 feet). Near the center of Imperial Vally, these deposits were not penetrated in a well bottoming at a depth of 4097 meters (13,443 feet) (Dutcher et al, 1972). The required vertical offset could be explained by a fault interpreted from geophysical surveys near the eastern margin of the Sand Hills (Kovach et al, 1962). The Sand Hills fault has been aligned with the Algadones fault southeast of Yuma, Arizona (Mattick et al, 1973). However, the Algadones fault cannot delineate the eastern margin of the Salton Trough in Sonora, Mexico, because a southeastern extension would lie east of exposures of basement rocks of possible Precambrian age in Sierra del Rosario (R. Merriam, personal communication).

Gravity and aeromagnetic data suggest 3 kilometers (2 miles) vertical separation at the top of basement rocks along a fault between sediments of the Salton Trough and basement rock exposed to the northeast in Sierra del Rosario (Sumner, 1972). Between the Salton Sea and Gulf of California, shifting sands and river flood plain deposits obscure any direct surface indications of faulting along the northeast edge of the Salton Trough. However, physiographic features appearing on Skylab imagery may be indicative of faulting along this trend. A prominent dark spot appears on the Skylab image on Fig. 4 on the approximate surface trace of the fault identified by Sumner. The dark spot is a lake (R. Merriam, personal communication) which, in this arid region, could be due to impoundage of ground water on the northeast side of a fault.

To the northwest, a remarkably straight tonal difference is located near the southwestern edge of the Sand Hills. The slightly darker tone on

the northeast side is the result of denser vegetation. The depth to the water table is 35 to 45 feet (10 to 14 meters) in six wells along the edge of the Sand Hills (Loeltz et al, 1975). There is no evidence that the water table is displaced along the tonal change, but well control is poor in this area (J. H. Robison, personal communication, 1975). Vegetation consists of shallow-rooted bushes, so it is doubtful that the vegetation change could be due to blockage of ground water. Loeltz et al (1975) have suggested that the dune sand may have been supplied by beaches along a fault-controlled shoreline at the southwest edge of the dune field. The straight vegetation break may be the result of soil differences along the fault-controlled shoreline. A fault is also suspected on the basis of a well drilled on the southwest margin of the dune field (S. L. Werner, personal communication). The well was drilled on a geothermal anomaly by the California Department of Water Resources, and silicified recent basin deposits were encountered (Werner and Olson, 1970).

Approximately half-way along the western edge of the Sand Hills, the dune field overlaps the line of vegetation and surficial evidence of faulting is obscured by cultivated fields and leakage along the Coachella Branch of the All American Canal. The overview provided by the Skylab images aided in the interpretation of this possible fault in the San Andreas set by showing the regional alignment of fault indicators at an appropriate scale.

SAN JACINTO FAULT ZONE

The San Jacinto fault zone extends from near the San Andreas fault in the San Gabriel Mountains southeast 500 kilometers (300 miles) to the Gulf of California. In contrast to the continuous trace of the San Andreas fault, the continuity of any one fault trace cannot be proven over the length of the San Jacinto fault zone. Maps prepared by Dibblee (1954), Sharp (1967, 1972), Bartholomew (1970) and others, show different locations, extensions, and names for some of the principal faults within a zone of subparallel and branching faults up to 20 kilometers (12 miles) wide. A microearthquake study of the San Jacinto fault zone in San Jacinto Valley by Cheatum and Combs (1973) also indicates a complex fault pattern in a zone 20 kilometers (12 miles) wide.

The San Jacinto fault zone is characterized by high seismic activity; thirteen large earthquakes have occurred along the fault zone north of the

Mexican border since 1890 (Lamar, Merifield, and Proctor, 1973). Surface faulting for a distance of about 31 kilometers (19 miles) with displacements of up to 38 centimeters (15 inches) occurred on the Coyote Creek fault during the 1968 Borrego Mountain earthquake (Clark, 1972). Surface rupture during an earthquake was also observed on the Imperial fault in 1940 and may have occurred in 1934 along faults in the San Jacinto fault zone in the Colorado River Delta (Allen et al, 1965). Sharp (1972) has compiled a map showing recently active breaks along the San Jacinto fault zone. According to Sharp (1967), fresh scarps and offset stream channels along the San Jacinto fault north of Anza indicate 730 meters (2400 feet) of recent right-lateral displacement.

Two prominent linears appear on the Skylab images of the Colorado Delta area (Fig. 4). The western linear in recent deltaic deposits corresponds to the segment of the San Jacinto fault believed to have been active in 1934 (Allen et al, 1965). The eastern linear appears as a straight, sharp boundary between deltaic deposits on the west and dune sand on the east. Merriam (1965) states that the southeast end of this linear is a fault and describes extensions of the San Jacinto fault zone to the southeast in Sonora.

To the northwest in Mexicali Valley, the fault traces are obscured by cultivated fields. However, an inferred northwest extension of the western linear passes through the Cerro Prieto geothermal field (De Anda and Parides, 1964); the geothermal activity may be related to the fault zone. Northwest of the geothermal area, faint differences in the tone of cultivated fields south of Mexicali can be seen across a line along the same trend (Figs. 2 and 4). No additional evidence concerning the origin of this linear was found during a field reconnaissance, but variations in the tone of the cultivated fields could be related to subtle differences in the soil. The lake sediments beneath Mexicali Valley are primarily interbedded silt and clay. Because of its better drainage qualities, silt is preferable for crops. Silt and clay juxtaposed along a fault could be reflected in different crops or land use. Because the subtle differences in tone along this possible strand within the San Jacinto fault zone occur over a wide area, the overview provided by the small-scale Skylab images was required for recognition of the strand.

The tonal difference cannot be traced northwest of a point 6 kilometers (4 miles) south of the international border, but a continuation of the same

trend lines up with a fairly straight segment of the New River. Exposures along the New River north of the border were examined, but no evidence of faulting was observed. If a fault along this trend curves slightly and is situated west of the New River, it would be aligned with a queried fault in the San Jacinto fault zone shown by Jennings (1973).

The Coyote Creek fault is a major strand of the San Jacinto fault zone exposed in Coyote Canyon (Sharp, 1967). Southeast of bedrock exposures of the fault, an abrupt linear contact between dark and light earth materials appears on Skylab imagery along the southwest edge of Coyote Mountain. This contact was field checked in a search for previously unrecognized evidence of faulting from the south end of Coyote Mountain to the north end of Borrego Valley. Bedrock and individual clasts in the alluvial fan deposits and talus on Coyote Mountain are stained dark brown to dark gray by desert varnish. In contrast, the younger windblown sand and alluvium in Borrego Valley are not varnished and are light gray to glistening white. Occasional floods and wind transport sediments from the outlet of Coyote Creek at the north end of Borrego Valley to the southeast along the edge of Coyote Mountain. The alluvium and windblown sand form a sharp, fairly straight contact with the older, varnished rocks primarily because the older, dark rocks in the canyons along the mountain front are shielded from the windblown sand and alluvium moving down the valley. This has the effect of straightening irregularities in the contact between light and dark rocks.

The field investigation revealed no evidence of recent fault movement along the southwest side of Coyote Mountain; however, the general straightness of the mountain front may be in part the result of erosional retreat parallel to a straight fault scarp. In this well-mapped area, Skylab images provided no new information. In an unmapped area, the straight trace of the mountain front would have surely directed attention to the possibility of a major fault along this trend.

EAST TRENDING FAULTS

The Transverse Ranges are characterized by a number of east trending faults. Left-slip of up to several kilometers is demonstrable on some of

these faults, and displacements in older alluvium and terrace deposits attest to movements in Quaternary time (Hope, 1966). Segments of these faults appear as linears on the Skylab image (Figs. 2 and 3).

Blue Cut Fault

The Blue Cut fault is one of the major east trending faults of the eastern Transverse Ranges. Correlation of lithologic units across the fault indicates left-slip of up to 5-6 kilometers (3-4 miles) on the western portion of the fault since Jurassic (Hope, 1966, 1969b). The western end of the Blue Cut fault curves northward and merges with the northwest trending Dillon fault (Rogers, 1965). Discontinuous fault zone exposures and physiographic evidence suggest that the Blue Cut fault may continue east for 80 kilometers (50 miles) and terminate against a northwest trending fault near the western edge of the Coxcomb Mountains. Because the evidence of faulting is discontinuous and separated by considerable distances, the alignment of fault indicators cannot be appreciated on the ground or from aircraft. A view eastward along the fault trend from a low-flying aircraft is shown in Fig. 10. The overview provided by small-scale Skylab imagery (Fig. 3) is ideal for recognizing the regional alignment of the geomorphic features described by Hope (1966) over the length of the fault.

Good exposures in Blue Cut, an east-west canyon in the Little San Bernardino Mountains, reveal a near-vertical fault zone several hundred feet wide. East of the Blue Cut, the fault is buried beneath recent alluvium in Pleasant Valley, and presumably reappears in El Dorado Canyon. The alignment of straight canyon segments eroded along the fault in the Blue Cut, the east end of Pleasant Valley, and along El Dorado Canyon, is quite apparent on the Skylab imagery (Fig. 3). A fault is located along the straight northeast edge of Pleasant Valley seen on Skylab imagery. The sharp linear at the east end of Pleasant Valley is formed by shadows on the north side of a ridge of fanglomerate uplifted on the south block of the Blue Cut fault (Hope, 1969b). The cluster of low hills in the western Pinto Basin outlines a north-northwest trending anticline in Tertiary or Quaternary sedimentary rocks. This anticline may be a drag fold formed as a result of left-slip along the proposed eastern extension of the Blue Cut fault beneath Pinto Basin (Hope, 1969b). At the east end of the Pinto Basin,

a southern branch of the fault may be located at the gently curving, abrupt north edge of the Eagle Mountains which is prominent on Skylab imagery.

Porcupine Wash, Substation and Victory Pass Faults

The Porcupine Wash fault can be traced from Pinto Basin westward into the Little San Bernardino Mountains where the trace ramifies and apparently ends. Left-separation of 2.4 kilometers (1.5 miles) on a near-vertical contact between granodiorite and gneiss is demonstrable, and scarps in older alluvium indicate Quaternary activity (Hope, 1966). To the east, the Substation and Victory Pass faults have been mapped in the Eagle Mountains. The Substation fault appears to offset a swarm of rhyolite dikes about 3 kilometers (2 miles) in a left-lateral sense. Displacement on the Victory Pass fault has not been determined (Hope, 1966).

Physiographic indicators along these faults are prominent on Skylab imagery (Fig. 3). Two straight canyons are aligned along the trace of the Porcupine Wash fault. To the east a straight canyon and a fairly straight break in slope can be seen along the trace of the Substation fault. The regional alignment of the Porcupine Wash and Substation faults can be seen on Skylab imagery. However, physiographic evidence of a connection between the faults cannot be found and we were unable to trace the Substation fault west of the termination shown on existing maps (Hope, 1966: Jennings, 1967).

A straight canyon and linear breaks in slope appear on Skylab imagery (Fig. 3) along the mapped trace of the Victory Pass fault. A western continuation of the fault is suggested by an east-west trending low-lying area within the Eagle Mountains. To the west, across the southern Pinto Basin, the photo linear is aligned with the east-west trending Pinkham Canyon. However, the fault could only be traced in the field about 1.5 kilometers (one mile) west of the termination shown by Jennings (1967) and 3 kilometers (2 miles) west of the termination shown by Hope (1966). The westernmost fault exposure is in a mine at the southwest corner of Sec. 36, T4S, R13E. At this location, the fault diverges from the photo linear and turns southwestward across Big Wash; the attitude of the fault is N62^{o}E, 42^{o}S parallel to foliation in metamorphic rocks. Three kilometers (2 miles) further west, almost continuous outcrops of metamorphic rock with a persistent north-south strike and east dip of foliation cross the photo linear; it is unlikely that

a western continuation of the fault can pass through this location. Further west, alluvium in the low-lying area along the photo linear would obscure any evidence of faulting.

Orocopia Linear

Jennings (1967) shows the Orocopia linear as a concealed fault extending parallel to Interstate Highway 10 for about 32 kilometers (20 miles) within the broad east-northeast trending valley between the Eagle Mountains on the north and the Orocopia Mountains on the south. A fault along this physiographic feature was first suggested by Hill (1928). Biehler et al (1964) describe a gravity low which may be the result of a fault-bounded, sediment-filled trough along the linear. Individual rock units and fault trends do not match across the linear (Jennings, 1967) which also suggests the presence of a fault. The overview provided by Skylab imagery shows that the Orocopia linear is the most prominent east-west trending, low-lying topographic feature in the region; based on parallelism with known left-slip faults to the north displayed on Skylab imagery, it is suggested that the Orocopia linear may have formed as a result of erosion of shattered rocks along a left-slip fault zone, but no verification has been obtained.

OTHER FAULTS IN THE SALTON TROUGH AREA

The Palm Canyon fault appears as a distinct but irregular line for about 16 kilometers (10 miles) along the axis of Palm Canyon. The irregular trace probably results from erosion along a thrust surface which dips 20° to 40° east (R. V. Sharp, personal communication, 1973). Faulting involves pre-Cretaceous metamorphic rocks only, and there is no evidence of displacement of Quaternary alluvium at the mouth of the canyon.

The Indio fault appears as a prominent, straight topographic break for 10 kilometers (6 miles) in Quaternary sediments along the northeast edge of the Indio Hills (Fig. 5). Prominent scarps can be seen on the ground along the fault but are not apparent on the Skylab images.

The Hidden Springs fault can be seen as a 20-kilometer (12-mile) long north-northwest trending, prominent, straight tonal change on Skylab imagery northeast of the Salton Sea. The origin of the tonal change is not known.

The pattern of linears in the Sierra de los Cucapas (Fig. 2) seen from Skylab (Fig. 4) is similar to the fault pattern field mapped by Gastil et al (1971). The linears identified southeast of Yuma (Figs. 2 and 4) have locations similar to faults shown on an unpublished field geologic map prepared by Richard Merriam (scale: 1:250,000). Extensions of these linars shown on Fig. 2 southeast of the Fig. 4 Skylab image can be seen on the Skylab 2, Roll 4, Frame 136 image.

With the exception of the Palm Canyon fault, the faults identified on the Skylab images are high-angle faults with straight traces. Other low-angle faults in the region are not recognizable because they have sinuous traces and lack diagnostic fault-controlled features which would allow their differentiation from geologic contacts of other origins.

CONCLUSIONS

The following indicators of faulting have been recognized in Skylab imagery of the Salton Trough area: (1) topographic features such as scarps, fault-line scarps, offset drainage, linear valleys and straight mountain fronts, (2) vegetation differences due to ground water barriers, and (3) lithologic differences across the fault producing contrasting tone, color or texture. High-angle, strike-slip faults are most apparent; low-angle faults are generally not identifiable. The scale and perspective of the Skylab imagery is advantageous for observing the regional alignment of faults tens of kilometers in length. For example, surface evidences of the Blue Cut fault are discontinuous and separated by as much as 10 kilometers (6 miles). The alignment of exposed segments of the Blue Cut fault is readily apparent in Skylab photos but cannot be appreciated in larger scale photos, and unless field studies disprove their connection, one continuous fault zone can be assumed. Utilizing this perspective, the following alignments of northwest trending linear features, which may reveal previously unrecognized segments of faults in the San Andreas set, were identified: (1) a tonal change across cultivated fields of the Mexicali Valley which is aligned with strands of the San Jacinto fault zone to the northwest and southeast, and (2) a straight break in vegetation and a lake in Sonora, Mexico, aligned with the active San Andreas fault zone to the northwest and a fault to the southeast previously

inferred from geophysical evidence.

This same perspective, however, can prompt incorrect interpretation of disconnected linear features which may have unrelated origins. Possible extensions of the Substation and Victory Pass faults, suggested by study of Skylab photos, could not be identified on the ground. The overview provided by Skylab images can greatly increase the efficiency of regional fault investigations; analysis of Skylab images should precede the study of larger scale imagery and detailed field investigations.

ACKNOWLEDGEMENTS

The work reported herein was accomplished under NASA Contract NAS 2-7698. Technical monitoring was provided by David Amsbury whose interest and helpful suggestions are gratefully acknowledged. We wish to acknowledge valuable discussions with Mason Hill, Richard Merrian, Shawn Biehler, Robert V. Sharp, G. A. Davis, S. L. Werner and James H. Robison. Mason Hill critically read the manuscript, Richard Merriam kindly provided us with unpublished maps of Sonora, Mexico, and Morlin Childers accompanied us on a reconnaissance of Mexicali and Imperial Valleys.

REFERENCES

Allen, C. R., 1957, San Andreas fault zone in San Gorgonio Pass, southern California: Geol. Soc. Amer. Bull., v. 69, p. 315-350.

Allen, C. R., St. Amand, P., Richter, C. F., and Nordquist, J. M., 1965, Relationship between seismicity and geologic structure in the southern California region: Seis. Soc. Amer. Bull, v. 55, p. 753-797.

Allen, C. R., Wyss, M., Brune, J. N., Grantz, A., and Wallace, R. E., 1972, Displacements on the Imperial, Superstition Hills, and San Andreas faults triggered by the Borrego Mountain earthquakes: in The Borrego Mountain earthquake of April 9, 1968; U.S. Geol. Survey Prof. Paper 787, p. 87-104.

Bartholomew, M. J., 1970, San Jacinto fault zone in the northern Imperial Valley, California: Geol. Soc. Amer. Bull., v. 81, p. 3161-3166.

Biehler, Shawn, 1964, Geophysical study of the Salton Trough of southern California, Calif. Inst. Technology, Ph.D. thesis, 139 p.

Biehler, S., Kovach, R. L., and Allen, C. R., 1964, Geophysical framework of northern end of Gulf of California structural province: Amer. Assoc. Petrol. Geol., Mem. 3, p. 126-143.

Cheatum, C. and Combs, J., 1973, Microearthquake study of the San Jacinto Valley, Riverside County, California: in Proc. Conf. on Tectonic Problems of the San Andreas Fault System, Stanford Univ. Publ., Geol. Sci., v. XIII, p. 1-10.

Clark, M. M., 1972, Surface rupture along the Coyote Creek fault: U.S. Geol. Survey, Prof. Paper 787, p. 55-86.

Crowell, J. C., 1962, Displacement along the San Andreas Fault, California: Geol. Soc. Amer., Spec. Paper 71, 61 p.

De Anda, L. F. and Parides, E., 1964, La falla de San Jacinto y su influencia sobre la actividad geothermica en el valle de Mexicali, B.C., Mexico: Boletin de la Association Mexicana de Geologos Petroleros, v. XVI, No. 7-8, p. 179-181.

Dibblee, T. W., Jr., 1954, Geology of the Imperial Valley region, California: Calif. Div. Mines and Geol., Bull. 170, contr. 2, Chapter II, p. 21-28.

Dibblee, T. W., Jr., 1968, Displacements on the San Andreas fault system in the San Gabriel, San Bernardino, and San Jacinto Mountains, Southern California: in Proc. Conf. on Geologic Problems of San Andreas fault system; Stanford Univ. Publ. Geol. Sci., v. XI, p. 260-278.

Dutcher, L. C., Hardt, W. F. and Moyle, W. R., Jr., 1972, Preliminary appraisal of ground water in storage with references to geothermal resources in the Imperial Valley area, California: U.S. Geol. Survey Circular 649, 59 p.

Elders, W. A., Rex, R. W., Meidev, T., Robinson, P. T. and Biehler, S., 1972, Crustal spreading in southern California: Science, v. 178, p. 15-24.

Gastil, R. G., Phillips, R. P., and Allison, E. C., 1971, Reconnaissance Geologic Map of the State of Baja California: Geol. Soc. Amer. scale 1:250,000.

Hill, M. L., 1965, The San Andreas rift system, California and Mexico; in The world rift system: Canada Geol. Survey Paper 66-14.

Hill, R. T., 1928, Southern California geology and Los Angeles earthquakes: Southern California Academy of Sciences, 232 p.

Hope, R. A., 1966, Geology and structural setting of the eastern Transverse Ranges, southern California: Ph.D. thesis, Univ. Calif., Los Angeles, 201 p.

Hope, R. A., 1969a, Map showing recently active breaks along the San Andreas and related faults between Cajon Pass and Salton Sea, California: U.S. Geol. Survey, Open File Report.

Hope, R. A., 1969b, The Blue Cut fault, southeastern California, Geological Survey Research, 1969: U.S. Geol. Survey Prof. Paper 650-D, p. D116-D121.

Jennings, C. W., 1967, Geologic map of California, Salton Sea sheet: Calif. Div. Mines and Geol.

Jennings, C. W., 1973, State of California, preliminary fault and geologic map, scale 1:750,000: Calif. Div. Mines and Geol., Preliminary Report 13.

Kovach, R. L., Allen, C. R., and Press, F., 1962, Geophysical investigations in the Colorado Delta Region: J. Geophys. Res., v. 67, p. 2845-2871.

Lamar, D. L., Merifield, P. M., and Proctor, R. J., 1973, Earthquake recurrence intervals on major faults in southern California: in Geology, Seismicity and Environmental Impact, Assoc. Eng. Geol., Spec. Publ., p. 265-276.

Loeltz, O. J., Irelan, B., Robison, J. H. and Olmsted, F. H., 1975, Geohydrologic reconnaissance of the Imperial Valley, California: U.S. Geol. Survey Prof. Paper 486-K, 54 p.

Mattick, R. E., Olmstead, F. H., and Zohdy, A. A. R., 1973, Geophysical studies in the Yuma area, Arizona and California: U.S. Geol. Survey Prof. Paper 726-D, 36 p.

Merifield, P. M. and Lamar, D. L., 1975a, Active and inactive faults in southern California viewed from Skylab: presented at the NASA Earth Resources Survey Symposium June 8-13, 1975, Houston, Texas, in: Proceedings Volume, NASA TM X-58168, JSC-09930, p. 779-797.

Merifield, P. M. and Lamar, D. L., 1975b, Faults on Skylab imagery of the Salton Trough area, southern California: CalESCO Technical Report 75-1.

Merriam, R., 1965, San Jacinto fault in northwestern Sonora, Mexico: Geol. Soc. Amer. Bull., v. 76, p. 1051-1054.

Proctor, R. J., 1958, Geology of the Desert Hot Springs area, Little San Bernardino Mountains, California: M.A. thesis, Univ. Calif., Los Angeles.

Proctor, R. J., 1973, Map showing major earthquakes and recently active faults in the southern California region: in Geology, Seismicity and Environmental Impact, Assoc. Eng. Geol. Spec. Publ.

Rogers, T. H., 1965, Geologic map of California, Santa Ana Sheet: Calif. Div. Mines and Geol.

Sharp, R. V., 1967, San Jacinto fault zone in the Peninsular Ranges of southern California: Geol. Soc. Amer. Bull., v. 78, p. 705-730.

Sharp, R. V., 1972, Map showing recently active breaks along the San Jacinto fault zone between the San Bernardino area and Borrego Valley, California: U.S. Geol. Survey Map I-675.

Sumner, J. R., 1972, Tectonic significance of gravity and aeromagnetic investigations at the head of the Gulf of California: Geol. Soc. Amer. Bull., v. 83, p. 3103-3120.

Tyley, S. J., 1971, Analog model study of the ground water basin of the Upper Coachella Valley, California: Water Resources Division, U.S. Geol. Survey, open-file report, 89 p.

Wallace, R. E., 1970, Earthquake recurrence intervals on the San Andreas fault: Geol. Soc. Amer. Bull., v 81, p. 2875-2890.

Werner, S. L. and Olson, L. J., 1970, Geothermal wastes and the water resources of the Salton Sea area: Calif. Dept. of Water Resources Bull. No. 143-7, 123 p.

PART V

ENHANCEMENT CHARACTERISTICS OF PSEUDOCOLOR TRANSFORMATION OF SKYLAB AND LANDSAT IMAGES AND TEST CHARTS

by

D. L. Lamar and P. M. Merifield
California Earth Science Corporation

and

Carl Gazley, Jr., J. V. Lamar, and R. H. Stratton
The Rand Corporation

PREFACE

Research on the application of Skylab and Landsat imagery to analysis of fault tectonics and earthquake hazards in California was accomplished by California Earth Science Corporation under contracts from the NASA-Johnson Spacecraft Center and the Earth Resources Observations System Program (EROS) Office, U.S. Geological Survey. One objective of this research was to evaluate the usefulness of pseudocolor transformation images in identifying faults and other geologic features. The appearance of selected geographic and cultural features was also analyzed. Pseudocolor transformations of selected Skylab and Landsat images and test charts were prepared under subcontracts to the Rand Corporation. Several of these transformations and a discussion of their enhancement characteristics are presented in this report. The results of our analysis of pseudocolor transformations of Landsat images were also presented in a previous report (Lamar et al., 1974).

CONTENTS

ILLUSTRATIONS

Note: Because of the expense of color photographic reproduction, color images of the figures are only included in copies submitted to NASA.

ABSTRACT

Pseudocolor transformations were prepared of Skylab and Landsat images of southern California. Tests were given to evaluate the relative ability to recognize representative faults and linears and selected physiographic and cultural features on single band, subtraction, and pseudocolor images. No significant improvement was found in the ability to detect and locate faults and linears on the pseudocolor transformations of Skylab and Landsat images. However, dry lake surfaces were enhanced on the subtraction images, and other geologic and geographic features characterized by minor tonal differences on relatively flat surfaces were enhanced on some pseudocolor transformations of the Landsat images. In addition, test charts of common symbols were prepared, and comparisons were made of the ability to identify the symbols in black and white and pseudocolor images. The tests revealed no significant enhancement of the symbols in the pseudocolor transformations. Significant differences between subjects in the ability to recognize symbols on charts and features on satellite images were observed and the effectiveness of the transformations varied with individuals. In view of the limited number of images studied, and subjects tested, these results should be considered preliminary.

INTRODUCTION

Comparison tests in which subjects are asked to identify the boundary between fields of differing brightness and chromaticity have demonstrated that the eye can distinguish, under varying levels of adaptation, millions of combinations of brightness, hue, and saturation, including about 150 shades of gray. However, at a given level of adaptation, the eye can distinguish only several thousand colors and only about 15 shades of gray (LeGrand, 1957). Discrimination is more difficult if the subject is asked to compare individual spots on a field (Sheppard et al., 1967) or areas in a complex image (Halsey and Chapanis, 1954); under these conditions the eye is still able to identify several hundred colors. Because of this ability of the eye to discriminate significantly more colors than shades of gray, it has been suggested that much smaller density differences and more information could be obtained from a complex black and white image if the grays in the image were transformed to colors in a pseudocolor image (Sheppard, Stratton, and Gazley, 1966).

Several electronic digital processing (Anonymous, 1972, 1974) and photographic (Gazley, Rieber, and Stratton, 1967; Anonymous, 1969; Maas, 1973) techniques have been developed to create such pseudocolor transformations. Most of the photographic methods have one or more of the following disadvantages: (1) Only discrete steps of up to 64 in the gray scale can be transformed into colors; (2) Laborious preparation of up to 64 individual separations; and (3) Loss of resolution. Stratton and Gazley (1971) have developed a photographic process which transforms a continuous gray scale into a continuous chromatic scale. The advantages of this method are that it employs only two intermediate black and white separations, introduces only a small loss in resolution, and should provide the maximum enhancement obtainable by photographic techniques. Photographic methods are limited in that adjacent shades of gray can only be transformed into adjacent colors on a chromatic scale. Electronic and digital processing methods of transformation have the potential for more flexibility in that adjacent shades of gray can be transformed into very different colors or density gradients could be transformed into colors; these methods would allow a much greater choice in enhancement characteristics.

Comparison of features on originals and pseudocolor transformations of complex black and white images is a subjective process and it is difficult to devise tests of enhancement characteristics. We have been unable to discover

any attempts to quantitatively evaluate the usefulness of pseudocolor images in the discrimination of features on remotely sensed or other complex images. As a portion of research on the recognition of faults and other geologic, geographic, and cultural features on satellite images, the method of Stratton and Gazley (1971) was used to prepare pseudocolor transformations of Skylab and Landsat images of the southern California area. Research was also accomplished on the ability to recognize simple symbols on charts. Black and white charts were generated by computer graphics with variations in the intensity of symbols and background so that some of the symbols could not be distinguished. Tests were given to compare the ability to recognize symbols on the original and pseudocolor images of the charts. The results of our study of pseudocolor transformations of Skylab and Landsat images and the symbol charts are presented in this report.

PHOTOGRAPHIC ENHANCEMENT TECHNIQUES

A number of photographic techniques are available for enhancement of black-and-white imagery. Contrast enhancement is accomplished by expanding a selected narrow density range to cover the gray scale range that can be discriminated by the human eye. Contrast is increased in a limited density range; however, the "highs" and "lows" beyond the selected intensity range are lost in the black and white ends of the gray scale. Fig. 1 illustrates a density vs. log E curve for contrast enhancement; by varying exposure this curve can be shifted to the right or left. A number of contrast enhancements can be made to cover the entire intensity range of the original. Thus, the total information in the original can be enhanced and retained, but not in a single image.

Another technique is extended-range contrast enhancement, which is the increase of contrast over the entire density range of the original (Fig. 1). This is accomplished by use of film having a high maximum density. Although all of the original information may be retained in such an enhancement, the eye cannot discriminate densities over such an extended range; a portion of the highs and lows are lost at any level of illumination. By changing illumination, and hence the eye's adaption, different segments of the density scale can be viewed; thus, a single extended range contrast enhancement can serve as a succession of contrast enhancements.

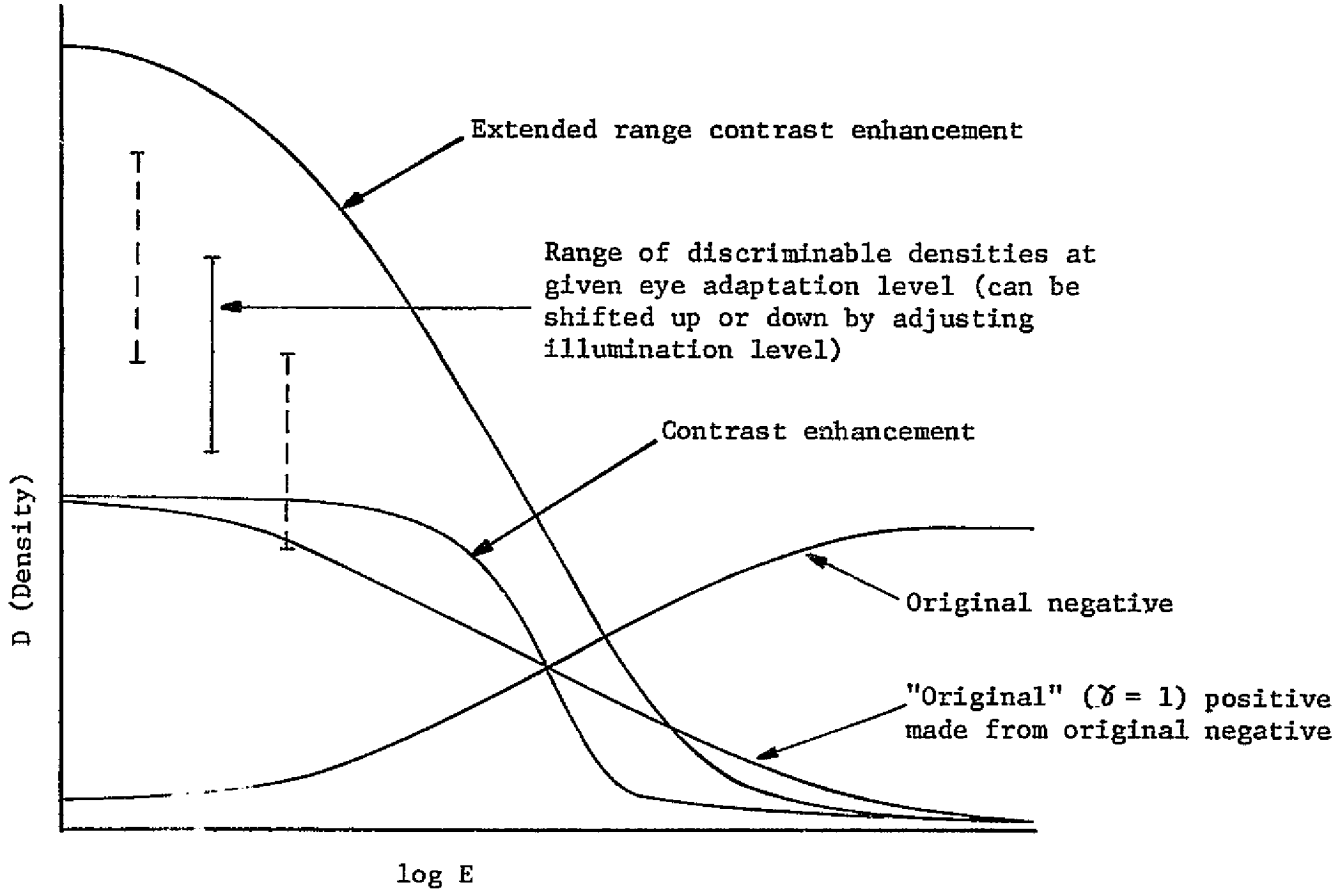

Figure 1 - Density versus log E (energy reaching film) curves for original positive and negative, contrast enhancement, and extended range contrast enhancement.

Because of the eye's ability to discriminate hundreds of colors and only about 10 to 15 shades of gray, much more of the density information should be discriminated in a pseudocolor transformation of an extended range contrast enhancement. Transparencies of positive and negative extended range contrast enhancements are prepared as steps in the pseudocolor process of Stratton and Gazley (1971) used to produce the pseudocolor transformations evaluated in this report.

Another type of image enhancement can be generated when two images, differing in time or wavelength, are available. A subtraction of two such images displays differences between the images; for example, a subtraction of two Landsat bands displays differences in the spectral characteristics of the scene. The subtraction, a black and white image, can be further enhanced by pseudocolor transformation. As a portion of our research, pseudocolor transformations of subtraction images of Landsat and Skylab images were prepared and analyzed.

The details of the procedure to produce the pseudocolor transformations and subtraction images are presented in Appendix 1.

DISCUSSION OF LANDSAT IMAGES

Fig. 2 shows principal faults and major geographic features annotated on Landsat image 1090-18012 of Band 7, which covers a portion of southern California. This particular image was chosen for study because it shows a number of faults with a wide range of characteristics. The San Andreas fault, the principal active fault in California, crosses the central portion of the image and intersects the prominent northeast-trending Garlock fault. The San Andreas and Garlock faults border the Mojave Desert Province. A number of other faults, as well as diverse geologic, geographic and cultural features, can be seen. These include the San Gabriel and Tehachapi Mountains, several dry lakes and alluvial fans in the Mojave Desert, and the street pattern and density of urban development in the Los Angeles Basin. Transparencies of the originals and pseudocolor transformations of Bands 4, 5 and 7, and a subtraction image of Bands 4 and 5 and its pseudocolor transformation of the Landsat image presented in Fig. 2 were prepared and analyzed. Images of all bands were generated from digital tapes; Band 6 and Band 7 were found to be similar, but geologic structure is somewhat better displayed on Band 7. Thus, Band 6 was not included in our

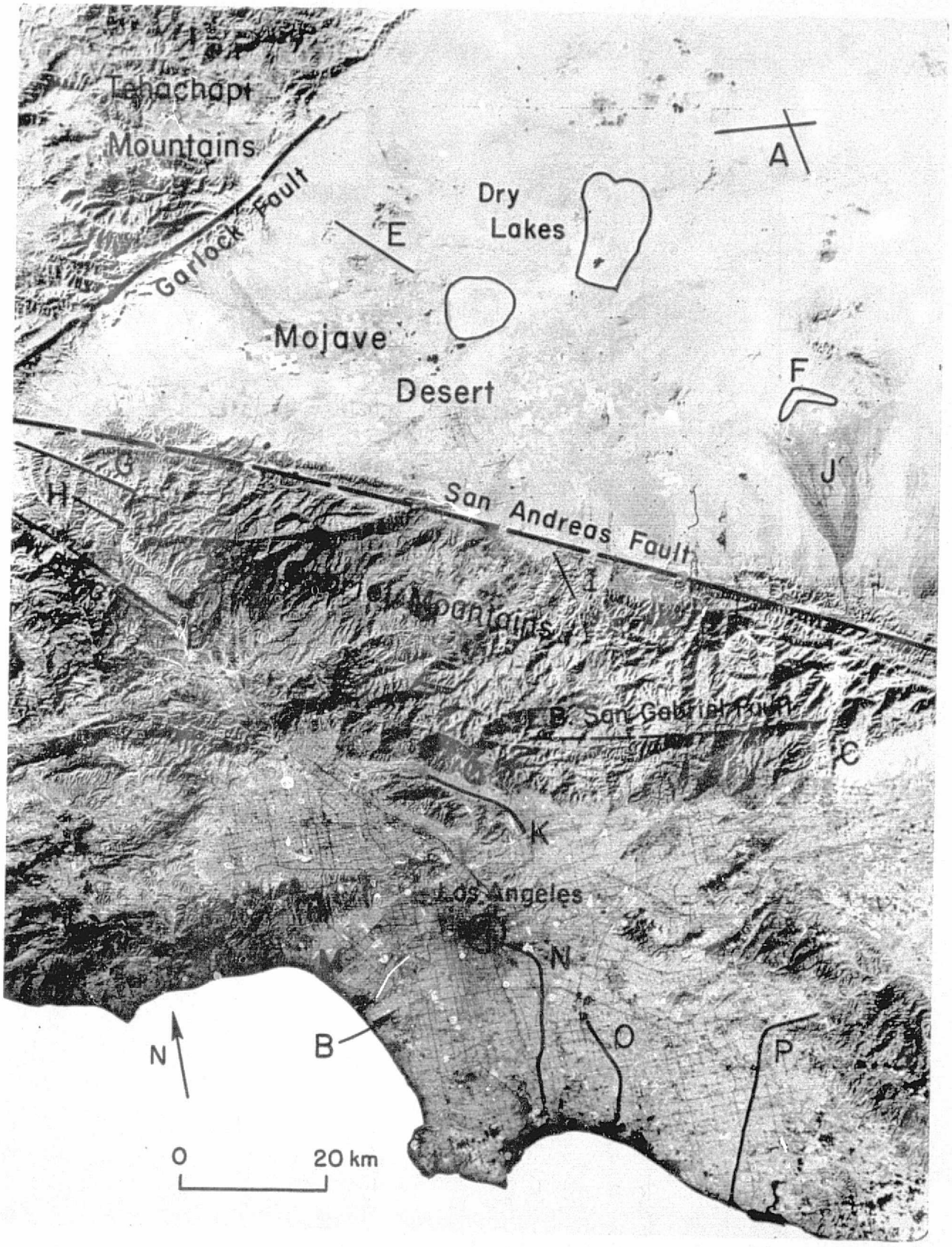

Fig. 2 - Landsat, Band 7 image 1090-18012 of a portion of southern California. W.B.S.G.F.: west branch San Gabriel fault; E.B.: east branch. See text for key to letters.

investigation. Fig. 3 is a print from an extended-range contrast enhancement of Band 7 used to prepare the pseudocolor image shown in Fig. 4. The extreme range from very dark to white gives Fig. 3 a "harsh" appearance, and no apparent improvement in the ability to discriminate features over the medium contrast originals could be detected. Note that this is a print, which cannot reproduce all parts of an extended-range contrast enhancement, and is more like a simple contrast enhancement. This image has been included to illustrate the individual steps in the production of pseudocolor transformations.

Major structural features, such as the San Andreas and Garlock faults, are well displayed in images of all bands, and the enhancements offer no obvious advantages. In the case of less obvious geologic and geographic features, however, there are distinctions between the originals and pseudocolor transformations. In order to define these differences a number of different types of features were compared in the originals and pseudocolor transformations. Admittedly, there is considerable subjectivity in this comparison. The pseudocolor may bring out a feature that was not seen in the original, but commonly it may be seen on re-inspection of the original after first being noticed on the pseudocolor.

As an independent evaluation of our comparisons, a test was devised and presented to 33 students in a field geology class at the University of California at Los Angeles. The results of the student test are included with our evaluations in Table 1.

The students were asked to indicate the relative appearance of six representative geologic and geographic features on 20.3 x 25.4-centimeter (8 x 10-inch) transparencies of originals and pseudocolor transformations of Bands 4, 5 and 7; the images were viewed on light tables. Hinged transparent overlays with letters A through F, shown as on Fig. 2, were provided to direct attention to the following individual features:

A. Highways which radiate from Kramer Junction in the Mojave Desert.

B. Street pattern in the Los Angeles Basin.

C. East branch of San Gabriel fault, an alignment of saddles and straight canyons directly north of the San Gabriel River.

D. West branch of San Gabriel fault, a lineament having a lighter tone than the background.

E. Margin of light-toned area in the Mojave Desert.

Fig. 3 - Extended range contrast enhancement of Landsat Band 7 image 1090-18012 of a portion of southern California. See Fig. 2 for features identified.

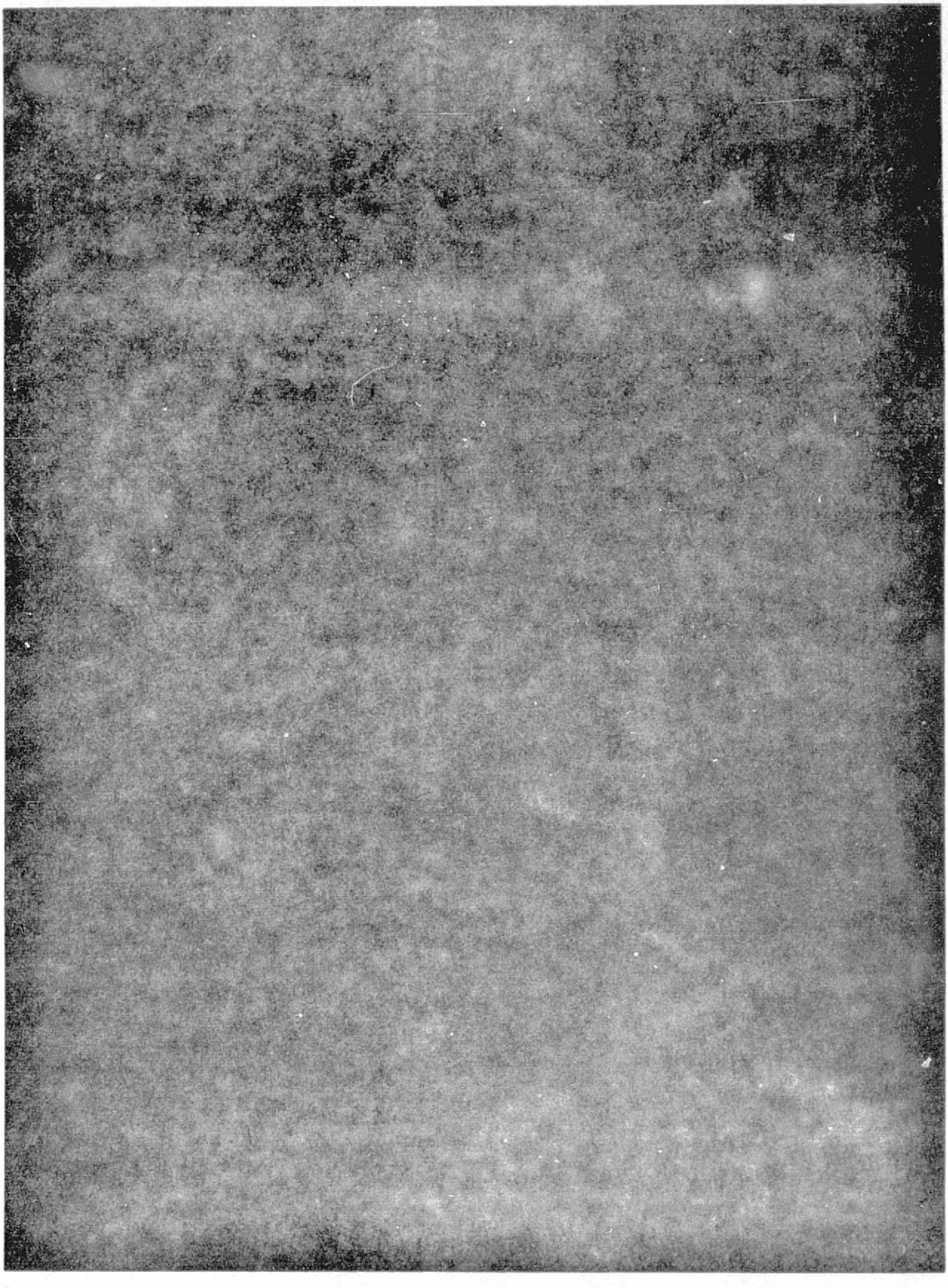

Fig. 4 - Pseudocolor image of Landsat Band 7 image 1090-18012 of a portion of southern California. See Fig. 2 for features identified.

	BAND 4		BAND 5		BAND 7		BANDS 4-5 Subtractions	
	Orig.	P.C.	Orig.	P.C.	Orig.	P.C.	Orig.	P.C.
FAULTS AND LINEAMENTS								
West branch of San Gabriel fault (D)	3 (3.6)	4 (3.7)	4 (4.1)	5 (3.9)	4 (4.1)	5 (4.1)	3	2
East Branch of San Gabriel fault (C)	2 (3.1)	2 (3.1)	2 (3.8)	3 (3.6)	3 (4.1)	4 (3.9)	3	3
Libre Mountain fault (G)	3	3	4	3	4	3	1	1
Clearwater fault (H)	2	2	2	2	3	3	1	1
Little Rock lineation (I)	3	2	4	3	5	4	1	1
Average value for faults and lineaments	2.6	2.6	3.2	3.2	3.8	3.8	1.8	1.6
NATURAL FEATURES ON MOJAVE DESERT								
South margin of light toned area (E)	1 (1.2)	2 (1.7)	2 (1.4)	3 (2.2)	2 (1.5)	3 (2.4)	1	1
El Mirage Dry Lake (F)	5 (4.5)	5 (4.7)	4 (3.4)	4 (4.1)	2 (2.5)	1 (2.1)	4	5
Alluvial fan (J)	4	3	4	3	4	5	2	2
LAND USE AND CULTURAL FEATURES								
Highways which radiate from Kramer Junction (A)	1 (1.4)	2 (2.2)	2 (1.8)	3 (3.6)	3 (2.3)	4 (3.6)	1	1
Street pattern in the Los Angeles Basin (B)	1 (2.0)	2 (2.3)	2 (2.2)	3 (2.5)	4 (4.3)	5 (4.5)	1	1
Density of urban development in Los Angeles region (K-M)	1	1	1	1	4	5	1	1
Concrete-lined drainage channels and new, unplanted freeway routes (N-Q)	4	2	4	3	2	2	1-2	1-2
Cultivated fields in Mojave Desert	4	4	5	5	3	3	2	2

TABLE 1 - Summary of results of analysis of geologic and geographic features which appear on originals and pseudocolor transformations of Landsat images. Letters (A-Q) refer to features on Fig. 2. Subjective scale of 1 (not seen) to 5 (very distinct) has been applied. The results of the student test analysis are included below the values assigned by the principal author . P.C.: pseudocolor image.

F. El Mirage Dry Lake, situated directly north of a prominent alluvial fan.

The students indicated the appearance of the above features on the following subjective scale:

1 Cannot be seen

2 Indistinct or difficult to see (poor)

3 Fairly easy to see (fair)

4 Distinct and easy to see (good)

5 Very distinct and extremely easy to see (excellent)

Additional information on the test is given in Appendix 2. The results are summarized on Figs. 5 to 7, in which the mean values and standard deviations of the observations are shown above the individual histograms. The student "t" distribution was used to test for differences in the mean values of observations of original black-and-white and pseudocolor images. In cases where the test revealed a difference in the mean values, the limits in the differences at 95% confidence level were calculated. The limits in the differences in the means, if any, are indicated between the histograms for the original and pseudocolor images.

The students taking the test felt that it was difficult to assign a subjective evaluation without comparing all of the images at once. This was not considered practical, and resulting discrepancies should have been averaged out by the number of students taking the test. The principal author of this report made a comparison of the images and applied the same subjective scale, except that all of the images were laid out and compared together. This method, while providing a more direct comparison of the value of images for detecting different kinds of features, makes it difficult to maintain a constant "feel" for the values of the subjective scale. The procedure was repeated and variations of 1 to 2 units in the subjective scale were obtained. This is comparable to the standard deviations of 0.5 to 1.1 obtained in the student test. In some cases the principal author's evaluation of the images differed significantly from the students; this can possibly be attributed to two factors: (1) the former observed the two images simultaneously, while the students viewed them sequentially, and (2) the senior author had experience in evaluating pseudocolor transformations and the students had not. These factors were both found to be significant in a short series of tests conducted by the Rand group with medical images. It was found that the efficacy of pseudocolor

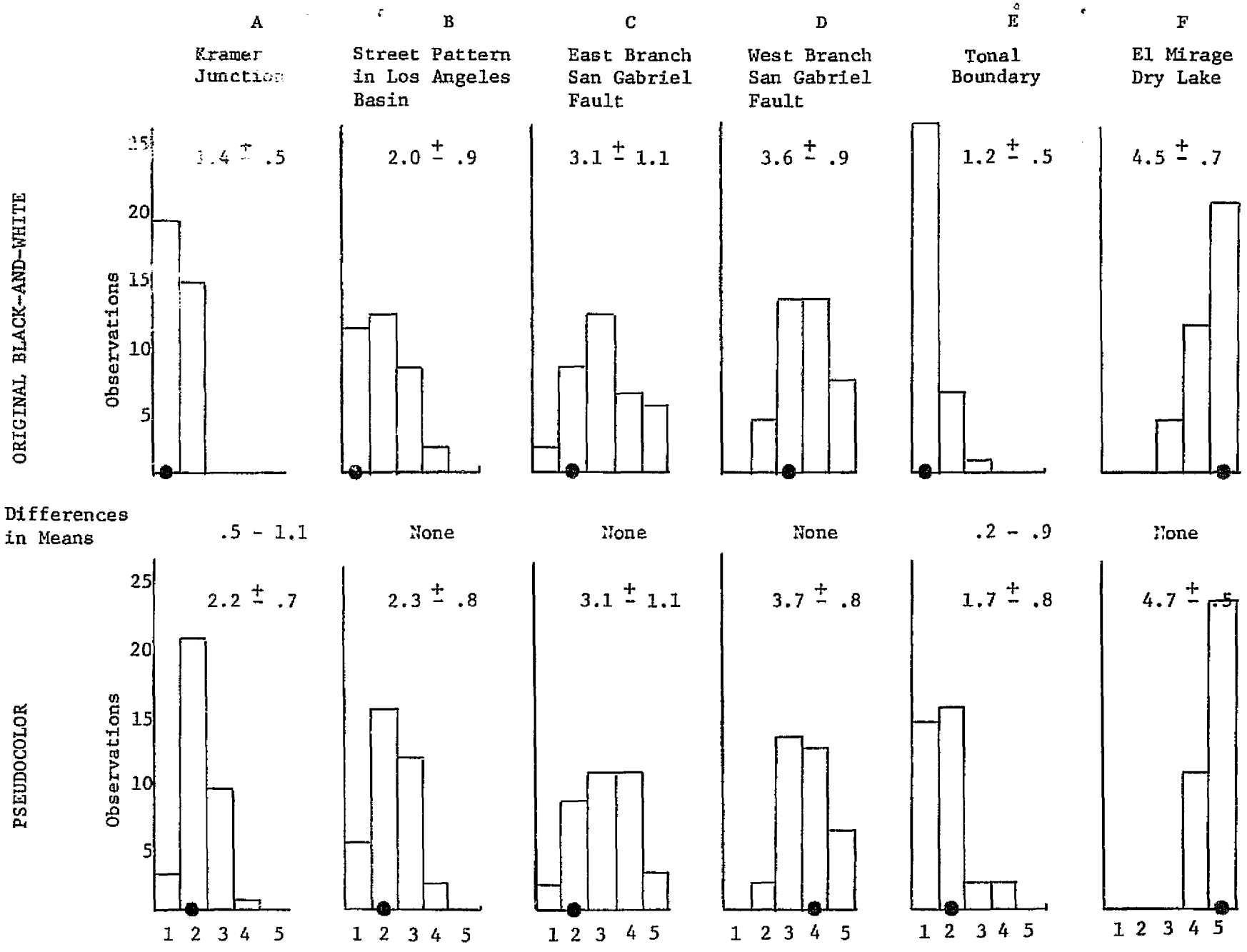

Fig. 5 - Histograms showing results of student test comparing original and pseudocolor images of Landsat Band 4. Dots on histogram indicate principal author's evaluation.

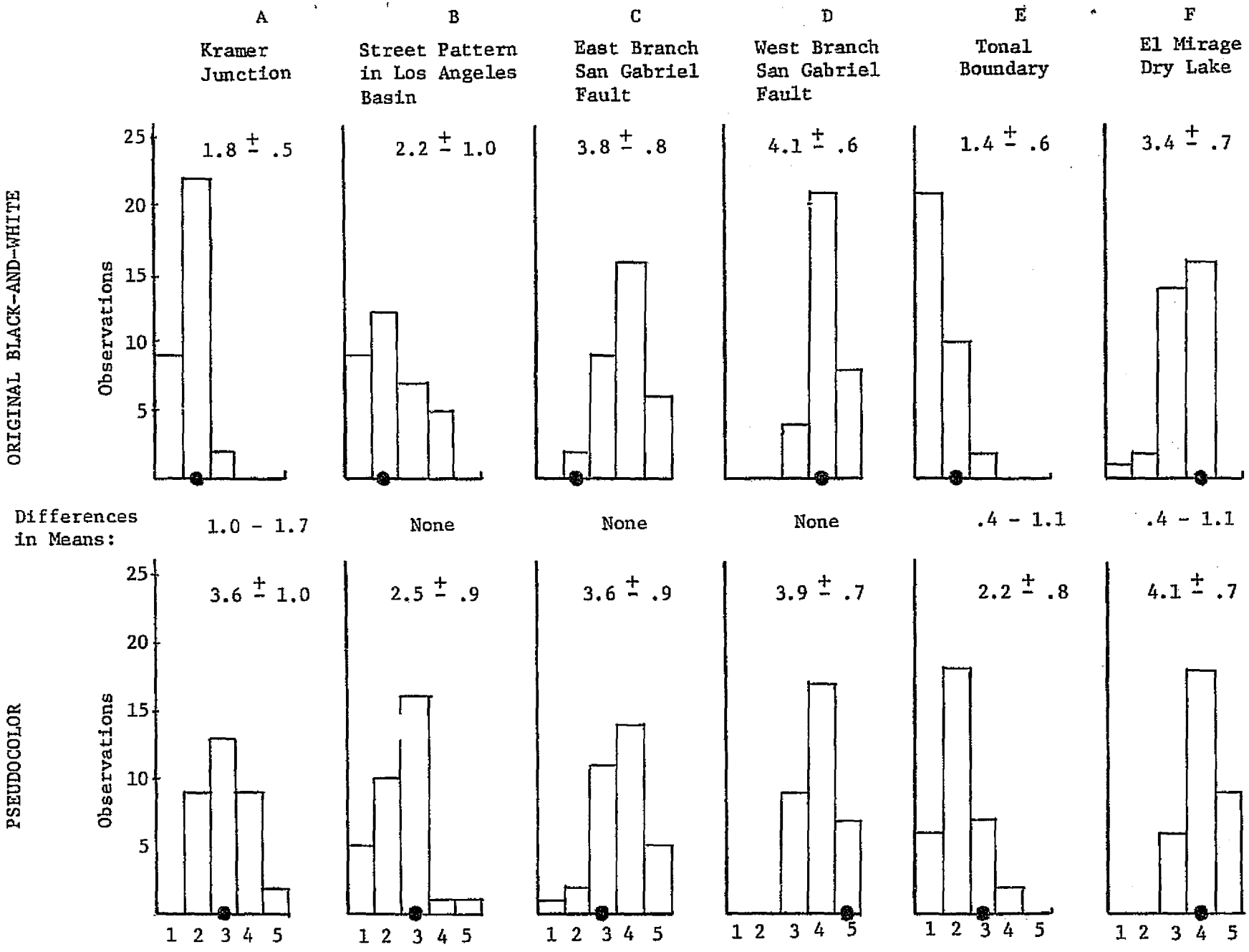

Fig. 6 - Histograms showing results of student test comparing original and pseudocolor images of Landsat Band 5. Dots on histogram indicate principal author's evaluation.

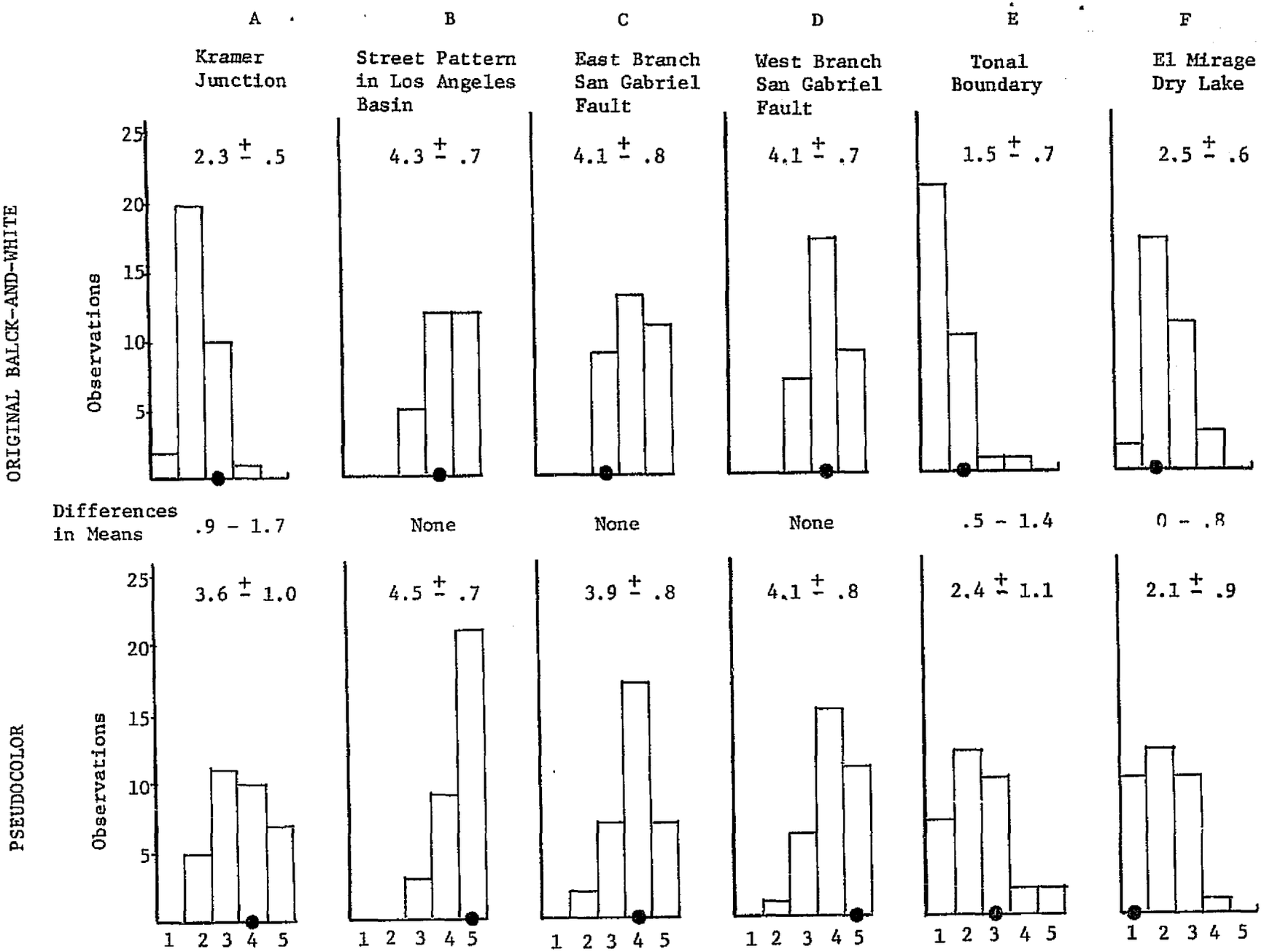

Fig. 7 - Histograms showing results of student test comparing original and pseudocolor images of Landsat Band 7. Dots on histogram indicate principal author's evaluation.

transformations is increased if the familiar black-and-white original is also present and if the observer has had some experience in evaluating pseudocolor images.

Our evaluations are summarized on Table 1; the results for those features on the student test are included for comparison. The appearance of individual features on the images and comparison of the principal author's evaluation with the student test results are discussed below.

Faults and Linears

The San Gabriel fault trends east-west to northwest across the central portion of the image shown in Fig. 2. This fault is presently inactive; the central portion of its trace cannot be seen on Fig. 2 because it is covered by younger, unbroken sediments (Ehlig, 1973). The western branch (D in Fig. 2) consists of two or more subparallel faults separating slivers of gneiss from sedimentary rocks to the east. A narrow band of breccia of Miocene to Pleistocene age occurs along the east side of the fault (Crowell, 1950); the breccia rapidly grades into finer grained rocks to the east. The trace of the west branch of the San Gabriel fault appears as a northwest trending light gray line on the Landsat image originals. In our opinion, the west branch of the San Gabriel fault is enhanced somewhat by the pseudocolor transformations, but the student test revealed no significant difference. The west branch of the San Gabriel fault can be seen (although not enhanced) on the Bands 4 and 5 subtraction images, but it is less obvious on the pseudocolor image than on the original.

The east branch of the San Gabriel fault (C on Fig. 2) trends east-west through pre-Cenozoic basement rocks of the San Gabriel Mountains. The prominent topographic expression of the fault trace is due to an alignment of deeply eroded canyons and low saddles. Alluvium shed from higher terrain to the north has displaced drainage channels, and canyon bottoms tend to lie south of the main fault zone (Ehlig, 1973). The topographic expression of the east branch of the San Gabriel fault (C on Fig. 2) is best illustrated on the pseudocolor image of Band 7; the sharpness of the topographic expression improves from west to east. We believe that the appearance is enhanced on the pseudocolor images of Bands 5 and 7, but the results of the student test do not support this conclusion. No significant difference in the appearance of the east branch of the San Gabriel fault can be seen on the Band 4 and 5 subtraction images.

The Libre Mountain fault appears as a northwest trending linear between lighter and darker gray terrane on the Landsat image originals (G on Fig. 2). The light gray area to the north is underlain by granitic and metamorphic basement rocks, and the darker gray areas to the south are underlain by Pliocene sedimentary rocks (Jennings and Strand, 1969). The fault appears to be less obvious in the Bands 5 and 7 pseudocolor images; no significant difference can be detected between the Band 4 original and pseudocolor images.

The northwest segment of the Clearwater fault (Jennings and Strand, 1969) is situated entirely in sedimentary rocks (H on Fig. 2). This feature is best displayed on the Band 7 image, and no enhancement of this feature is discernible on the pseudocolor image. Neither the Libre Mountain nor Clearwater fault can be detected on the Bands 4 and 5 subtractions.

Segments of Little Rock Creek and Bare Mountain Canyon appear as a prominent linear on the Landsat image (I on Fig. 2). Published geologic maps (Jennings and Strand, 1969) do not show a fault along this linear. The linear is situated in basement complex consisting of highly fractured and sheared granitic and metamorphic rocks which lack persistent foliation direction or prominent jointing. Considerable field work would be required to map the distribution of rock types and structure in sufficient detail to determine the nature of this linear. Our reconnaissance examination was inconclusive and the existence of a fault could not be established. Regardless of its origin, it is typical of linears seen in Landsat images. Our analysis indicates that this linear is more difficult to detect on the pseudocolor images than on the originals.

Natural Features on Mojave Desert

Slight differences in tone appear in images of the Mojave Desert because of variations in vegetation, soil and rock type. The faint line at E (Fig. 2) corresponds to a vegetation change. South of the tonal boundary (darker region), vegetation consists mostly of brown sage brush spaced 0.6-2 meters (2-6 feet), but dark green Joshua trees and creosote bushes are interspersed throughout the sage. The lighter region to the north supports brown sage spaced 2-4 meters (6-13 feet); dark green Joshua trees and creosote bushes are rare to absent. In both areas the soil is light brown, fine-grained sand and silt with scattered granules and pebbles. The lighter tone is believed to result from the sparser sage and lack of dark green Joshua trees and creosote bushes.

This boundary is barely detectable on the originals, and our analysis indicates a consistent one step enhancement of its appearance in the pseudocolor transformations of all bands. The student test also indicated a .2 to 1.4 enhancement in the pseudocolor images. This feature is not visible in the Band 4 and 5 subtractions.

Large dry lakes appear as prominent light areas on Band 4 originals, and even more prominent on the Band 4 and 5 subtraction; they are somewhat less prominent on Band 5 and 7 images. El Mirage Dry Lake (F on Fig. 2) was included on the student test, and no significant improvement in the pseudocolor image over the Band 4 original was noted, but the student test shows a .4 to 1.1 improvement of the pseudocolor over the Band 5 original. The principal author did not believe that this lake could be differentiated on the Band 7 pseudocolor images, but it was seen by a majority of the students. The test results also indicate that it is more difficult to detect in pseudocolor than in the Band 7 original. On the other hand, El Mirage Dry Lake is further enhanced in the pseudocolor image of the Band 4 and 5 subtraction.

A prominent dark alluvial fan can be seen at the east edge of the image (J on Fig. 2). This feature is most prominent on the Band 7 pseudocolor image. It is less prominent on Bands 4 and 5 pseudocolor images than on the originals, and is barely detectable on the Band 4 and 5 subtraction images. The dark tone of the fan relative to the adjacent desert surface results from a thin veneer of dark gray Pelona schist debris deposited by mudflows, notably one of 1941 (Sharp and Nobles, 1953).

Land Use and Cultural Features

Our study indicated a consistent one step enhancement in the appearance of highways which radiate from Kramer Junction (A on Fig. 2) on the pseudocolor transformations of all bands. The student test indicated a similar enhancement of .5 to 1.7. This feature appears most prominently on the pseudocolor transformation of Band 7. Similar results were obtained in our study of street patterns in the Los Angeles Basin (B on Fig. 2). In contrast, the student test revealed no significant difference in the appearance of street patterns on originals and pseudocolor images. Streets and roads are not visible on the original and pseudocolor transformation of the Band 4 and 5 subtraction.

The dense urban development of downtown Los Angeles appears as a darker gray area on the Band 7 original. Areas of less intensive development fade

into lighter shades in the peripheral areas. Darker gray areas corresponding to outlying urban centers in Pasadena (K on Fig. 2), Long Beach (L), and Santa Monica (M) can also be differentiated and are most prominently displayed on the pseudocolor transformation of Band 7. These urban areas are not detectable on the originals and pseudocolor transformations of the other bands, or in the Band 4 and 5 subtractions.

The concrete-lined channels of the Los Angeles (N on Fig. 2), San Gabriel (O), and Santa Ana (P) rivers appear as white lines on the originals of Bands 4 and 5. A recently completed segment of the Foothill Freeway (Q) has a similar appearance. Older segments of the freeway system do not appear as white lines because they become darker with use and originally barren land along the freeways is planted. These light-colored linear features are less well displayed on Band 7 and all the pseudocolor images. Only the new segment of the Foothill Freeway can be seen in the Band 4 and 5 subtractions.

Cultivated fields in the Mojave Desert appear as rectangles with varying shades of gray on the originals and as different hues on the pseudocolor images. These features are best displayed on Band 5 images; the pseudocolor images offer no obvious advantages in viewing these features.

DISCUSSION OF SKYLAB IMAGES

Fig. 8 shows an image taken by the S-190A camera on Skylab Mission 2 (SL2) from camera station 5 (bandwidth: .6 to .7 μm), Pass 2, Track 63, Frame 111. This Skylab frame covers portions of the Mojave Desert, Tehachapi Mountains, and San Gabriel Mountains shown on the Landsat image (Figs. 2-4) previously discussed. Fig. 9 is a high contrast image and Fig. 10 is a pseudocolor transformation of this image. Similar to the Landsat image, major structural features, such as the San Andreas and Garlock faults, are well displayed and the pseudocolor image offers no obvious advantages.

Transparencies of the original and pseudocolor images were carefully compared to see if any features were visible on the pseudocolor image which could not be delineated on the original. No such features were recognized. The appearances of eight features were compared on the original (Fig. 8), the high contrast positive (Fig. 9), and the pseudocolor transformation (Fig. 10). The results of the comparisons using the subjective scale presented above are tabulated on Table 2. Features characterized by slight tonal differences can best

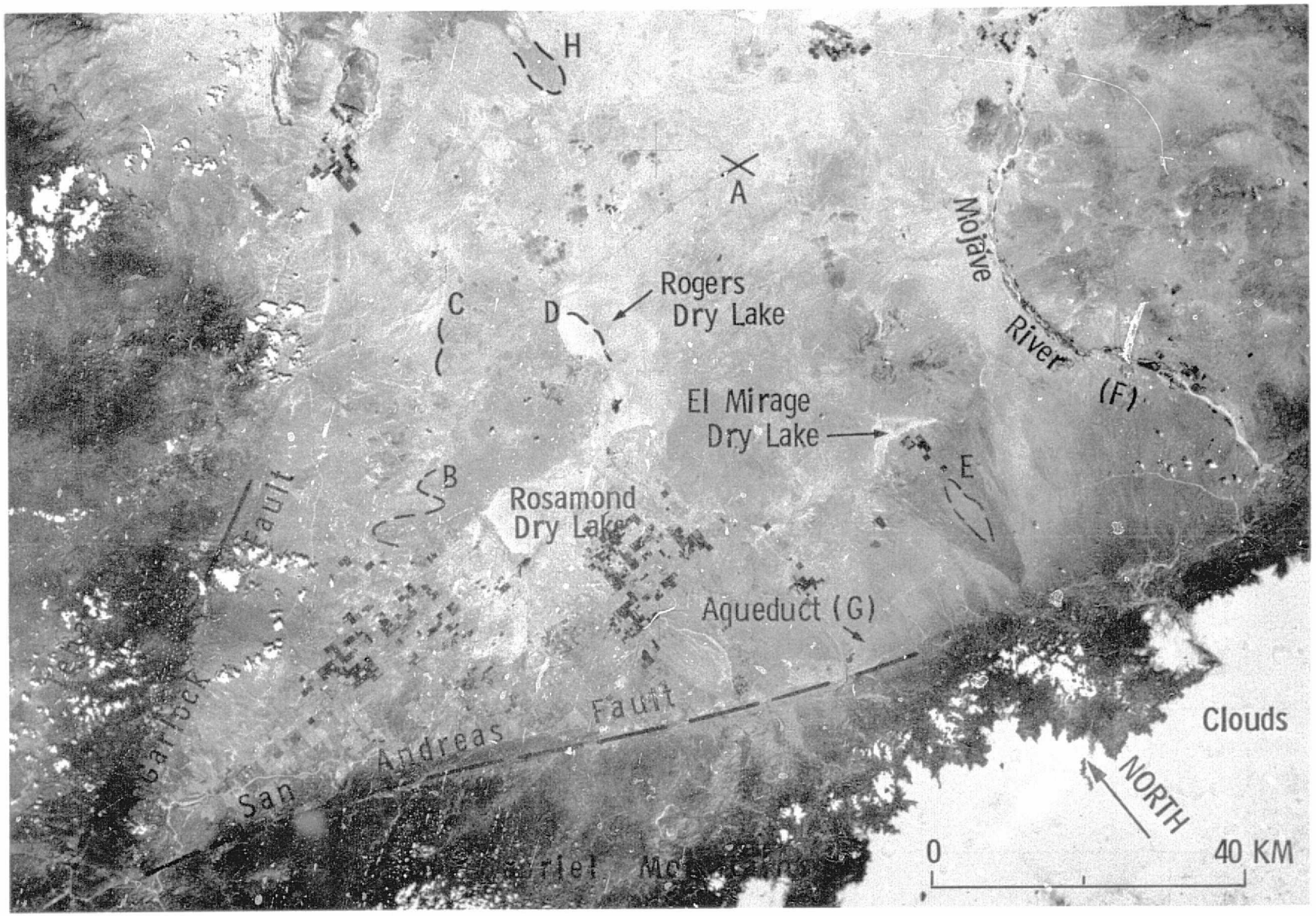

Fig. 8 - Portion of Mojave Desert, Tehachapi Mountains, and San Gabriel Mountains, southern California. Portion of Skylab 2, 190A camera image, bandwidth .6 to .7 μm, Pass 2, Track 63, Roll 2, Frame 111. See text for key to letters.

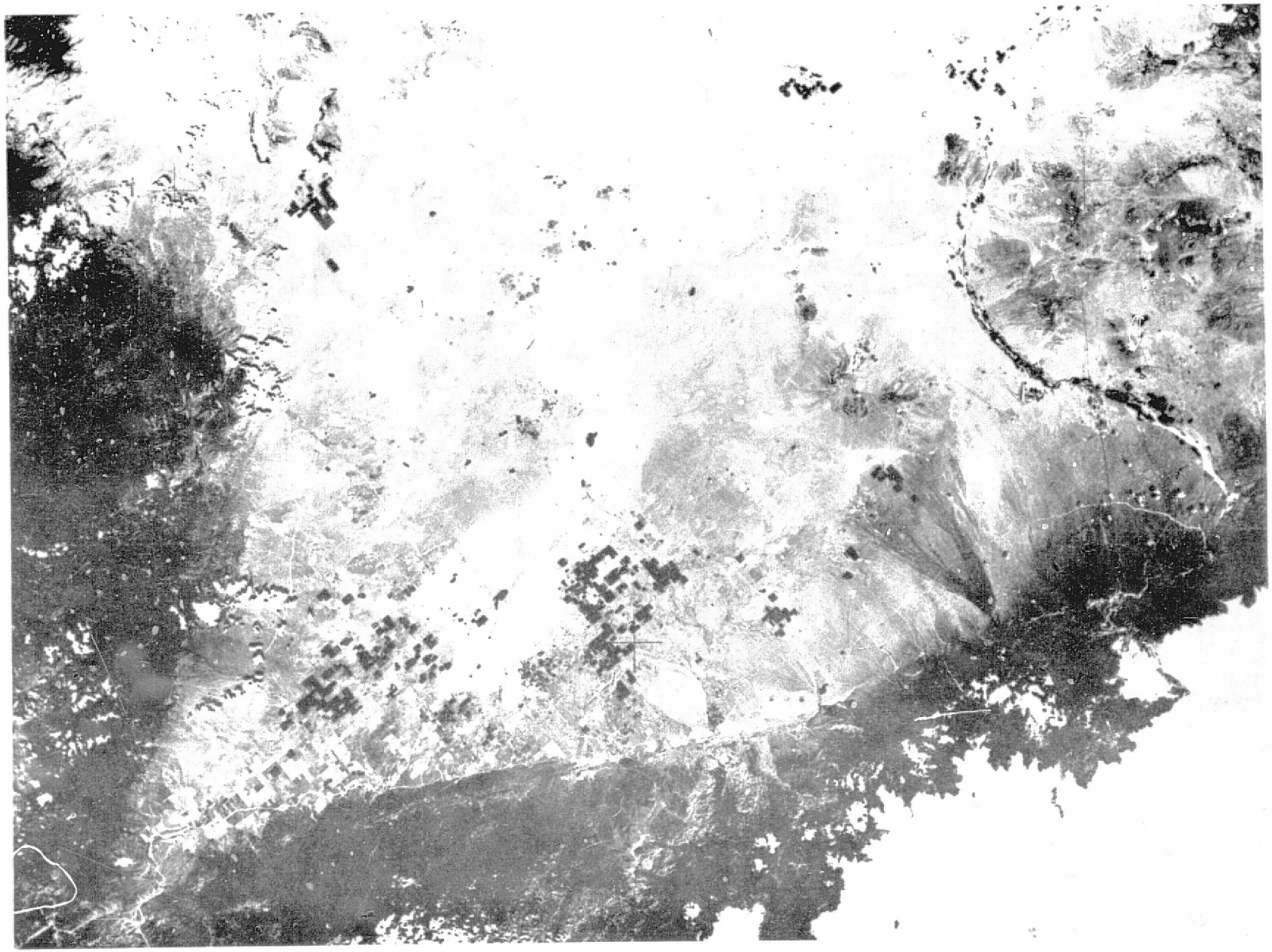

Fig. 9 - Portion of Mojave Desert, Tehachapi Mountains, and San Gabriel Mountains, southern California. Extended range contrast enhancement of portion of Skylab 2, 190A camera image, bandwidth .6 to .7 μm, Pass 2, Track 63, Roll 2, Frame 111. See Fig. 8 for features identified.

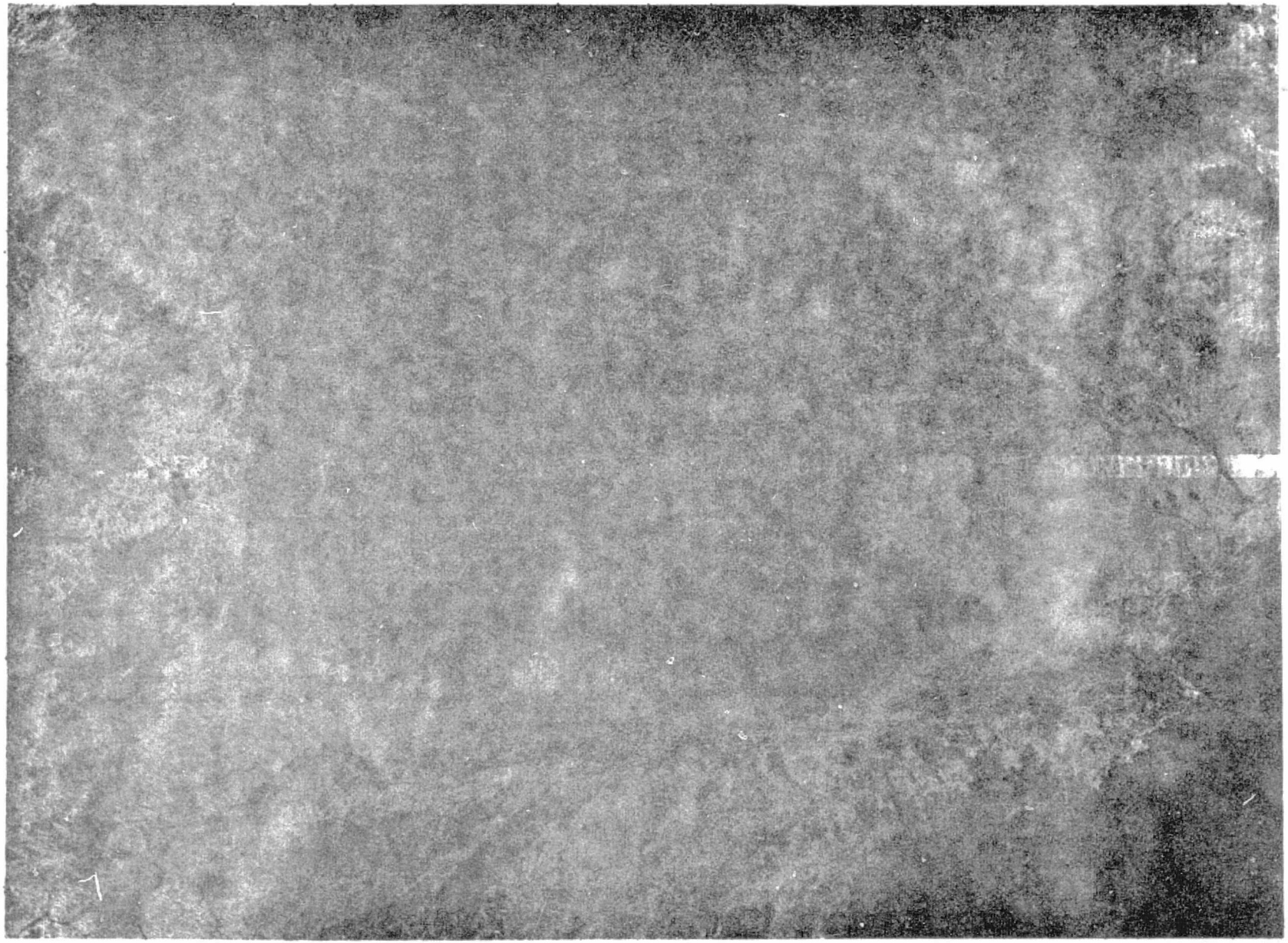

Fig. 10 - Portion of Mojave Desert, Tehachapi Mountains, and San Gabriel Mountains, southern California. Pseudocolor image of portion of Skylab 2, 190A camera image, bandwidth .6 to .7 μm, Pass 2, Track 63, Roll 2, Frame 111. See Fig. 8 for features identified.

Feature	Original	High Contrast	Pseudo-color
A. Highways radiating from Kramer Junction	4	4	4
B. Sharp tonal boundary on desert surface northwest of Rosamond Dry Lake	3	4	4
C. Diffuse tonal boundary on desert surface northwest of Rogers Dry Lake	2	3	3
D. Tonal boundary within Rogers Dry Lake	3	4	3
E. Tonal pattern within alluvial fan south of El Mirage Dry Lake	3	3	2
F. Course of Mojave River	3	4	3
G. Course of aqueduct	3	4	4
H. Tonal boundary north of Rogers Dry Lake	3	4	4
Average	3.0	3.8	3.4

Table 2 - Comparison of features which appear on original, high contrast black and white, and pseudocolor transparent images of Skylab image of Mojave Desert (Figs. 8-10). Subjective scale of 1 (not seen) to 5 (very distinct) was applied.

be seen on the high contrast black and white image, and the pseudocolor image provides no significant improvement in the ability to discriminate features.

Fig. 11 was taken by the S-190A camera on Skylab Mission 2 (SL2), camera station 5 (bandwidth: .6 to .7 μm), Pass 2, Track 63, Roll 5, Frame 114. This Skylab frame covers Coachella Valley at the northwest end of the Salton Trough and mountains and valleys located to the northeast and southwest. Fig. 12 is a pseudocolor transformation of this image. The major structural features are well displayed on all of the images and the pseudocolor transformation offers no obvious advantages. Transparencies of the black and white original, high contrast, and pseudocolor images were compared to see if any features or slight differences in tone could be seen on the pseudocolor image which could not be seen on the black and white images. No such features were identified, and no difference in the ability to discriminate individual features on the black and white and pseudocolor images could be detected. Comparison of the yellow portions of the pseudocolor image with the corresponding gray areas on the high contrast black and white image indicates that details appear to be washed out on the pseudocolor image relative to the black and white. However, somewhat greater detail can be seen in the blue areas which appear as dark gray or black on the black and white originals.

Fig. 13 is a subtraction image prepared from camera stations 5 (.6 to .7 μm) and 6 (.5 to .6 μm) of Skylab mission 2 (SL2), Pass 2, Track 63, Roll 5, Frame 114 of the north end of Salton Sea and adjacent areas, southern California. Fig. 14 is a pseudocolor transformation of this image. Changes in tone or color from the margins of the image due to the projection are apparent, and no advantages in the subtraction image and its pseudocolor transformation can be detected.

ANALYSIS OF SYMBOL CHARTS

For the Skylab and Landsat images studied, it was concluded that, for geologic applications, the enhancement provided by the pseudocolor transformations is not sufficient to justify their preparation. This result was unexpected because of previous tests which suggested that observers should be able to extract significantly more information from a pseudocolor transformation of an original complex black and white image. Because of the discouraging results in our analysis of Skylab and Landsat images, the research was redirected toward a study of the ability to recognize simple symbols on charts.

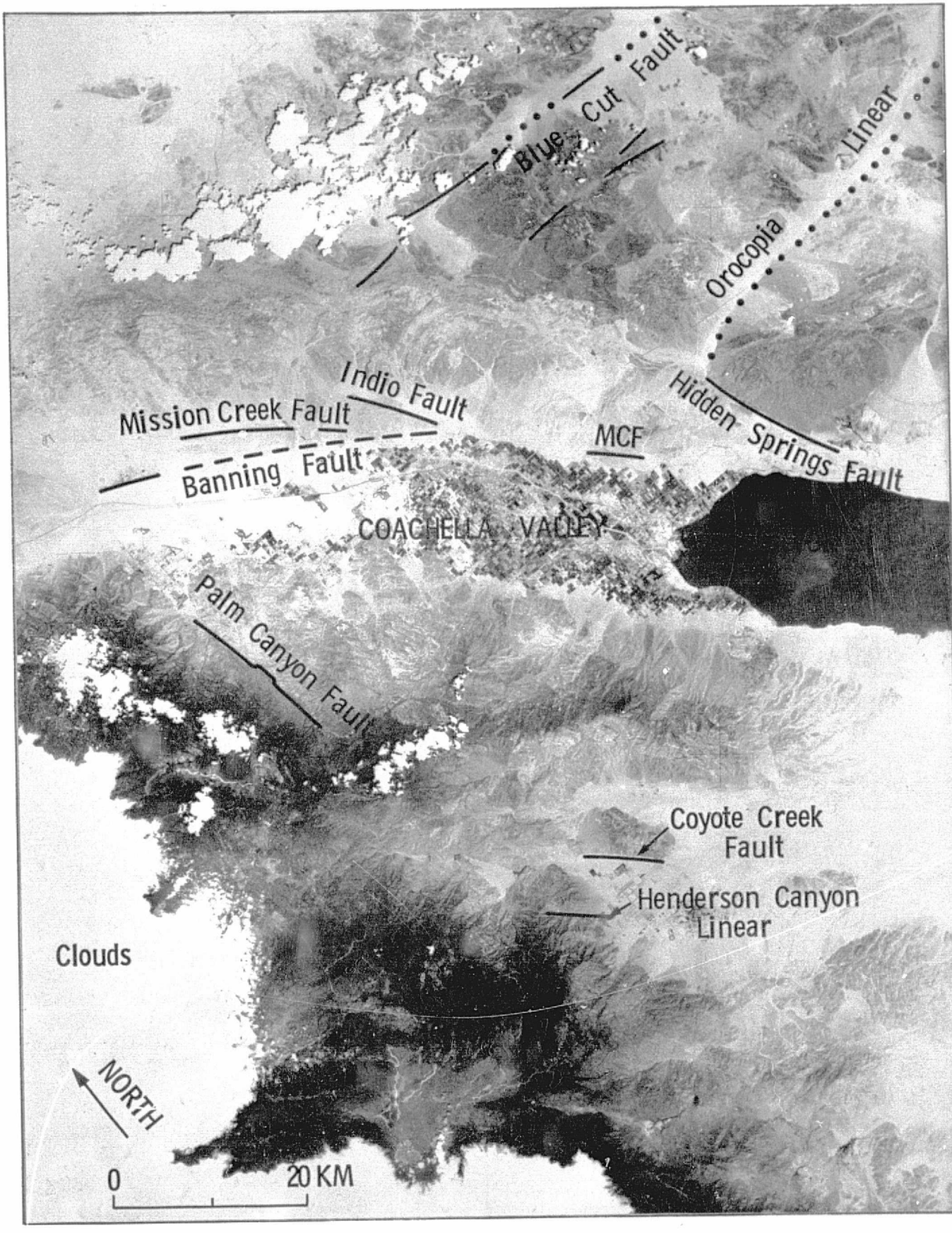

Fig. 11 - North end of Salton Sea and adjacent areas, southern California. Portion of Skylab 2, 190A camera image, bandwidth .6 to .7 μm, Pass 2, Track 63, Roll 5, Frame 114. Abbreviation: MCF: Mission Creek fault.

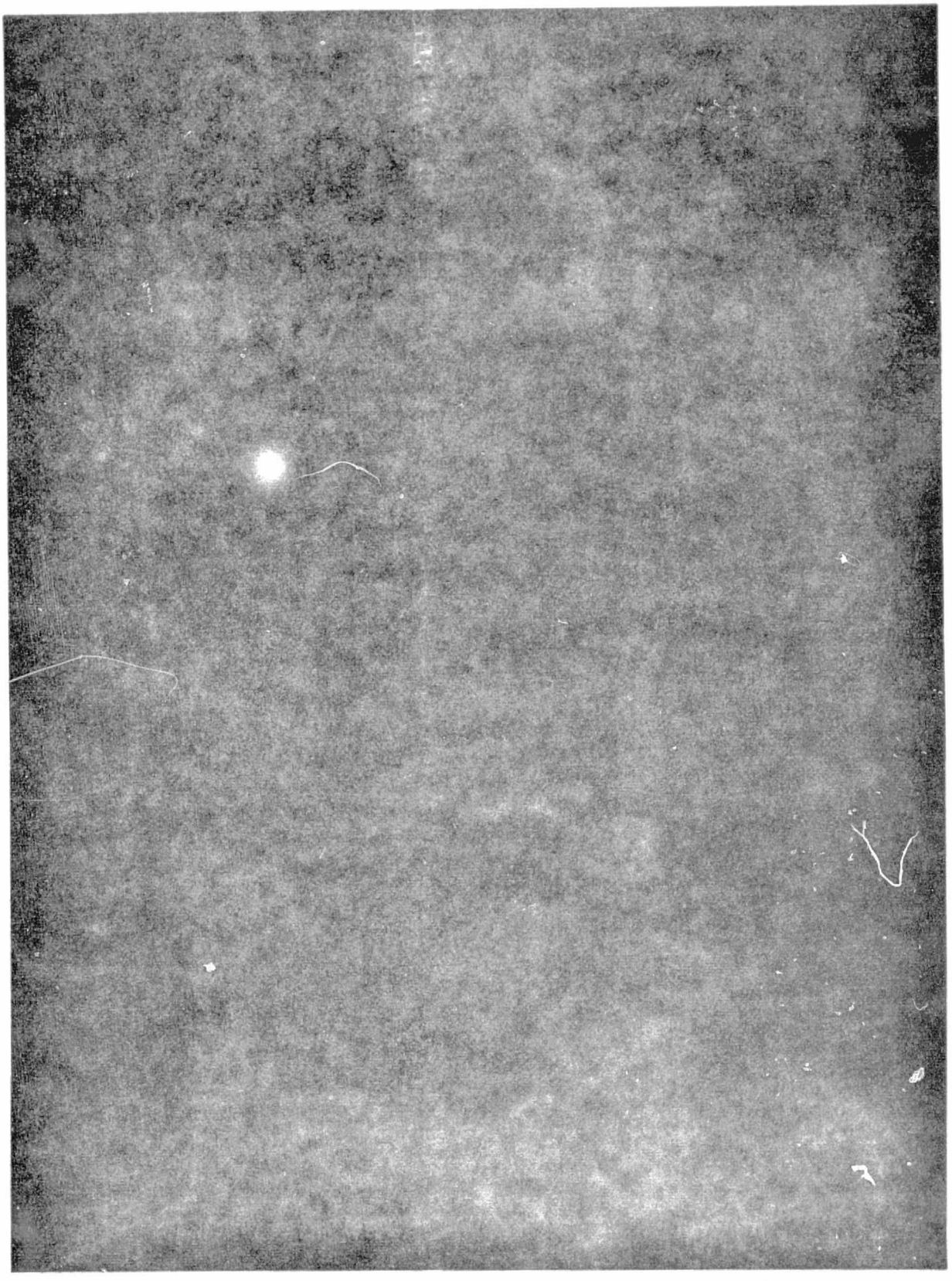

Fig. 12 - North end of Salton Sea and adjacent areas, southern California. Pseudocolor image of portion of Skylab 2, 190A camera image, bandwidth .6 to .7 μm, Pass 2, Track 63, Roll 5, Frame 114. See Fig. 11 for features identified.

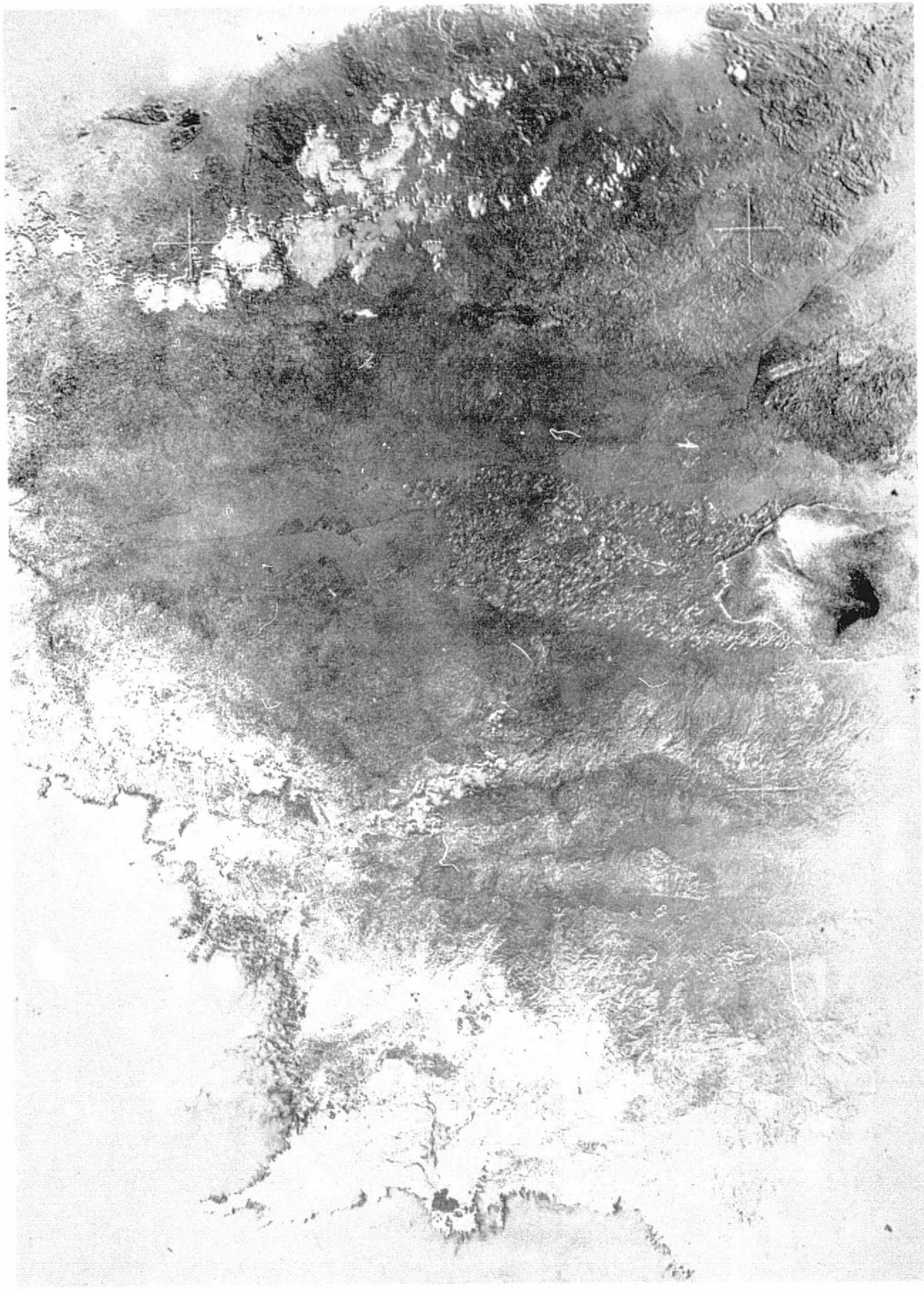

Fig. 13 - North end of Salton Sea and adjacent areas, southern California. Subtraction image prepared from Skylab 2, 190A camera images of bandwidths .5 to .6 μm and .6 to .7 μm, Pass 2, Track 63, Roll 5, Frame 114. See Fig. 11 for features identified.

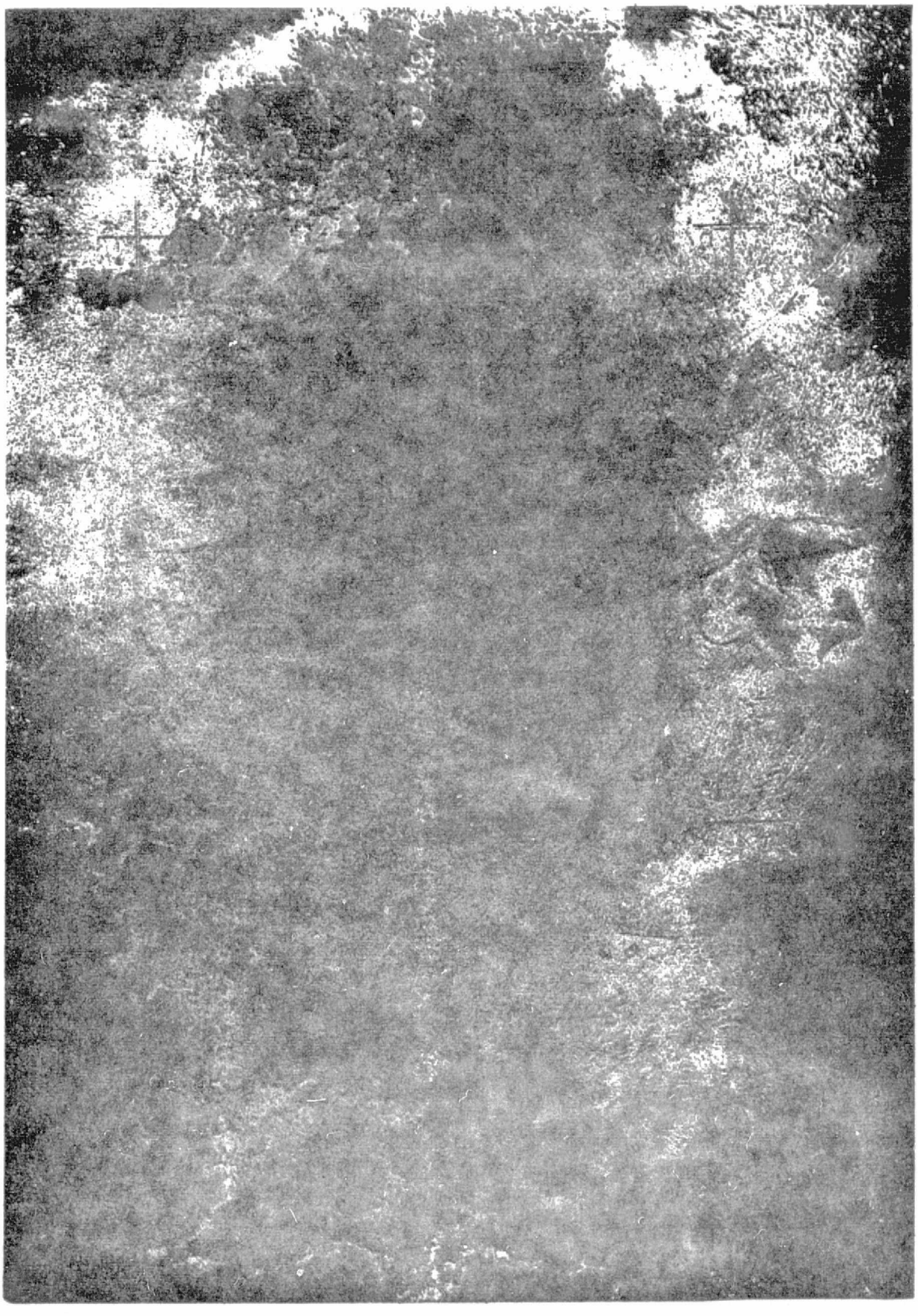

Fig. 14 - North end of Salton Sea and adjacent areas, southern California. Pseudocolor of subtraction image prepared from Skylab 2, 190A camera images of bandwidth .5 to .6 μm and .6 to .7 μm, Pass 2, Track 63, Roll 5, Frame 114. See Fig. 11 for features identified.

A number of charts with symbols and backgrounds of varying intensity were generated by computer graphics methods. Fig. 15 shows the chart of symbols which were displayed on each image. The intensities of symbols and backgrounds were varied so that in many cases the intensity of the symbol and background are so similar that the symbol cannot be recognized. Tests were conducted in order to evaluate the usefulness of the pseudocolor transformations in enhancing the symbols. Subjects were asked to identify symbols on backlighted transparencies of black and white originals and pseudocolor transformations. Fig. 16 is a black and white and Fig. 17 a pseudocolor transformation of chart B. Because of the difficulty in photographic reproduction of faint differences in color and tone, not all of the symbols apparent on the original transparencies used in the tests can be seen on the prints.

The results of the comparisons between the charts are tabulated in Table 3. The totals indicate that subjects were able to do somewhat better in the identification of symbols in pseudocolor versus black and white. However, as summarized in Table 4, analysis of variance shows no significance at the 5% confidence level in the pseudocolor results. On Table 4, values of F below the 5% confidence values indicate no significance at the 5% confidence level. In contrast, the results on Table 3 and the F values on Table 4 greater than 5% confidence show significant variation between individual ability to read the charts. Subjects JL and WA have had more experience in identifying computer-generated symbols and their scores were consistently higher.

Our tests indicate no significant enhancement in the ability to recognize symbols on pseudocolor transformations; however, because of differences in subjects, many more tests are required to verify this conclusion.

CONCLUSIONS

Five representative faults and linears appearing on Landsat images of the Los Angeles County area were studied. The faults appear on the originals as light lines in contrast to their surroundings, as contacts between areas of slightly different tone, and as topographic linears. Some of the structural features appeared to be enhanced on the pseudocolor transformations; others were not. However, the average value on a subjective scale of detection and identification of the five faults and lineaments was found to be the same for the originals and pseudocolor transformations. Some geographic and geologic

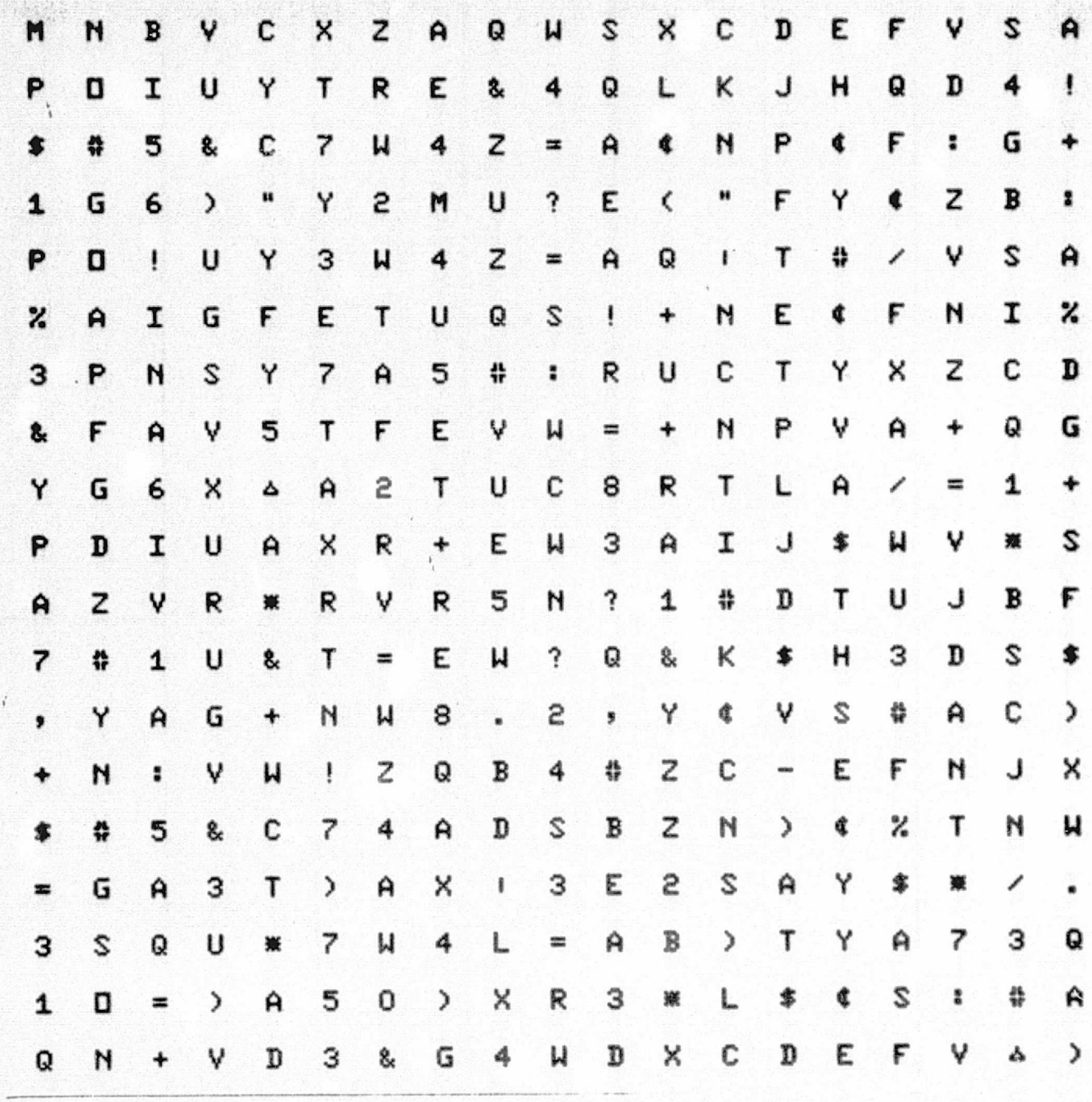

Fig. 15 - Symbols used on charts for pseudocolor tests.

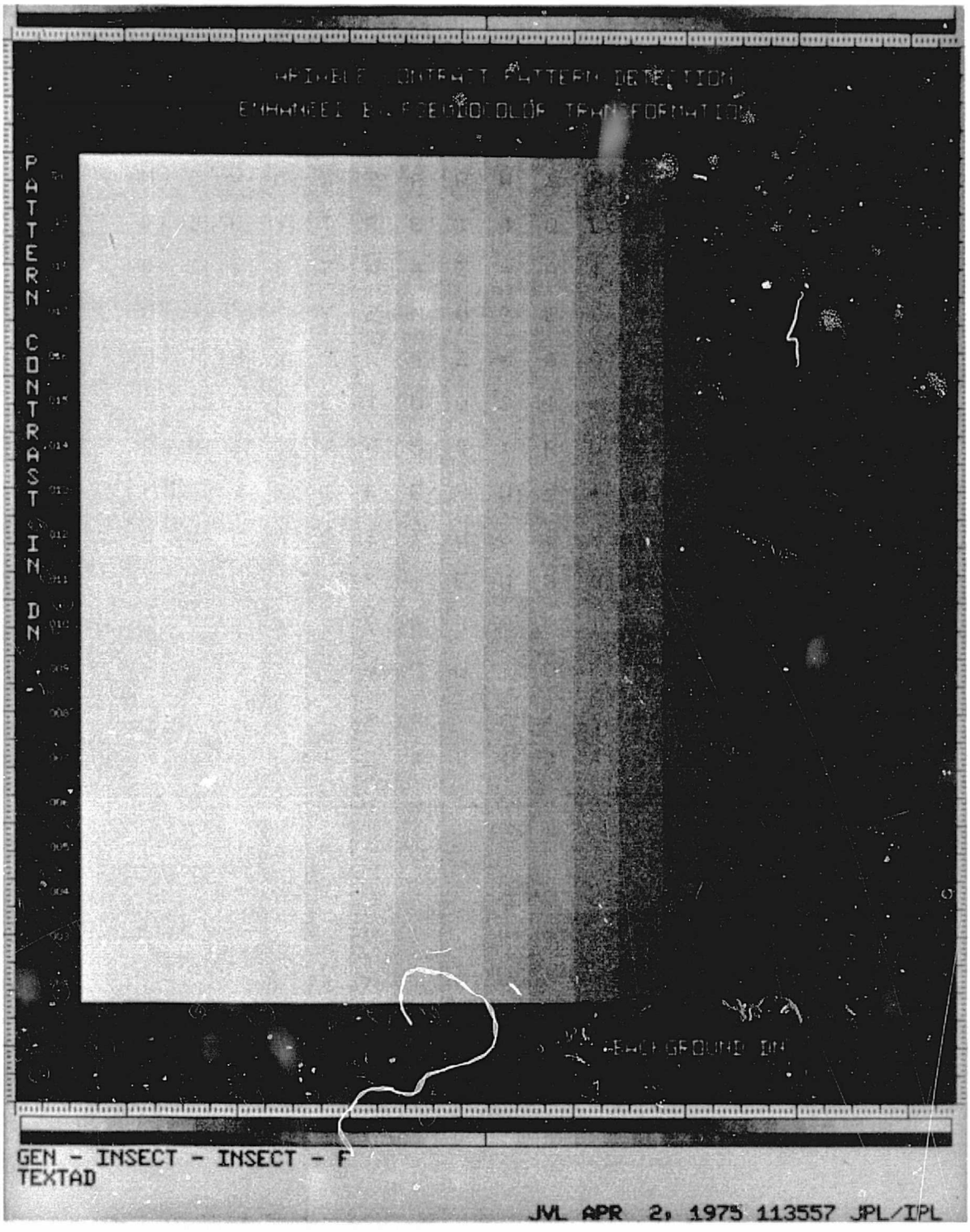

Fig. 16 - Black and white image of chart B used in pseudocolor test.

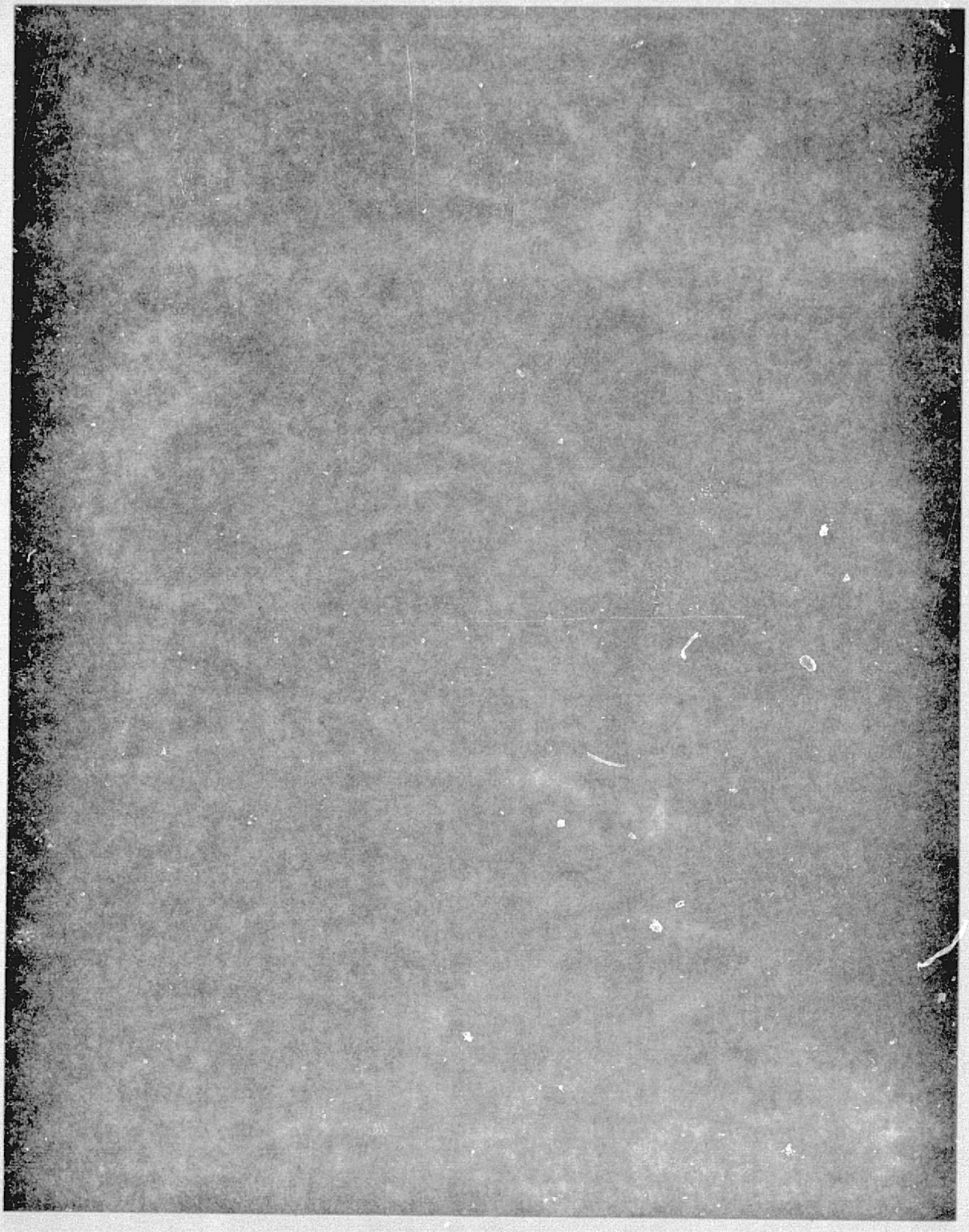

Fig. 17 - Pseudocolor transformation of chart B used in pseudocolor tests.

	SUBJECT						
	DL	RR	JL	H	WA	JB	TOTAL
Chart A							
Black and White	61		83	36			180
Pseudocolor	61		70	39			170
Chart B							
Black and White	67	55	78	55			255
Pseudocolor	74	56	86	59			275
Chart D							
Black and White	59		98		104	62	323
Pseudocolor	64		117		108	37	326
Total Black and White	187	55	259	91	104	62	758
Total Pseudocolor	199	56	273	98	108	37	771

Table 3 - Summary of results of identification of symbols on black and white test charts and pseudocolor transformations. Numbers of symbols correctly identified on each chart by subjects are indicated.

	Comparison of black and white and pseudocolor		Comparison of subjects	
	Calculated F value	F value required for 5% confidence	Calculated F value	F value required for 5% confidence
Chart A	2.17	200	21.3	19.0
Chart B	10.0	10.1	62.3	9.28
Chart C	152	216	10.5	9.28

Table 4 - F values from analysis of variance of results (Table 3) of tests of black and white and pseudocolor transformations of charts of symbols.

features, such as light-colored drainage channels, new freeway alignments, cultivated fields, dry lakes and alluvial fans, are generally either not enhanced or are more difficult to see on the pseudocolor transformations. However, pseudocolor images did provide enhancement of road intersections, street patterns, density of urban development, and slight differences in soil and vegetation tone. These results indicate that pseudocolor transformations of Landsat images provide some enhancement of certain features characterized by minor tonal differences on relatively flat surfaces. The study of pseudocolor transformations of Skylab images of southern California failed to reveal any significant enhancement of the appearance of geologic or geographic features. For the Landsat and Skylab images studied, it was concluded that for geologic applications the enhancement provided by the pseudocolor transformations is not sufficient to justify their preparation. These results were unexpected because of previous tests which indicated that observers should be able to extract significantly more information from a pseudocolor transformation of an original complex black and white image.

In view of the discouraging results in our analysis of Landsat and Skylab images, the research was redirected toward a study of the ability to recognize simple symbols on charts. The charts were generated by computer graphics with variations in the intensity of symbols and background so that some of the symbols could not be distinguished. High and low contrast black and white transparencies and pseudocolor transformations of the charts were prepared and tests were given to compare the ability to recognize symbols on the original and pseudocolor images. We were unable to detect any significant difference in the ability to recognize symbols on either the high-contrast black and white or on the pseudocolor transformations as compared to the original black and white images.

Our studies of selected Landsat and Skylab images and computer generated charts of symbols do not show any significant enhancement of features on photographically produced pseudocolor images. These results should be considered preliminary because of the limited number of images studied and, in view of the application to remotely sensed images, additional quantitative tests should be accomplished for comparison with our results.

ACKNOWLEDGMENT

We wish to acknowledge valuable assistance from Dr. Robert R. Rapp on the statistical analysis of the data.

APPENDIX 1

Method of Producing Pseudocolor Transformations and Subtraction Images

A complete explanation of the method for producing a full spectral gamut of colors in Ektacolor using only two separations and a discussion of colorimetry, film calibration and sensitometry appears in Stratton and Gazley (1971). The method described by Stratton and Gazley has been improved to allow emulsion-to-emulsion printing in all steps of the process.

The current photographic technique for the production of a pseudocolor transformation of an image is shown in the schematic diagram (Fig. 18). With the exception of the originally supplied 70 mm positive, the films are 8 x 10-inch sheets; the 8 x 10 inch sheets are pre-punched and contact printed emulsion-to-emulsion in a pin-register vacuum frame to provide the required registration.

The details of the procedure are as follows:

1. The medium contrast black-and-white intermediate, 0_i, is made from the supplied 70 mm positive image by projection printing onto Kodak commercial film 4127 and developed in DK 50 diluted 1:1. Exposure and developing time are such as to yield a density range of approximately .50 to 1.50.

2. The high contrast black-and-white positive separation, 0_p, is printed from 0_i on Kodak contrast process ortho film 4154 and developed in D-11 diluted 1:1. Exposure and developing time are such as to yield a density range of approximately .30 to 2.70.

3. The high contrast black-and-white negative separation, 0_n, is printed from 0_i on Kodak high speed duplicating film 4575 and developed in DK 50 diluted 1:1. Exposure and developing time are such that the density range is approximately the same as 0_p.

4. To obtain the final pseudocolor transformation, 0_n and 0_p are printed onto a single sheet of Kodak Ektacolor print film 4109. The 0_n exposure is accomplished with a red light source (tungsten lamp plus wratten 23A filter), and subsequently the 0_p exposure is accomplished with a blue light source (tungsten lamp plus wratten 47A filter). The exposures of each separation are controlled to yield a transformation which contains all the spectral hues. The light areas in the original 70 mm positive black-and-white image appear as red, the medium areas as yellow-green, and the dark areas as blue. The Ektacolor film is developed in unmodified Kodak C-22.

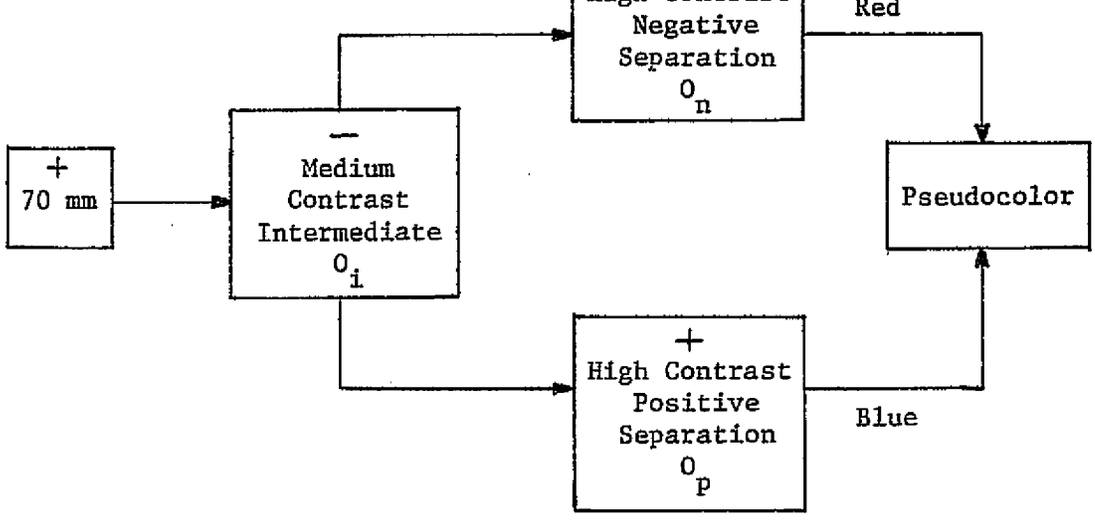

Fig. 18 - Diagram of two separation pseudocolor transformation process.

The intermediate 0_i required for a pseudocolor transformation of subtraction of two different spectral bands of the same image is produced as follows:

1. A positive image is printed on 8 x 10 inch commercial black-and-white film from one band and a negative image is printed from the other band. The film is exposed and developed to a gamma of approximately one.

2. These 8 x 10 images are positioned in register with rear illumination and copied photographically (not by contact), and developed to produce the medium black-and-white intermediate 0_i with a nominal density range of .50 to 1.50.

3. The pseudocolor transformation is produced from the 8 x 10 intermediate 0_i following the method outlined above in steps 2, 3, and 4.

APPENDIX 2

Details of Student Test

Transparencies of Landsat images were placed at 12 stations on two rows of light tables. Station numbers for the images are as follows:

Station Numbers	Band	Description
1, 10	4	Original
2, 7	4	Pseudocolor
3, 11	5	Original
4, 8	5	Pseudocolor
5, 12	7	Original
6, 9	7	Pseudocolor

Twelve students were assembled, one at each station, and the following written instructions were given:

A number of stations with Landsat images of a portion of southern California have been made up. The purpose is to test your ability to detect different features on different types of images. It is important that you visit the stations in the order indicated on the answer sheet; do not go out of turn or look at adjacent stations. You will be allowed 2 minutes at each station. Do not waste time looking for features which are difficult to see on some images. Lettered overlays have been prepared to direct your attention to the particular features.

Indicate your impression of how well these features can be seen on the images by placing numbers 1 to 5 in the appropriate boxes for each image and feature. Use the following subjective scale:

1 Cannot be seen
2 Indistinct or difficult to see (poor)
3 Fairly easy to see (fair)
4 Distinct and easy to see (good)
5 Very distinct and extremely easy to see (excellent)

It was found that more than two minutes were required for each of the first few images; however, as the students became more familiar with the test, less time was required.

The sequence of viewing individual images could have influenced the student's opinion of the appearance of individual features. To avoid this bias, the students visited the stations in different sequences. The different sequences of stations and the number of students who visited each sequence are tabulated as follows:

Number of Students	Station Sequences						Number of Students	Station Sequences					
4	1	2	3	4	5	6	1	6	5	4	3	2	1
1	2	3	4	5	6	1	1	5	4	3	2	1	6
1	3	4	5	6	1	2	1	4	3	2	1	6	5
1	4	5	6	1	2	3	1	3	2	1	6	5	4
1	5	6	1	2	3	4	1	2	1	6	5	4	3
1	6	1	2	3	4	5	1	1	6	5	4	3	2
2	7	8	9	10	11	12	1	12	11	10	9	8	7
2	8	9	10	11	12	7	1	11	10	9	8	7	12
2	9	10	11	12	7	8	1	10	9	8	7	12	11
2	10	11	12	7	8	9	1	9	8	7	12	11	10
2	11	12	7	8	9	10	1	8	7	12	11	10	9
2	12	7	8	9	10	11	1	7	12	11	10	9	8

It is believed that the sequence of visiting stations was sufficiently random to eliminate any "learning bias" in favor of the pseudocolor images.

Each of the students was given a standard color blindness test; no evidence of color blindness was detected.

REFERENCES

Anonymous, 1969, Color this brain visible: Life, March 7.

Anonymous, 1972, System 800 Model 805 color display: Spatial Data Systems, Inc., Goleta, Calif.

Anonymous, 1974, Image 100; Ground Systems Department, Space Division, General Electric, Daytona Beach, Florida.

Crowell, J. C., 1950, Geology of Hungry Valley area, southern California; Amer. Assoc. Petrol. Geol., Bull., V. 34, p. 1623-1646.

Ehlig, P. L., 1973, History, seismicity and engineering geology of the San Gabriel Fault; in Geology, Seismicity, and Environmental Impact, Assoc. of Engineering Geologists Special Publication, p. 247-251.

Gazley, C., Jr., Rieber, J. E., and Stratton, R. H., 1967, Pseudocolor processing of electronic photographs: The Rand Corp., RM-5297-PR.

Halsey, R. M., and Chapanis, A., 1954, Chromaticity-confusion contours in a complex viewing situation: J. Opt. Soc. Am., v. 44, p. 442.

Jennings, C. W., and Strand, R. G., 1969, Los Angeles Sheet of Geologic Map of California; Calif. Div. Mines and Geology.

Lamar, D. L., Merifield, P. M., Stratton, R. H., Lamar, J. V., and Gazley, Carl, Jr., 1974, Analysis of pseudocolor transformations of ERTS-1 images of southern California area: CalESCO Technical Report 74-2, 23 p.

LeGrand, Y., 1957, Light, color and vision: Chapman & Hall, Ltd., London, Chap. 13.

Maas, K. A., 1973, Building color images; Technical Photography, February.

Sharp, R. P., and Nobles, L. H., 1953, Mudflow of 1941 at Wrightwood, Southern California; Geol. Soc. Am. Bull., V. 64, p. 547-560.

Sheppard, J. J., Stratton, R. H., and Gazley, C., Jr., 1966, Pseudocolor as a means of image enhancement: The Rand Corp. P-3988.

Sheppard, J. J., Moshin, H. L., Stratton, R. H., Dugas, D., and Madansky, A., 1967, Color discrimination in static displays: The Rand Corp. RM-5303-ARPA.

Stratton, R. H., and Gazley, C., Jr., 1971, A photographic technique for image enhancement: Pseudocolor two-separation process: The Rand Corp. R-597-PR.

PART VI

ANALYSIS OF S-192 IMAGERY OF THE WESTERN MOJAVE DESERT, CALIFORNIA

by

P. M. Merifield, D. L. Lamar and
J. V. Lamar

PREFACE

Images of single spectral bands and ratios of bands generated from Skylab S-192 multispectral scanner data were studied as a portion of a broader investigation to apply Skylab imagery to the analysis of fault tectonics and earthquake hazards of southern California. In most cases, faults were not significantly enhanced on spectral band ratio images in the area studied, but it was discovered that certain other features became visible or were more clearly delineated. The results of study of these features are presented in this report. A summary of this material was presented at a meeting of the American Geophysical Union (Lamar, Merifield, and Lamar, 1975).

CONTENTS

ILLUSTRATIONS

ABSTRACT

A number of geologic features in the western Mojave Desert and adjacent mountainous areas can be seen on images generated from Skylab S-192 multispectral scanner data. The appearance of some features is enhanced on images generated from ratios of the individual bands. A change in vegetation across a segment of the San Andreas fault in the San Gabriel Mountains is enhanced on the Band 9 (1.09 to 1.19 μm) to Band 2 (.46 to .51 μm) ratio image. A marble unit being quarried for cement in the Tehachapi Mountains cannot be distinguished on the single band images, but the marble is sharply differentiated from granite and other metamorphic rocks on the ratio images. Alluvial deposits of different age are more readily distinguished on the ratio images than the single band images. Subtle differences in soil color resulting from variations in iron-oxide content as a function of age are apparently enhanced in the ratio images. Variations in rock type, soil and alteration products within the Mojave Mining District are also more clearly differentiated on the ratio images than on the single band images.

INTRODUCTION

Skylab 2, EREP Pass 2 provided S-192 multispectral data of a portion of the test site. The western Mojave Desert and adjacent mountainous areas (Fig. 1) were selected for evaluation because of the variety of soil and rock types and the presence of two major fault zones, the San Andreas and Garlock. The images were generated from digital tapes at the Image Processing Laboratory of the Jet Propulsion Laboratory. Contrast stretching and spectral band ratioing were applied to the data; these techniques are described in Billingsley (1973) and Billingsley and Goetz (1973). Usable data were obtained in the following bands: 2 (.46 to .51 μm), 3 (.52 to .56 μm), 6 (.68 to .76 μm), 8 (.98 to 1.08 μm), 9 (1.09 to 1.19 μm), 10 (1.20 to 1.30 μm), and 11 (1.55 to 1.75 μm). The four bands (2, 6, 9 and 11) reproduced in Figs. 2 to 5 are representative of the seven usable bands. Three images generated from ratios of the bands (9/2, 11/2 and 11/6) are shown in Figs. 6 to 8. In ratio images, the variation in gray levels is a function of the slope of the reflectivity curves between the two bands. If the denominator is greater than the numerator, the area appears dark. If the numerator is greater than the denominator, the area is comparatively light. Subtle reflectivity differences are enhanced by the process, and variations in reflectivity owing to topography are minimized.

FAULTS

The San Andreas and Garlock faults, two of the most prominent faults in California, are recognizable on the single bands (Figs. 2 to 5), largely due to topographic expression. (Refer to annotations, Fig. 6, and Index Map, Fig. 1, for features discussed.) On the segment of the San Andreas fault between Quail Lake and Elisabeth Lake, no significant tonal difference is present across the fault in the single band images. A distinct tonal difference appears across the fault in ratio image 9/2 (Fig. 6), which is not apparent in the other ratio images (Figs. 7 and 8). The tonal contrast results from a vegetation difference on either side of the fault, dense forest

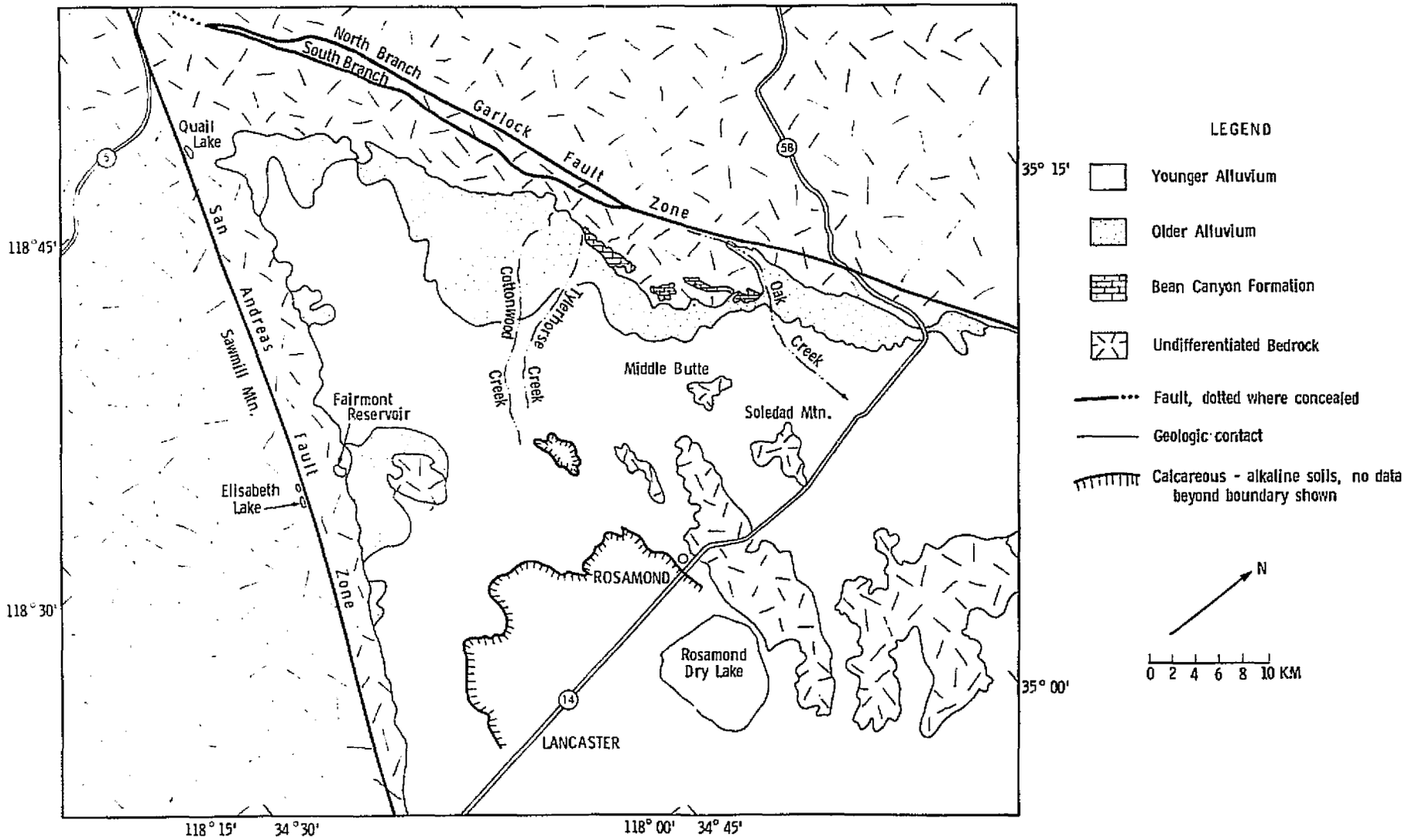

Fig. 1 - Map showing generalized geology of area covered by multispectral scanner images (Figs. 2-8), (after Dibblee, 1967).

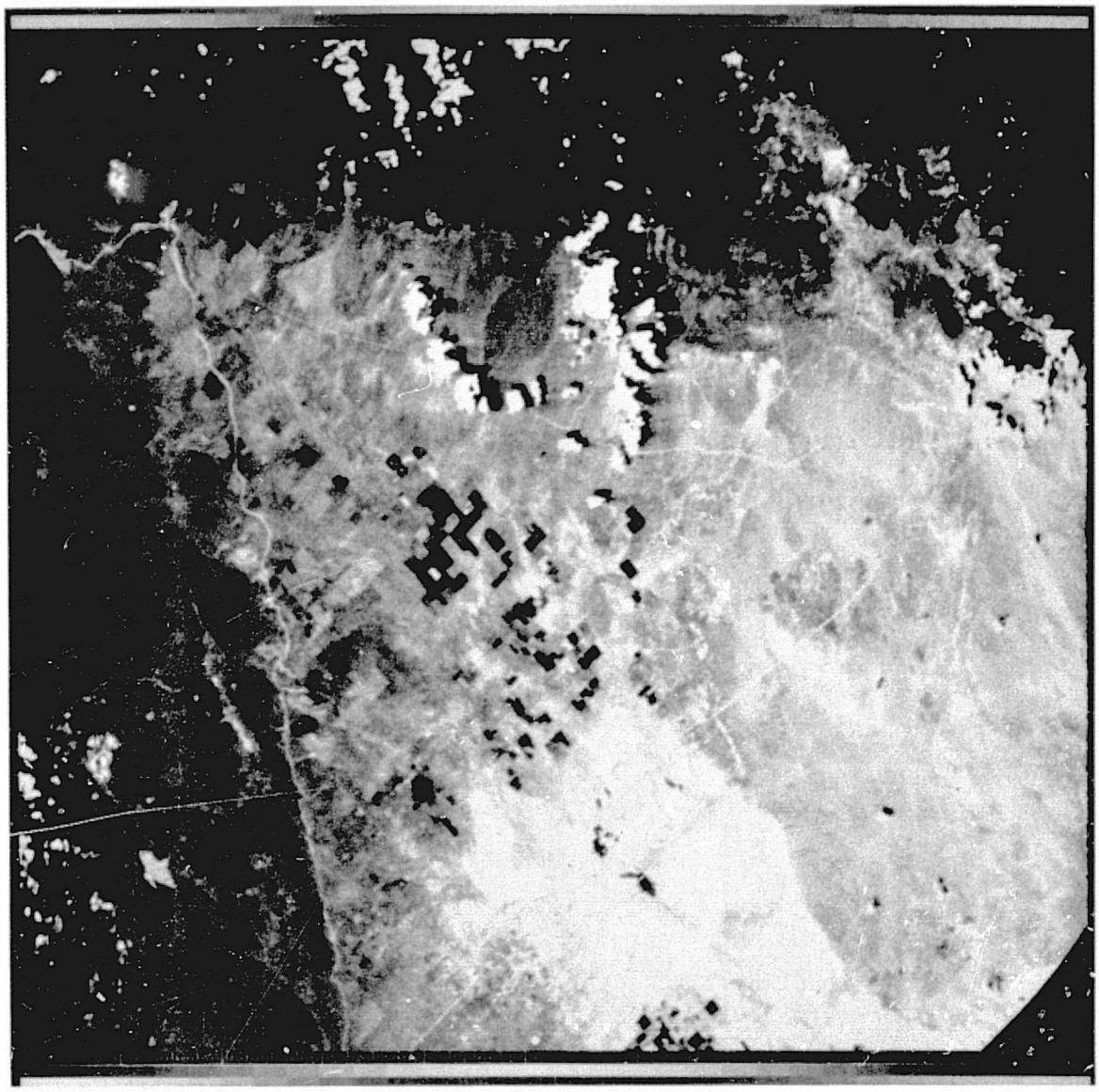

Fig. 2 - Portion of western Mojave Desert, California; Skylab 2, S-192 multispectral scanner data, Band 2 (.46 to .51 μm), Roll 936, June 1973. See Figs. 1 and 6 for features identified.

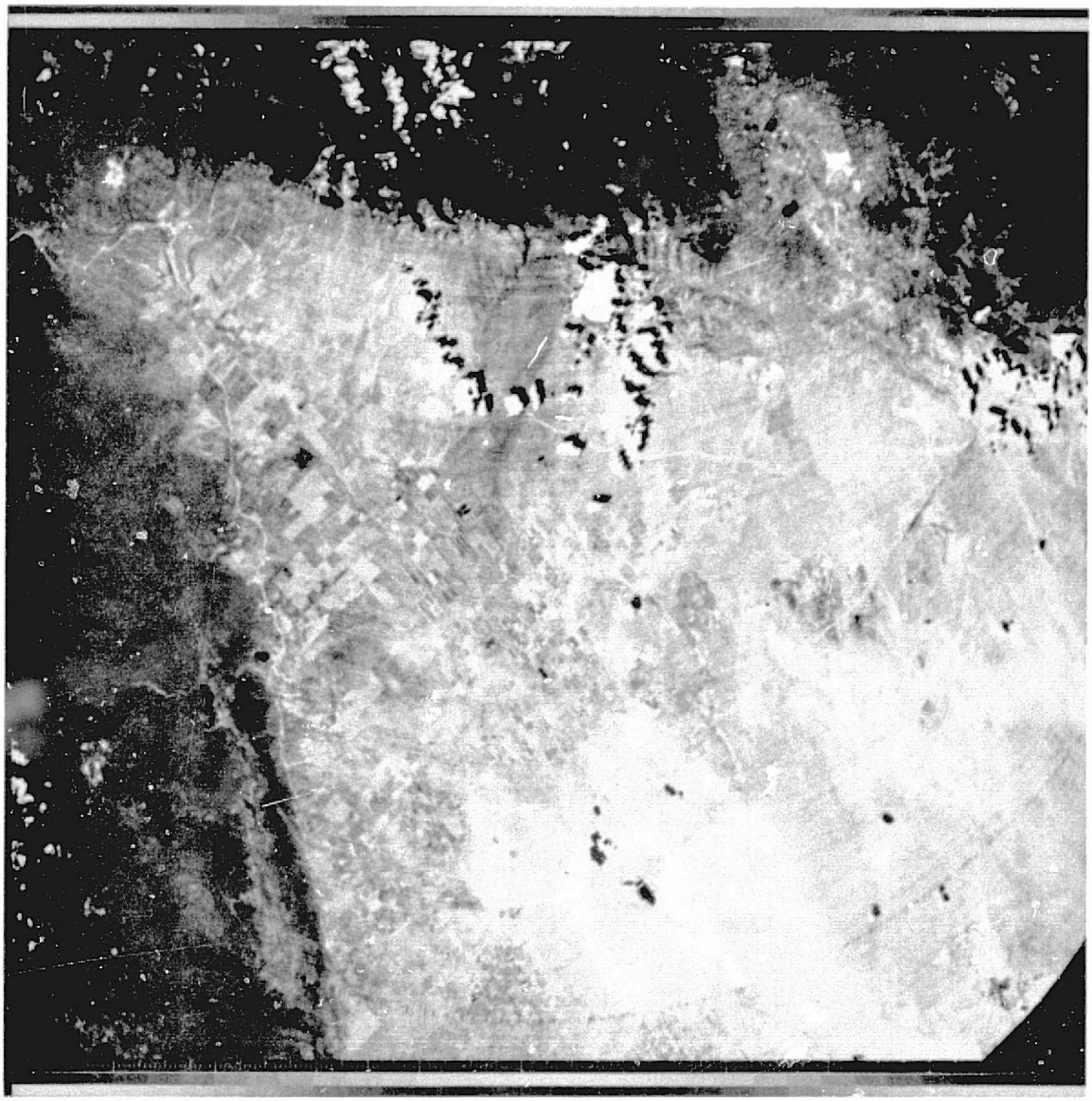

Fig. 3 - Portion of western Mojave Desert, California; Skylab 2, S-192 multispectral scanner data, Band 6 (.68 to .76 μm), Roll 936, June 1973. See Figs. 1 and 6 for features identified.

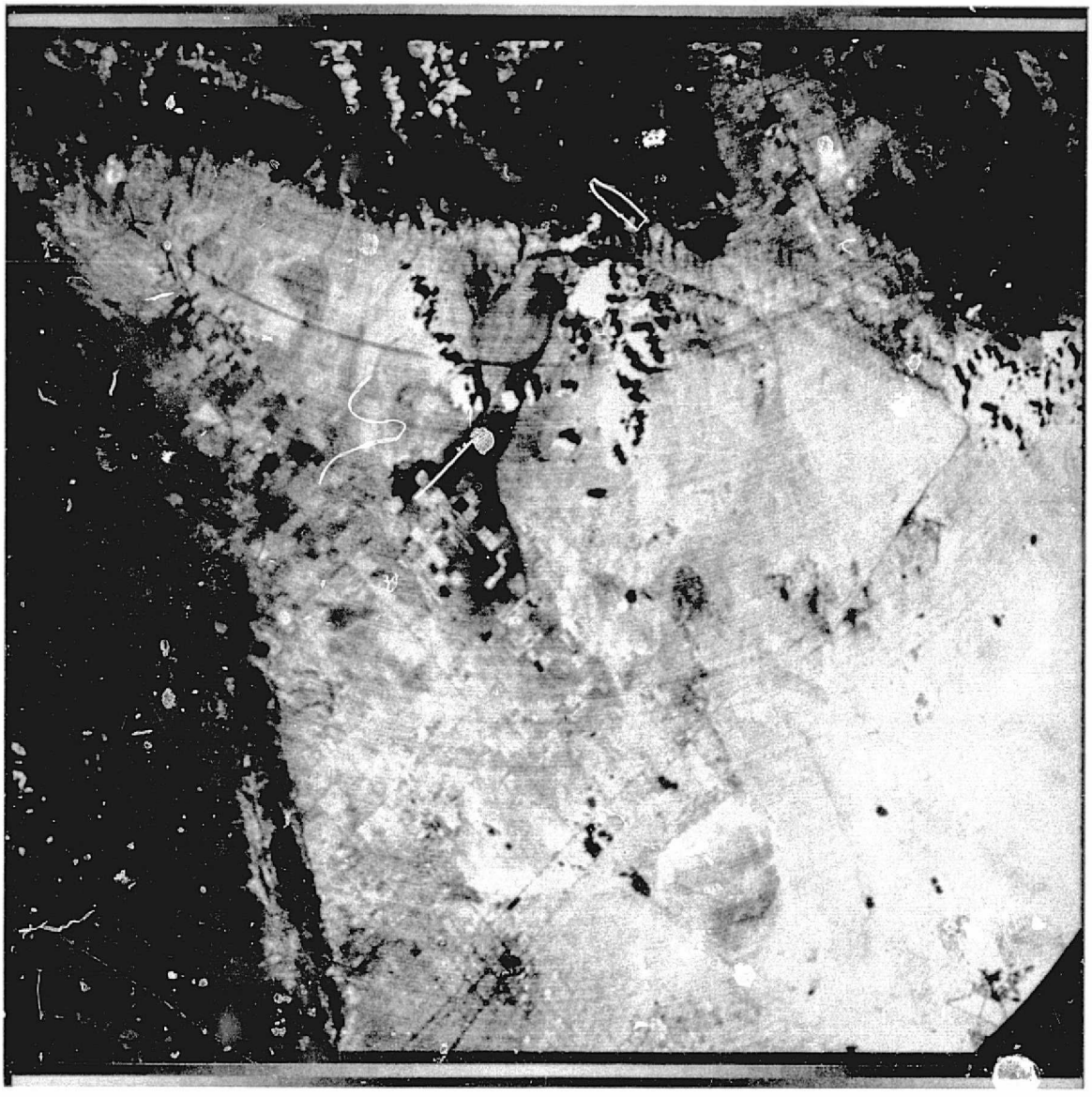

Fig. 4 - Portion of western Mojave Desert, California; Skylab 2, S-192 multispectral scanner data, Band 9 (1.09 to 1.19 μm), Roll 936, June 1973. See Figs. 1 and 6 for features identified.

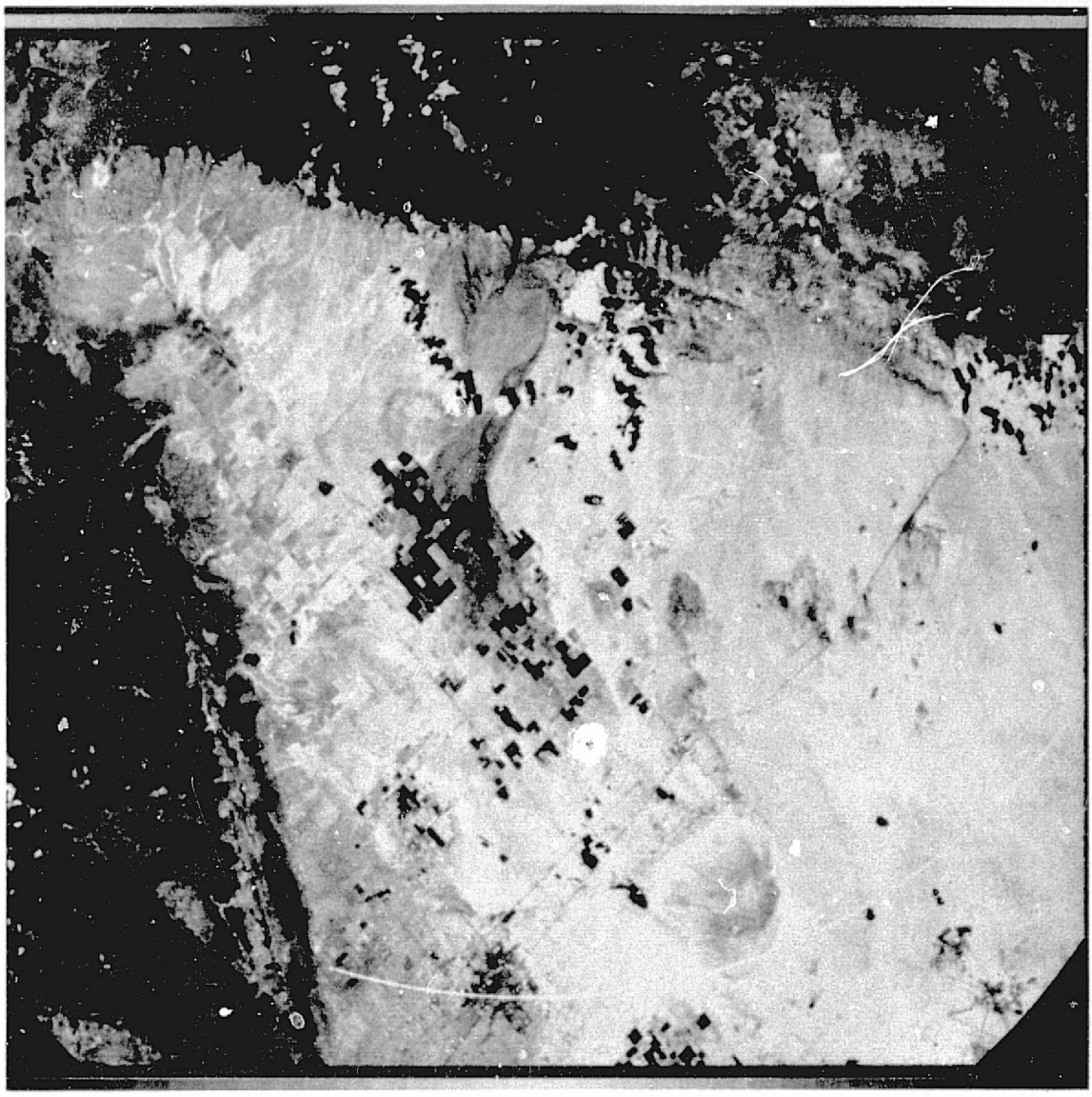

Fig. 5 - Portion of western Mojave Desert, California; Skylab 2, S-192 multispectral scanner data, Band 11 (1.55 to 1.75 μm), Roll 936, June 1973. See Figs. 1 and 6 for features identified.

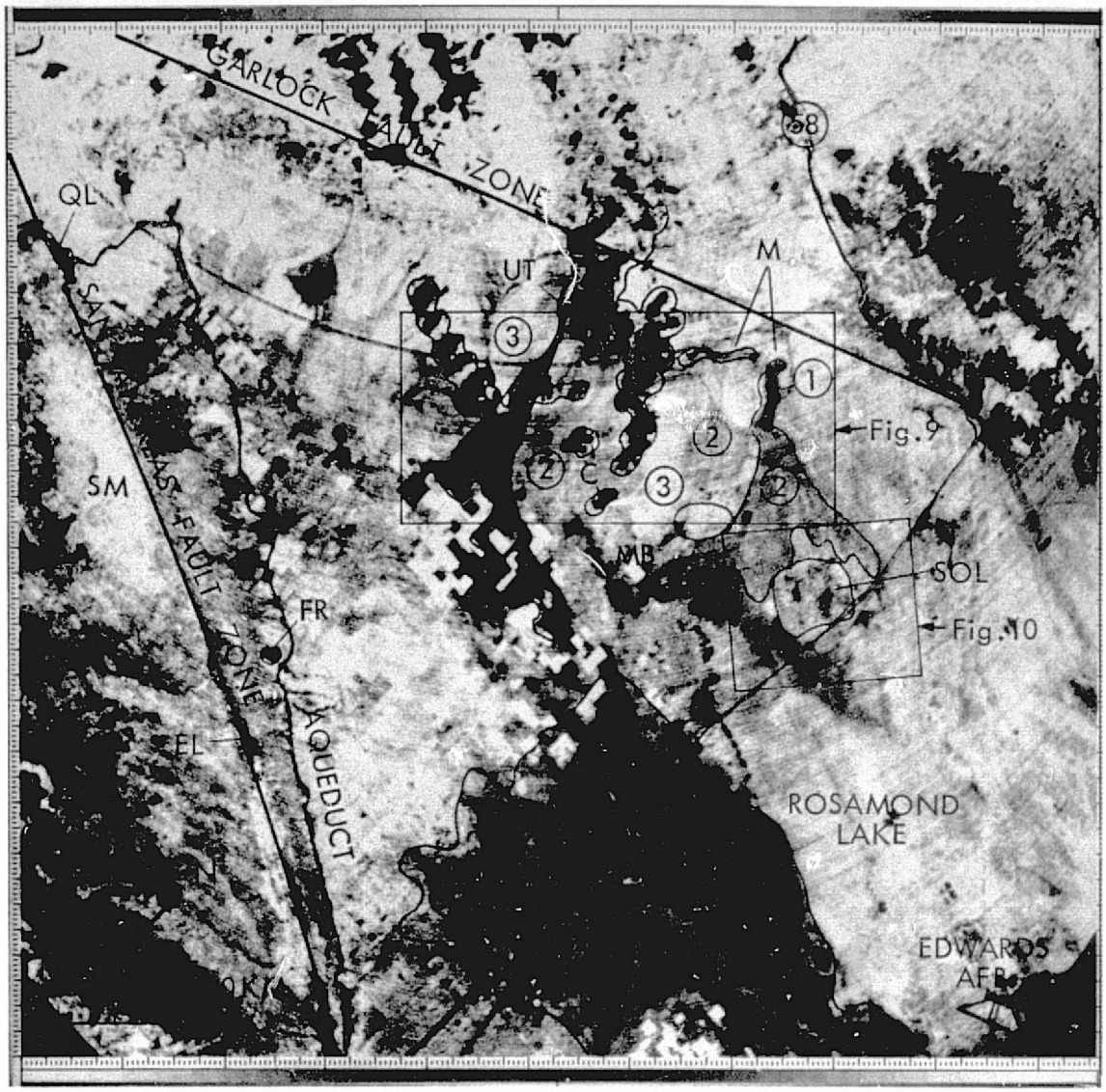

Fig. 6 - Portion of western Mojave Desert, California; Skylab 2, S-192 multispectral scanner data; ratio of Band 9 (1.09 to 1.19 μm) to Band 2 (.46 to .51 μm), Roll 936, June 1973. Brightness levels in alluvial deposits: 1: dark; 2: intermediate; 3: light. Abbreviations: EL: Elisabeth Lake; FR: Fairmont Reservoir; M: Bean Canyon Marble; MB: Middle Butte; QL: Quail Lake; SM: Sawmill Mountain; Sol: Soledad Mountain; UT: Upper Tylerhorse Canyon.

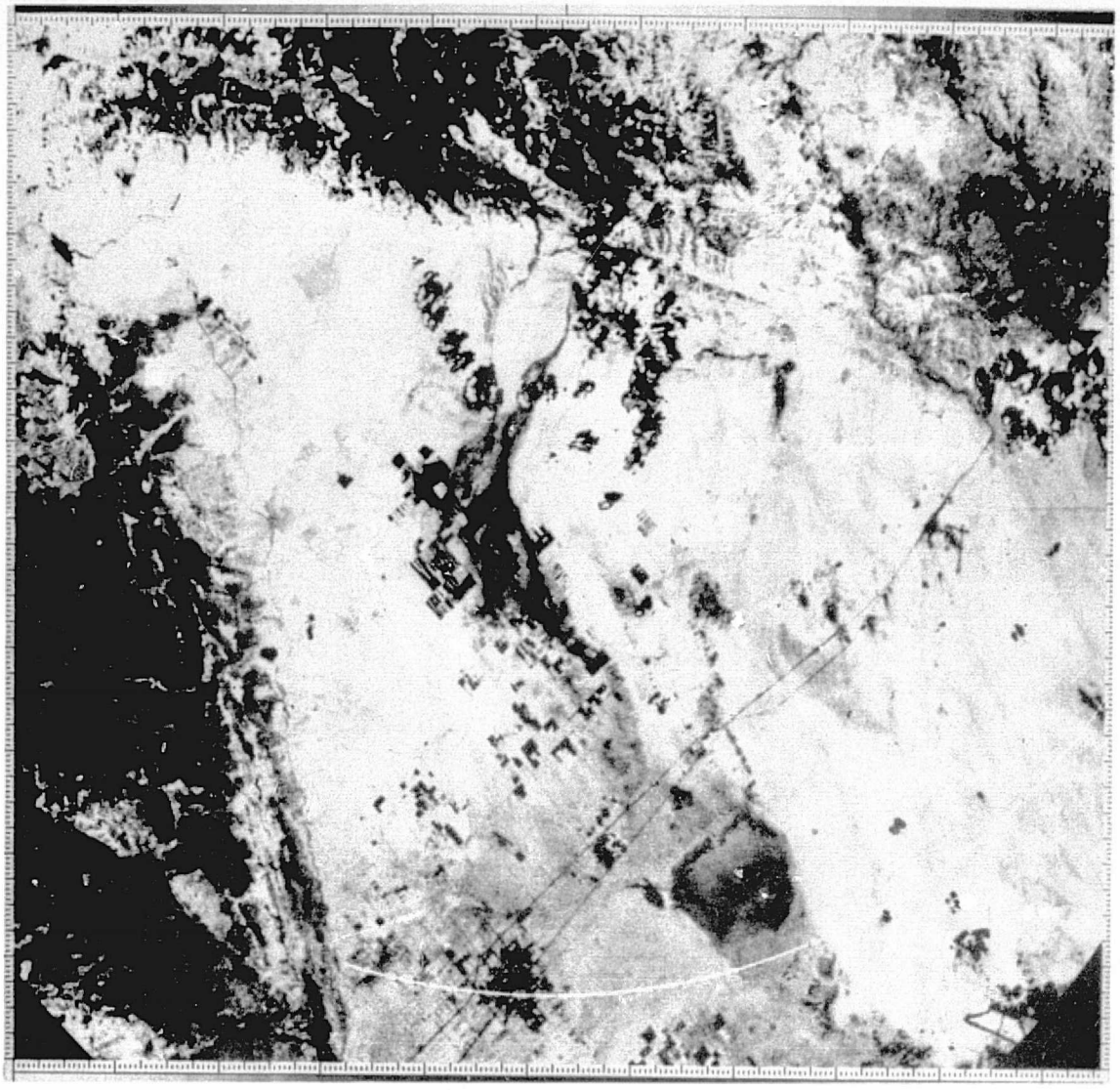

Fig. 7 - Portion of western Mojave Desert, California; Skylab 2, S-192 multispectral scanner data; ratio of Band 11 (1.55 to 1.75 μm) to Band 2 (.46 to .51 μm), Roll 936, June 1973. See Figs. 1 and 6 for features identified.

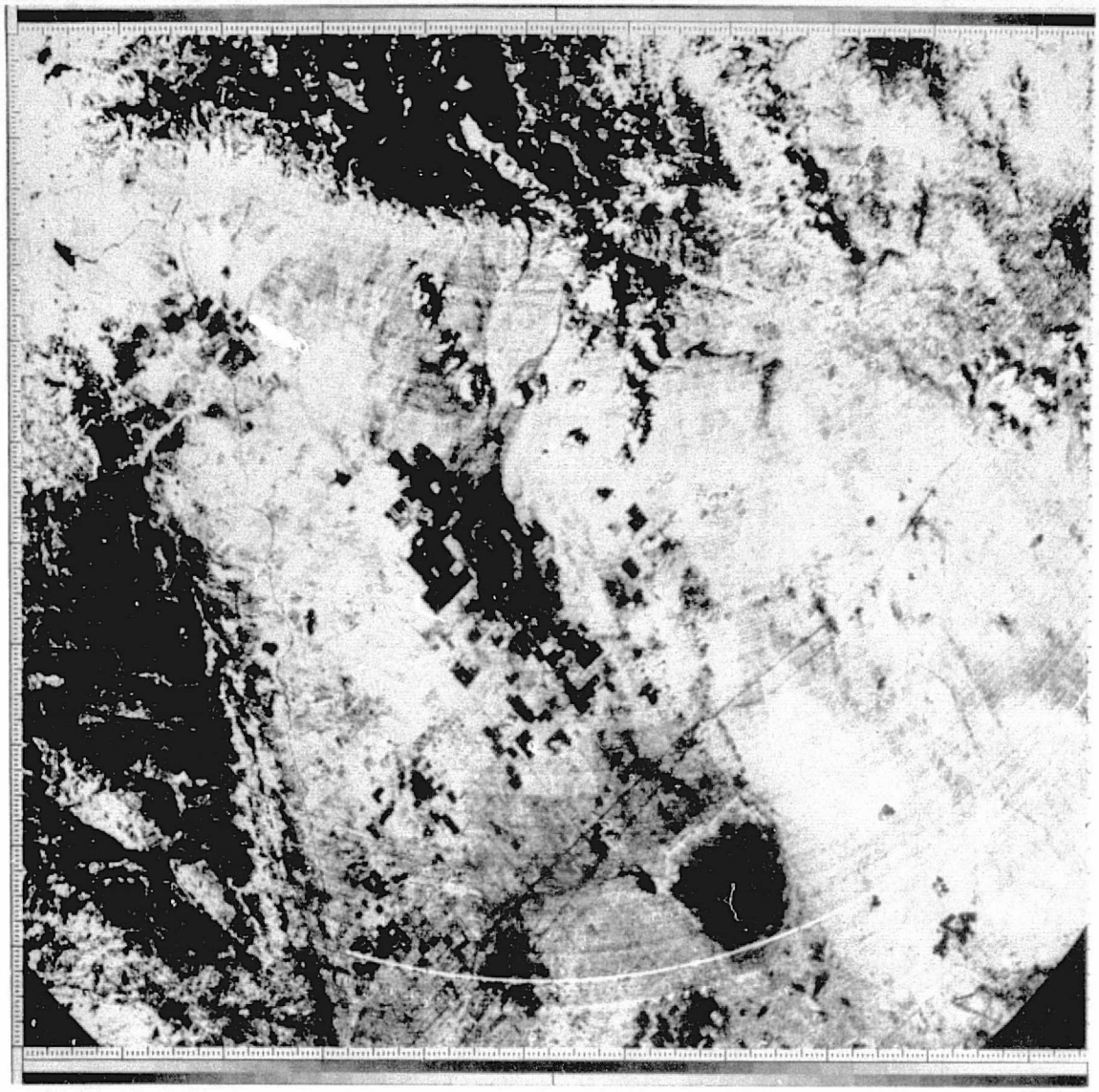

Fig. 8 - Portion of western Mojave Desert, California; Skylab 2, S-192 multispectral scanner data; ratio of Band 11 (1.55 to 1.75 μm) to Band 6 (.68 to .76 μm), Roll 936, June 1973. See Figs. 1 and 6 for features identified.

cover on Sawmill Mountain to the southwest, and sparser scrub vegetation on the northeast. The Garlock fault is more difficult to see in the ratio images, presumably because no vegetation differences occur across the fault, and the topographic shadowing has been eliminated by the ratioing process.

DISCRIMINATION OF ROCK AND SOIL TYPES

Bean Canyon Marble

The Paleozoic Bean Canyon Formation has been mapped by Dibblee (1967). About one-third of the formation consists of white to light-gray marble, here referred to as the Bean Canyon Marble. The remainder of the formation consists of meta-argillite or fine-grained mica schist, with minor amounts of quartzite and metabasalt. These metamorphic rocks occur as roof pendants in granitic rocks in the southwestern Tehachapi Mountains southeast of the Garlock fault (Fig. 1). In the single band images (Figs. 2 to 5), the marble is not distinguishable from other basement rocks. However, it is distinct on the ratio images, especially ratio 11/6 (Fig. 8). The two particularly dark spots at the northeast end of the marble outcrops are quarries where fresh marble is exposed. Vegetation is sparse and not different on adjacent units; therefore, vegetation does not play a significant role in the appearance of the marble on the ratio images.

Alluvium and Soil

Alluvial fan deposits spread outward from the Tehachapi Mountains across a broad bajada sloping gently toward Rosamond Dry Lake. These deposits were derived from granitic and schistose rocks and consist of gravels in stream channels of the Tehachapi foothills which grade into clay and silt in Rosamond Dry Lake. Dissection of surfaces developed on the older alluvial deposits indicates periodic uplift of the area during the Pleistocene. Dibblee (1967) has differentiated two alluvial units in this area, older alluvium and alluvium (Fig. 1). Alluvial fan deposits of different ages are more easily distinguished in the ratio images than the single band images, particularly in ratio image 9/2 (Fig. 6). On Fig. 6, alluvial fan deposits range from dark gray to white in tone. The darkest areas are delineated on the Fig. 6 overlay and labeled

number one. Intermediate gray and light areas are labeled numbers two and three, respectively. The boundaries between intermediate gray and light areas are indistinct, and were therefore not delineated on the Fig. 6 overlay. Observations of soil and vegetation characteristics were made from low-flying aircraft and the ground to determine the cause of the gray level differences.

Representative soil samples were collected from the dark, medium gray and light alluvial areas seen on Fig. 6 and compared with respect to color, texture and percent $CaCO_3$, determined by visual inspection and treatment with dilute hydrochloric acid. The sample localities are shown in Fig. 9 and the soil characteristics are summarized in Table I. An imperfect correlation between brightness level and soil color is present. Red-brown to yellow-brown soils are bright to medium bright, and gray soils are mostly dark. The highly calcareous soils (Samples 3 and 4) were collected from surface alluvium washed down from the marble quarrying and processing operations in Upper Oak Creek. These and other soil samples were treated with acid to determine if a high $CaCO_3$ content was common to dark areas. (As discussed previously, the Bean Canyon Marble appears dark gray in ratio image 11/6, Fig. 8.) Table I reveals no correlation between reflectance level and either texture or $CaCO_3$ content.

The influence of natural desert vegetation on reflectance levels is difficult to evaluate. Some bright areas support light brown annual grasses that may contribute to the brightness, but as mentioned below, Middle Butte is light in tone but barren of vegetation. Several of the dark areas support relatively dense stands of Joshua trees (Yucca brevifolia) and Creosote bushes (Larrea divaricata), such as the middle and lower Tylerhorse and Cottonwood Creek fans. These areas also show up darker than their surroundings on the single bands in the IR region of the spectrum, e.g., Bands 9 (Fig. 4) and 11 (Fig. 5). It is significant that although the lower part of the Tylerhorse fan is darker than its surroundings on the IR band images, the upper part is not. The upper reaches of Tylerhorse Canyon, which are very dark in ratio image 9/2 (Fig. 6), are essentially barren of vegetation, but the soil is light gray. The dark tone of upper Tylerhorse Canyon, therefore, is evidently due to soil color alone. Desert surfaces exposing partly soil and partly mixed vegetation types should yield complex spectral signatures. Kondratyev,

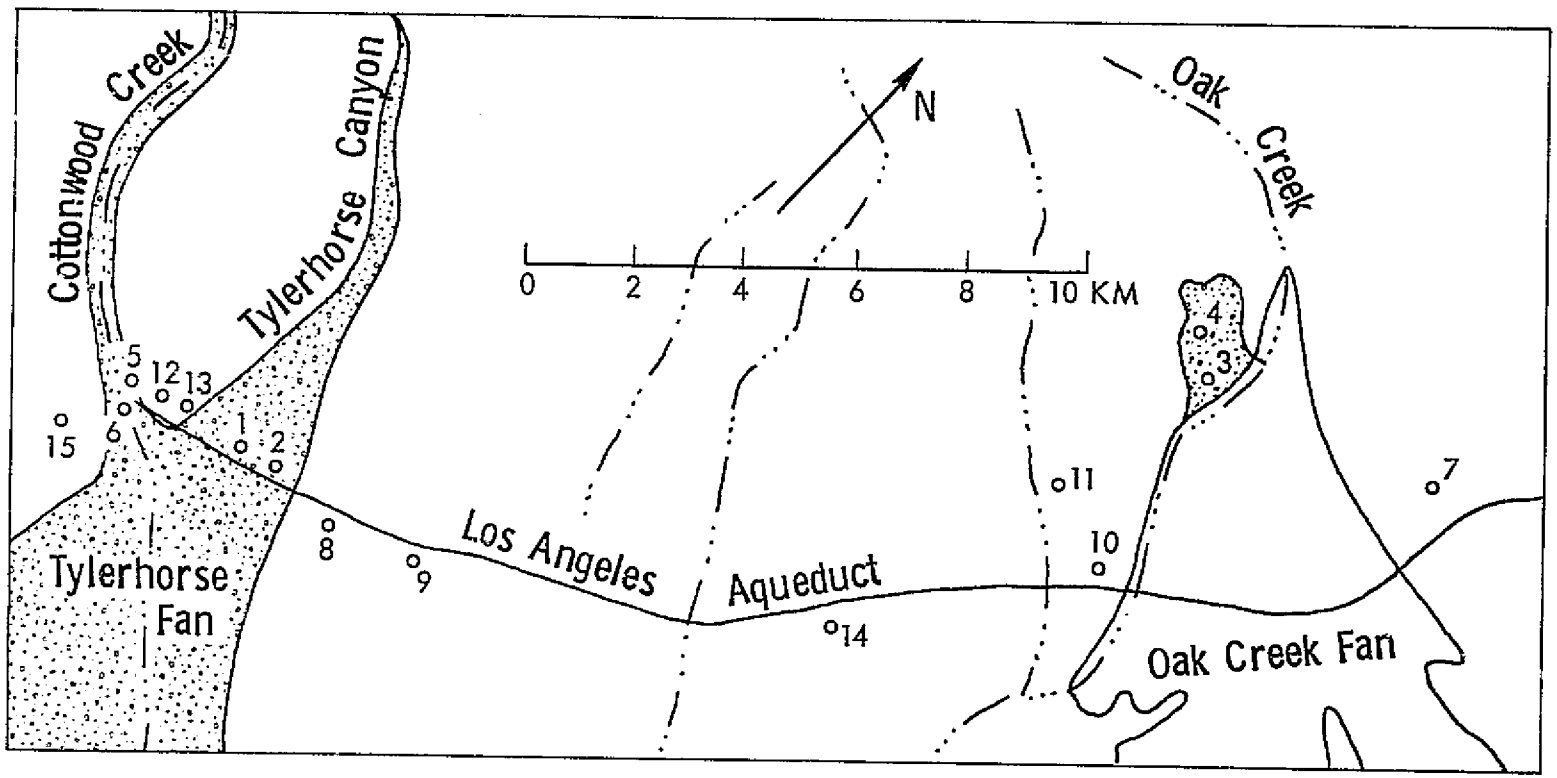

Fig. 9 - Location of surface samples listed in Table I. Stippled area corresponds to dark areas on Fig. 6. See Fig. 6 for area covered.

Sample No.	Relative Brightness	Color	Texture	Percent $CaCO_3$
1		brownish-gray	fine and medium sand	*
2		gray	gravel and granules	1.3
3	dark	gray	clay and silt	43.7
4		gray	clay and silt	39.6
5		gray	gravel and granules	*
6		gray	gravel and gran	*
7		light-brown	fine and medium sand	*
8		gray	gravel to fine sand	*
9	intermediate	brownish-gray	gravel and granules	0.75
10		yellow-brown	coarse sand	*
11		light-brown	fine and medium sand	*
12		red-brown	silt and fine sand	6.8
13		red-brown	silt and fine sand	*
14	light	yellow-brown	coarse sand	*
15		light-brown	fine and medium sand	*
16		brown	silt and fine sand	*

* not measurable

Table I -- Summary of soil characteristics, sample locations shown on Fig. 9.

et al (1974) present a spectral response curve for xerophilic semidesert vegetation which is negative between the blue-green and IR wavelengths; such a curve would produce the dark tone on the 9/2 ratio image (Fig. 6).

It is interesting that there is a general correlation between the gray levels and the age and elevation of the alluvial surfaces on the 9/2 ratio image (Fig. 6); the older, more dissected surfaces are brighter. A possible explanation for this correspondence is that the older the soil, the more mature it is and the greater the percentage of alteration products, including iron oxide which supplies the yellow-brown or red-brown color. The detection of hydrous iron oxides by spectral band ratioing has previously been discussed by Vincent (1972), Rowan, et al (1974), and Merifield, et al (1974, 1975).

Rosamond Dry Lake and adjacent areas on the west and south appear extremely bright on single bands in the visible region of the spectrum (Bands 2 and 6, Figs. 2 and 3). In longer wavelength bands (Bands 9 and 11, Figs. 4 and 5), these areas become less distinctive, although more detail appears within the playa itself. In ratio image 9/2 (Fig. 6), the same areas appear dark. These areas correspond to calcareous-alkaline soils (Fig. 1) delineated by the Soil Conservation Service (1970). The calcareous-alkaline soils do not support irrigated crops, and natural vegetation is very sparse or absent. Farther west, fertile soils support extensive fields of irrigated crops. The spectral response of the calcareous-alkaline soils is believed to be due to the whiteness of the soil resulting from the presence of evaporite minerals, and the near absence of vegetation.

Nearly identical results in the study of alluvium and soil on single band and ratio images from Landsat of the same general area were obtained (Merifield, et al, 1974, 1975). However, better differentiation of alluvial deposits was possible on the Band 5 (.6 to .7 μm) to Band 4 (.5 to .6 μm) ratio of Landsat multispectral data than was possible with any of the available S-192 ratio images. Bands 4 (.56 to .61 μm) and 5 (.62 to .67 μm) of S-192, which correspond most closely to Band 5 of Landsat, were not usable, so a direct comparison of Skylab and Landsat ratio images was not possible.

Mojave Mining District

The groups of hills north and west of Rosamond comprise the Mojave

Mining District, which in the past has yielded considerable gold and silver. Bedrock consists largely of quartz latite and rhyolitic tuff, which in places have been highly altered to clay and iron oxide. The most highly altered area is Middle Butte, which is barren of vegetation and mantled almost entirely with pinkish to reddish soil; the coloration is due to hydrous iron oxides. Middle Butte appears bright in the ratio images, especially 9/2 (Fig. 6). However, Middle Butte cannot be distinguished from the reddish-brown alluvial deposits immediately north of it. Dense, leafy vegetation in the checkerboard pattern of irrigated fields adjacent to Middle Butte also appears bright in the 9/2 ratio image, but can be discriminated from earth materials by virtue of its high reflectivity in the single band near IR images (e.g., Band 9, Fig. 4) and low reflectivity in Band 2 image (Fig. 2).

Figure 10 is an enlarged portion of an S-192 Band 8 (.98 to 1.08 μm) to Band 3 (.52 to .56 μm) ratio image covering the Soledad Mountain area, which is the largest outcrop area within the Mojave Mining District. Considerable variation in gray levels reflecting the distribution of rock types, alteration products and soils can be seen. A finer discrimination of rock types and alteration products within the Mojave Mining District is possible on the S-192 images as compared to the Landsat images (Merifield, et al, 1974, 1975). This is presumed to be due to the narrower bandwidths of the S-192 scanner. Additional field work is required to determine the physical characteristics of the various gray levels on the S-192 images. The existing geologic map of Dibblee (1967) is not adequate because it is not of sufficiently large scale, and soil types and altered rock are not differentiated from unaltered rock.

SUMMARY AND CONCLUSIONS

A number of geologic features are enhanced in ratio images of S-192 multichannel scanner data. Ratio images 8/2 and 9/2 are equally useful and are generally better than the remaining ratio images for the features studied. In ratio images 8/2 and 9/2, older alluvium and iron-oxide gossans of the Middle Butte Mining District appear anomalously bright. The older alluvium is red-brown or yellow-brown, presumably due to the presence of iron oxides, and the gossans are reddish- to pinkish-brown in color. The Bean Canyon Marble, calcareous-alkaline soils and recently deposited stream

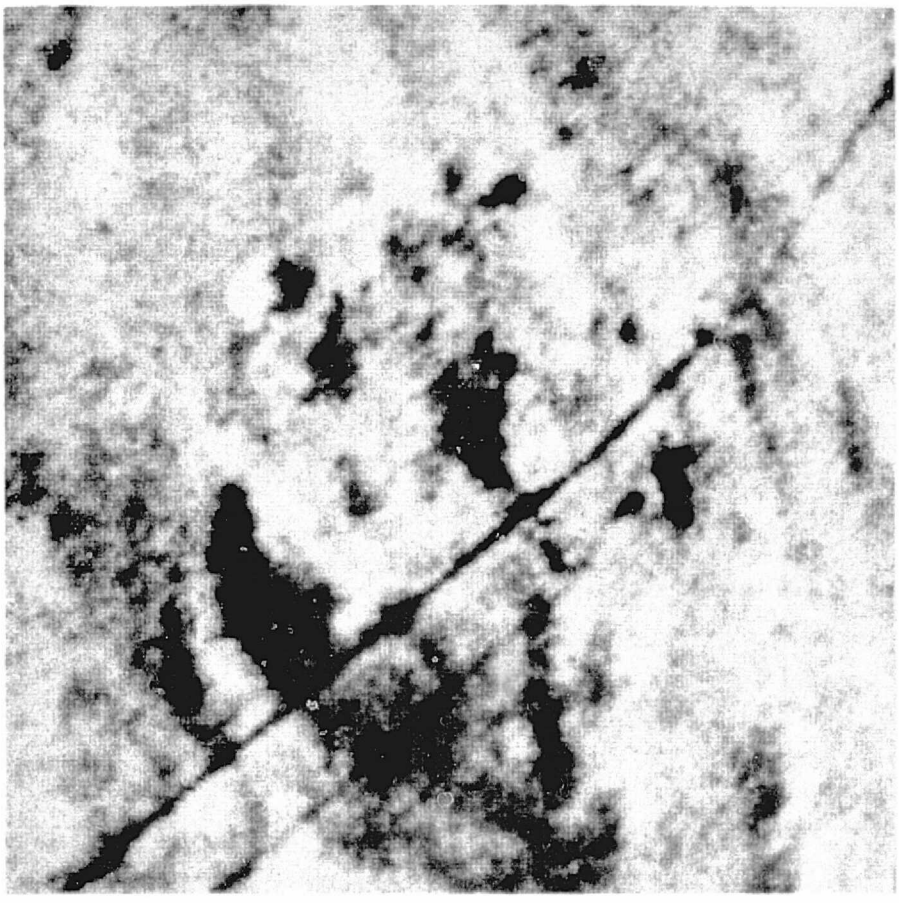

Fig. 10 - Soledad Mountain area of Mojave Mining District; Skylab 2, S-192 multispectral scanner data; ratio of Band 8 (.98 to 1.08 μm) to Band 3 (.52 to .56 μm), Roll 936, June 1973. See Fig. 6 for area covered.

and fan alluvium appear anomalously dark in ratio images 8/2 and 9/2. These earth materials have one characteristic in common, they are white to light-gray in color. It is concluded that the 8/2 and 9/2 ratio images enhance differences between grays and red-browns in natural rocks and soils which are not readily apparent in single band images. The role of sparse desert vegetation is not easily determined. Denser stands of Joshua trees and creosote bushes are associated with some of the gray soils and probably contribute to the low reflectance. Dry, brown, annual grasses are commonly associated with the dissected surfaces of older alluvium and may contribute to their brightness.

In heavily vegetated areas, rock and soil types cannot be discriminated in the images. Vegetation differences may be enhanced, however. A vegetation change across the San Andreas fault is more clearly discernible on 8/2 and 9/2 ratio images than on single band images or color photography. Forested areas appear bright relative to areas of sparser xerophilic vegetation on opposite sides of the fault.

Several applications of S-192 ratio images are indicated by this preliminary investigation: (1) the discrimination of marble from other metamorphic and igneous rocks, (2) the delineation of alluvial deposits of different ages, (3) the detection of faults where vegetation differences, not apparent in single bands or color photography, are enhanced, and (4) the detection of iron-oxide gossans. The latter application is being investigated by others, but its importance and potential warrants additional study. The Mojave Mining District is an ideal test site because several degrees of alteration are present, and the area is easily accessible and barren of vegetation.

REFERENCES

Billingsley, F. C., 1973, Some digital techniques for enhancing ERTS imagery: Symposium Proceedings, Management and Utilization of Remote Sensing Data, Am. Soc. Photogram. Fall Meeting, Oct. 29-Nov. 1, 1973, Sioux Falls, So. Dakota.

Billingsley, F. C. and Goetz, A. F. H., 1973, Computer techniques used for some enhancements of ERTS images: Symposium on significant results obtained from the Earth Resources Technology Satellite-1, NASA SP-327, v. 1, Sec. B., p. 1159-1168.

Dibblee, T. W., 1967, Areal geology of the western Mojave Desert, California: U.S. Geological Survey Prof. Paper 522.

Kondratyev, K. Ya., Buznikov, A. A., Vasilyev, O. B., and Sevastyanov, V. I., 1974, Results of spectrophotometric measurements of natural formations from the spacecraft "Soyuz-9" and investigations of environment from space: Remote Sensing of Environment, v. 3, p. 15-27.

Lamar, J. V., Merifield, P. M., and Lamar, D. L., 1975, Digital enhancement of ERTS and Skylab S-192 multispectral scanner images of the Mojave Desert, California; presented at annual meeting of American Geophysical Union, EOS, v. 56, p. 347.

Merifield, P. M., Lamar, D. L., Keaton, J. R., and Lamar, J. V., 1974, Enhancement of geologic features near Mojave, California, by spectral band ratioing of ERTS MSS data: Tech. Report No. 74-4, Calif. Earth Science Corp., Santa Monica, CA., 17 p.

Merifield, P. M., Lamar, D. L. and Lamar, J. V., 1975, Enhancement of geologic features near Mojave, California, by spectral band ratioing of Landsat MSS data: Proc. 10th Intern. Symp. Remote Sensing of Environment, Ann Arbor, Mich. (in press).

Rowan, L. C., Wetlaufer, P. H., Goetz, A. F. H., Billingsley, F. C. and Stewart, J. H., 1974, Discrimination of rock types and detection of hydrothermally altered areas in south-central Nevada by the use of computer-enhanced ERTS images: U.S. Geological Survey Prof. Paper 883, 35 p.

Soil Conservation Service, 1970, Soil Survey, Antelope Valley Area, California, U.S. Dept. of Agriculture.

Vincent, R. K., 1972, An ERTS multispectral scanner experiment for mapping iron compounds: Proc. 8th Intern. Symp. Remote Sensing of Environment, Ann Arbor, Mich. p. 1239-1247.

END
DATE
FILMED
1-6-76